A tailored viro-immunotherapy combination approach for the treatment of BRCA1/2 mutated breast and ovarian cancers

Taylor Rae Jamieson-Datzkiw

A thesis submitted in partial fulfillment of the requirements for the
Doctorate in Philosophy degree in Microbiology and Immunology

Department of Biochemistry, Microbiology and Immunology
Faculty of Medicine
University of Ottawa

Abstract

Hereditary breast and ovarian cancers (HBOC) represent 5-10% of breast and 10-15% of ovarian cancer cases. These cancers tend to be aggressive and curative treatment strategies are scarce. Poly(ADP-ribose) polymerase inhibitors (PARPi), a family of drugs that inhibit DNA repair, are a promising therapy for cancers harbouring mutations in their DNA repair machinery, such as HBOC. Unfortunately, nearly all patients ultimately become resistant to PARPi, leaving limited options for definitive treatment. Oncolytic or "cancer-killing" viruses are an innovative immunotherapeutic platform capable of selectively targeting cancer cells, leaving healthy tissues unharmed. Our group has demonstrated that oncolytic rhabdoviruses may be used to deliver therapeutic payloads by encoding targeting sequences to act on genes via RNA interference. In the present work, I have engineered the oncolytic virus, vesicular stomatitis virus (VSV), to express a variety of microRNA (miRNA) sequences that target genes essential for DNA repair, sensitizing resistant cancer cells to PARPi therapy. After initial experiments revealed hurdles concerning the functionality of artificial miRNAs which specifically target BRCA1 and BRCA2 I encoded the naturally occurring hsa-miR-182 into VSV to knockdown BRCA1 and additional genes essential for DNA repair. Using a 3D spheroid model, I have demonstrated sensitization of initially resistant MDA-MB-231 breast cancer cells to the PARPi, rucaparib. Complementary work exploring the shuttling of miRNAs into small extracellular vesicles, or EVs, has also shown that we can take advantage of the EV packaging facilities in infected cells, inducing the packaging of miRNAs over-expressed by VSV (EV-miRNAs) into EVs. Future work will address the functionality of these EV-miRNAs, testing their ability to knockdown targets in uninfected cancer cells.

Acknowledgments

I would like to begin by sending out a huge thank you to my supervisors Drs. Carolina Ilkow and John Bell. I am so grateful that you were both willing to welcome me into your groups to complete my PhD. Coming in with no prior experience in graduate studies or virology, I have learned more over the last three years than I ever could have imagined. You have taught me many lessons in the lab, but along the way I have also been exposed to the fields of biotechnology development and intellectual property. Thank you to the members of my thesis advisory committee – Drs. Christine Pratt, Doug Gray and Harry Atkins. Your expertise and advise have helped to move this project forward from the first TAC meeting until the last.

Thank you to current and past members of the Bell and Ilkow groups. Dr. Taha Azad, I have learned so much from my involvement in the biosensor project, from the actual experiments to the process of manuscript preparation, the efforts you have made to teach me valuable skills have not gone unnoticed. Dr. Mathieu Crupi, thank you for always being excited to bounce ideas around after lab meeting and for your willingness to teach new techniques whenever the opportunity arose, but most of all thank you for helping to get those last few westerns finished! Dr. Adrian Pelin, you have provided both moral and technical support throughout this entire project, thank you for taking the time to share your expertise (and humour) throughout my PhD studies. Emily Brown and Jaahnavi Dave, you made early mornings in TC so much more enjoyable, thank you for always being there to troubleshoot issues with experiments and life in general. A big thank you to Christiano Tanese De Sousa, Julia Petryk,

Ricardo Marius, Xiaohong He and Bradley Austin for your providing technical expertise throughout this project.

To the past and present Ilkow ladies (Marie-Ève Wedge, Dr. Joanna Poutou, Hayley McKay, Abera Surendran, and Sarah Tucker) thank you for your endless support throughout my PhD studies. You have all made important contributions to this project whether it was teaching an important technique, helping with a big experiment or providing moral support along the way; I am thankful to have worked with every one of you. Thank you to Dr. William Chen, my lab mate by marriage, for the countless coffee and food dates and enough gossip to always keep me laughing! To the members of my MD/PhD family (Melissa Phuong, Adam Pietrobon, Clayton Hall, and Laura Forrest) thank you for being there for support, guidance and many laughs through every transition from MD to PhD and back again.

And finally, I would not have made it through these last few years with a smile on my face if I did not have the love and support of my friends and family. Thank you to my mama bear and grandma for your weekly phone calls and endless support. I am grateful to my entire family for believing in me even more than I believe in myself sometimes. Thank you to Holly Yim for taking that fateful bus ride with me during our first months of medical school. Our friendship has carried me through the first years of medical school and has continued to grow (you also have one of the best roommates I have ever met…Jaz!). Lastly, thank you to my amazing husband for being the most caring and understanding partner anyone could ever hope for and most of all thank you for cooking all of my meals, you make sure that everyday is a good one filled with lots of love and plenty of yummy food.

Table of Contents

List of Abbreviations

APC – antigen presenting cell
ATM – ataxia-telangiectasia mutated
BCS – breast conserving surgery
BiTE - bispecific T-cell engager
BRCA1 - BReast CAncer gene 1 or breast cancer associated protein 1
BRCA2 - BReast CAncer gene 2 or breast cancer associated protein 2
CAF – cancer associated fibroblast
CAR T - chimeric antigen receptor T cell
cGAMP – cyclic guanosine monophosphate–adenosine monophosphate (GMP-AMP)
cGAS - cyclic GMP-AMP synthase
CSC – cancer stem cell
DC – dendritic cell
DGCR8 – DiGeorge syndrome critical region gene 8
DMEM - Dulbecco's minimal essential medium
DNA-PKcs - catalytic subunit of the DNA-dependant protein kinase
DSB – double strand break
EBV – Epstein-Barr virus
ECM – extracellular matrix
EGFR – epidermal growth factor
EV – extracellular vesicle
FBS – fetal bovine serum
g – glycoprotein
HBOC – hereditary breast and ovarian cancer (carcinoma)
HGSOC – high-grade serous ovarian cancer
HR – homologous recombination
HSV – herpes simplex virus
IAV – influenza A virus
ICB – immune checkpoint blockade
ICI – immune checkpoint inhibitor
IFN – interferon
iNKT – invariant natural killer T
LDLR – low density lipoprotein receptor
LOH – loss of heterozygosity
miRNA- microRNA
MOI – multiplicity of infection
MSC – mesenchymal stem cell
NF – normal fibroblast
NHEJ – non-homologous end joining
NK – natural killer
NSCLC – non-small cell lung cancer
OV – oncolytic virus

PALB2 – partner and localizer of BRCA2
PAMP – pathogen associated molecular pattern
PARG – poly(ADP-ribose) glycohydrolase
PARP – poly(ADP-ribose) polymerase
PARPi – poly(ADP-ribose) polymerase inhibitor
PD-1 - programmed cell death protein 1
PD-L1 – programmed death-ligand 1
PEG – polyethylene glycol
PFU – plaque forming units
P-gp – P-glycoprotein
PRR – pattern recognition receptor
scFv – single chain variable fragment
STING – stimulator of interferon genes
T reg cell – T regulatory cell
TAA – tumour associated antigens
TAM – tumour associated macrophage
TME – tumour microenvironment
TNF – tumour necrosis factor
VSV – vesicular stomatitis virus
VUS – variants of unknown significance
XRCC1 – X-ray repair cross-complementing protein 1
53BP1 – p53 - binding protein 1

List of Figures

List of Tables

Chapter 1: General introduction and objectives

Preface

The contents of this thesis contain the work of my PhD studies which have been completed over the course of three years as a part of the combined MD/PhD program. The large disruptions due to the COVID-19 pandemic have made it challenging to complete all the original objectives for this project and have resulted in some experiments being completed once or in a limited collection of cell lines. Fortunately, our group was able to make significant contributions during lab shutdowns/slowdowns by working to develop a biosensor for testing various COVID-19 treatment and prevention modalities as well as a multi-pronged approach to vaccine development using oncolytic virus backbones to act as vaccine vectors against SARS-CoV-2. The main body of this thesis contains the work of my original project, divided into three main result chapters, while the appendix contains two additional chapters outlining a concise summary of the work I contributed to the SARS-CoV-2 projects in addition to a Journal of Visualized Experiments methods paper I have written outlining the neutralization assay I took the lead on developing for our group. The SARS-CoV-2 projects are highly collaborative and for the most part are still a work in progress, I have highlighted aspects for which I was closely involved.

Also of note, Chapter 1 (particularly subsections – 'Tumour microenvironment' and 'Oncolytic viruses') and the General Discussion contain direct excerpts and figures from a review written by myself and post doctoral fellow, Dr. Joanna Poutou, entitled 'Redirecting oncolytic viruses: Engineering opportunists to take control of the tumour microenvironment'. The text has been adjusted where necessary. The use of this material has been allowed based on the Elsevier policy on use of published text within a dissertation.

Introduction

1.1 Tumour microenvironment

Tumours are now recognized as complex entities comprised not only by tumour cells but also, cancer stem cells (CSC), cancer-associated fibroblasts (CAFs), endothelial cells (EC), tumour infiltrating immune cells (T lymphocytes, B lymphocytes, natural killer (NK), tumour-associated macrophages (TAMs), dendritic cells (DCs) etc.), in addition to the extracellular matrix (ECM) that constitutes the scaffold to create a collaborative, interwoven entity known as the tumour microenvironment (TME)[1]. As a member of this "society", each cell type is in close communication with neighboring cells. Cancer cells interact with non-malignant components within the TME not only by direct contact between cells but also paracrine signal exchange of cytokines and growth factors (**Figure 1.1**). It is now recognized that extracellular vesicles (EVs), 30-150 nm heterogenous population of cell-derived membrane vesicles, secreted by tumours have specialized functions as intercellular communicators. These tumour-associated EVs can transport nucleic acids, oncogenic proteins and signaling molecules, contributing to tumour progression and metastases[2].

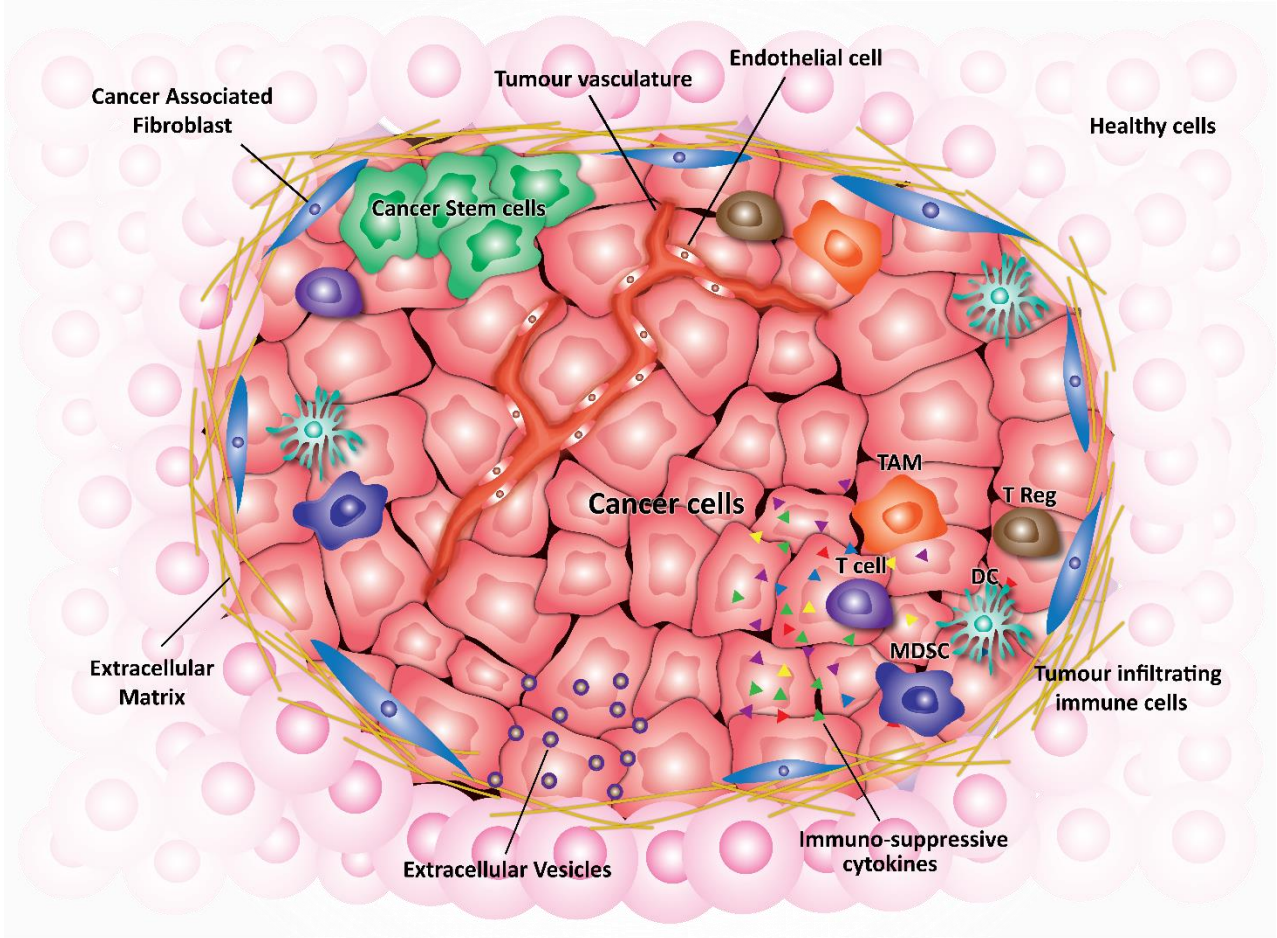

Figure 1.1 The tumour microenvironment is a dynamic and constantly adapting entity. The constant crosstalk among TME components, not only influences tumorigenesis, tumor progression and metastasis but also plays a crucial role in the resistance to anti-cancer therapies. The **ECM** provide structural scaffold and contains growth factors and cytokines, for survival and proliferation of the cancer cells. **CAFs** are the major contributor to depositing and remodeling ECM, in addition fostering angiogenesis, tumor progression and metastases. **CSCs** are involved in metastases and resistance to therapy and cancer recurrence. **Tumor associated vasculature** is required for tumor progression, favor metastases and contribute to tumor evasion of immune system destruction. **Tumor infiltrating immune cells** stimulate the proliferation of cancer cell and other cells type in the stroma, also contribute to remodeling the ECM by the secretion of proteolytic enzymes. In addition, the immunosuppressive tumor microenvironment which usually contain immune cells associated with immune suppression or tolerance impose additional challenges to anticancer therapies. The understanding of the tumor microenvironment makes it increasingly evident that successful antitumor cancer therapy must target not only on tumour cells but also on the other components of the tumor microenvironment. TAM: tumour associated macrophage, DC: dendritic cell, MDSC: myeloid derived suppressor cell. (This figure has been reproduced from Jamieson *et al.* Cytokine and Growth Factor Reviews 56:102-114, 2020)[3]

The TME is a dynamic, constantly evolving network influenced by the interactions between its components and the host. The ECM not only provides a structural scaffold of fibrous proteins, but also contains growth factors and cytokines, establishing a permissive niche for survival and proliferation of the cancer cells[4]. Cancer-associated fibroblasts, a heterogeneous cell population within the TME, contribute to the depositing and remodeling of the ECM, and secrete growth factors and chemokines that may induce the survival and growth of cancer cells, induce angiogenesis, and recruit tumour infiltrating immune cells[5]. Tumor infiltrating immune cells can directly or indirectly provide signals (e.g. TGF-β, TNF-α, FGFs, EGF) that stimulate the proliferation of cancer cells and other cell types within the stroma, and also contribute to remodeling the ECM by the secretion of proteolytic enzymes[6]. CSCs have the capacity for self-renewal and are capable of seeding new tumours during metastases. These cells tend to be resistant to conventional therapy and they are often responsible for cancer relapse[1,7]. The complexity of the TME as well as its critical role in the initiation and development of tumour progression make evident that a successful anticancer therapy should not only target cancer cells but also multiple components of the tumour niche, particularly the immune microenvironment.

1.2 Targeted therapies take advantage of key components of the TME

Systemic cancer therapies have traditionally been designed to indiscriminately kill rapidly dividing cells, leaving behind a wake of damage to the surrounding tissues and a wide range of side effects[8]. As more targeted therapies, such as antibody-drug conjugates[9,10], tyrosine kinase inhibitors[11] and hormone blocking agents[12], have entered the playing field researchers have also looked beyond directly targeting tumour cells and set their sights on breaking down the TME as

a whole. For example, targeting immunosuppressive TAMs and myeloid derived suppressor cells (MDSCs) via colony-stimulating factor-1 (CSF-1) and CSF-1 receptor (CSF-1R) inhibition, disrupting the supporting stroma and vasculature of the tumour by targeting fibroblast activation protein (FAP) expressing CAFs or applying antiangiogenic therapies (eg. anti-FAP and anti-VEGFA monoclonal antibodies), and activating the anti-tumour immune response by providing granulocyte-macrophage colony stimulating factor (GM-CSF)[13,14]. While considering the diverse components of the TME as therapeutic targets, it is important to also keep in mind the mutational signature that has contributed to the development and overall behaviour of the disease. Genetic changes are the driving force behind the altered phenotypes we see within tumour cells and the surrounding TME, meaning that the development of targeted therapies also includes those which aim to take advantage of specific genetic alterations within the tumour and surrounding cells. Two of the most notorious 'cancer genes' in mainstream media are *BRCA1* and *BRCA2* (BReast CAncer gene 1 and gene 2) owing to their strong connection with breast and ovarian cancer[15,16].

1.3 BRCA1 and BRCA2

The association of *BRCA1* and *BRCA2* with increased risk of breast cancer was established in 1994[15,16]. *BRCA1*, located on chromosome 17, was originally named by Mary-Claire King after tracing a large cluster of early-onset breast cancer cases via linkage analysis back to *BRCA1*[17]. It was later determined that truncating mutations of the BRCA1 protein were the culprit[15]. *BRCA2*, located on chromosome 13; was associated with increased risk of breast cancer while investigating families with a high incidence of male breast cancer without a *BRCA1* mutation present[16,18,19]. Hereditary breast and ovarian cancer (HBOC) has now been defined as a genetic

tumour syndrome most commonly due to inherited mutations in *BRCA1* or *BRCA2*; cancers caused by mutations in the *BRCA1/2* genes currently make up 5-10% of breast cancer and 10-15% of ovarian cancer cases[20,21].

BRCA1 and *2* are tumour suppressor genes that play important roles in DNA damage repair via homologous recombination (HR)[22]. Individuals born with a heterozygous mutation in either of these genes typically undergo loss of the non-mutated (or wild-type) allele at the *BRCA1* or *BRCA2* locus, also known as locus-specific loss of heterozygosity (LOH), leading to genomic instability and tumour growth[23,24]. The lifetime risk of developing breast and ovarian cancers for individuals who carry a mutation in either gene is extremely high. In the general population, the risk of developing breast cancer is approximately 13% (about 1 in 8 women) and ovarian cancer is 1.2%[25,26]. Women who inherit a deleterious mutation in BRCA1 or BRCA2 have a profound increase in their chances of developing breast and ovarian cancer; 55-72% of women who inherit a BRCA1 mutation and 45-69% who inherit a BRCA2 mutation develop breast cancer by 70-80 years of age, and the risk of ovarian cancer increases to 39-44% for women who inherit a BRCA1 mutation and 11-17% for those with a BRCA2 mutation[27–29]. Additionally, the risk of contralateral breast cancer increases for women who carry a BRCA1 or 2 mutation with 20-30% of women developing cancer in the opposite breast 10-years after the original malignancy is diagnosed and 40-50% after 20 years[27]. The observed variation in penetrance of mutations in *BRCA1* or *BRCA2* is relatively high due to the wide range of mutation type and location that may occur[30].

BRCA1 mutated breast cancers tend to fall into a distinct pathological group manifesting common features including high grade invasive ductal morphology, usually falling within the "basal-like" subtype of breast cancer, with low or lack of expression of genes associated with

estrogen receptor (ER), progesterone receptor (PR) and human epidermal growth factor receptor 2 (HER2)[31]. In contrast, BRCA2 mutated tumours tend to resemble those of noncarrier, or sporadic tumours, usually falling withing the "luminal-type" subtype (luminal A) with expression of genes expressed by the luminal breast epithelium and those associated with ER[32–34]. Ovarian cancers associated with BRCA1/2 mutation are generally high-grade serous carcinomas, this is also the most common subtype overall in the general population, comprising up to 90% of ovarian cancer cases[31]. Other ovarian cancer subtypes that have been associated with BRCA1/2 mutations include endometrioid, mucinous and clear cell carcinomas[31].

The tissue specificity of BRCA1/2 mutated tumours has been a contentious topic for many years now[35,36]. It has been long understood that the most common tissues impacted by inherited germline mutations are breast and ovarian; however, BRCA1 and BRCA2 are both expressed by nearly all cell types without significant differences in the level of expression between different tissues[37]. Plasma estrogen and progesterone levels in BRCA1 mutation carriers have been shown to be elevated, moreover both estrogen and progesterone receptor signalling have been shown to be repressed by BRCA1 via transcriptional repression as well as protein-protein interaction[38,39]. This suggests a theoretically clear path for the development of hormone-dependant tumours in BRCA1 mutation carriers; however, most breast tumours arising in this group do not express ER or PR. Another probable trigger for tumour development may be the high levels of genotoxic metabolites resulting from estrogen-inactivating pathways in tissues such as the breast or ovary leading to elevated rates of DNA damage leading to genetic instability especially in cells lacking sufficient BRCA1 or 2 expression[40,41]. Other groups have suggested that ER and PR signaling impact tumorigenesis in BRCA mutation carriers via paracrine mediate mechanisms or that an

over expression of ER and PR are required to initiate tumour development, but these are lost at a certain point in the development[42,43]. These and many other possibilities still require further exploration to fully elucidate the mechanism of tissue specificity of BRCA mutated tumours.

Hereditary breast and ovarian cancers (HBOCs)

While a majority of HBOCs can be attributed to mutations in BRCA1 or 2[37], a number of other genes have been shown to contribute to a hereditary phenotype when mutated including ATM[44–46], BARD1[47], BRIP1[48,49], PALB2[50–52], RAD51C[49], RAD51D[49], and Chk2[53–55]. The term 'BRCAness' has been used to describe tumours which share molecular similarities with BRCA mutated tumours, those of which may also respond to similar therapeutics[56]. In short, tumours which fall into the category of BRCAness generally have an HR defect, but do not have a BRCA1/2 germline mutation. The examples listed above are in fact all key genes involved in the HR DNA repair pathway in addition to other important cellular processes required for maintaining genomic stability, such as cell cycle checkpoints[56]. Attempts have been made to identify a distinct third breast cancer susceptibility gene (*BRCA3*); to date, it is understood that many different genes can contributed to the hereditary breast cancer phenotype and no single gene can be associated with families that have a high incidence of breast cancer with no *BRCA1/2* mutation identified[57].

Other types of BRCA1/2 mutated cancers

A number of cancer types in addition to breast and ovarian have been associated with BRCA1 or 2 mutations including melanoma, fallopian tube and endometrial cancers, pancreatic cancer[58], prostate cancer[59], and gastric cancer[60]. The association of BRCA mutations with certain

familial cancers aside from those involving reproductive organs has been somewhat under debate however, multiple large-scale studies have confirmed the association of BRCA2 with familial pancreatic cancer (FPC) with 17% families with three or more cases of pancreatic cancer among close relatives (first-and second-degree)[56,61,62]. Conversely, there have been a trends observed for increased risk of melanoma among BRCA1 mutation carriers and some studies have even shown a link to melanoma in families which carry BRCA2 mutations; still, a definitive association of either gene with increased risk of melanoma has not been concluded[62,63].

1.4 Mechanisms of DNA repair

Single strand DNA repair

The two main pathways of ssDNA repair are nucleotide-excision repair (NER) and base-excision repair (BER). NER can repair a wide variety of lesions; the two sub-pathways of NER include global genome NER (GG-NER) and transcription-coupled repair (TCR). GG-NER is responsible for surveying the entire genome for distortion due to disrupted base-pairing[64]. TCR takes place at the site of stalled RNA polymerase where the polymerase must be displaced by TCR-specific factors for subsequent repair to take place and resume transcription[65]. BER is the main mechanism for the repair of damage incurred by cellular metabolism, including reactive oxygen species, methylation, deamination and hydroxylation, as well as single stand breaks caused by X-rays[66,67].

Double strand DNA repair

DSBs may be caused by environmental factors such as ionizing radiation, cell intrinsic contributions including metabolic products, such as reactive oxygen species, and during replication[68]. The repair of DSB is critical for cell survival as these lesions can promote genomic instability and ultimately lead to cell death[69,70]. The mechanisms of DNA double strand break (DSB) repair can be broadly classified into two pathways, non-homologous end-joining (NHEJ) and homologous recombination (HR). DSB are preferentially repaired by NHEJ during G1 phase of the cell cycle and HR during S and G2 phases[68,71]. In general, due to the availability of intact homologous sequences during replication, DSBs occurring during replication are repaired by HR and those caused by ionizing radiation when DNA is more tightly packed are repaired by NHEJ[68]. Importantly, the main difference between NHEJ and HR is the requirement for recombination between sister chromatids during HR resulting in a nearly error-free process[71,72].

NHEJ begins with DNA end-binding proteins, Ku70 and Ku80 (also known as XRCC5 and XRCC6 or heterodimer Ku), binding at the break and recruiting the catalytic subunit of the DNA-dependant protein kinase (DNA-PKcs)[73]. This complex then recruits the repair enzyme DNA ligase IV which completes the repair[74]. Ku70/80 has high affinity for blunt DNA ends and those that possess very short overhangs, while breaks with longer ssDNA ends are less likely to bind the Ku heterodimer and undergo NHEJ[75]. Overall, NHEJ represents an error-prone process as DSBs are repaired via direct ligation without the requirement of a homologous template strand.

HR starts with strand resection, resulting in 3' single-strand (ss) overhangs. DNA end resection is carried out by the MRN (MRE11-Rad50-NBS1) complex; MRE11 first nicks the strand with a free 5' terminus up to 300 nucleotides away from the DSB and exerts its exonuclease activity to extend the nick to the DNA end[76]. The MRN complex then acts as a DSB sensor which

recruits ataxia-telangiectasia mutated (ATM) to the site of the break[77]. The ssDNA is then coated with RPA complex (replication protein A; RPA1, RPA2, RPA3) to prevent binding with another ssDNA. BRCA2 along with PALB2 then interacts with the ssDNA, RAD51 monomers which assemble into a filament, and BRCA1-BARD1, facilitating the displacement of RPA[78]. The recruitment of RAD51, a DNA strand-exchange protein, via BRCA1 interaction is dependant on CHK2-mediated phosphorylation of BRCA1[79]. The BRCA1-BARD1 complex then enables RAD51 homology searching and pairing[76]. Once sufficient pairing is in place, the synapse is stabilized, and the non-paired strand of the invaded DNA is displaced to form a displacement or D-loop[80]. The free 3' end of the invading DNA strand then interacts with DNA polymerase δ along with RAD51, RAD54 and RPA to extend the invading strand using the paired donor DNA as a template[76,80].

BRCA1 and BRCA2 protein-protein interactions and diverse functions

The amino acid sequences of BRCA1 and BRCA2 provided some initial insight into the function of these proteins soon after their association with increased risk of breast cancer was established. The BRCA1 protein is comprised of 1863 amino acids and is present in most proliferating cells[81]. Early investigations demonstrated that BRCA1 localized to sub-nuclear foci during the S and G2 phases of the cell cycle in addition to forming complexes with Rad51, another protein required for homologous recombination[82]. BRCA2, the larger of the pair, consists of 3418 amino acids and has also been shown to co-localize with BRCA1 and Rad51[83–85].

BRCA1 plays a number of well-defined roles in processes ranging from DNA-repair, cell-cycle checkpoint control and genome integrity maintenance, chromatin remodelling to

ubiquitination[57,86]. The BRCA1 protein can be separated into three main regions including a RING (Really Interesting New Gene) domain at its amino terminus, followed by a relatively unstructured region encoded by its large central exon [11], a coiled-coil domain, and finally tandem BRCA1 carboxy-terminal repeats (BRCTs)[87]. BRCA1 forms its complex with BARD1 through interactions with its RING domain and as previously discussed this is essential to the HR pathway. The BRCA1-BARD1 complex can also interacted with the RING domain of E3 ubiquitin ligase, inducing either mono- or polyubiquitination[88]. Additionally, the BRCA1-BARD1 complex can catalyze the formation of non-canonical lysine 6-linked ubiquitin (K6-polyUb) chains[89]. The coiled-coil domain of BRCA1 interacts with PALB2 (partner and localizer of BRCA2) and is responsible for bringing BRCA1 in close proximity with BRCA2 and RAD51 during HR. The BRCT repeat domain recognizes a phosphorylated serine within a specific motif present in Abraxas, BRIP1 and CtIP; the BRCT domain may only interact with one of these proteins at a time with each complex serving a unique function[78,90]. The interaction with Abraxas (BRCA1-A complex) targets BRCA1 to ubiquitin conjugates at DSBs which are needed for DNA-damage signaling and repair, it also binds RAP80 which recognizes ubiquitinylated histones including H2AX to recruit to the site of DNA damage. Phosphorylated BRIP1 is recruited by BRCA1 to form the BRCA1-B complex which acts as helicase to unwind secondary DNA structures during S phase, it is also required for S-phase checkpoint activation[91]. BRCA1 interacts with CtIP (BRCA1-C complex) to complete DNA end resection alongside the MRN complex during HR[92].

BRCA1 also plays important roles in the response to DNA damage at the initial signaling step required to initiate cell cycle arrest and the start of DNA repair. In response to DNA damage, BRCA1 is phosphorylated by ATM or ATR, depending on the type of stimuli[22]. In response to IR

damage, ATM phosphorylates BRCA1 as well as the checkpoint kinase CHK2 which can also phosphorylate BRCA1; phosphorylation by CHK2 has also been shown to inhibit the error-prone pathway of NHEJ and promote HR[93]. ATR is activated by UV-damage and hydroxyurea-induced replication arrest, activating BRCA1 during G_2-M, the interaction of BRCA1 and ATR has also been implicated in the response to stalled replication forks[94,95]. Overall, the phosphorylation of BRCA1 at multiple sites is essential for its activation and functions in cell cycle control and DNA repair.

While the implications of BRCA2 in HR have been well described there is relatively little known about the functions of BRCA2 outside the HR pathway[57]. BRCA2 has been shown to interact with PALB2 at its WD40 domain forming the BRCA2-PALB2-BRCA1 complex during HR[96]. The binding of RAD51 occurs at repeated motifs (BRC repeats) located near the centre of the BRCA2 protein as well as the carboxyl terminus, binding at these sites has be shown to contribute to RAD51 filament formation[83,97]. BRCA2 also interacts with DNA and DSS1 (deleted in spilt hand/spilt foot) protein at a conserved DNA-binding domain that follows the centrally located BRC repeats, binding of DSS1 has been shown to be essential for maintaining the stability of BRCA2[98,99].

Most (approximately 80%) of the known pathological mutations in BRCA1/2 result in protein truncations or in-frame deletions, as well as mutations resulting in mRNA decay[100–102]. Interestingly, there have been specific regions identified on both BRCA1 and BRCA2 which have been defined as either “breast cancer cluster” or “ovarian cancer cluster” regions owing to their conferred risk of triggering the development of each type of cancer when truncating mutation arises within that location[103]. There are also a number of pathogenic missense mutations resulting in unstable, full-length versions of each protein; a majority of deleterious missense

BRCA1 mutations occur at the N-terminal RING domain or the BRCT domain, while BRCA2 missense mutations tend to occur at the BRC repeat domains or the ssDNA binding region[100]. A large proportion of mutations, particularly those of the missense variety, have been classified as variants of unknown significance (VUS) meaning that the implications of the mutation have not been clinically defined and can therefore be difficult to manage[100,104].

1.5 PARP inhibitors are a perfect match for the treatment of BRCA1/2 mutated cancers

The loss of BRCA1/2 impairs the ability of cells to accurately repair DSBs by HR, often making them initially sensitive to chemotherapeutics that stall the replication fork and lead to DSBs, such as platinum salts and mitomycin C[56,105]. Unfortunately, as previously mentioned, most ovarian cancer patients will experience disease progression following initial treatment. For those who become resistant to platinum therapy, the response rate to further chemotherapeutics is only 6-30%[106]. The approval of Poly(ADP-ribose) polymerase inhibitors (PARPi) for the treatment of *BRCA1/2* mutated cancers has opened the door to enhancing therapeutic outcomes in both breast and ovarian tumours with pathogenic BRCA1/2 mutations. This treatment modality represents a **targeted synthetically lethal approach** to specifically eliminate cancer cells deficient in HR.

The poly(ADP-ribose) polymerase (PARP) was first described in 1963 as a DNA-dependent polyadenylic acid-synthesizing nuclear enzyme, PARP enzymes now encompass a superfamily of 17 different proteins, with PARP1 and 2 being essential to the base excision repair (BER) process to repair DNA single-strand breaks (SSB)[107–109]. PARP1 is the most active member of family; under normal circumstances PARP1 binds to SSBs where it is activated, then using NAD^+ as a substrate,

it catalyzes ADP-ribose polymers (PARylation) which mark the site of damage and attract XRCC1 (X-ray repair cross-complementing protein 1)[110,111]. XRCC1 then serves as a scaffold for DNA polymerase (Polβ) and DNA ligase (Lig3α) to fill and ligate the break[112]. PARP1 plays an additional role in HR by activating ataxia-telangiectasia mutated (ATM) as well[113].

PARPi typically interrupt DNA repair by interacting with the PARP enzyme co-factor β-nicotinamide adenine dinucleotide (β-NAD+) in the catalytic domains of PARP1 and 2[114]. The synthetic lethality of BRCA-mutation combined with PARP inhibition has been demonstrated previously by Farmer (2005) and Bryant (2005)[115,116] (summarized in **Figure 1.2**). Since then, several groups have demonstrated a similar effect by transient knockdown of BRCA1/2 prior to PARPi treatment[117–119]. The synthetic lethality of PARPi with BRCA1/2 mutation has been attributed to multiple mechanisms. Initially, it was thought that the inhibition of PARP results in persistent SSBs and stalling of the DNA replication fork, leading to the production of DSBs[120] . As discussed previously, cells rely on two main mechanisms for the repair of DSB, HR and NHEJ[121]. BRCA-mutated cells lack the ability to repair DNA breaks using the high-fidelity process of HR, rendering them vulnerable to further mutations, genomic instability, cell cycle arrest and even apoptosis when errors occur during NHEJ[122]. Interestingly, PARP1 knockdown or knockout eliminates the cytotoxicity elicited by PARPi, implying that the physical presence of PARP is required to induce cell death in BRCA mutated cells. It is now understood that the process of 'PARP trapping' plays a very important role in the efficacy of PARPi[123,124]. Essentially, PARP becomes trapped on the damaged DNA strand which not only prevents repair of the DNA, but also leads to collapsed replication forks and eventually leads to cell death as double stranded breaks persist and accumulate in the cell[125]. The PARPi currently under investigation have been

ranked according to their trapping potency with talazoparib coming out on top, followed by niraparib, olaparib and rucaparib are virtually tied, and veliparib comes in last[123]. These rankings are relatively reflective of the cytotoxic potency of each drug *in vitro* as well[123,126].

PARPi in the clinic

The first PARPi to be approved for use as a single agent was olaparib (Lynparza; AstraZeneca) in 2014 for the maintenance treatment of advanced ovarian cancer in patients with germline BRCA mutation after three or more lines of chemotherapy[127,128]. Since then, a number of additional PARPi have been approved with additional applications including olaparib (extended use to BRCA-mutated breast and ovarian cancer), rucaparib (BRCA-mutated ovarian cancer), niraparib (ovarian cancer, regardless of BRCA mutation status), and talazoparib (BRCA-mutated locally advanced/metastatic breast cancer); additional PARPi are currently being developed at the pre-clinical and clinical stages alongside studies exploring the application of approved PARPi for other types of cancer (eg. prostate and pancreas)[114,129,130]. Indeed, two recent clinical trials have led to the approval of olaparib and rucaparib for the treatment of prostate cancer in men with mutations in genes altering DNA repair, whose disease has metastasized or become resistant to typical hormone therapies[131].

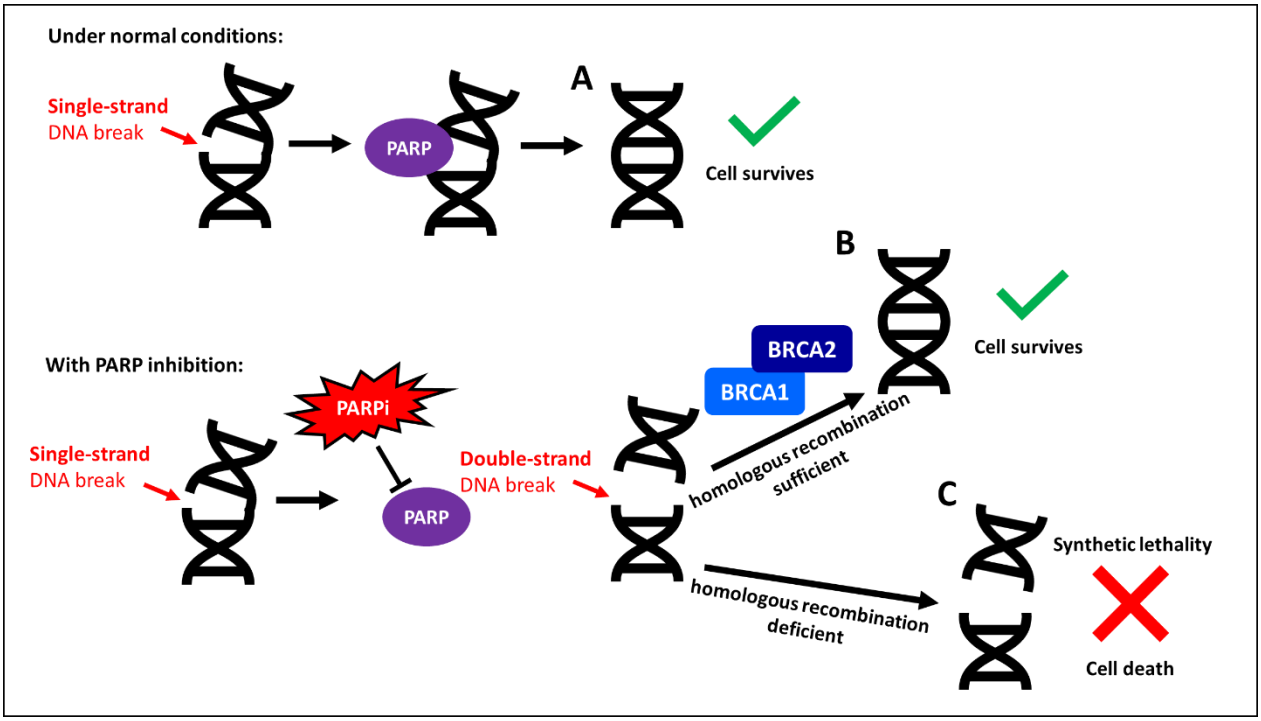

Figure 1.2 Synthetic lethality of BRCA1/2 mutations and PARPi. (A) A cancer cell with wild-type BRCA1 and BRCA2 along with fully function PARP is viable. (B) A cancer cell with mutated BRCA1 or BRCA2 is still viable if it has intact PARP function. (C) A cancer cell with a mutation in either BRCA1 or BRCA2 will no longer be viable when treated with PARPi (such as olaparib or rucaparib).

1.6 The problem - PARPi resistance

While the approval of PARPi for the treatment of *BRCA* mutated cancers initially emerged with great promise as the first class of drugs to take advantage of synthetic lethality against cancer in the clinical setting, tumour heterogeneity and genomic instability of these tumours has been shown to promote PARPi resistance when BRCA1/2 function is ultimately restored[114,132]. While it is difficult at this time to estimate the frequency of resistance in patients given that PARPi are relatively new to the clinic, acquired resistance in several preclinical models has been extensively studied[133]. Methods for enhanced screening techniques are currently contributing to our understanding of PARPi resistance overall, but some clinic studies have began to provide insight[133]. Currently, four main mechanisms of resistance have been identified: upregulation of drug efflux proteins, restoration of homologous recombination (often by reversion mutations of *BRCA1/2* or other HR genes), partial restoration of PARylation and renewal of stalled replication fork protection[133–135].

Upregulation of drug efflux pumps is a common mode of resistance among various tumour types and is not specific to PARPi drugs. The over expression of P-glycoprotein (P-gp) pumps has been associated with PARPi resistance, in fact, cancer cells treated with the P-gp pump inhibitor tariquidar are re-sensitized to PARPi treatment[136,137]. Unfortunately, the clinical use of P-gp pump inhibitors has been associated with toxicity in previous studies, likely due to a lack of specificity; thus, alternative mechanisms of overcoming resistance caused by efflux pump overexpression need further development[138].

Down regulation of PARP1 and PARG expression leading to decreased PARP trapping can confer resistance to PARPi. A recent study has identified multiple potential PARPi mutations using

a genome-wide CRISPR-Cas9 screening approach, several mutations impacted PARP trapping but interestingly many also led to distinct sensitivity to chemotherapeutic treatment. This same group identified a specific mutation of PARP1 which conferred resistance to PARPi, the mutation did not impact the ability of PARP1 to bind DNA but was located near the catalytic domain and was therefore not able to be "trapped" by PARPi[139]. PARP glycohydrolase (PARG) is needed for the degradation of PAR chains, preventing PAR accumulation, thus the loss of PARG has also been shown to contribute to PARPi resistance as PARylation can be partially restored in cells lacking PARG[140].

Stalled replication fork protection is achieved in part by BRCA1/2, in their absence this task can be rescued by inhibiting the recruitment of MRE11, an nuclease which can accomplish excessive DNA end resection in the absence of BRCA1/2, by depleting its interacting partners[141,142]. There exist a number of potential mechanisms to describe how replication fork stability may exert PARPi resistance, many of which are still under investigation.

Restoration of homologous recombination is currently the most widely accepted mechanism of resistance[134,135] and will therefore be the focus of this project. Several studies have mapped secondary BRCA reversion mutations in tumours after developing resistance to DNA damaging agents including PARPi and platinum-based chemotherapies[143]. Moreover, reversion mutations of other proteins involved in HR have been shown following platinum-based therapy[144]. Both genetic and epigenetic alterations can be attributed to the restoration of HR and PARPi resistance with loss of *BRCA1* promotor methylation also restoring BRCA1 function, leading to sufficient HR to overcome PARPi treatment[145]. HR can also be restored with the loss of 53BP1

(p53-binding protein 1), loss of 53BP1 protein promotes ATM-dependant processing of damaged DNA, in turn permitting HR to take place in the absence of BRCA1[146].

Additional mechanisms of resistance are also being explored including disruption of cell cycle control, alterations of miRNA expression patterns and changes to cell signalling pathways[135]. Overexpression of proteins associated with cell cycle regulation including CDK12 and WEE1 have been shown to promote PARPi resistance while inhibition can in fact confer sensitivity to PARPi[147]. Altered miRNA expression has been reported in several studies investigating PARPi resistance, for example miRNA-622 has been shown to enhance the HR pathway by directly inhibiting the expression of Ku70/80 which are essential to NHEJ[148]. Multiple signaling pathways have been shown to contribute to PARPi resistance as well including MET, PI3K/AKT, and ATM/ATR by promoting activation of PARP1, upregulating growth/proliferation and actively recruiting DNA repair factors, respectively[149–151].

1.7 Proposed solution - Oncolytic viruses

A large proportion of tumours have a common characteristic, aside from specific genetic alterations which may make them more susceptible to certain drug therapies; cancer cells tend to share an inherent susceptibility to viral infection[152]. Viruses are obligate parasites, they invade living cells to replicate their viral genome and spread. For their part, cells have developed several mechanisms to detect and fight the invaders. Host cells sense viruses and initiate the antiviral program by means of a group of surface and intracellular proteins collectively known as pattern recognition receptors (PRRs). These receptors detect conserved pathogen-specific molecules termed as pathogen associated molecular patterns (PAMPs). The host antiviral response is

versatile and results in the induction of type I interferons, chemokines and proinflammatory cytokines, which activate and recruit innate immune cells to the site of infection and promote adaptive immunity[153].

Oncolytic virotherapy exploits the inherent propensity of cancer cells to be infected by viruses[152]. During malignant transformation, normal cells progressively undergo genetic transformations, acquiring biological capabilities that distinguish them from healthy cells, these critical changes are described as "the hallmarks of cancer"[1]. Acquiring these cancer inherent characteristics including increased angiogenesis, insensitivity to anti-growth signals, sustained proliferative signals, evasion of apoptosis, avoiding immune cell destruction and attenuated host antiviral response, make cancer cells coincidentally more susceptible to viral infection[154,155].

Cancer-killing or oncolytic viruses (OVs) are viruses that occur either naturally or have been genetically engineered to infect, replicate in, and kill cancer cells while leaving normal cells unharmed. These anti-tumour agents have promising safety profiles in patients[156], with the first OV product Talimogene laherparepvec (T-Vec, Imlygic®), approved by the U.S. FDA in 2015 for the treatment of advanced melanoma[157]. Initially designed as cancer killers, OVs are now recognized as a promising multi-mechanistic therapy for the treatment of cancer. OVs can reshape the tumour microenvironment[158,159], activate the immune system to induce a robust long-lasting anti-tumour immunity[159], and can express and deliver therapeutic payloads in the TME[160–163]. In addition, these agents are the ideal candidates to synergize with other immunotherapies such as immune checkpoint inhibitors [164,165].

Despite advances, the efficacy of OV therapy is still limited by the variability of the immune response observed in patients, tumour heterogeneity as well as physical barriers (e.g.

fibrotic tumours) and immunosuppressive milieu imposed by the TME[166,167]. Several strategies have been developed to improve OV specificity and therapeutic efficacy. Examples include but are not limited to improving OV safety profiles by re-directing OVs towards receptors that are preferentially expressed in cancer cells (cancer cell-induced tropism). Multiple strategies have also been developed to improve OV efficacy including encoding tumour associated antigens (TAAs) or immunomodulatory cytokines (e.g. granulocyte-macrophage colony-stimulating factor; GM-CSF) to overcome tumour immune suppression, and finally increasing penetration and diffusion through the tumour by targeting supportive components within the TME which contribute to the difficult to penetrate stroma (summarized in **Figure 1.2**)[168,169].

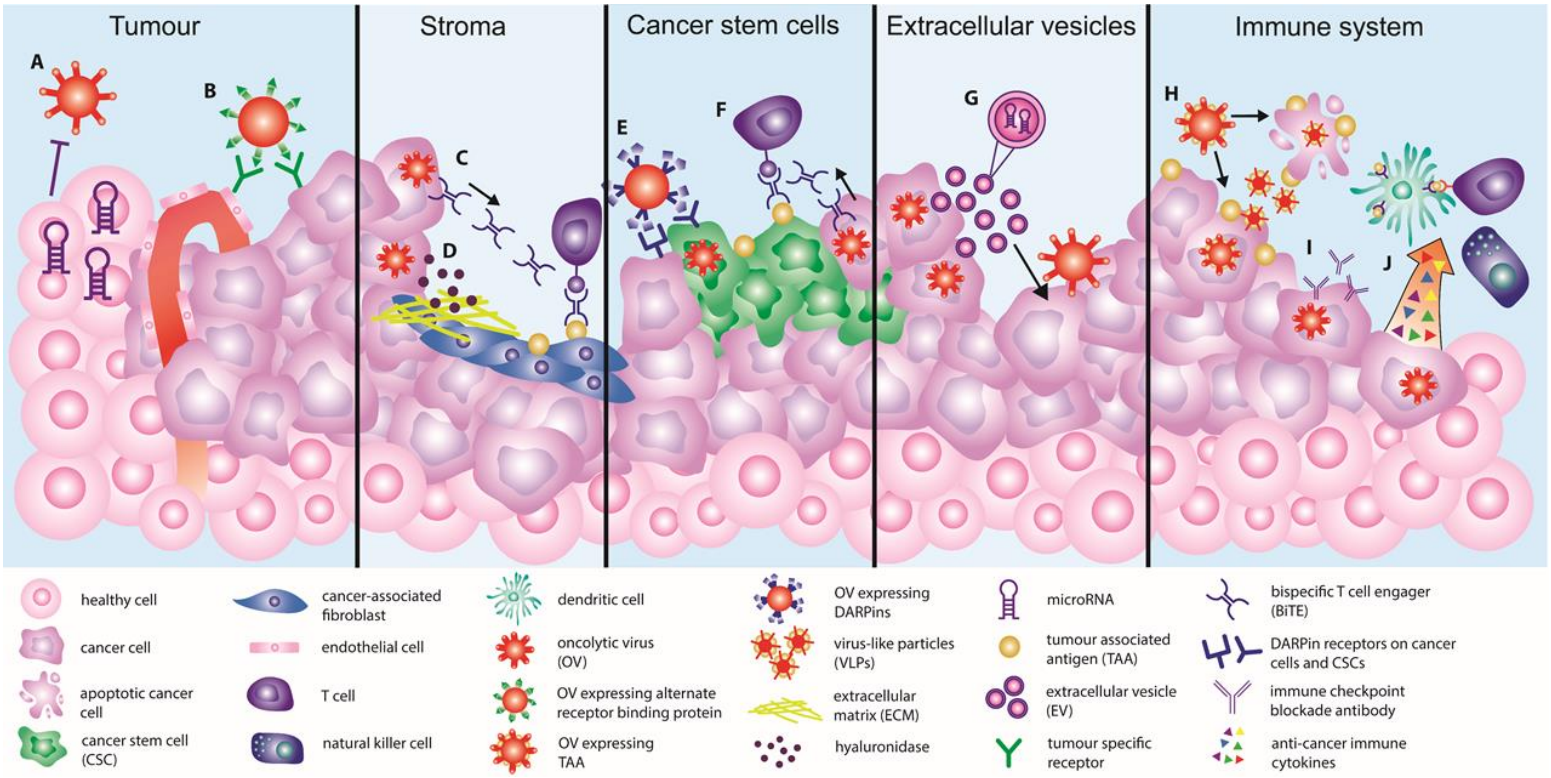

Figure 1.3 Summary of recently developed therapies redirecting oncolytic viruses (OVs) to the diverse components of the tumour microenvironment. (A) Expression of miRNA binding sites for miRNAs highly expressed in healthy cells reduces off-target infection. (B) Expression of alternate tumour specific receptor binding proteins directs viral entry to tumour cells as well as endothelial cells of the tumour vasculature. (C) Expression of bispecific T cell engagers (BiTEs) targeted to antigens expressed by cancer-associated fibroblasts (CAFs) direct T cell mediated killing to CAFs. (D) Hyaluronic acid (HA) expressed from OVs breaks down the extracellular matrix (ECM). (E) Designed ankyrin repeat proteins (DARPins) expressed from the virus simultaneously target tumour cells and cancer stem cells (CSCs). (F) BiTEs expressed by OVs specifically engage T cells with antigens on CSCs. (G) Extracellular vesicles (EVs) produced by infected cells promote a pro-virus niche, enhancing infection of neighbouring cells. (H) OVs expressing tumour associated antigens (TAAs) enhance TAA presentation by dendritic cells. Virus-like particles (VLPs) expressing similar antigens can boost the anti-tumour immune response. (I) Immune checkpoint blockade antibodies (anti-PD1 and anti-PD-L1) act synergistically with OVs when expressed from the virus or administered exogenously to overcome late-stage disease. (J) Cytokines expressed from OVs activate and expand cells of the innate and adaptive immune systems including dendritic cells, T cells, and natural killer cells. (This figure has been reproduced from Jamieson *et al.* Cytokine and Growth Factor Reviews 56:102-114, 2020)[3]

1.8 Vesicular stomatitis virus

The wild-type and oncolytic versions of vesicular stomatitis virus

Vesicular stomatitis virus (VSV) is a small enveloped, non-segmented negative sense single-stranded RNA virus belonging to the family Rhabdoviridae[170]. VSV has proven to be a promising OV candidate due to its unbiased tissue tropism, capacity to be genetically manipulated, and its ability to induce interferon signaling upon infection[170,171,172]. The 11kb genome of VSV comprises 5 genes which encode nucleocapsid protein (N), phosphoprotein (P), matrix protein (M), glycoprotein (G), and large polymerase (L)[173]. The major VSV serotypes, Indiana (IN) and New Jersey (NJ), are endemic to some parts of the United States and Central/South America, with the natural hosts of VSV including cattle, pigs, horses, as well as insects[173]. Seroprevalence in the human population is very low, adding to VSVs potential as an OV[174]. VSV G protein is necessary for viral attachment to the host cell and its broad tissue tropism can be attributed to the relatively ubiquitously expressed cell surface low density lipoprotein receptor (LDLR) serving as the primary receptor for viral entry[175].

The attenuation of VSV to prevent viral replication in normal tissues, leaving cancer cells susceptible, was based on the notion that many types of cancer have impairments within their interferon signaling pathway[176,177]. The growth of VSV is severely inhibited by interferon, consequently this virus has developed methods to block interferon production during infection (described below)[178]. Thus, an attenuated version of the virus (VSVΔ51) which induces a heightened interferon response has been developed to protect healthy cells[179]. VSVΔ51 contains a mutation within the matrix (M) protein, removing the virus's inherent ability to block interferon production in infected cells. The M protein is required to carry out several viral functions

including budding and virion assembly, as well as inhibition of host gene expression. VSV's impact on host gene expression has been ascribed to the M proteins ability to inhibit the nuclear transport of host proteins and mRNAs into and out of the host nucleus[180,181]. Stojdl *et al.* demonstrated that cells possessing intact interferon signaling are protected from VSVΔ51 replication, while those that do not mount an effective antiviral response are susceptible due to VSVΔ51's loss of ability to block host cell transcription of antiviral genes[171,179]. [All experiments performed and proposed throughout this thesis utilize VSVΔ51 and will often be referred to simply as VSV].

VSV replication

Following attachment, VSV enters the cell via endocytosis, a drop in endosomal pH occurs and VSV G catalyzes the fusion of the viral membrane with the cell membrane, releasing the viral ribonucleoprotein into the cell cytoplasm[171]. Viral genes are then transcribed by the RNA-dependant RNA-polymerase complex, made up of the nucleoprotein, phosphoprotein, and large polymerase protein[182]. The transcription of VSV occurs within the cell cytoplasm in a stop-start fashion with the polymerase entering the genome at a single site and stuttering at each intergenic region during the polyadenylation of the transcript, transcription of downstream genes depends on the termination of transcription of the upstream gene[183]. The RNA-dependant RNA polymerase plays double duty, facilitating transcription of mRNA necessary for production of viral particles and also producing full-length copies of the genome to complete the replication cycle[183]. N, P, M, and L proteins are translated by free cytoplasmic ribosomes, while G proteins are translated by ribosomes bound to the endoplasmic reticulum[184]. As G proteins are synthesized

they move through the secretory pathway where they are glycosylated, eventually associating with the M proteins and nucleocapsid at the host membrane where the assembled viral progeny are released by budding[185].

VSV is ready for the clinic

One of the most important characteristics when introducing a new therapeutic to the clinic is safety. Following several *in vivo* studies, investigating both safety and efficacy of VSV, this virus has entered clinical trials. VSV-IFNβ-NIS (Voyager-V1™), an attenuated recombinant version of IN strain VSV, expressing human interferon-β (IFNβ) and the sodium-iodide symporter (NIS) was developed by Dr. Russell's team at the Mayo Clinic in Rochester, Minnesota. IFNβ serves to protect normal tissues from viral replication (as this virus does not possess the M mutation present in VSVΔ51) while also stimulating the cross-priming of T cells during infection while NIS permits non-invasive tracking of viral infection by nuclear imaging of (123)I-iodine distribution[186–188]. The potency of this recombinant VSV has been demonstrated in one study which highlighted its "curative one-shot" potential against an *in vivo* model of myeloma[189]. Early dose escalation trials have established a tolerable and safe dose in adults with late stage endometrial cancer[190]. VSV-IFNβ-NIS is currently in multiple phase I/II clinical trials as a single therapy or in combination with immune checkpoint inhibition and other chemotherapeutics in endometrial cancer, non-small cell lung cancer (NSCLC) and head and neck squamous cell carcinoma (HNSCC)[191]. OVs represent a powerful delivery agent capable of sending therapeutic cargo directly to the site of the tumour, this cargo may include proteins as described above or RNA interference machinery such as microRNAs.

1.9 MicroRNAs

The first microRNA (miRNA), lin-4 in *Caenorhabditis elegans*, was discovered in 1993 by Dr. Ambros and colleagues[192]. There are now more than 2000 miRNAs estimated to be present in the human genome[193,194]. MicroRNAs are small (usually ~20-23 nucleotides) non-coding RNAs that play a crucial role in post-transcriptional gene expression[195,196]. miRNAs modulate protein synthesis by pairing with complementary sequences of target mRNAs within their 3' – untranslated region (UTR); miRNAs may repress translation or induce degradation of the mRNA, a small selection of miRNAs has also been reported to activate translation[195]. These small RNAs are located throughout the genome often within noncoding areas, they may also be located within introns or untranslated regions (UTRs) of protein coding genes[197]. The unifying characteristic of all miRNAs is a stem-loop precursor RNA structure. miRNAs may be present as individual genes or organized as clusters of "miRNA families" which are related by sequence and/or function, they are generally transcribed by RNA polymerase II from either their own promotor or the promotor of their host gene[198]. Primary-miRNA (pri-miRNA) precursors contain a 5' – cap (7MGpppG) and a 3' – poly(A) tail[198].

Canonical miRNA processing occurs as a stepwise process in which Drosha (RNase III enzyme) associates with the RNA binding protein DGCR8 (DiGeorge syndrome critical region gene 8) to cleave the primary hairpin (pri-miRNA) sequence, this releases the stem-loop precursor structure from the pri-miRNA transcript, the pre-miRNA is then exported out of the nucleus by Exportin5[199]. The next step occurs in the cytosol with cleavage of the pre-miRNA by the endonuclease Dicer (RNase III enzyme), yielding a double-stranded miRNA/miRNA* duplex (miRNA* = passenger strand)[200,201]. One strand will preferentially complex with an Argonaute

(Ago) protein (Ago1-4), a member of the RNA induced silencing complex (RISC), guiding it to target mRNA transcripts[201]. For some miRNAs it is known that both strands will associate with RISC at high frequencies, thus there is not a clear guide strand versus passenger strand in these cases[202].

Non-canonical pathways for miRNA processing also exist for specific types of miRNAs, the most common being the miRtron class of miRNAs. The processing of miRtrons is unique due to their location within introns at the exon junction site meaning the initial cleavage step does not require Drosha, instead they are processed during splicing[203,204]. The subsequent cleavage of the pre-miRtrons remains dependant on Dicer. An alternative Dicer independent pathway also exists with the most described Dicer-independent miRNA being miR-451[201]. Following cleavage of the pri-miRNA sequence by Drosha, miR-451 binds directly to Ago2 which cleaves the passenger strand and trims the stem-loop, yielding the mature miR-451.

1.10 Extracellular vesicles as therapeutic delivery agents

Small extracellular vesicles (EVs), which include exosomes and some microvesicles, are (30-150 nm in diameter), membrane-bound, vesicles that are released from a wide variety of cell types, including tumour cells[205,206]. EVs can carry a wide variety of cargo including protein, nucleic acids and lipids depending on their cell of origin serving as delivery agents between cells to assist in communication and maintaining homeostasis[207,208]. EVs have also been shown to play an important role in the development and spread of cancer when produced by cancer cells; cancer-derived EVs are able to regulate gene expression within recipient cells to create their own customized metastatic niche via protein interactions, receptor transfer and horizontal transfer of

genetic information[209]. While EVs can carry functional mRNA, the majority of RNA carried by EVs is of the non-coding variety, including miRNA[210]. The presence of both pre- and mature miRNAs within EVs has been reported, in fact, a number of miRNAs isolated from EVs have been associated with specific disease states and in certain cases can even contribute to estimates of prognosis[211]. We have chosen to take advantage of this natural form of cell-to-cell communication, as cancer cells have been shown to produce higher numbers of EVs than normal cells. In fact, there have even been reports of enrichment of miRNAs in cancer-derived EVs compared to normal cells[212].

Thesis rationale

Aiming to take down the most clinically relevant cause of PARPi resistance, this project centres on overcoming the restoration of HR due to BRCA1/2 reversion mutations to wild-type, this mechanism has strong pre-clinical and clinical evidence with multiple reports of PARPi-resistant clones emerging due to either a reversion mutation or demethylation in the case of *BRCA1*[134]. Polyclonality has also been demonstrated among circulating cell-free tumour DNA indicating multiple reversion mutations within one patient[134], reinforcing the need for a treatment protocol to eradicate unique resistant clones as they arise over time. Our group has recently demonstrated the ability of oncolytic virus VSV to deliver artificial miRNAs (amiRNAs) developed via a library screen of random miRNA sequences *in vitro* and *in vivo*, these miRNAs can successfully knock down predicted targets at the level of the mRNA and protein. By using OVs as a delivery agent, this work aims to overcome current limitations of miRNA therapeutics. Taking the technology one step further, we now know that miRNAs are a common passenger within EVs, thus the project described here aims to take advantage of this cell to cell trafficking system by strategically selecting miRNAs to express from VSV which are more likely to be loaded into EVs.

Objectives

1. Design and engineer VSV expressing microRNAs and validate their ability to knock down known and predicted targets.
2. Determine if microRNAs expressed from VSV are loaded into EVs.
3. Assess the synthetic lethality of infection with VSV expressing a microRNA capable of knocking down BRCA1 or 2 in combination with PARPi.

Chapter 2: Material and methods

2.1 Cell lines and tissue culture

All cell lines were previously purchased from the American Type Culture Collection (ATCC, Manassas, VA), except the ID8 and ID8 $p53^{-/-}$ cell lines (gift from Dr. Iain McNeish, Barts Cancer Institute, Queen Mary University of London, UK), T47D (gift from Dr. Christine Pratt, University of Ottawa, ON) and T-Rex™-293 cells were purchased from Invitrogen. Vero, MiaPaCa2, 293T, T-Rex™-293, 786-O, and U-2 OS cells were maintained in Dulbecco's minimal essential medium (DMEM; Corning) containing 10% fetal bovine serum (FBS; Hyclone). T-Rex™-293 cells were also maintained in 5 ug/mL blasticidin and 300 ug/mL zeocin (Thermo Fisher Scientific) to preserve inducible expression of VSV G protein. SKOV3, 4T1, ZR-75 and MDA-MD-231 cells were maintained in RPMI-1640 medium containing 10% FBS. ID8 and ID8 $p53^{-/-}$ were maintained in DMEM supplemented with 5% FBS and ITS (5 µg/mL insulin, 5 µg/mL transferrin, and 5 ng/mL sodium selenite; Gibco). T47D cells were maintained in RPMI-1640 medium supplemented with 10% FBS and 5 µg/mL insulin (Insulin human recombinant; Thermo Fisher Scientific). All cell lines were cultured under 5% CO_2 at 37°C and were routinely tested for mycoplasma contamination using the e-Myco VALiD Myco PCR detection kit (FroggaBio). All cell lines have tested negative for mycoplasma contamination prior to their use the experiments described here.

2.2 VSV cloning and rescues

To insert miRNA sequences into the VSV backbone, single stranded oligonucleotides for each miRNA were designed with flanking XhoI and NheI restriction enzyme cut sites and ordered from

IDT (Integrated DNA Technologies). Single stranded oligos were annealed by reconstituting each to a final concentration of 0.5 µg/µL in nuclease free H_2O and combining 20 µL sense strand, 20 µL antisense strand with 10 µL (5X) annealing buffer (500mM potassium acetate, 150mM HEPES-KOH pH 7.4, and 10mM magnesium acetate; Fisher Scientific). This mixture was then placed in a thermocycler at 95°C for 5 minutes, 80°C for 10 minutes, and ramped down to 4°C (-0.5°C every 2.5 minutes). Single and double miR-182 hairpins were ordered from Genscript in the pUC57 plasmid vector with flanking XhoI and NheI restriction enzyme cut sites. All miRNA insert sequences may be found in Supplementary **Table 1**. VSVΔ51-GFP vector (containing GFP between G and L) was digested using XhoI and NheI restriction enzymes to remove GFP (New England Biolabs) and gel extracted (Takara NucleoSpin Gel Extraction and PCR Clean Up Kit). Each miRNA was ligated into the VSVΔ51 backbone (with the full G sequence or an interrupted G version) by combining 50 µg vector with 50 µg annealed miRNA and ligating for 10 minutes at room temperature (Thermo Scientific Rapid DNA Ligation Kit). Constructs were then transformed into NEB10 competent *E. coli* (New England Biolabs) following the manufacturer's protocol and plated on LB plates (with 100 µg/mL ampicillin) and allowed to grow ~24 hours at 30°C. Single colonies were picked and grown overnight at 30°C in LB broth (with 100 µg/mL ampicillin) and plasmid DNA was isolated (Bio Basics Inc EZ-10 Spin Column Plasmid DNA Minipreps Kit).

VSVΔ51 rescue and propagation protocols have been previously described[179]. Briefly, 293T cells (~1E6 cells per well) were plated in 6 wells, incubated overnight and infected with Vaccinia virus expressing the T7 promotor for 1.5 hours at a multiplicity of infection (MOI) of 0.5 in 0.5 mL serum free DMEM per well at 37°C. After removing the inoculum, cells were transfected with a

mixture of T7 RNA polymerase-driven expression plasmids containing essential VSV genes N (1 µg), P (1.25 µg), and L (0.25 µg) and 2-3 µg of the recombinant VSVΔ51 backbone to be rescued in 500 µL Opti-MEM media with 2 µL Lipofectamine 2000 (Thermo Fisher Scientific) per well and incubated at 37°C for at least 4 hours (or overnight). Wells were topped up with 1.5 mL DMEM (containing 10% FBS) and after 48 hours transfection supernatants were transferred to vero cells in 6-well plates for 24 hours. Supernatants were spun down at 500 xg to remove cell debris and filtered using 0.22 µM (Millex-GV, low binding filters; Millipore Sigma) syringe filter onto fresh vero cells in 6-wells. After 24 hours incubation (or until sufficient cytopathic effect was evident) at 37°C, cell debris was removed similarly to the previous step and rescued viruses were aliquoted and stored at -80°C. G-less versions of each virus were rescued using a similar protocol with the following exceptions: all steps were completed using T-Rex™-293 (VSV G expression was induced prior to each step using 1 µg/mL doxycycline (Sigma-Aldrich)), supernatants were filtered a second time after 24 to 48 hours and transferred to new cells, and the final rescue often required an additional 24 to 48 hours on freshly plated cells requiring an additional supernatant transfer (this final step is variable depending on the virus being rescued).

2.3 VSV purification

Vero cells were seeded in roller bottles (1900cm^3 TC treated roller bottles; Ultident) at 4E7 cells per bottle (for 3 days) or 8E7 cells per bottle (for two days incubation) in 220 mL DMEM (supplemented with 10% FBS and 25mM HEPES) and incubated at 37°C without CO_2 in a rotating incubator. Cells were infected at MOI 0.05 for approximately 36 hours (until significant cytopathic effect was evident and ~50% cell detachment). Cell supernatants were pre-cleared by

centrifugation at 1500 rpm for 10 minutes at 4°C (Beckman Coulter, Allegra X-14R benchtop centrifuge). Supernatant was carefully decanted onto 0.45 µM bottle top filters (500mL PVDF filter system; EMD Millipore) followed by 0.22 µM bottle top filter (500mL Stericup polyethersulfone (PES) filter system; EMD Millipore). Virus was pelleted by centrifugation at 13, 500 rpm for 1.5 hours at 4°C (JLA 16.250 rotor; Beckman Coulter Avanti JE centrifuge). Media was removed by aspiration and pellets were pooled (if necessary) in cold PBS and centrifuged at 13, 500 rpm for 1.5 hours at 4°C (JA 25.5 rotor; Beckman Coulter Avanti JE centrifuge). Supernatant was removed by aspirating and virus pellets were resuspended in 500 to 750 µL in cold 'Solution C' (0.15M NaCl, 10mM EDTA, 50mM Tris-HCl pH 7.4). Viruses were passed through a syringe multiple times to homogenize the viral particles using needles starting at ~22 gauge up to 30 gauge. Virus stocks were aliquoted for single use and stored at -80°C.

2.4 Titer by plaque assay

Viral titers were determined by serial dilution plaque assays. Vero cells (6E5 cells per well) were plated in 6-well plates and incubated overnight at 37°C. A 10-fold serial dilution for each virus was completed either in 1.5 mL microfuge tubes or deep-well plates by adding virus stock to serum free DMEM in a total volume of 1 mL per dilution. Dilutions 10^{-3} to 10^{-10} were typically added to each well in 500 uL after removing media from each well. After 45 minutes incubation at 37°C (with rocking every 15 minutes), inoculum was removed by aspirating and replaced with a 1:1 mixture of 6% Carboxymethyl cellulose (CMC; Sigma) : DMEM (2X concentrated with 20% FBS) overlay. After 48 hours incubation at 37°C, overlay was removed, monolayer was washed gently with PBS and plates were stained with crystal violet (0.1% crystal violet in 80% MeOH in

H_2O) for approximately 20 minutes followed by two washes with PBS and left to dry overnight. Similar to the viral rescue protocol, G-less versions of each virus were titered using T-Rex™-293 cells treated with 1 µg/mL doxycycline prior to infection for inducible expression of VSV G (replenished after 24 hours). Viral titers were calculated using the following equation using plaque counts from wells containing 10 to 100 plaques:

$$\text{pfu/mL} = \frac{\#\ \text{plaques}}{\text{dilution factor} \times \text{volume (mL)}}$$

2.5 PCR (polymerase chain reaction)

The pri-miR-150 sequence was amplified via PCR from the Addgene plasmid pcDNA3.2/V5 hsa-mir-150 (Addgene plasmid # 26310) following the Phusion DNA polymerase master mix protocol (Phusion High-Fidelity DNA Polymerase; New England Biolabs) with 10 ng of plasmid DNA and 10 uM of forward and reverse primers. XhoI and NheI cut sites for cloning into the VSVΔ51 backbone were added during this amplification step (primers listed in Supplementary **Table 2**). PCR products were amplified using the Bio-Rad T100™ Thermal Cycler using the recommended settings for Phusion master mix.

2.6 RNA extraction and Quantitative Real Time PCR

Total RNA was extracted from cells and EVs using NucleoZOL reagent (Macherey-Nagel). Cells were lysed and homogenized in NucleoZOL reagent and RNA was isolated following the manufacturer's protocol. RNA pellets were resuspended in 20 µL nuclease free water and RNA

concentration was determined using NanoDrop™ One Microvolume UV-Vis Spectrophotometer (Thermo Fisher Scientific). RNA was converted to cDNA using iScript™ cDNA Synthesis Kit (Bio-Rad) for knockdown studies using 1 µg of RNA, SuperScript™ VILO™ cDNA Synthesis Kit (Invitrogen) for pre-miRNA amplification experiments and TaqMan™ MicroRNA Reverse Transcription Kit (Thermo Fisher Scientific) for mature miRNA amplification using 20 ng of RNA. Primers for knockdown studies are listed in Supplementary **Table 2** and probes for pre-miRNA/mature miRNA were ordered as pre-designed probes for each miRNA (Applied Biosystems™ TaqMan™ MicroRNA Assay for mature miRNAs and TaqMan® Gene Expression Assays for pre-miRNAs). A schematic depiction of mature miRNA quantification using the TaqMan system is shown below, highlighting the requirement for a fully processed single-stranded product due to the use of a stem-loop primer during Step 1 – reverse transcription (**Figure 2.1**) Gene knockdown samples were amplified using QuantiTect SYBR Green PCR Kit (Qiagen) and miRNA samples were amplified using Applied Biosystems™ TaqMan™ Fast Advanced Master Mix (Fisher Scientific) following the recommended protocols. All samples were analyzed using the Applied Biosystems™ 7500 Fast Real-Time PCR System and qPCR measurements were normalized to 18S or Rplp0 genes for knockdown experiments and Let-7a for miRNA expression experiments. Relative expression was determined using the delta delta Ct [2^-(ΔΔCt)] equation.

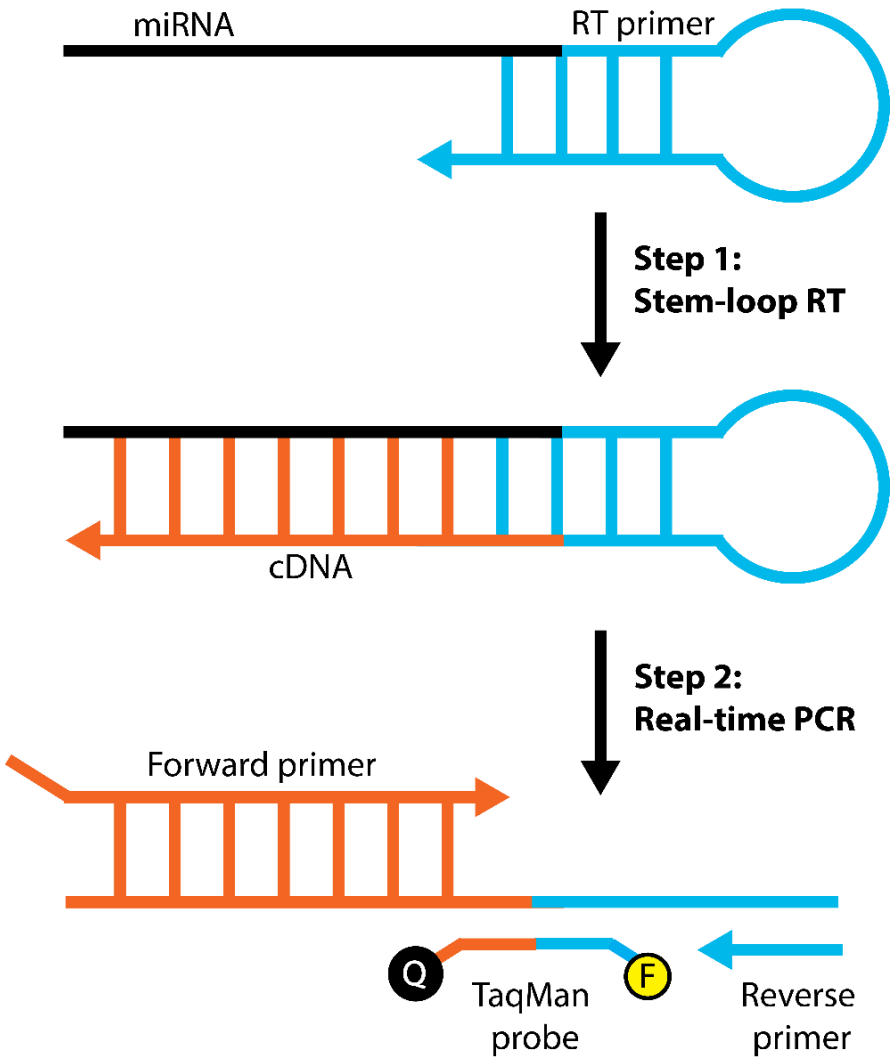

Figure 2.1 Schematic representation of TaqMan miRNA assay for mature miRNA detection. In Step 1, stem-loop primers bind the 3' end of the miRNA molecules (specific stem-loop primers are required for each individual miRNA) and miRNA molecules are reverse transcribed via reverse transcriptase to cDNA. In Step 2, the RT product is quantified by TaqMan PCR using a miRNA-specific forward primer, a reverse primer which binds the stem-loop sequence and fluorescent dye-labelled TaqMan probes. RT = reverse transcription; cDNA = complementary DNA; Q = quencher; F = fluorescent dye. (Adapted from Chen *et al.* 2005[213])

2.7 Western blot analysis

Cells were lysed for 10 minutes on ice using RIPA lysis buffer (Pierce™ Ripa Buffer; Thermo Scientific) with protease/phosphatase inhibitor cocktail (Thermo Fisher Scientific). Whole cell lysates were centrifuged at 13, 000 rpm for 15 minutes at 4^{o}C to remove cell debris and stored at -20^{o}C until time of use. Protein concentrations were determined using BCA protein assay kit (Pierce™ BCA® Protein Assay; Thermo Scientific) and an equal quantity of protein was prepared for each gel (20 – 30 µg per sample) with loading dye (5x Laemmli loading buffer; Bio-Rad) and boiled for 5 minutes at 100^{o}C. Proteins were loaded onto 4-12% gradient Bis-Tris gels (NuPAGE; Thermo Fisher Scientific) and run for approximately 1.5 hours at 100 volts in 1X MOPS running buffer (20X running buffer; 50 mM MOPS, 50 mM Tris Base, 0.1% SDS, 1 mM EDTA, pH 7.7), followed by transfer to nitrocellulose membrane for 1.5 hours at 100 mA (transfer buffer; 25 mM Tris, 192 mM glycine, 20% methanol). Membranes were Ponceau stained (Millipore Sigma) prior to blocking in 5% milk (in TBS-T) (Thermo Fisher skim milk power; 50 mM Tris-Cl pH 7.5, 150 mM NaCl, 1% Tween-20) for 30 minutes at room temperature. Membranes were incubated with primary antibodies overnight at 4^{o}C with gentle rocking diluted in 5% milk (in TBS-T). Primary antibodies were applied at the following concentrations: BRCA1 (abcam ab191042; 1:500), BRCA2 (abcam ab27976; 1:500), Chk2 (abcam ab109413; 1:1000), vinculin (Cell Signaling 4650S; 1:1000), and beta-tubulin (Cell Signaling 4970L; 1:1000). After removing primary antibodies, membranes were washed three times with TBS-T (5 minutes each) and secondary antibodies were added in 1:3000 dilutions in 5% milk (in TBS-T) for 1 hour at room temperature with gentle rocking (goat anti-mouse IgG antibody HRP catalogue #G-21040 and goat anti-rabbit IgG antibody HRP catalogue #31490; Thermo Fisher Scientific). Membranes were washed three times in TBS-T

(5 minutes each) and imaged following incubation with ECL substrate (Clarity™ Western ECL Substrate; Bio-Rad). Membranes were exposed using X-ray film exposure and development (quantified using ImageJ software) or Bio-Rad ChemiDoc imaging system (quantified using Bio-Rad Image Lab software). (Chemicals used in the buffers listed above were purchased from Fisher Scientific)

2.8 Colony forming assays

Cells were transfected with BRCA1, BRCA2 or control non-targeting siRNA by reverse transfection by combining 20 nM siRNA in 250 µL Opti-MEM medium (Opti-MEM™ Reduced Serum Medium, GlutaMAX™ Supplement; Thermo Fisher Scientific) with 250 µL Opti-MEM medium containing 5 µL Lipofectamine™ RNAiMAX Transfection Reagent (Thermo Fisher Scientific). RNAi complexes were added to each well and 5E5 cells per well were added in a volume of 1.5 mL in RPMI-1640 medium (supplemented with 10% FBS). Cells were incubated for 24 hours at 37°C, then counted and re-plated at equal cell densities for colony formation on 12-well plates in RPMI-1640 media (supplemented with 10% FBS) containing 5 µM of each PARPi (rucaparib AG014699, olaparib AZD2281; SelleckChem) or DMSO control (Dimethyl Sulfoxide; Sigma). 4T1 and ZR-75 cells were seeded at 500 cells per well and grown for 7-10 days and 14-16 days respectively. Cell media was changed (with fresh PARPi added) weekly. Once visible colonies containing at least 50 cells were present, wells were washed gently with PBS and stained with crystal violet (0.5% crystal violet in 80% MeOH in H_2O) for approximately 30 minutes followed by two washes with PBS and left to dry overnight. Colonies were imaged using ArrayScan VTI HCS (Thermo Fisher Scientific) and counted using ImageJ software. (See **Appendix A1** for full counting script developed for ImageJ)

2.9 Spheroid models

Cells were plated at 1E4 cells per well in U-bottom cell- repellent plates (CELLSTAR, cell-repellent 96-well; greiner bio-one) in RPMI (supplemented with 5% FBS, 0.12% methyl cellulose – filtered with 0.22 µM syringe filter). Spheroids were incubated without disruption for 48 hours at 37^{o}C prior to treatment. All treatments were added in a volume of 10µL (in RPMI) including control wells (10µL DMSO or media alone). MDA-MB-231 cells were plated in cold media with 2.5% Matrigel (Corning® Matrigel® Growth Factor Reduced (GFR) Basement Membrane Matrix) and centrifuged at 1000 xg for 5 mins at 4^{o}C before incubating. 4T1 Spheroids were infected at MOI 1 with each virus and MDA-MB-231 spheroids were infected at MOI 0.05, after 24 hours infection, 5 µM of each PARPi was added (rucaparib AG014699, olaparib AZD2281; SelleckChem) or DMSO control (Sigma). PARPi was replenished every two days for the duration of each experiment. Cells were imaged using the EVOS cell imaging system (Thermo Fisher Scientific) at 5X magnification and diameters were calculated using ImageJ software (relative diameter based on scale bar) and/or evaluated by alamar blue viability assay.

2.10 Cell viability assay (alamar blue and crystal violet)

Cell viability (metabolism) was assessed using the Alamar blue assay with the REDOX indicator resazurin (Sigma Aldrich) according to manufacturer's protocol. Briefly, Resazurin (2.5 mM) was added in a 1:10 dilution, spheroids were incubated with resazurin for approximately 48 hours. Fluorescence was measured (excitation 530 nm, emission 590 nm) using the BioTek Synergy™ Mx Microplate Reader.

Cytotoxicity was assessed using a crystal violet assay. Media was removed from wells and cells were washed once with PBS, then 0.5% crystal violet (80% MeOH in water) was added to each well. Plates were incubated at room temperature on a shaker for 20 minutes, then crystal violet solution was removed, and fixed cells were washed three times with water. Plates were left to air dry overnight. Once dry, plates were scanned and were then subjected to crystal violet lift (with 100 µl of methanol per well for a 96 well plate). Plates were incubated at room temperature on a shaker for 45 minutes, then the OD570 was read using the Multiskan Ascent plate reader.

2.11 Immunofluorescence staining

Cells were grown on glass coverslips and infected for one hour in serum free DMEM/RPMI, inoculum was removed by aspiration and replaced with FBS containing media for up to 72 hours at the listed MOI for each experiment. Cells were washed twice with PBS containing 1 mM Mg and 0.5 mM Ca (PBS-CM) and fixed in 4% paraformaldehyde (PFA; Thermo Fisher Scientific) for 20 minutes at 4^{o}C, then quenched with 50 mM NH4Cl (in PBS) for 5 minutes at room temperature. Cells were permeabilized using 0.2% triton X-100 (Sigma Aldrich) for 4 min at room temperature, then washed twice with PBS-CM for 5 minutes each. Coverslips were blocked using 1% BSA (in PBS-CM) for 20 minutes at room temperature prior to applying primary antibodies in 1% BSA (in PBS-CM) for one hour at room temperature or overnight at 4^{o}C. Primary antibodies were used at the following concentrations: BRCA1 (abcam catalogue #ab191042; 1:250) and VSV-N (Kerafast catalogue #EB0009; 1:500). Coverslips were washed three times with 0.1% BSA (in PBS-CM) for 10 minutes each then incubated with secondary antibodies for 1 hour at room temperature before washing again with PBS-CM three times and once with PBS. Secondary antibodies were

used at the following concentrations: Donkey anti Mouse IgG Secondary Antibody Alexa Fluor 568 (Invitrogen catalogue #A10037; 1:1000) and Goat anti-Rabbit IgG (H+L) Highly Cross-Adsorbed Secondary Antibody Alexa Fluor 488 (Invitrogen catalogue #A-11034; 1:500). Coverslips were mounted using Invitrogen™ ProLong™ Gold Antifade Mountant with DAPI (Invitrogen) and allowed to dry overnight.

2.12 Extracellular vesicle (EV) purification

Small EVs (SEVs) were collected using differential centrifugation of conditioned media from infected cell monolayers. Cells (MiaPaCa2) were seeded on 15 cm tissue culture plates at approximately 3E6 cells per plate, after incubation for 3 days at 37^{o}C cells were infected at MOI 3 with G-less (non-spreading) VSVΔ51 expressing various miRNAs. Media was replaced after 2 hours incubation with DMEM supplemented with EV depleted FBS (prepared by ultracentrifugation at 120, 000xg at 4^{o}C overnight). Media containing EVs was collected after incubating 48 hours and cell debris was removed by centrifugation at 2000xg for 20 minutes at 4^{o}C (Beckman Coulter, Allegra X-14R centrifuge). Cells were harvested at this time for RNA extraction. Supernatants were then centrifuged at 12, 000xg for 45 minutes at 4^{o}C (Beckman Coulter Avanti JE centrifuge) and filtered through a 0.22 µM Whatman filter (Fisher Scientific). EVs were then pelleted by ultracentrifugation at 120, 000xg for 1.5 hours at 4^{o}C, media was carefully removed by aspiration, EVs were resuspended in 80 to 100 µL fresh PBS and stored at -80^{o}C. This protocol has been previously described and validated by our group (Wedge et al. Nature Cancer, under revisions). A summary of the SEV identification steps is shown below (**Figure 2.2**).

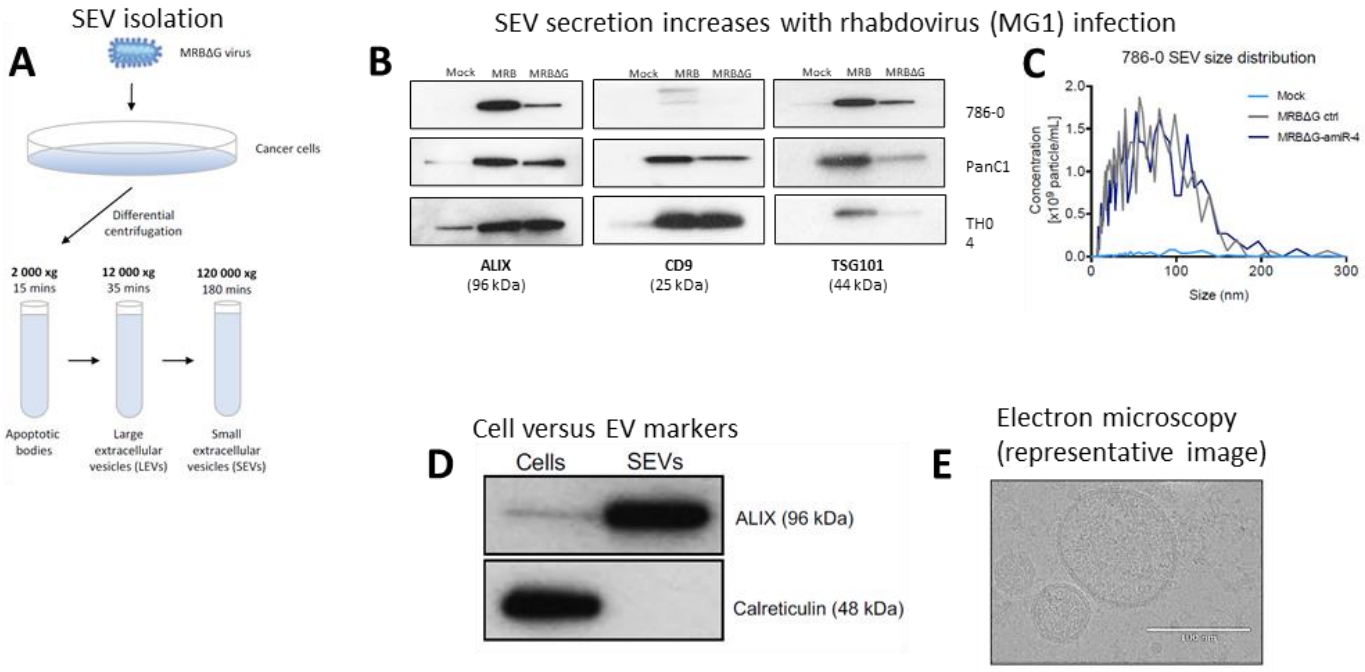

Figure 2.2 Small extracellular vesical isolation and identification. (A) Schematic depiction of the small extracellular vesical (SEV) isolation method using differential centrifugation. (B) Immunoblotting analysis of SEV markers (ALIX, CD9, and TSG101) demonstrates increased expression in multiple cell lines following rhabdovirus infection (MRB = Maraba virus) at MOI 1. (C) Nanoparticle tracking analysis (NTA) representing size distribution and quantification of SEVs isolated from uninfected (mock) or MRBΔG-infected 786-O cells at MOI 5 for 24 hours. (D) Immunoblotting analysis for ALIX (SEV marker) and calreticulin (cell-associated marker) in SEVs purified from Mel888 human melanoma cells and whole cell lysates infected with MRBΔG at MOI 1. (E) Representative electron microscopy image of SEVs collected from Mel888 cells infected with MRBΔG at MOI 1 (scale bar = 100nm). (This figure has been adapted from Wedge *et al.* Nature Cancer, under revisions)

2.13 Dual-Fluorescent reporter (LSB-mKate)

293T cells were plated in black-walled, clear-bottom 96-well tissue culture plates at 4E4 cells per well and incubated 24 hours at 37°C. Each well was transfected for 6 hours with 200 ng of each LSB-mKate plasmid (unless otherwise noted) and 0.5 µL of Lipofectamine 2000 (Thermo Fisher Scientific) in 50 µL Opti-MEM media (Opti-MEM™ Reduced Serum Medium, GlutaMAX™ Supplement; Thermo Fisher Scientific). Cells were infected at MOI 0.1 by adding virus in a volume of 50 µL DMEM to each well. Fluorescence was measured at multiple timepoints (mKate excitation 588 nm, emission 635 nm; EBFP2 excitation 383 nm, emission 448 nm) using the BioTek Synergy™ Mx Microplate Reader.

2.14 Animal studies and tumour models

All animal studies complied with ethical regulations and were approved by the Institutional Animal Care Committee of the University of Ottawa and carried out in accordance with guidelines of the National Institutes of Health and the Canadian Council on Animal Care. Animals were blindly randomized to treatment groups upon arrival. For the orthotopic 4T1 model, 2E5 cells were injected into the fat-pad of 6-week old female Balb/C mice (Charles River Laboratories) and tumours were treated starting on day 7 or 10 with 1E8 plaque forming units (PFUs) of VSVΔ51-miR-BRCA1 versus control VSVΔ51 or an equal volume of PBS on daily on days 7 – 11 or alternating days for a total of 6 injections. Combination groups received either 1 or 5 mg/kg rucaparib (AG014699; SelleckChem) in DMSO (diluted in 30% PEG with 2% Tween-80) or an equal volume of vehicle control. For the ID8 $p53^{-/-}$ intraperitoneal model 5E6 cells per animal were injected IP in 6-week old female C57BL/6 mice (Jackson Laboratory). To compare the survival

rates of mice treated with VSVΔ51 versus PBS (control), 3E8 PFUs were injected IP on days 7-9 and 14-16 (or an equivalent volume of PBS). Mice were euthanized at humane endpoint once severe ascites was present. For the flow cytometry experiment, MC38 cells were injected subcutaneously in 6-week old female C57BL/6 mice (Jackson Laboratory). After 14 days tumours were injected with 3E8 PFUs of VSVΔ51-miR-150 versus control VSVΔ51 or an equal volume of PBS once daily for 3 days. Six days after the last injection mice were sacrificed for tissue collection.

2.15 Flow cytometry analysis

Tumours and spleens were collected in RPMI-1640 media (without serum) and placed on ice. Spleens were placed in 6-well plates in RPMI-1640 (supplemented with 10% FBS and 1% penicillin/streptomycin) and dissociated using the back of a sterile syringe. Tumours were collected in Miltenyi Biotec Gentlemacs^{TM} C Tubes and dissociated using Miltenyi's Murine Tumour Dissociation kit (Miltenyi Biotec) following manufacturer's protocol for soft tumours and tumour infiltrating lymphocyte preservation. Tumour and spleen samples were filtered through a 70 µm sterile cell strainer (Fisher scientific) after diluting with 5 mL media to wash the cells from the tubes/plates. Cells were pelleted by centrifuging at 500xg for 5 minutes at 4^{o}C and media was removed. Red blood cells were lysed using 2 mL Ammonia Chloride Potassium (ACK)-lysis buffer (Thermo Fisher Scientific) for 5 minutes at room temperature, 5 mL PBS was added, and cells were pelleted by centrifuging at 500xg for 5 minutes at 4^{o}C. Media was carefully removed and splenocytes were resuspended in 4 mL RPMI (with 10% FBS) and tumour cells were resuspended in 1 mL RPMI (serum free). Cells were counted and approximately 1E6 splenocytes per well and 2E6 tumour cells per well were plated in V-bottom 96-well tissue culture plates

(Corning® 96-well Clear V-Bottom TC-treated Microplate). Cells were pelleted by by centrifuging at 500xg for 5 minutes, then washed using FACS buffer (0.5% BSA in PBS). Fc block (Mouse BD Fc Block™; BD Biosciences) was diluted 1:200 in FACS buffer and added in a volume of 50 µL to each well for 30 minutes (incubated at room temperature protected from light). Antibodies were prepared in FACs buffer (antibody information may be found in Supplementary **Table 3**) and 50 µL was added to each well in addition to fluorescence minus one controls (FMOs). Plates were incubated for 1 hour at 4°C (protected from light), followed by one wash with FACs buffer, one wash with PBS and fixing in 1% PFA (Sigma). Plates were stored at 4°C overnight. All samples were transferred to 1.1 mL tall microtubes (Thermo Scientific™ Microtubes for 1.1 mL Microtube System) prior to running on BD LSR Fortessa flow cytometer. Compensation beads (UltraComp eBeads™ Compensation Beads; Thermo Fisher Scientific) were prepared by adding 1 µL of each antibody to one drop of bead for single colour controls. Data was analyzed using FlowJo v10 (FlowJo, LLC, Ashland, OR) (gating strategy is outlined in supplemental **Figure S2.1**).

2.16 Statistical analysis

Statistical analyses were performed using GraphPad Prism 6.0 software (San Diego, CA). Unless otherwise indicated, data is presented as the mean of at least 3-5 technical replicates (and additional biological replicates where noted). Error bars represent the standard error of the mean. Statistical significance was evaluated using unpaired two-tailed Student's t-test unless otherwise noted and *P*-values less than 0.05 were deemed significant.

Chapter 3: VSVΔ51 expressing artificial microRNAs targeting BRCA1/2 fail to establish sensitization of resistant cancer cells to PARP inhibitor therapy

3.1 Introduction

Patients with BRCA1/2 mutated breast and ovarian cancers need more options

Breast cancer is the most common type of cancer impacting women in Canada (excluding non-melanoma skin cancer)[214]. Ovarian cancer remains the deadliest form of gynecological cancer worldwide and the 5th leading cause of cancer death among women in Ontario[215,216]. A common attribute among inherited forms of these two cancer types is germline mutation in either *BRCA1* or *BRCA2*. The treatment of hereditary breast and ovarian cancers (HBOCs) tends to be difficult as many *BRCA* mutated breast cancers are resistant to conventional hormone therapeutics (specifically *BRCA1*) and ovarian cancer cases tend to present in the late stages of disease[217,218].

To date, the most effective risk-reduction strategies to prevent breast and ovarian cancers in BRCA1/2 mutation carriers is prophylactic mastectomy and salpingo-oophorectomy (removal of the ovaries and fallopian tubes)[219]. While there is some evidence supporting the use of chemoprevention in these groups including estrogen receptor modulators (tamoxifen and raloxifene) and aromatase inhibitors, there is a significant risk of side effects associated with these therapies[220]. Bilateral mastectomy can reduce the risk of breast cancer by at least 90% and salpingo-oophorectomy can reduce the risk ovarian cancer by 80-90%[221]. Due to the recent understanding that ovarian cancer often arises from the fallopian tube rather than the ovary

itself, salpingectomy (remove of fallopian tubes) alone is also under consideration. Current recommendations state that salpingo-oophorectomy should be offered to BRCA1/2 mutation carriers, usually after childbearing; however, tubal ligation and salpingectomy have been shown to reduce ovarian cancer risk in the general population by 30% and 42-77% respectively and are therefore considered feasible prevention strategies[222].

The usual course of treatment for HGSOC starts with surgical debulking, the goal being total resection at the macroscopic level. Unlike low-grade subtypes of ovarian cancer, nearly all patients will be offered adjuvant chemotherapy following surgical resection, regardless of a successful initial resection[223]. While an estimated 70% of patients with ovarian cancer initially respond to platinum-based chemotherapy, a staggering 80% or more eventually experience disease progression[215]. Currently, the 5 year survival rate for ovarian cancer in Canada is only 45%[224]. Overall, the 5-year survival of patients with ovarian cancer has remained nearly unchanged since an initial improvement with the introduction of platinum based therapy as standard of care in the 1980's[225]. Surgical intervention also remains the first line of treatment for breast cancer management, including those with pathogenic BRCA1/2 mutations; however, the extent of surgical intervention remains an area of debate[226]. Breast conserving surgery (BCS) is the preferred route for early stage disease in patients with sporadic breast cancer and while the risk of both ipsilateral and contralateral breast cancer in BRCA1/2 mutation carriers is higher than non-carriers multiple studies have shown that risk of recurrence is in fact higher with BCS there was no difference in overall survival[227]. Platinum based chemotherapy is generally offered in the adjuvant/neoadjuvant setting for advanced cases; poly(ADP-ribose) polymerase inhibitors (PARPi) are the preferred nonplatinum chemotherapy options in advanced/metastatic cases,

however, there is yet to be sufficient data gathered to recommend the use of PARPi for nonmetastatic disease[228].

MicroRNAs are naturally expressed from certain viruses

Virally encoded miRNAs play a complex role in viral infection by acting on both host and viral gene expression[229]. The functions of viral miRNAs range from regulation of the latent-lytic cycle (for certain viruses), encouraging viral replication by promoting host cell survival, and modulating the host immune system[230]. The first viral miRNAs were discovered in the Epstein-Barr virus (EBV), a γ-herpesvirus, in 2004[229]. EBV is now known to encode at least 44 viral miRNAs; more than 250 viral miRNAs have been identified overall with a majority being found within the herpesvirus family[231]. Shortly after the identification of miRNAs within the EBV genome other members of the γ-herpesvirus family in addition to α- and β-herpesviruses were shown to express viral miRNAs as well[231]. Virally expressed miRNAs have also been identified within the genomes of a number of other DNA viruses including human papillomavirus, hepatitis B virus, adenovirus and polyomavirus[231].

Viral miRNAs have also been implicated in virus-mediated tumorigenesis. For example, bovine leukemia virus (BLV) has been associated with B-cell tumorigenesis in in cattle. One group has successfully identified a cluster of miRNAs within the BLV genome containing BLV-miRNA-B4 which in fact shares common targets with miRNA-29, of which overexpression has been associated with B-cell neoplasms[232,233]. Kaposi's sarcoma-associated herpesvirus has also been implicated in the development of Kaposi's sarcoma via manipulation of the immune system to maintain viral latency, specifically the TGF-β pathway[234].

MicroRNAs have a history of pairing with oncolytic viruses

The relationship between OVs and miRNAs is well established, but not in the context we are exploring for the project described here. Rather, the OV field has taken advantage of miRNAs to gain control of viral infection to fine-tune the tropism of viruses toward specific tissues as a method of avoiding off-target toxicities. This strategy was initially used to prevent off-target infection of lentiviral based transgene delivery and has since been incorporated into many OV vectors[235,236]. By taking advantage of the unique miRNA expression landscape of tumour tissues compared to surrounding healthy tissues, miRNA recognition sequences for miRNAs primarily expressed in normal tissues have been incorporated into a number of OV genomes to control their replication by impairing the translation of important viral genes[237]. Importantly, this method can increase the therapeutic index of OVs by creating a specific "off switch" which only normal cells can access rather than traditional methods of viral attenuation which can lead to safer viruses, but often sacrifice potency[236]. This strategy has also been used to specifically inhibit the expression of potentially toxic transgenes in normal tissues.

A collection of microRNAs are selectively exported into extracellular vesicles (AKA - 'EV-miRNAs')

miRNAs are commonly transported from cell to cell within extracellular vesicles (EVs)[238]. The importance of extracellular miRNAs has recently come to light with extracellular miRNAs emerging as prognostic markers for diseases, such as cancer, in addition to their proven ability to modulate gene expression in recipient cells[239–241]. Multiple studies have also shown that the miRNA content found within EVs does not necessarily reflect cellular expression levels,

alternatively, specific miRNAs appear to be selectively shuttled into EVs[242,243]. While the exact mechanism by which EV miRNAs are selected and packaged into EVs is not known, a comparative study which combined data from multiple cell lines has shown that there is in fact a small group of miRNAs which are preferentially exported into EVs by comparing the ratio of expression in EVs versus cells[238]. The most notable miRNA present in EVs is miR-451, this study also demonstrated that miRNA loading into EVs could be enhanced via over-expression of the specific miRNA.

3.2 Rationale and hypothesis

Strategically designing artificial miRNAs for export into EVs using the miRNA-451a cassette

For the initial viral constructs described here, I have strategically utilized the hsa-miRNA-451a cassette to encourage packaging of therapeutic artificial miRNAs (amiRNAs) into EVs with the goal of eliciting a bystander effect toward uninfected cells. It is well understood that the mechanism of OV killing goes far beyond the basic cell lysis due to infection, it has been demonstrated that many cells within a tumour will in fact never be infected by the virus[167]. We must therefore rely on various secondary mechanisms to take down the entire tumour, including cells that remain clear of infection.

Several publications have reported miR-451 as one of the most common miRNAs present in EVs[238]. Moreover, RNA sequencing analysis performed previously by our group has demonstrated that the presence of miR-451 in EVs in fact increases following infection with VSV (**Figure 3.1**). Furthering our interest in miR-451 as the optimal cassette for our amiRNAs is the

non-canonical Dicer-independent processing of this miRNA[244]. The unique processing of miR-451 fulfills several characteristics that can potentially contribute to an ideal amiRNA delivery system. To begin, several studies have shown a global downregulation of miRNA expression in tumour cells compared to normal tissues leading to investigations into the function of miRNA processing machinery in tumour cells[245]. Indeed, the expression of the main miRNA processing proteins Drosha and Dicer1 are decreased in multiple cancer types including ovarian cancer, lung cancer and neuroblastoma. Low levels of both proteins have also been associated with advanced tumour stage and poor prognosis[246,247]. By selecting a miRNA that is capable of skipping one of the canonical steps of processing, we aim to broaden the scope of this therapy to tumours which may or may not have alterations in proteins of the miRNA processing pathway as commonly seen in tumour cells. The specific Ago2 processing step of miR-451 also means that miR-451 can avoid competition with other canonical miRNAs which may be processed by alternative Ago proteins, potentially preventing interference of natural miRNA expression when over-expressed. Additionally, Ago2 slicer activity performs differently from Dicer1 in that a star-strand or passenger-strand is not produced, reducing the potential for off-target effects[200,248]. Finally, while the previously mentioned study identifying miR-451 as the top exported miRNA across multiple cell lines did not necessarily separate the population of EVs to distinguish small versus large vesicles, more recent work as shown miR-451 is in fact enriched specifically in small EVs[249]. Evidently, this group has also demonstrated that amiRNAs designed by replacing the mature sequence of the miR-451 with an siRNA targeting a protein of interest are in fact loaded into EVs following transient expression from cells. The functionality of these amiRNAs has also been established[249].

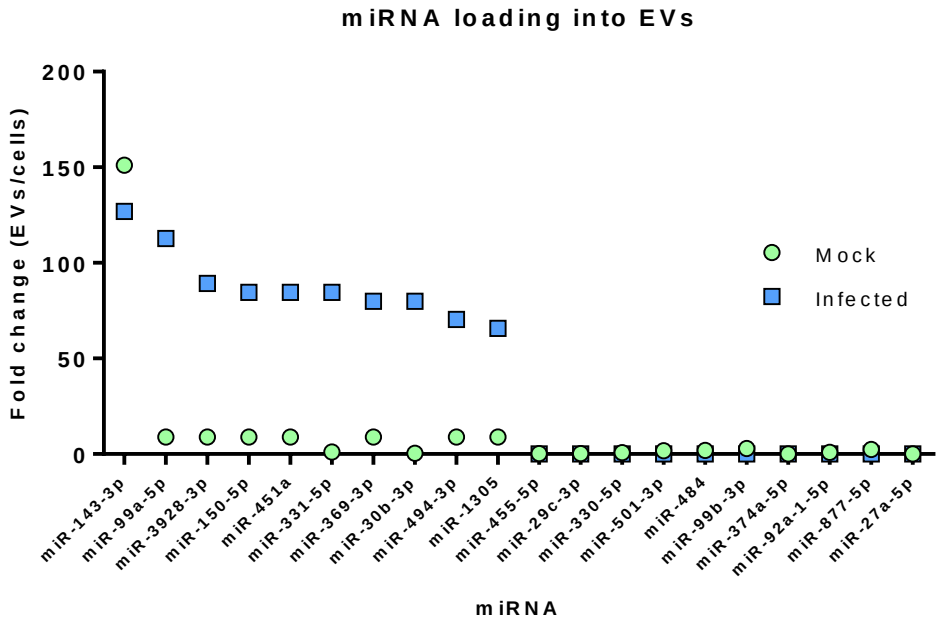

Figure 3.1 RNA sequencing data representing the top ten microRNAs enriched in EVs versus those retained in cells following infection with VSVΔ51 in MiaPaCa2 cells (completed by Marie-Ève Wedge and Adrian Pelin). Cells were infected at MOI 1 for 48 hours and small EVs were purified by ultracentrifugation.

Artificial microRNAs can be expressed from an RNA virus

The expression of miRNAs from RNA viruses has naturally been an area of uncertainty for several reasons. RNA viruses generally replicate in the cytoplasm of the host cell meaning that they may not have access to the required miRNA processing proteins which are primarily housed within the nucleus, processing of the pre-miRNA from the primary transcript could result in damage to the viral genome itself, and finally the virally encoded miRNA may target the viral genome as well[231]. Despite these potential roadblocks, a small collection of miRNAs have been identified from the genomes of RNA viruses (summarized in [250,251]). Expectedly, a majority of naturally occurring viral miRNAs expressed from RNA viruses have been documented in retroviruses, likely due to their inherent access to miRNA processing machinery during replication in the nucleus[251]. However, a majority of RNA viruses including VSV replicate in the cytoplasm, thus multiple groups sought to investigate miRNA processing from cytoplasmic RNA viruses and have since proven that functional miRNAs can be expressed from these viruses through non-canonical processing that can take place outside the nucleus[252,253].

To investigate the processing of miRNAs from cytoplasmic RNA viruses, pri-miR-124 was inserted into the Sindbis virus genome where it was shown to undergo full processing yielding a functional mature miR-124 without hindering replication of the virus[254]. By demonstrating a compromised cellular response to viral infection after deletion of Drosha, tenOever *et al*. elucidated that infection with several RNA viruses leads to the export of Drosha into the cytoplasm serving as an antiviral response agent against the RNA based genome. Moreover, this group has demonstrated the ability to express artificial miRNAs from influenza virus A using the pri-miRNA-124 cassette[255].

Hypothesis

Infection with engineered oncolytic viruses encoding artificial miRNAs targeting BRCA1 and/or BRCA2 will sensitize resistant breast and ovarian cancer cells to PARP inhibitor therapy via EV delivery of miRNAs.

3.3 Results

Engineering unique OVs to express BRCA1/2 targeting artificial miRNAs within the hsa-miRNA-451a cassette

Artificial miRNA sequences to target BRCA1 and 2 were selected based on commercially available siRNA target sites. To streamline future experiments and easily compare viruses, I elected to select miRNA sequences for each gene that were complementary to both the human and mouse reference mRNA sequences. A BRCA1 targeting sequence which was previously validated against human BRCA1 was selected as it shared perfect complementarity with the mouse sequence as well. Two different BRCA2 sequences were tested prior to cloning into VSV as there was not one commercially tested sequence which perfectly matched both species; however, it was predicted that either would knockdown BRCA2 based on the notion that the seed sequence, nucleotides 2-8, is the most crucial for successful mRNA recognition and knockdown and this requirement was met by both[256,257]. Validation of knockdown using each sequence was completed via siRNA transfection in the following cell lines: 293T (transfection control, human embryonic kidney), U2OS (human osteosarcoma), and 4T1 (mouse breast cancer). qPCR analysis on these cell lines revealed that the siBRCA1 sequence was a suitable candidate for viral targeting

in addition to the siBRCA2a sequence given that these siRNA sequences can produce a > 50% knockdown of BRCA1 and BRCA2 mRNA in all cell lines tested (**Figure 3.2**). Western blot analysis revealed that knockdown of the BRCA2 protein would require either an increased concentration of the siRNA or a second dose. Indeed, successful knockdown could be achieved following the application of a second siRNA treatment. The results of the western blot confirmed siBRCA1 knockdown and superior targeting of siBRCA2a over siBRCA2b (**Figure 3.3**); therefore, the BRCA2a sequence was used to engineer the BRCA2-targeting VSV construct.

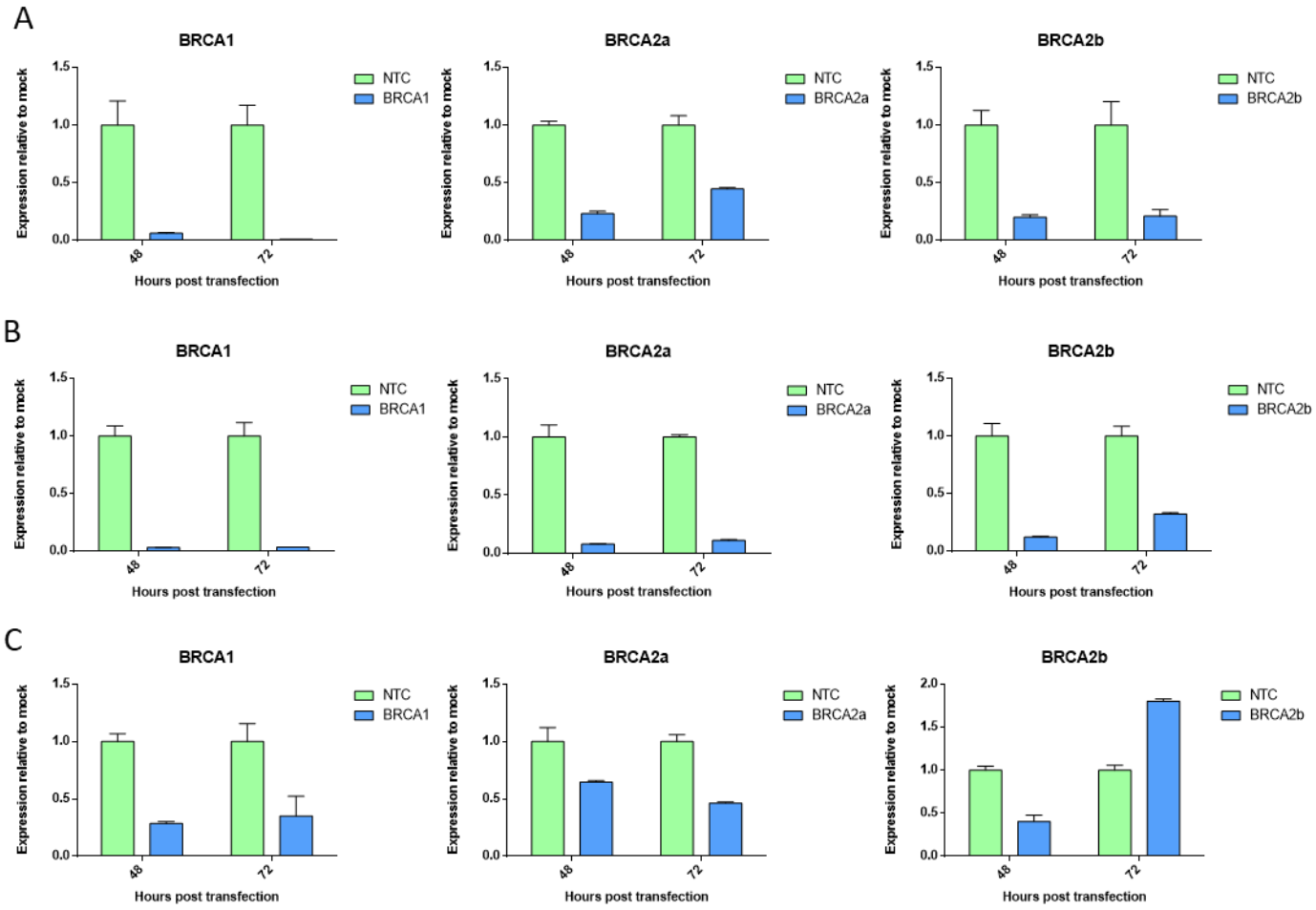

Figure 3.2 Selection and validation of siBRCA sequences demonstrated by qPCR analysis in (A) 293T (human), (B) U-2 OS (human), and (C) 4T1 (mouse) cell lines. Relative expression has been analyzed via the ΔΔCt method, normalizing each sample to an endogenous control gene (hRplpO for human cell lines and 18s for mouse cell lines). Error bars represent standard error of mean (n=1, 3 technical replicates).

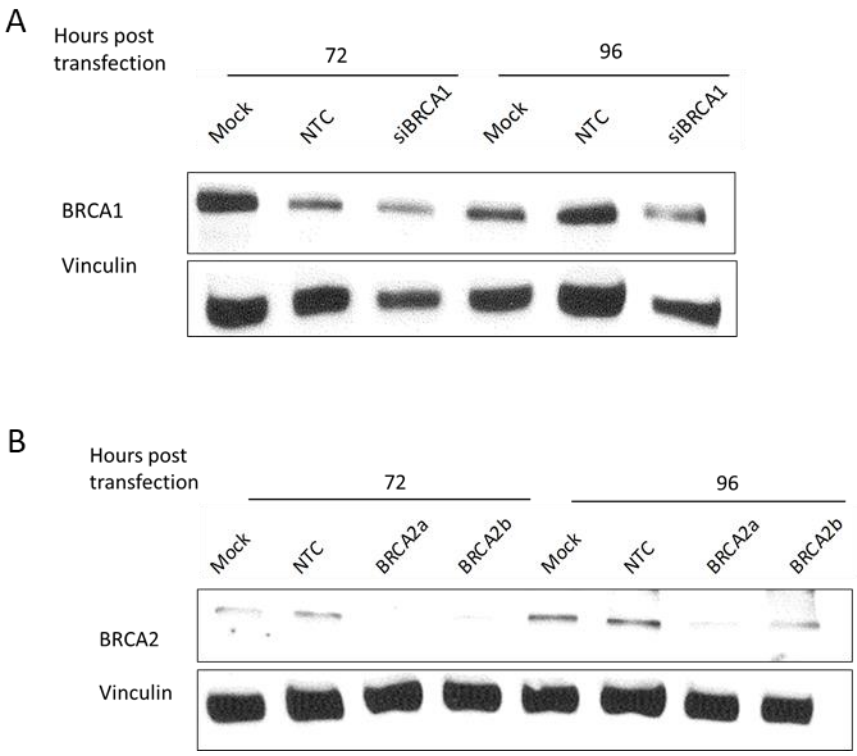

Figure 3.3 Selection and validation of siBRCA sequences demonstrated by western blot analysis. Transfection with either (A) siBRCA1 or (B) siBRCA2 was carried out alongside a non-targeting control sequence (NTC) in U-2 OS cells. Cell lysates were collected at 72 and 96 hours post transfection. Vinculin was used as a loading control.

Following validation of siRNA knockdown, sequences targeting both BRCA1 and BRCA2 were cloned into the VSVΔ51 vector within a miR-451 cassette. miRNAs were generated by replacing the mature miRNA sequence (as annotated by miRNAbase.org) with selected siRNA sequences, single-stranded DNA oligos with restriction enzyme cut-sites at each end corresponding to sites within the VSVΔ51 backbone between the G and L genes were obtained (**Figure 3.4**). Oligos were annealed and ligated into the VSVΔ51 plasmid followed by transformation into competent *E. coli*. Each construct has been sequenced to confirm presence of the amiRNA of interest and viruses were rescued. The resulting viruses have been named VSVΔ51-451miR-BRCA1 and VSVΔ51-451miR-BRCA2.

To determine if these newly engineered OVs could knockdown BRCA1 and BRCA2, qPCR an analysis was completed following infection of both human and mouse BRCA wild-type breast cancer cell lines. Following 24 hours of infection at least 50% or more knockdown of each target transcript could be observed (**Figure 3.5 A+B**). Western blot also revealed a significant decrease in BRCA1 and 2 protein level (**Figure 3.5 C+D**).

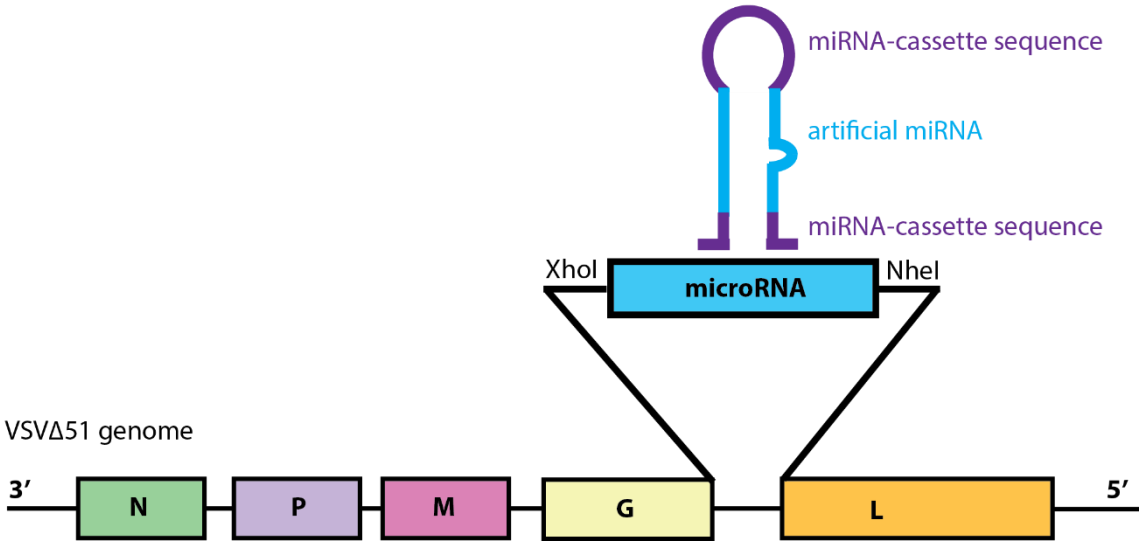

Figure 3.4 Schematic of miRNA expressing VSVΔ51 construct design.

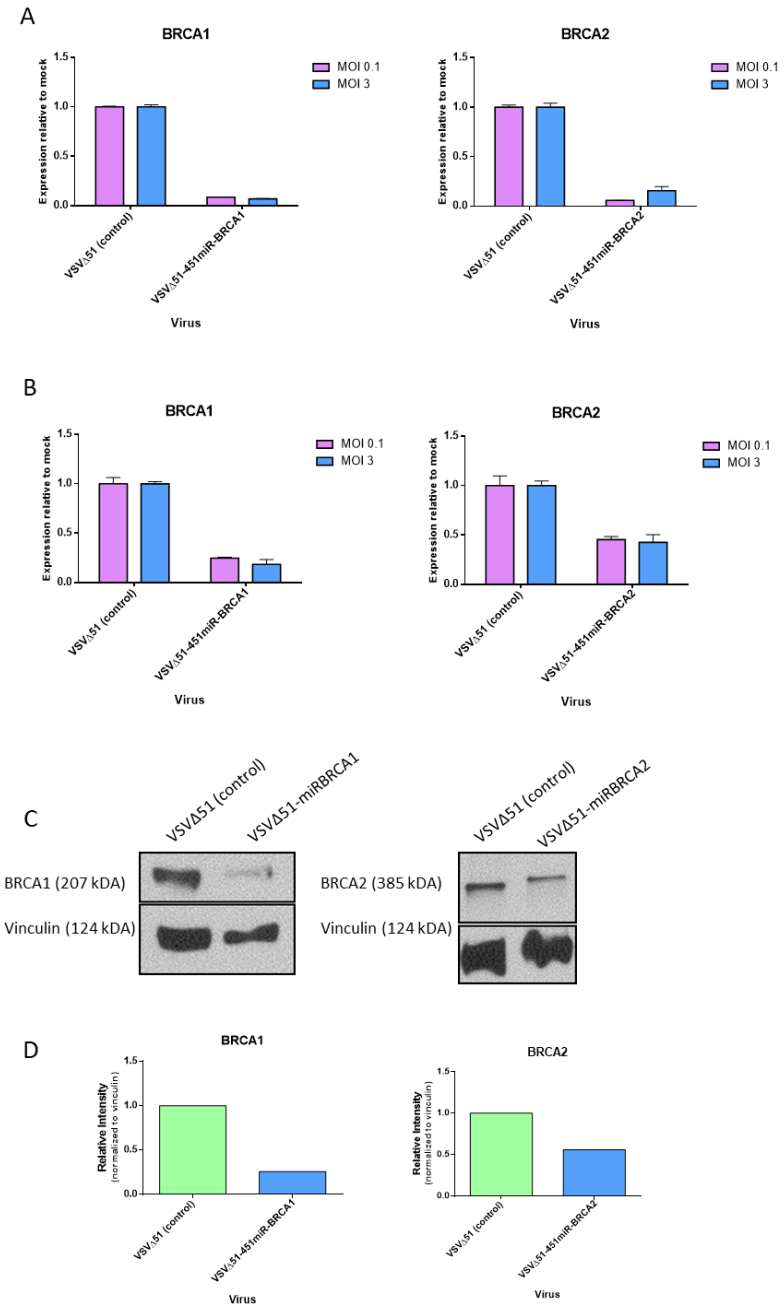

Figure 3.5 VSVΔ51-451miR-BRCA1/2 virus validation. Downregulation of BRCA1 and BRCA2 was evaluated by both qPCR of (A) T47D and (B) 4T1 cells and (C) Western blot analysis of T47D cells. Cells were infection for 24 hours at MOI 0.1 and 3 for RNA extraction and MOI 0.1 for western blot. qPCR results were analyzed using the ΔΔCt method, normalized to mock (uninfected) cells and 18s endogenous control gene. Error bars represent standard error of mean (n=1, 3 technical replicates). (D) Western blots were quantified using ImageJ software to determine relative expression.

siRNA knockdown of BRCA1 and/or 2 is synthetic lethal with PARPi treatment

To ensure the mRNA target sequence corresponding to each virus reduced the growth of both human and mouse cancer cell lines when combined with PARPi treatment an initial validation experiment was completed. To determine if there was a reduction in clonogenic capacity of cells following the combination therapy, transient transfections using siRNA (identical to the sequences that were cloned into each virus, targeting both mouse and human versions of *BRCA1/2*) were carried out in 6-well plates for 24 hours and 500-1000 cells (depending on cell line) were re-plated onto 12-well plates in media containing 5 µM PARPi (olaparib or rucaparib). Cells were incubated 1-3 weeks until colonies containing a minimum of 50 cells could be visualized under a light microscope, after which the media was removed, and colonies were stained with 0.5% (w/v) crystal violet in 20% methanol. Colony counts were determined via imaging by the Cellomics Array Scan followed by ImageJ software analysis (full counting protocol for ImageJ is in **Appendix A1**). A concentration of PARPi was selected based on previously reported values, in addition to my own initial screen of human and mouse cell lines which demonstrated via alamar blue and crystal violet metabolic activity and viability assays, respectably, that no decrease in viability was observed after 3 days with either olaparib or rucaparib at a concentration of 5 µM (**Figure 3.6**).

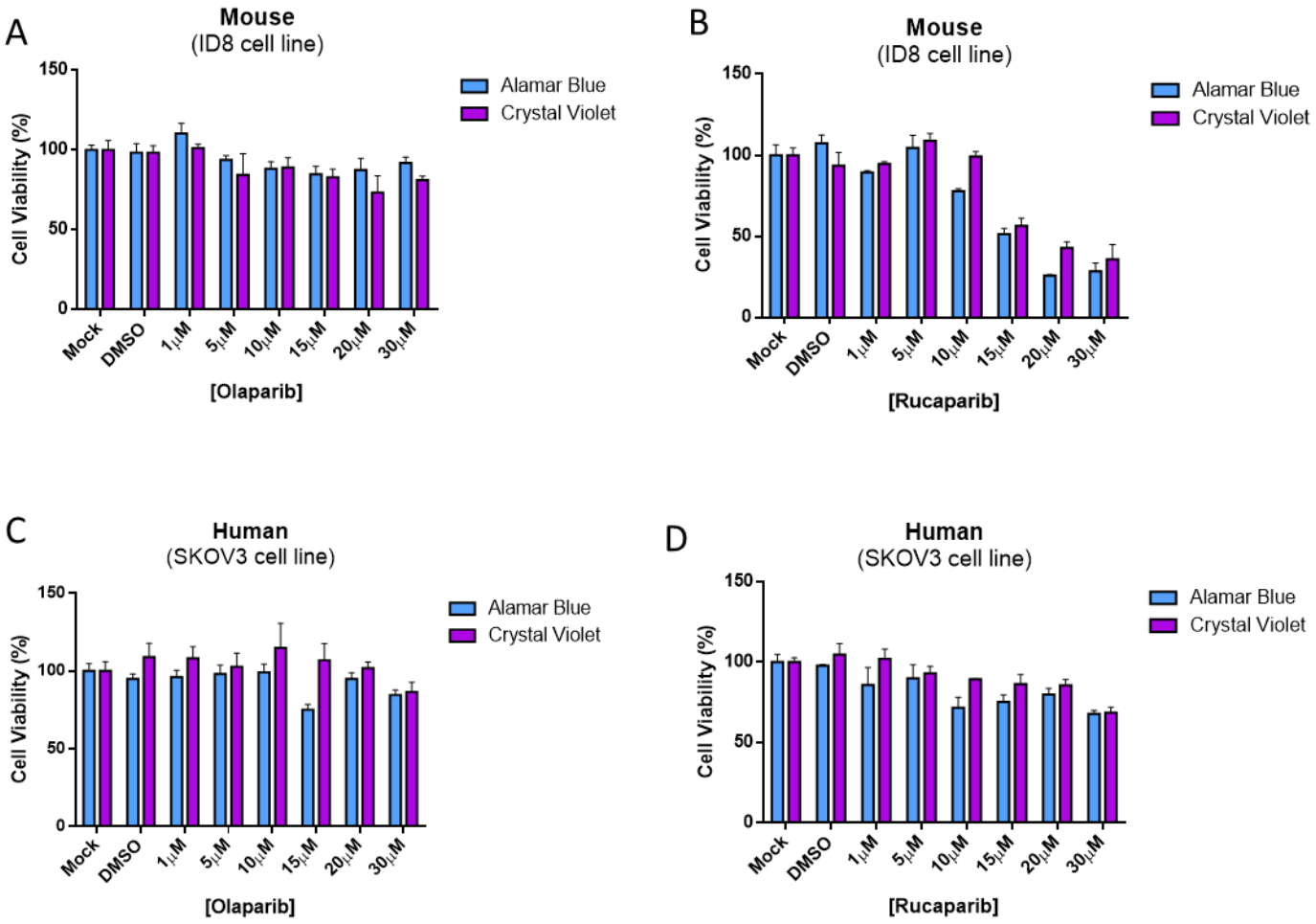

Figure 3.6 PARP inhibitor dose optimization. Each cell line was treated with varying concentrations of PARPi (listed above) and assessed by alamar blue and crystal violet assays at 72hrs post-treatment. The following cell lines were tested: (A) ID8 with olaparib (B) and rucaparib, and (C) SKOV3 with olaparib and (D) rucaparib. Error bars represent standard error of mean (n=1, 3 technical replicates).

Treatment with both PARPi agents reduced the surviving fraction of ZR-75 (human breast cancer) cells slightly, additionally BRCA1/2 knockdown alone resulted in a decrease of surviving fraction. Overall, a much larger reduction was observed when BRCA1/2 knockdown was combined with PARPi, reducing the surviving fraction of colonies to approximately 10 percent (**Figure 3.7 A**). This result confirms that sensitization to PARPi following BRCA1/2 depletion can occur using the miRNA sequence encoded into my recombinant VSV; however, a lower concentration of PARPi may be required depending on the cell line tested. The 4T1 (mouse breast cancer) cell line demonstrated more variability in terms of colony count (likely due to lower transfection efficiency) and interestingly appeared to be less sensitive to olaparib than rucaparib following BRCA1/2 knockdown; nonetheless, the combination of both BRCA1 and BRCA2 knockdown with rucaparib produced a substantial drop in the proportion of colony forming cells, with olaparib performing slightly less effectively (**Figure 3.7 B**).

A

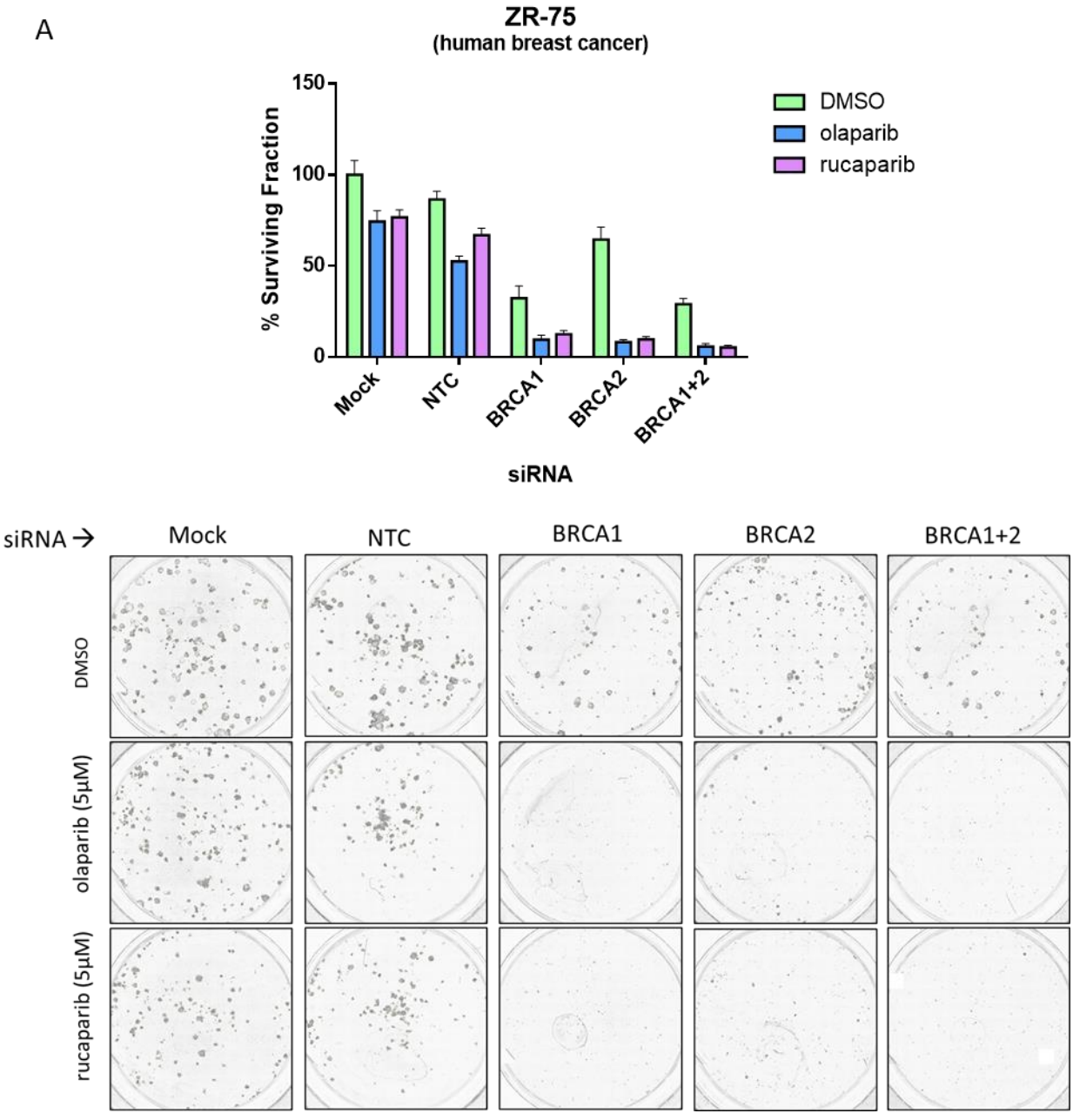
ZR-75
(human breast cancer)
% Surviving Fraction
150
100
50
0
DMSO
olaparib
rucaparib
Mock
NTC
BRCA1
BRCA2
BRCA1+2
siRNA
siRNA →
Mock
NTC
BRCA1
BRCA2
BRCA1+2
DMSO
olaparib (5μM)
rucaparib (5μM)

B

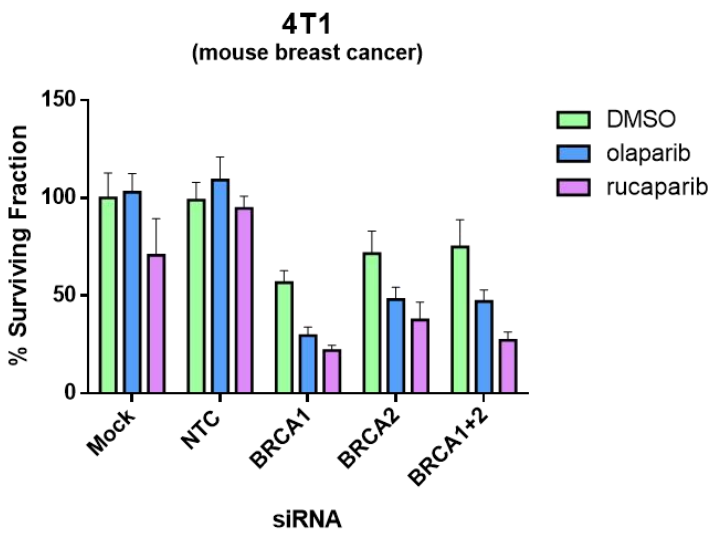

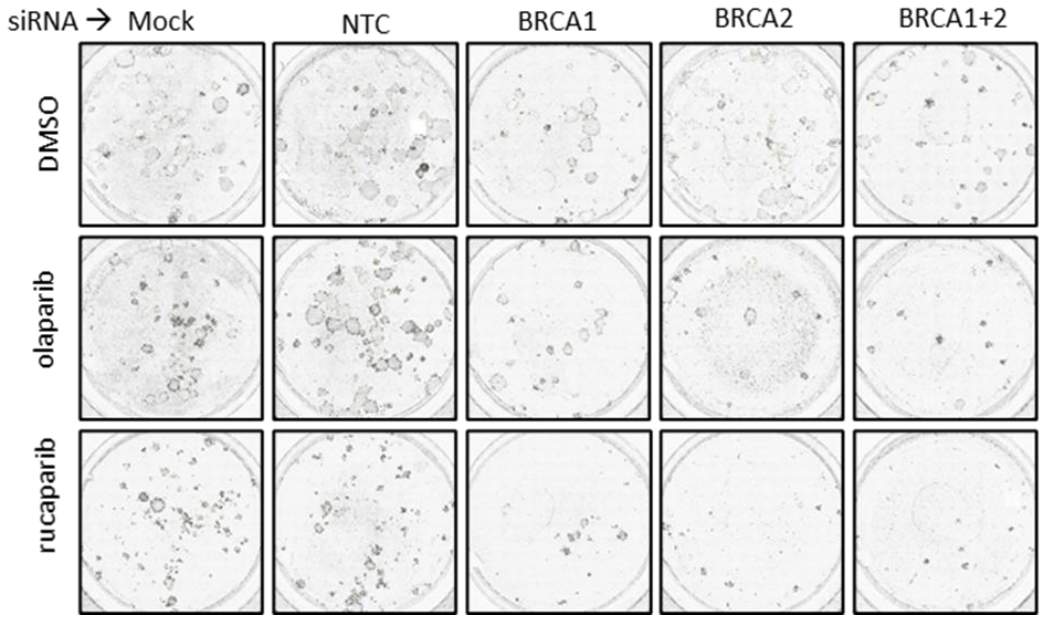

Figure 3.7 Colony formation assays demonstrate a significant decrease in the clonogenic capacity of breast cancer cells (human and mouse) following BRCA1 and/or 2 siRNA knock down and PARPi therapy. (A) ZR-75 and (B) 4T1 cells were transfected with siRNA targeting BRCA1/2 (or a non-targeting control siRNA; NTC), plated in PARPi-containing media after 24 hours and grown until colonies reached 50 cells or more. Colonies were stained with 0.5% crystal violet and imaged using Cellomics ArrayScan at 5X magnification (all images were processed and quantified using ImageJ software analysis). Percent surviving fraction has been calculated relative to DMSO treated control cells. Error bars represent standard error of mean (n=1, 6 technical replicates).

BRCA1/2 knockdown by VSV-amiRNA-BRCA1/2 is not sufficient to sensitize BRCA1/2 wildtype cancer cells to PARPi in vitro and in vivo

The 4T1 mouse breast carcinoma model was selected for an initial *in vivo* pilot experiment based on the criteria that this model is known to be quite resistant to OV treatment alone[165], the 4T1 cell line represents a triple-negative phenotype that is BRCA wild-type[258], these cells may also be grown sub-cutaneous or within the fat-pad in immunocompetent mice to allow for regular tumour volume monitoring. I have completed two *in vivo* experiments using the 4T1 model to date, both yielding similar results. I did not observe any significant differences in tumour burden or survival for the first experiment (**Figure S3.1**). Therefore, a few modifications to the treatment protocol were made including beginning treatment earlier (7 days post tumour implantation as opposed to 10) as well as intratumoural delivery of the virus (VSVΔ51-451miR-BRCA1) over a shorter period (five days as opposed to two weeks) combined with a higher concentration of rucaparib (5 mg/kg). The animals tolerated this treatment well with minor weight-loss during virus treatment, recovering within three days. Unfortunately, the tumours were quite aggressive and very little difference in survival was observed between groups (**Figure S3.2**).

Given the resistant nature of the 4T1 *in vivo* tumour model against VSV infection I opted to assess the impact of the combination therapy using a 3D spheroid model. By using spheroids, we could compare OV treatments over a longer period of time as opposed to 2D cultures. Prior to optimizing the growth of spheroids, I also attempted to carry out colony formation assays similar to those described in the above section. Unfortunately, after infection (regardless of using

a very low MOI) it was challenging to achieve a high enough number of colonies to make any reliable comparisons between treatments.

4T1 cells grown as spheroids were infected at an MOI of 1 for 24 hours, followed by treatment with olaparib or rucaparib at the previously tested dose of 5 μM. To assess the impact of the treatment, spheroid diameters were measured daily via microscopy. While the combination of olaparib and rucaparib with both viruses did produce spheroids of the smallest diameter over time (initial diameter measurements were all quite similar with no discernable outliers), there was a rather small decrease in diameter compared with viral infection alone (**Figure 3.8**). While these decreases are statistically significant technically, it is unclear what the biological significance of a ~25% loss of diameter would be. Furthermore, it was observed that the diameter of the spheroids did not increase over time, even in those that were not treated with either PARPi or virus. Thus, future experiments will aim to optimize the growth of these 3D cultures, potentially beginning treatment before they reach their maximum size to further reveal differences between treatments. These results combined with the lack of efficacy seen *in vivo* have led me to re-think these artificial miRNAs and rationally design new and improved versions of these viruses to enhance the combination effect with PARPi treatment as described below.

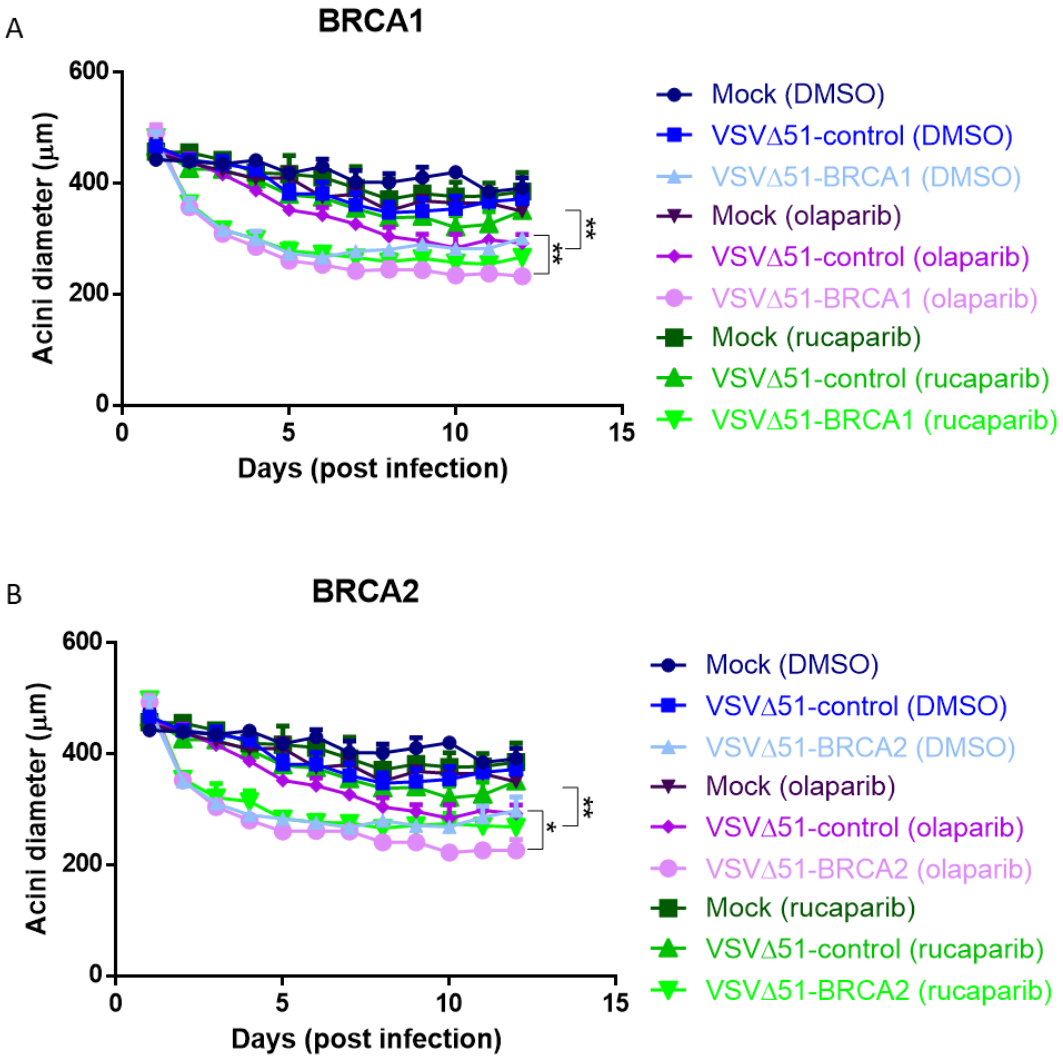

Figure 3.8 Infection of 3D spheroid cell cultures with VSVΔ51-451miR-BRCA1/2 leads to minor sensitization to PARPi treatment. (A) 4T1 cells were plated at 1E4 cells per well in greiner bio-one U-bottom CELLSTAR, cell-repellent surface plates and allowed to grow for 48 hours prior to treatment. All treatments were delivered in a 10 µL volume, including control wells (10µL DMSO or media alone). Cells were infected at MOI 1 and treated with 5 µM olaparib or rucaparib 24 hours later, PARPi were replenished every 2 days. (B) Spheroids were imaged using the EVOS microscope at 4X magnification and diameters have been determined using ImageJ software. Error bars represent standard error of mean (n=3 biological replicates). Unpaired two-tailed t-test was used to evaluate statistical significance (*P<0.05, **P<0.01). (Note: (A)** denotes significant difference between VSVΔ51-control with olaparib/rucaparib and VSVΔ51-BRCA1 with olaparib/rucaparib, (B)* denotes significant difference between VSVΔ51-control with olaparib and VSVΔ51-BRCA2 with olaparib, ** denotes significant difference between VSVΔ51-control with rucaparib and VSVΔ51-BRCA2 with rucaparib)

Re-thinking and re-designing artificial miRNAs to knockdown BRCA1

While functional validation of each virus was initially completed using qPCR and western blot to demonstrate a downregulation of BRCA1 or BRCA2 following infection, it was unfortunately difficult to replicate this western blot result in the originally tested cell line (T47D) as well as others. Similar challenges regarding the validation of miR-451 cassette encoding viruses have been encountered by others in our group (for viruses encoding miRNAs targeting a variety of other genes) with one successful example of an amiRNA which mediates PD-L1 expression. These issues combined with the lack of combinatorial effect with PARPi treatments have raised concerns regarding the unique processing pathway of miR-451a and encouraged us to re-evaluate the design of our miRNA encoding viruses. We have herein developed a new strategy to improve the design of amiRNAs within the miR-451 cassette. I have used data summarized in two publications by Lai *et al.* in which mutant constructs of miR-451 were systematically engineered to interrogate their accessibility for complete processing to their mature/functional form to re-design a BRCA1 targeting virus (**Figure S3.3**)[200,201].

Additionally, the previously mentioned RNA-sequencing experiment carried by our group demonstrated that a number of miRNAs become enriched in EVs produced by cancer cells following VSVΔ51 infection (Wedge and Pelin, unpublished data) (**Figure 3.1**). Selecting miRNAs which are highly enriched in EVs, I have designed single-stranded oligonucleotides containing identical targeting sequences for BRCA1 (same as the previously validated sequence) within the miR-143, miR-99a, miR-150 and miR-331 cassettes, in addition to the commonly used miR-30 cassette[259]. I elected to focus solely on BRCA1 as a target to easily compare these new viruses;

taking into consideration that knockdown of BRCA1 or BRCA2 alone can sensitize cells to PARPi treatment[260].

To mitigate concerns regarding the processing of our miRNAs I have also incorporated qPCR validation step using TaqMan technology to specifically probe for the mature form of each newly engineered amiRNA[213]. I have completed qPCR analysis to confirm expression and processing of each miRNA on the following cell lines: T47D, ZR-75, ID8 and E0771 (**Figure S3.4**). As discussed previously, it has been difficult to assess the functionality of these miR-BRCA1 expressing viruses via western blot in the cell lines tested. Therefore, I have completed qPCR to evaluate downregulation of BRCA1 mRNA in multiple cell lines (**Figure 3.9**) as well as immunofluorescent imaging to evaluate BRCA1 protein levels (**Figure 3.10**). Unfortunately, while there does appear to be varying levels of downregulation at the mRNA level, evident by qPCR, these results are not consistent with a decrease in BRCA1 at the protein level (addition timepoints shown in **Figures S3.5** and **S3.6**). The sub-optimal knockdown of BRCA1 could be due to a variety of reasons. As described previously, I chose to use validated siRNA target sequences which target early exons within BRCA1/2 for the design of each amiRNA using commercially available siRNA sequences. Under natural circumstances, a miRNA typically targets sequences within the 3'UTR an mRNA transcript[261]; of note, the successful example mentioned above of a PD-L1 targeting amiRNA designed by our group did in fact target the 3'UTR of the gene. Additionally, while it is difficult to predict exactly how many copies of a miRNA are necessary to knock down a target, the expression of the amiRNAs against BRCA1 may have not been high enough to result in significant downregulation of BRCA1/2.

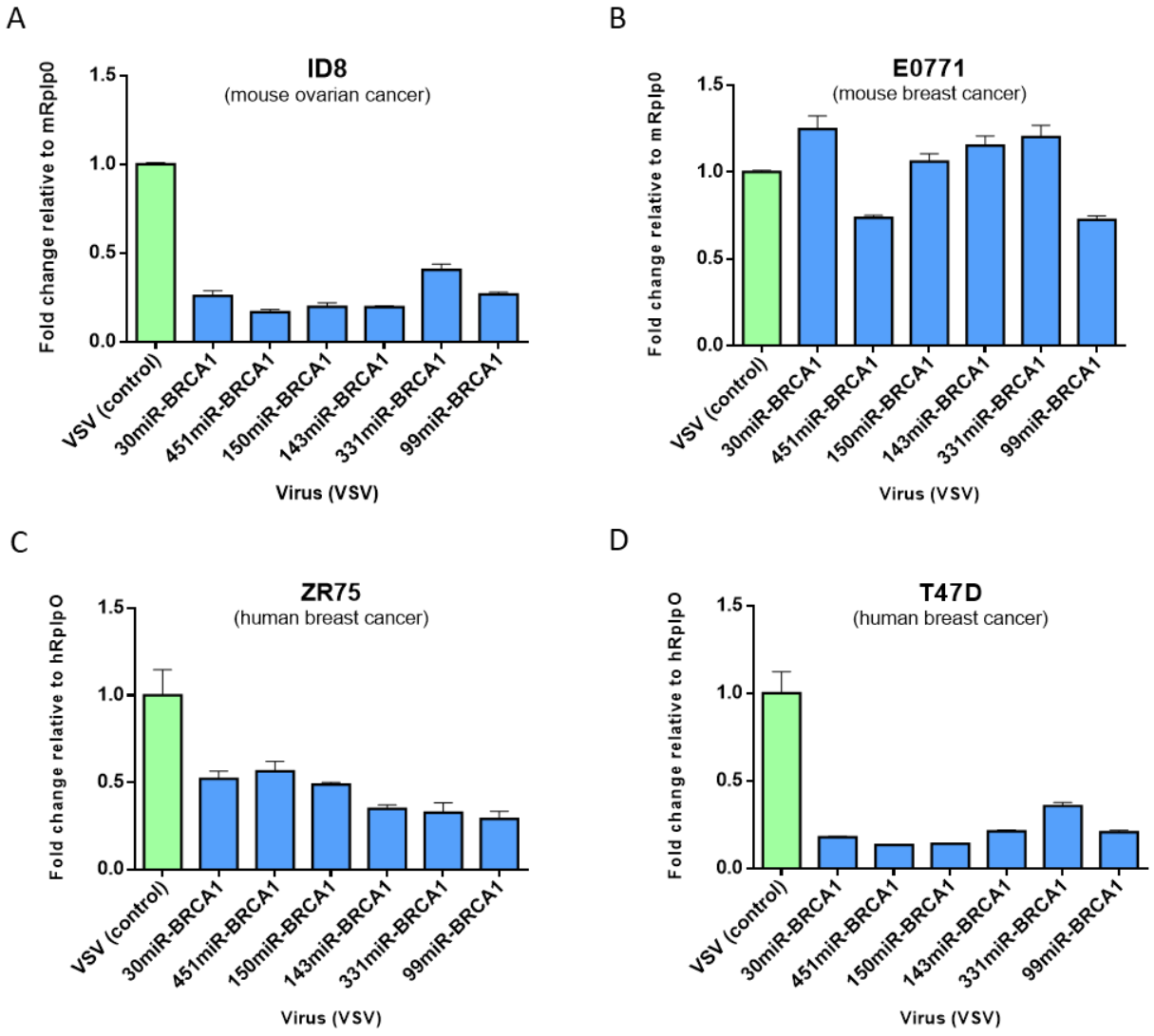

Figure 3.9 qPCR analysis demonstrating downregulation of BRCA1 mRNA following infection with VSVΔ51-miR-BRCA1 in (A) ID8, (B) E0771, (C) ZR-75, and (D)T47D cells. Three plaques for each virus have been screened and shown here are the results of the plaques which demonstrated the most promising downregulation. All cell lines were infected at MOI 0.1 with each respective virus for 24 hours. Error bars represent standard error of mean (n=1, 3 technical replicates).

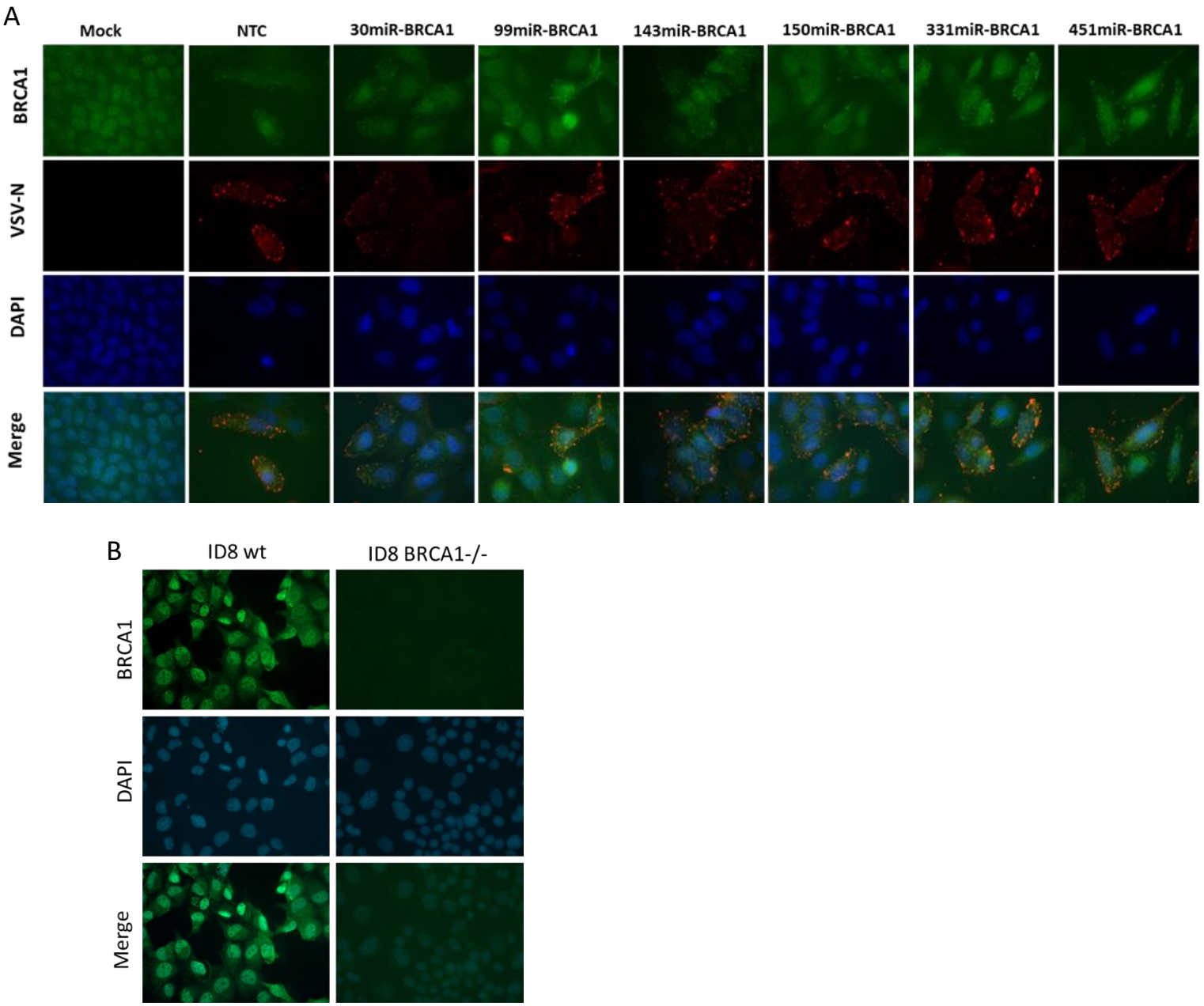

Figure 3.10 Immunofluorescence demonstrating no change in BRCA1 protein expression following infection with VSVΔ51-miR-BRCA1 viruses. (A) ID8 cells were infected at MOI 1 with G-less (non-spreading) versions of each virus for 48 hours (24 and 72hrs are in supplemental information). (B) ID8 BRCA1$^{-/-}$ knockout cell line was used to validate the primary BRCA1 antibody.

3.4 Discussion and future directions

Current state of amiRNA-BRCA1 expressing VSV and potential pitfalls to address

While the outcome of this chapter may not have been ideal in terms of therapeutic impact, there are many roads to take from here to improve this therapy and learn more about amiRNA expressing viruses. An initial concern when beginning this project was whether the RNA processing machinery would even be able to access miRNAs expressed from VSV. As previously mentioned, work by tenOever *et al.* has shown that processing of miRNAs is in fact possible in the cytoplasm; while this work was limited to one miRNA (miR-124), they have also done more extensive investigations revealing that Drosha is in fact exported out of the nucleus following infection with multiple RNA viruses including VSV[254]. Further work by this group has proven that amiRNAs designed using miR-124 as a cassette can function when expressed from influenza A, again this example only utilizes one miRNA cassette, however a very large library of miRNAs was successfully expressed[262]. An important difference to note when comparing VSV with influenza is the replication of influenza does in fact take place in the nucleus, thus, miRNA processing is likely more efficient for this virus. Additionally, previous work by Wedge *et al.* (Nature Cancer, in revisions) in our group has shown that at least some amiRNAs can be functional when expressed from VSV, again, this work utilized a specific miRNA cassette (miR-30) which is processed differently from miR-451.

After reviewing the sub-optimal function of the miR-451 viruses, further review of the literature revealed that the unique processing of this miRNA goes beyond simply replacing Dicer1 cleavage with Ago2, there are many specific motifs within the hairpin which, if altered, could lead

to a significant decrease in processing. Critically important features included the presence of specific nucleotides within predicted Ago2 binding sites in addition to maintaining strict levels of G-C content in certain areas. Accordingly, I have created a list of step-by-step instructions to produce amiRNA sequences using the miR-451 cassette as a backbone (**Figure S3.3**).

After adjusting the design of the amiRNAs to incorporate several of the important characteristics described above in addition to other potential miRNA cassettes it became evident that there are likely other obstacles at play. Another potential issue could be the choice of target site within the mRNA of interest. Naturally occurring miRNAs almost exclusively bind the 3' – UTR of target genes, often taking advantage of multiple repeated miRNA recognition sequences within the same mRNA. While there have been miRNA target sites identified within coding regions, they appear to be far less frequent and may also be less amendable to regulation by miRNAs[263]. Several suggestions have been made to explain the propensity for miRNA targeting and enhanced efficacy at the 3' – UTR including greater conservation of miRNA binding sites within this region as well as cooperation between RNA binding proteins within close proximity in these 'geographically' small regions[264].

While the processing of amiRNAs must have taken place to some extent, demonstrated by the qPCR specifically probing for the mature form of each miRNA (**Figure S3.4**), there may not have been enough mature miRNAs present to produce a measurable knockdown with any obvious phenotype. While the exact number of miRNA or siRNA copies necessary to produce a measurable knockdown of any given gene, various studies have shown that anywhere between 300 and 2,000 copies of a given siRNA are required per cell[265,266]. It would be interesting to determine how many copies of each miRNA are produced per cell and determine if

expression/processing is in fact the culprit leading to sub-optimal knockdown of our given targets given that siRNA treatment could successfully knockdown both BRCA1 and BRCA2 in the initial validation experiments (**Figure 3.3**). Finally, it is important to consider the plethora of compensatory mechanisms involved in PARPi resistance, including upregulation of several genes involved in DNA repair[133,134]; compensation by upregulation of gene expression could very well have protected the cell lines tested here considering very little, if any, BRCA1/2 knockdown was evident after infection. A number of these additional genes will be discussed in the following chapter as I describe the advantages of encoding naturally occurring miRNA sequences into VSVΔ51. Time limitations did not allow for BRCA1 expression after infection with each miRNA-bearing virus to be explored further by either repeating the fluorescent microscopy analysis in the same or a different cell line or further optimizing the western blot protocol; however, these additional experiments will be needed to fully interpret potential reasons why the miR-BRCA1 viruses may not have knocked down their expected target. Additionally, it is important that the targeting sequences be confirmed by repeating the initial western blot experiments in relevant cell lines. To confirm the concentration of PARPi used here significantly inhibits PARP1/2 activity enzymatic assays may be carried out in addition to the detection of PAR chains by immunoblotting analysis on PARPi treated cell lines.

Alternative models for in vitro and in vivo infection

Initial experiments have been carried out in BRCA1/2 wild-type cell lines to recapitulate the resistance that could occur after reversion mutations. It would be very interesting to compare treatment outcomes for paired cell lines before and after resistance to either platinum-based

therapy or PARPi occurred as there are a number of genetic alterations that may occur in the background in addition to reversion mutations of BRCA1/2. Previously established cell lines that could be quite informative on this front include the PEO1 and PEO4 patient derived cell lines, acquired from the same patient before and after cisplatin resistance developed. These cell lines were derived from the ascites of a patient with poorly differentiated ovarian serous adenocarcinoma[267]. The patient was a heterozygous carrier of a *BRCA2* nonsense mutation, her tumour expressed the same (hemizygous) mutation. Prior to cisplatin treatment the patient had undetectable BRCA2 protein expression, but over time became resistant and two new cell lines with reversion mutations resulting in restored BRCA2 protein were generated, PEO4 and PEO6[267]. Differing sensitivities to PARPi have already been established for these cell lines with the clonogenicity of PEO1 being significantly impaired by low dose treatment of talazoparib[268] in addition to significant cytotoxicity observed after low doses of olaparib[106]. PEO4 was unaffected in both cases. We have recently been gifted the PEO1 and PEO4 cell lines kindly from Dr. Vanderhyden (OHRI) and they will be incorporated into future experiments following up on this project.

Based on our observation that OV treatment alone had very little impact when tested *in vivo* in the 4T1 model (**Figure S3.1** and **S3.2**), we have also considered the use of an alternative model that exhibits at least a minor response to the virus, as viral replication is essential for propagation of our therapeutic miRNAs. I have begun optimization of the ID8 ovarian cancer model and successfully demonstrated a small survival benefit with VSVΔ51 treatment alone (**Figure 3.11**), further optimization will be necessary for the combination of VSV-amiR-BRCA1 with PARPi after a successful viral candidate has been established. Another interesting course would

be to incorporate resection of the previously utilized 4T1 model. Previous work within our group has shown strong therapeutic potential of oncolytic Maraba virus (MG1), a rhabdovirus similar to VSV, against triple negative breast tumour models including 4T1, EMT6 and E0771[165]. In this study tumours were initially infected with MG1, surgically resected and finally re-implanted. The anti-tumour immune response could protect against re-growth of these tumour models leading to a significant improvement of survival and complete cures in some cases.

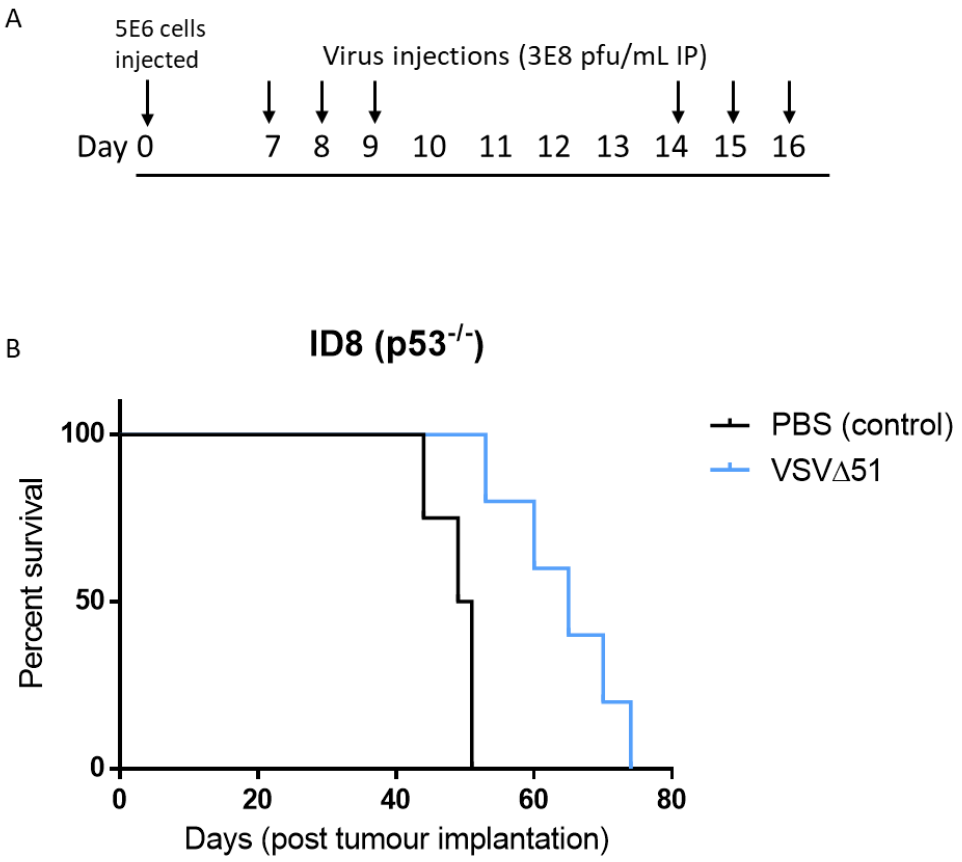

Figure 3.11 VSVΔ51 improves survival in the ID8 p53-/- intraperitoneal *in vivo* model. (A) Treatment was performed as shown above beginning 7 days post-tumour implantation, virus was injected intraperitoneally. (B) Survival was determined when mice reached human end-point due to the accumulation of ascites.

PARPi and immunotherapy are a dynamic duo in the making

The therapeutic potential for PARPi combined with immunotherapeutic agents including OVs is currently gaining momentum[269–272]. It has become clear that elevated levels of DNA damage may provide the spark needed to re-ignite the immune system in treatment resistant tumours. A "triple-threat" treatment strategy combining OV infection with PARPi and immune checkpoint blockade could likely yield greater survival benefit than OVs with PARPi alone.

PARP inhibition has been shown to have a significant impact on the immune system with olaparib treatment increasing the number of CD4 and CD8 effector T-cells both intratumorally and peripherally in initial studies of a BRCA1-deficient ovarian cancer *in vivo* model [273]. The exact mechanism(s) by which PARPi provokes an immune response is still an evolving area of investigation, but DNA damage is clearly a large contributor. PARPi treatment has predictably been associated with increased levels of cytosolic DNA which may be detected by cGAS (cyclic GMP-AMP synthase), eventually leading to the activation of STING (stimulator of interferon genes)[274,275]. The expression of several genes is impacted following STING activation including elevated expression of type 1 interferons and T-cell recruiting chemokines (CCL5 and CXCL10), subsequently increasing T cell infiltration at the site of the tumour. A comparison of HR-deficient versus HR-proficient *in vivo* TNBC treated with olaparib has shown that activation of the cGAS/STING pathway and T-cell recruitment is enhanced in HR-deficient tumours. This same study demonstrated that $CD8^+$ T-cell depletion could in fact reduce the anti-tumour efficacy of PARPi treatment, highlighting the critical role the immune system plays in the anti-tumour impact of PARPi therapy[276]. PARP1 can also contribute to the non-canonical pathway of STING activation;

by recruiting ATM to the site of DBSs, ubiquitin ligase TRAF6 is then activated and translocated to the cytosol where it interacts with IFI16 and p53 to activate STING[277,278].

The introduction of immune checkpoint blockade (ICB) by immune checkpoint inhibitors (ICI) has led to a significant evolution in the field of cancer therapeutics. CTLA4 (cytotoxic T lymphocyte antigen 4) blockade was the frontrunner, approved in 2011, quickly followed by antibodies targeting PD1 and PD-L1 (programmed cell death 1 and programmed cell death ligand 1)[279]. In short, ICB removes the inhibitory signals of T-cell activation allowing T-cells to mount an effective anti-tumour response[280]. PD-1's main function is to regulate the action of T-cells by interacting with PD-L1 in a negative feedback loop to attenuate the T-cell response in the periphery, prevent tissue damage and promote "self-tolerance" when the immune system becomes activated against a pathogen[281]. PD-1 is expressed on activated T and B lymphocytes, upon engagement with PD-L1 a negative co-stimulatory signal is emitted to attenuate T-cell activation[280]. Many tumour types have learned to outsmart and evade the immune system by expressing high levels of PD-L1 on tumours cells themselves in addition to myeloid cells within the TME[281,282].

Increased expression of PD-L1 in breast cancer cells treated by olaparib, talazoparib and rucaparib (as well as PARP1 knockdown) *in vitro* and *in vivo* has been reported; interestingly, increased PD-L1 expression could occur regardless of BRCA mutation status[283]. This finding has opened the door to the potentially lethal combination of ICB therapy in the form of anti-PD-1 or PD-L1 with PARPi. Multiple mechanisms have been proposed to rationalize the increase in PD-L1 expression following PARPi treatment, including increased binding of transcription factor NF-κB to the PD-L1 promotor in response to STING activation and induction of PD-L1 by JAK1/2

activation due to the JAK/STAT signaling which occurs downstream of cGAS/STING and type 1 interferon[284,285]. As mentioned previously, pre-clinical combinations of PARPi with ICB have been quite successful and thus a number of clinical trials are now underway to fully elucidate the therapeutic potential of this combination therapy using already approved PARPi and ICB agents[273,274,286]. Interestingly, tumours lacking BRCA1/2 have recently been shown to express increased levels of programmed cell death protein 1 (PD-1) and programmed cell death ligand 1 (PD-L1) even before PARPi treatment, further confirming ICB may be a suitable addition to current therapeutic options[287–289].

Oncolytic viruses which induce a DNA damage response including adenovirus (AdV) *dl*922-947 and oncolytic HSV (oHSV) have also led to promising outcomes when combined with PARPi[269,271]. The interplay between viral replication and host antiviral response have entangled infection with the DNA damage response in a number of ways which may work both for and against OV efficacy[290,291]. While cells may use their DNA damage response pathway as an antiviral pathway by recognizing viral genomes as damaged DNA, many viruses have evolved to modulate important proteins in the response pathway often via degradation[292]. One group has demonstrated that oHSV can sensitize GBM stem cells (GSCs) to PARPi treatment in a synthetic lethal manner both *in vitro* and *in vivo*, resulting in increased DNA damage, apoptosis and cell death overall[271]. This sensitization occurs as a result of oHSVs ability to mediate proteasomal degradation of Rad51 and Chk1, both key players in the DNA damage response. Taking the OV/PARPi combination approach from another perspective, another group has established that olaparib can in fact enhance the oncolytic activity of oncolytic adenovirus (AdV)[269]. Initial investigations established that AdV *dl*922-947 could trigger a DNA damage response due to

replicative stress leading to decreased replication of the virus[293]. Hence, the addition of PARPi combined with the DNA damage which naturally accumulates during AdV infection was able to produce higher levels of DNA damage and cell death. While the results of these initial studies are promising, the use of OVs with PARPi therapy is relatively unexplored territory, leaving much to be discovered and boundless opportunity for improved therapeutic outcomes. In the following chapter we look beyond BRCA1/2 to target additional components of the HR DNA repair pathway, aiming to elicit a more potent synthetic lethal combination with PARPi.

Chapter 4: Over-expression of miR-182 via oncolytic virus delivery can sensitize resistant breast cancer cells to PARPi therapy

4.1 Introduction

microRNAs and cancer

microRNAs may be small, but they play a very large role in the development and progression of multiple cancers and can often contribute to treatment response as well[237]. Shortly after their discovery it was established that the broad scope of miRNA regulation on the genome could impact nearly all cellular functions whether it be directly or indirectly. The first evidence of miRNA involvement in human cancer was the case of chronic lymphocytic leukemia (CLL). One group sought to determine which proteins may be expressed from a frequently deleted area on chromosome 13 only to discover that this deletion does not impact a protein-coding region, rather miR-15a and miR-16 are located in this area[294]. Shortly thereafter, this same group mapped all of the documented miRNA sequences and found that many were in fact located in unstable regions of the genome which are commonly deleted or amplified in tumour tissues[295]. It is now understood that the miRNA expression landscape between normal tissue and tumours is often quite distinct, in fact, specific subtypes of disease can even be distinguished in some cases (eg. basal versus luminal breast cancer)[296]. The dysregulation of miRNA expression in cancer can occur via several routes. Initial reports, including the CLL case, demonstrated structural genetic changes leading to miRNA dysregulation. It is now understood that a variety of genetic and epigenetic factors are at play including hyper or hypomethylation, and histone deacetylation[237].

Loss of expression of proteins necessary for processing miRNAs, most commonly Dicer and Drosha, can also play a crucial role in tumorigenesis and prognosis in a number of cancers including ovarian carcinomas[247]. And finally, miRNA dysregulation can also occur along with alternations in transcription factor activity[237].

The inhibition and overexpression of specific miRNAs has been explored to improve responses to certain therapeutics. For example, one of the first studies to take advantage of miRNA expression in tumour tissues demonstrated that inhibition of miR-21 and miR-200b could increase sensitivity to gemcitabine in cholangiocarcinoma cell lines[297]. The overexpression of certain miRNAs has also shown promise with miR-205 overexpression increasing responsiveness to tyrosine kinase inhibition in some cancers[298]. To date, an extensive collection of miRNAs have been associated with resistance to drug and hormone therapies in breast and ovarian cancers, some miRNAs due to increased expression and some due to loss or decreased expression levels (summarized in [299,300]).

miR-182

While exploring the possibility of using different miRNA cassettes to deliver amiRNAs in Chapter 3 it became evident that it may be even more effective to encode an endogenous miRNA capable of targeting multiple genes rather than an amiRNA which targets one specific gene. This would also mitigate concerns regarding processing of the pre-miRNA structure of amiRNA sequences. Moskwa *et al.* have shown that BRCA1 is a target of miR-182, with 4 potential recognition sites in the 3'UTR of BRCA1[301]. This group has also demonstrated that ectopic expression of miR-182 can result in persistent DNA damage following ionizing radiation

treatment. To look specifically at the therapeutic potential of miR-182 overexpression in a relevant breast cancer model they used MDA-MB-231 cells which express low endogenous miR-182 and a high level of BRCA1 protein. They first demonstrated that overexpression of miR-182 led to decreased expression of BRCA1 and increased DNA damage via comet assay following ionizing radiation treatment *in vitro*, followed by an *in vivo* combination of miR-182 expression with PARPi treatment which led to slowed tumour growth. Further work by Krishnan *et al.* has shown that miR-182-5p not only targets BRCA1, it also downregulates a variety of other genes involved in DNA repair and cell cycle, including CDKN1B, CHEK2, SMARCD3, ATF1, hRGS17 TP53BP1, FOXO3, and RAD17, BARD1[302].

4.2 Rationale and hypothesis

Targeting multiple genes may increase the potential for overcoming PARPi resistance

Shortly after it was determined that deleterious mutations of BRCA1/2 could render cells sensitive to PARPi a number of additional genes required for successful DNA damage repair by HR were shown to contribute to PARPi sensitivity when mutated, termed 'BRCAness' phenotype genes (reviewed by Lord & Ashworth 2016)[56]. miR-182 is predicted to downregulate a number of these genes, thus this miRNA is a prime candidate to overcome PARPi resistance. Unsurprisingly, miR-182 overexpression has the potential to act as both a cancer promotor in some settings while acting to sensitize cells to drug therapy in others. miR-182 has been reported to be tumorigenic in melanoma, endometrial cancer, prostate cancer, colon cancer and in primary gliomas while it

acts as a tumour suppressor in lung and gastric cancers (summarized in[302]). Interestingly, Krishnan *et al*. have also determined that miR-182 expression is often upregulated in breast cancers; importantly, expression tends to be higher in the ER^+/PR^+ subtype whereas triple negative tumours, the subtype in which BRCA1 tumours tend to fall, are highly variable[302].

Targeting genes that are required for DNA repair could likely lead to genomic instability, producing more aggressive tumour phenotypes due to an increased mutational load. When taking into consideration the potential for a pro-tumour effect of miR-182 expression from VSV, it is important to note is the proposed application of miR-182 here would always be in combination with systemic PARPi treatment with the goal of inducing apoptosis quickly after miRNA expression is able to take place. Considering a clinical context, miRNA expression would only be present during infection while PARPi treatment is often provided as a daily oral medication and has been shown to be tolerated as maintenance therapy for many months[127].

Hypothesis

Overexpression of miR-182 via expression from oncolytic VSV will sensitize resistant, BRCA1/2 wildtype, cancer cells to PARPi treatment.

4.3 Results

miR-182 is expressed by VSV and knocks down predicted targets

Two miR-182 expressing versions of VSV have been designed and validated (via sequencing), the first expresses one miR-182 hairpin and the second expresses two [referred to as VSVΔ51-miR-182(x1) and VSVΔ51-miR-182(x2)]. Both versions are expressed within the VSV genome between the G and L protein sequences. miR-182 is predicted to interact with BRCA1 at four potential target sequences, three of which have been verified via a luciferase reporter assay previously[301]. I was also interested in determining if the potency of knockdown could be enhanced by expressing two hairpins compared to one. The double hairpin virus was designed following the recommended minimal spacing strategy outlined in a previous publication which tested the expression of tandem miRNAs expressed from HIV by adding 30 nucleotides to either side of each hairpin[303].

An alternative option to increase expression of the miRNA would be to change the location of the miRNA to a position upstream of the G protein, unfortunately our current VSV plasmid has been optimized for cloning between G and L. After attempting to insert miR-182 at an upstream location I have determined that cloning in alternative locations will require further optimization. While the expression of miR-182 from the two viruses was quite similar with the double hairpin virus expressing a slightly higher amount of processed miR-182 (**Figure 4.1**), the ability to knockdown multiple targets at the mRNA level was in fact enhanced by the presence of a second copy of miR-182 (**Figure 4.2 A**). Multiple mRNA targets in addition to BRCA1 were substantially knocked down following infection with the double hairpin virus as well. Further,

preliminary western blot analysis revealed enhanced knockdown of BRCA1 in MDA-MB-231 cells infected with VSVΔ51-miR-182(x2) compared to VSVΔ51-miR-182(x1). This experiment has since been repeated (using the double hairpin virus only), revealing that infection at a low MOI using the replication competent version of the virus can effectively knockdown BRCA1 in addition to the ΔG (non-spreading) version (**Figure 4.2 B, C, D**). Here, the additional target CHEK2 has been included. While the qPCR results were not overly compelling for *CHEK2,* this target was of particular interest due to its previously reported implications in PARPi sensitization. Western blot analysis has revealed that CHEK2 is in fact knocked down at the protein level as well by both the replicating and ΔG versions of the miR-182 double hairpin virus (**Figure 4.2 B, C, D**). Future experiments should aim to repeat and confirm these important findings, in the interest of time we moved forward to determine if these viruses could sensitize BRCA1/2 wildtype breast cancer cells to PARPi treatment and whether miR-182 could be enriched in EVs.

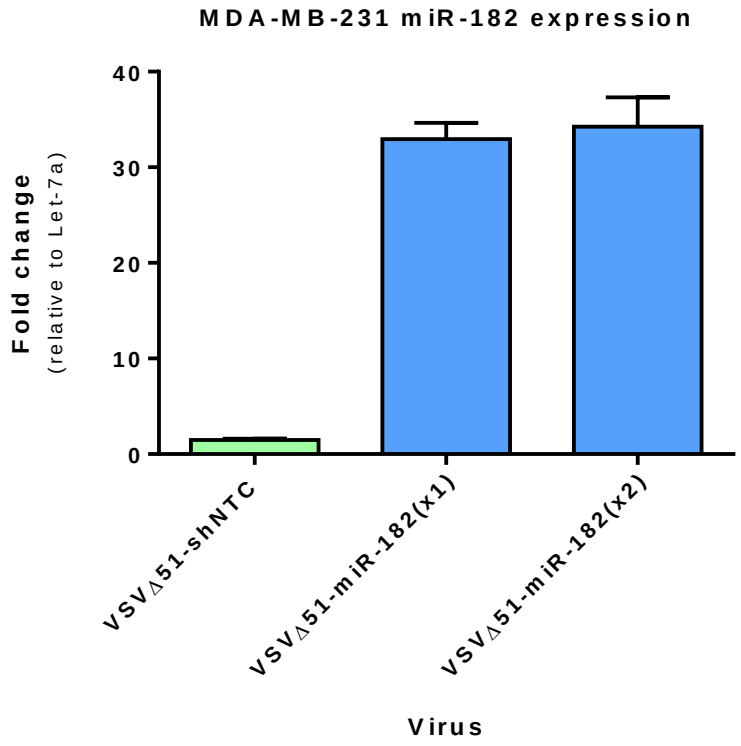

Figure 4.1 qPCR analysis demonstrates mature miR-182 expression from MDA-MB-231 cells infected at MOI 0.1 for 48 hours. Error bars represent standard error of mean (n= 1, 3 technical replicates).

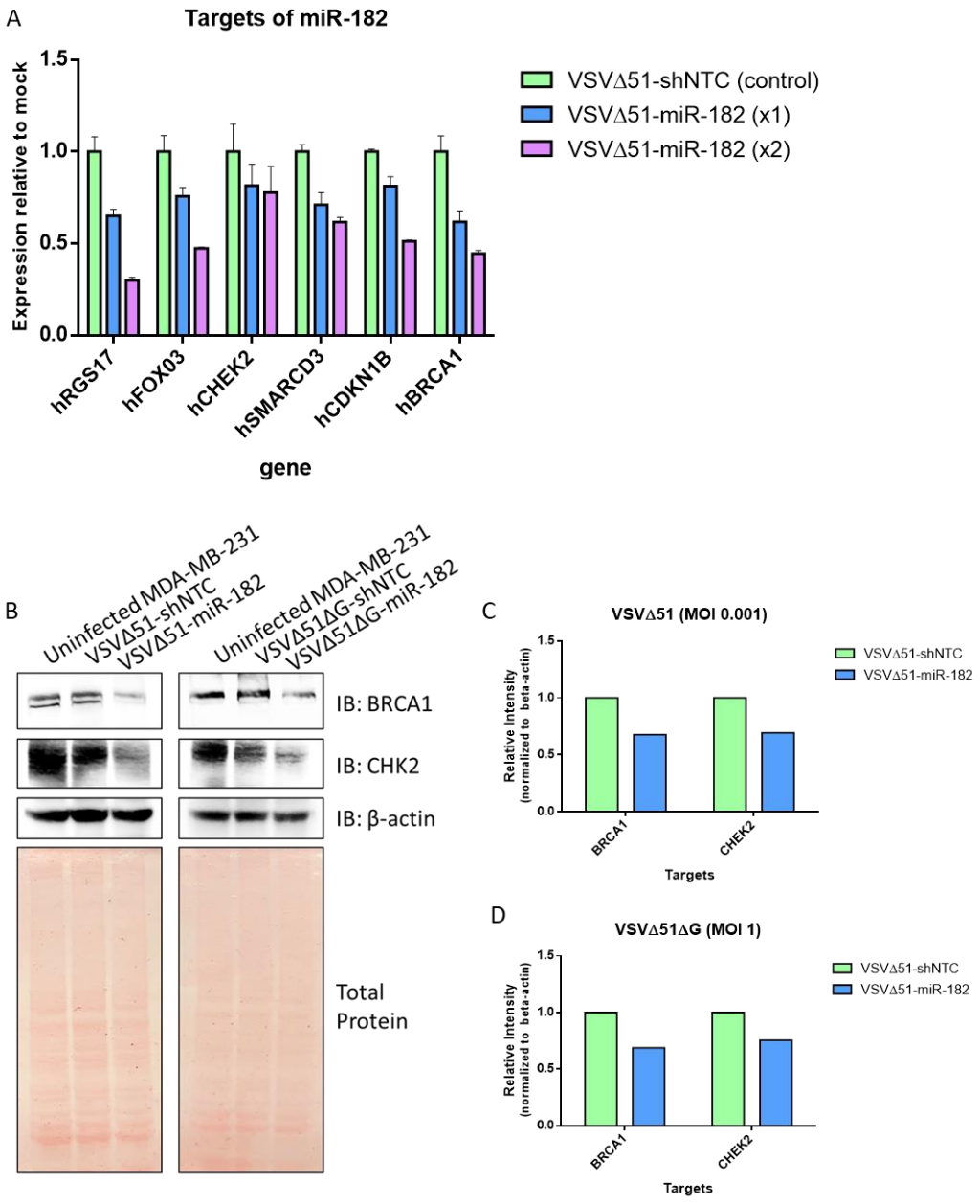

Figure 4.2 qPCR and western blot analysis demonstrates miR-182 target knockdown in MDA-MB-231 cells. (A) Cells were infected at MOI 3 with G-less versions of each virus for 48 hours prior to RNA extraction and qPCR. Error bars represent standard error of mean (n= 1, 3 technical replicates). (B) Cells were infected with the replicating version of each virus at MOI 0.001 for approximately 50 hours and G-less virus at MOI 1 for approximately 60 hours prior to lysis and western blot analysis. (C + D) Relative intensity was determined using densitometry analysis on the Bio-Rad Image Lab software.

miR-182 is present in EVs when overexpressed by VSV

While miR-182 was not necessarily identified as an EV-miRNA in the previously discussed RNA-sequencing experiment, additional work by our group (Wedge *et al.* Nature Cancer, in revisions) has demonstrated that artificial miRNAs expressed by VSV within the commonly used miR-30 cassette can in fact be loaded into EVs. Therefore, we hypothesized that the same could occur for miR-182 when overexpressed from VSV. Infecting with VSVΔ51-shNTC (non-targeting control virus) interestingly resulted in an undetectable level of mature miR-182 in EVs after 48 hours; however, miR-182 could in fact be detected in EVs following infection with VSVΔ51-miR-182(x2) (**Figure 4.3 A**). Importantly, the total amount of RNA present in each reaction was normalized via nanodrop spectroscopy and the nearly identical Ct values of the housekeeping miRNA, Let-7a, confirmed this. The results of this experiment have been displayed as Ct value rather than fold expression, due to the lack of expression following VSVΔ51-shNTC infection. VSVΔ51-miR-182(x2) infection also resulted in preferentially loading of the pre-miR-182 species into EVs relative to copies retained within the cell (**Figure 4.3 B**).

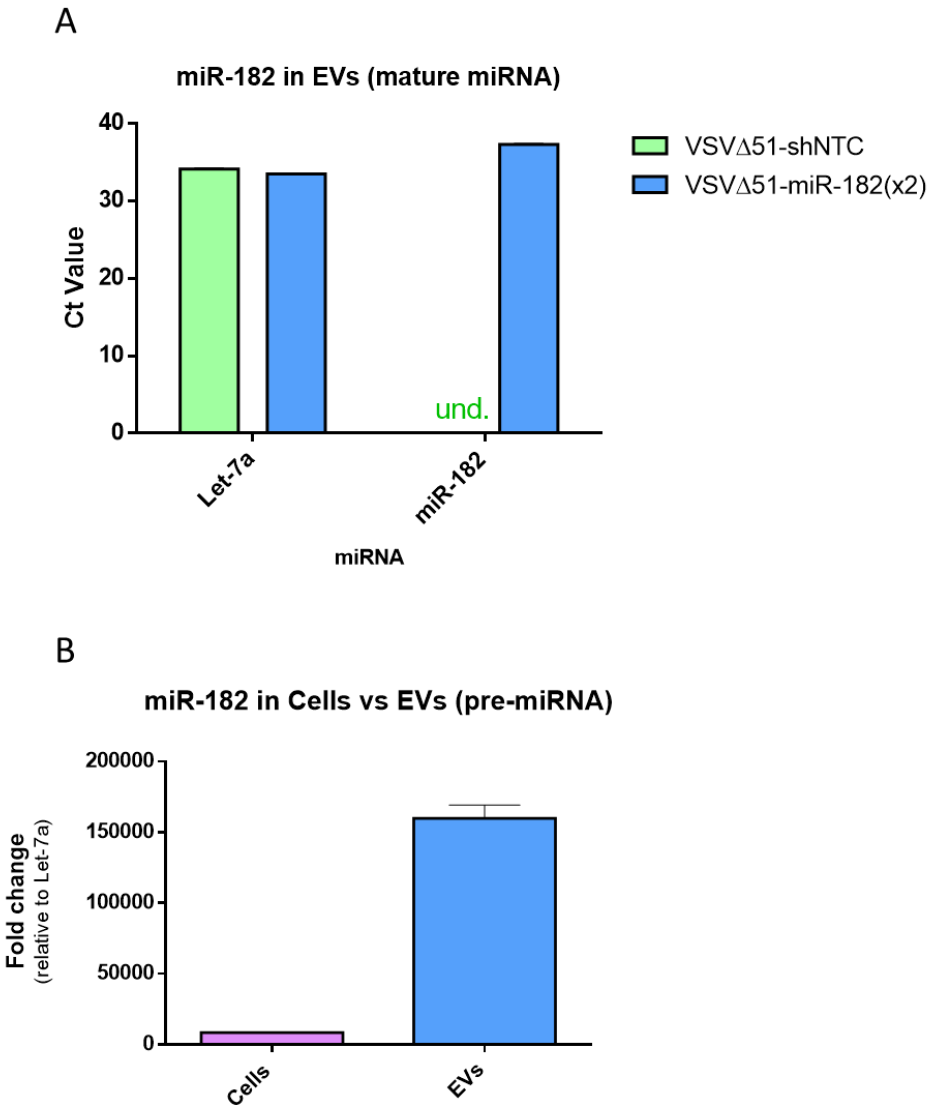

Figure 4.3 qPCR analysis reveals that expression of mature and pre-miR-182 can be detected in cells and EVs. MDA-MB-231 cells were infected at MOI 3 with VSVΔ51 (G-less) miR-182 (double hairpin) for 48 hours. TaqMan probes for the (A) mature miR-182 versus the (B) pre-miR-182 were used to measure expression relative to the shNTC expressing virus. Error bars represent standard error of mean (n= 1, 3 technical replicates).

miR-182 sensitizes MDA-MB-231 breast cancer cells to rucaparib

To determine if VSVΔ51-miR-182 could sensitize BRCA1/2 wildtype cells to PARPi treatment, MDA-MB-231 cells were grown as 3D spheroids and infected with either VSVΔ51-miR-182(x1) or VSVΔ51-miR-182(x2) and subsequently treated with olaparib or rucaparib. While significant changes in the diameter of these spheroids were not observed (likely due to the less uniform shape this cell line tends to produce when grown in 3D compared to the previously tested 4T1 model), changes in the viability (specifically cellular metabolism) could be determined via alamar blue. The MDA-MB-231 cell line is quite susceptible to infection, even when grown as spheroids, thus a relatively low MOI was necessary to distinguish changes due to the combination treatment compared to virus alone. Infection of these spheroids at such a low MOI led to significant variability between spheroids; thus, the results of two combined experiments, each completed in triplicate, are shown. As high as 50% loss of viability could be observed with the combination of VSVΔ51-miR-182(x2) with rucaparib in some cases, no combination effect was observed after olaparib treatment (**Figure 4.4**).

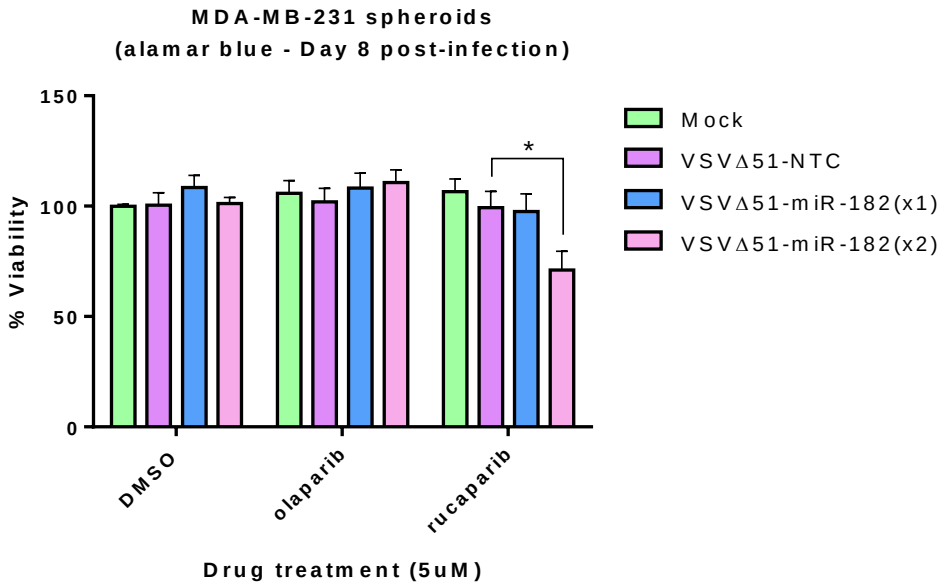

Figure 4.4 Cell viability measured via alamar blue of spheroids infected with VSV-miR-182(x2) is significantly lower when treated with PARPi combination therapy (rucaparib). Spheroids were treated with each virus at MOI 0.05 and treated with 5 µM of each PARPi starting one day after infection, replenished every two days. Alamar blue was added on day eight post infection and read on day ten. Error bars represent standard error of the mean (n=6, 3 technical replicates x 2 biological replicates). Unpaired two-tailed t-test comparing VSV-miR-182(x1) and VSV-miR-182(x2) with VSV-shNTC was used to evaluate statistical significance (*P<0.05).

4.4 Discussion and future directions

VSVΔ51-miR-182 can sensitize cells to PARPi

Demonstrating the functionality of amiRs expressed from VSV has proven to be rather complex, thus, I opted to explore the expression and function of the naturally occurring human miR-182. As previously mentioned, multiple versions of miR-182 expressing VSV were initially designed with the objective of comparing upstream versus downstream expression in addition to single versus multiple copies of the miRNA. The viral gene order of VSV has been determined to be 3'-N-P-M-G-L-5' with the abundance of mRNA decreasing with distance from the promotor (N > P > M > G > L) as 30% of polymerase molecules at each intergenic point fail to transcribe the subsequent gene[304,305]. Thus, we can modify the quantity of expression for the transgene which has been inserted based on the location of insertion. Unfortunately, while the insertion of genes between G and L has been well established within our group, the insertion of miR-182 at an upstream location presented logistical challenges which will require further optimization to overcome. Nevertheless, the expression of a single versus double hairpin was put to the test and despite initial concerns regarding potential recombination of the identical hairpins expressed from a single vector, the knockdown efficacy of the double hairpin was in fact more significant at the mRNA and protein level compared to a single hairpin (**Figure 4.2**). When combined with rucaparib treatment, the potency of the double hairpin virus was in fact confirmed by a more significant decrease in the viability of spheroids treated with the combination therapy (**Figure 4.4**). Interestingly, the synthetic lethal effect was only observed when infection was combined with rucaparib, not olaparib. It is well understood that not all PARPi have been created equal, as

described previously olaparib and rucaparib both have a similar propensity for PARP trapping however rucaparib does tend to be a more promiscuous drug in terms of interacting partners. Olaparib primarily inhibits PARP1 and 2 while rucaparib has been shown to act on PARP3 as well in addition to exhibiting more potent inhibition of PARP1 compared to olaparib (summarized in[306]). Based on previous reports, we could potentially see different levels of sensitivity for different PARPi depending on the cell line tested as each line tends to exhibit rather unique susceptibility profiles[306]. Thus, future experiments will include the use of multiple cell lines, specifically expressing various levels of BRCA1.

MicroRNAs expressed from VSVΔ51 are packaged into EVs regardless of 'EV-miRNA status'

While previous work by our group and others has shown that over-expression of miRNAs can lead to packaging into EVs, there is little information available in this area[238]. It is unclear whether there is a certain threshold of expression needed to induce exportation into EVs or if certain miRNAs can be retained within the cell regardless of the level of expression. Interestingly, miR-182-5p has very recently been detected in EVs secreted by GBM cells under hypoxic conditions[307]. This is yet another reassuring piece of evidence which leads us to believe that the content of EVs is often changing and may be modified under altered physiologic conditions including infection. Consequently, we predicted that miR-182 would be loaded into EVs. It was interesting to determine a higher proportion was of the pre-miRNA variety compared to the mature sequence; however, the presence of any copies of miR-182 whatsoever in EVs was an encouraging finding (**Figure 4.3**).

Due to the very low or non-existent presence of mature miR-182-5p in EVs produced from cells infected with VSV-shNTC, it was not feasible to calculate the fold-change following infection with VSV-miR-182 compared to a non-targeting miRNA. While it is clear that the expression of miR-182 from the virus was able to encourage packaging into EVs, if we would like to gain a better grasp of exactly how large the difference between treatments might be, future experiments could incorporate the use of a cell line which is known to express higher levels of miR-182 and would therefore be more likely to have at least trace amounts present in the EVs or a standard curve approach could be applied. Additionally, it should be noted that the MDA-MB-231 cells are quite susceptible to VSV infection; therefore, a slightly more robust cell line that can withstand infection for a longer period of time may be able to produce more of the miRNA leading to enhanced knockdown of the respective targets and increased loading into EVs. This proof of concept for miRNA loading in to EVs regardless of EV-miRNA status is encouraging and will be explored in future experiments using miR-182 and potentially other cancer therapeutic miRNAs under investigation.

A clear advantage of expressing miRNAs from an OV is the specific delivery to the site of the tumour, but if we are encouraging the export of therapeutic miRNAs into EVs the opportunity for off-target effects could increase. Previous work has shown that EVs may be specifically targeted to cancer cells by expressing specific markers on their surfaces, such as an epidermal growth factor receptor (EGFR) binding ligand, recognized primarily by cancer cells[308]. Our group is currently working to test and optimize EV targeting systems for various types of cancer which could be applied here as well if needed.

Can we improve the efficacy of our miRNA expressing oncolytic viruses?

While only a small portion of breast and ovarian cancers harbour mutations in either *BRCA1* or *BRCA2,* recent studies have demonstrated that nearly 50% of sporadic high-grade serous ovarian cancers and 15% of triple-negative breast cancers are homologous recombination deficient (HRD), due to mutations in other key genes needed for HR, falling under the umbrella term BRCAness[56,309,310]. Mutations in an extensive list of HR-related genes have been identified including *ATM*, ATR*, BARD1, BRIP1, CHK1, CHK2, PALB2*, RAD51, FANC*, WEE1, RAD51C, NBS1,* and *PTEN* (*mutation sensitizes to PARPi)[56,114,132,311]. The following genes have in fact been targeted by either small molecule or siRNA inhibition in resistant or BRCA-proficient cell lines and demonstrated synthetic lethal effect with PARPi therapy: CDK1[312], CDK12[313], ATM[314], ATR[315], WEE1[316,317] and c-Met[318]. The list of possible genes for targeting to increase sensitivity to PARPi continues to grow via genome surveillance studies and siRNA screening, many of which have known miRNA recognition sites[319,320].

Indeed, additional miRNAs have already been identified which when overexpressed increase the susceptibility of resistant breast cancer cells to olaparib therapy by targeting Rad51, a protein required for HR[321]. In contrast, other miRNAs have been shown to promote resistance (summarized in[299,300]). Taken altogether it is clear that the miRNA profile of both resistant and sensitive tumours has the potential to impact the development of targeted therapies through the modulation of multiple genes. Thus, future work to enhance the potency of our miRNA expressing OVs could include the expression of multiple miRNAs either from one virus or co-infection with single miRNA expressing viruses. A multi-miRNA approach may also be an interesting method to overcome potential resistance against the miRNA itself due to mutations

in the 3' – UTR among genes of interest, as previous work has shown that small mutations or single nucleotide polymorphisms within the 3' – UTR of oncogenes could allow escape from regulation by miRNAs[322].

There is much to be explored regarding the impact of VSVΔ51-miR-182 alone and in combination with PARPi treatment

Now that I have established a functional miRNA which can be expressed from VSV and sensitize breast cancer cells to rucaparib treatment there are several experiments to complete to further elucidate the potential applications for this therapy. First, the scope of this treatment should be tested on multiple cell lines to determine if VSV-miR-182 is able to sensitize genotypically and phenotypically different cell lines. Next, it is critical to ensure the newly engineered virus maintains a similar safety profile to the parental virus, importantly, replicating primarily at the site of the tumour. Thus far, our group has not encountered off-target toxicity related to infection with VSVΔ51, but this should be confirmed for each new virus. Initial safety experiments comparing the ability of the virus to infect and replicate in normal tissues can be completed *in vitro* by measuring cytotoxicity with infection in normal cell lines which should not be susceptible to infection. Follow-up *in vivo* studies should also include biodistribution studies wherein normal tissues are excised after infection and processed either for titering or immunohistochemistry (IHC) staining to determine if the virus is replicating outside the site of the tumour. Additionally, single- and multi-step growth curves should be completed to determine of the addition of the transgene has rendered the new virus unable to replicate and infect, at a similar rate to the parental virus. After initial safety experiments, tumour control and survival

can be measured following treatment. Our group has established a maximally tolerated viral dose for intratumoural injection into mice and I have begun testing multiple doses of PARPi (rucaparib) to ensure toxicity does not occur with drug treatment alone.

The potency of BRCA1 knockdown can also be explored *in vivo*. To assess the degree of knockdown at the protein level within injected tumours, immunohistochemistry (IHC) staining can be performed on excised tumours 48 to 72 hours post infection. It would also be interesting to determine if the degree of BRCA1 knockdown correlates with the location of the virus or if EV delivery of miR-182 from infected cells is in fact enough to knockdown BRCA1 in neighbouring cells. IHC can also be employed to localize the virus within the tumour. Additionally, RNAscope technology can be used to probe tumours for viral RNA while simultaneously probing for multiple gene targets[323]. Looking beyond knockdown of BRCA1, we can explore deeper into the mechanism of synthetic lethality, beginning with methods to measure DNA damage. For example, one of the most commonly used methods to quantify double strand breaks is the detection of RAD51 and γ-H2AX foci via antibody staining and fluorescent microscopy, wherein decreased Rad51 foci and increased γ-H2AX would represent the presence of persistent DNA breaks within the nucleus[313].

The successful sensitization of MDA-MB-231 cells to PARPi via infection with VSV-miR-182 represents, to our knowledge, the first example of sensitization to PARPi therapy by an OV encoded miRNA. While the results of this study have not been fully refined, this novel therapy has the potential to overcome multiple barriers of currently available treatments by acting specifically on cancer tissues owing to the specificity of VSV replication, as well as efficiently delivering therapeutic miRNA directly to the site of the tumour and to uninfected cells within the

TME via EVs. In the following chapter we move beyond targeting the cellular DNA repair machinery to explore additional miRNAs which are preferentially loaded into EVs and may act on other components of the TME.

Chapter 5: Unleashing the potential for virally derived 'EV-miRNAs' in cancer therapy

5.1 Introduction

miR-150

While investigating the application of different miRNA cassettes to carry amiRNAs in Chapter 3, I was interested in confirming that the naturally occurring miRNA sequences could be fully processed and functional when expressed from VSV prior to incorporating artificial sequences. While the selection of miRNAs was based solely on their propensity to enter EVs following infection, a brief literature review of the top five miRNAs resulted in one particular miRNA standing out as an interesting immunotherapeutic candidate itself, miR-150. After early experiments (discussed in more detail below) revealed that miR-150 could be carried by EVs at high levels in both its pre-miRNA and mature miRNA state I focused follow-up experiments on this miRNA. As an endogenous miRNA it is unsurprising that miR-150 is able to exert its effect on multiple genes, interestingly two main themes emerge when reviewing the genes under miR-150 regulation – cancer and the immune system.

miR-150 and cancer

miR-150 has been shown to have direct anti-tumour effects by targeting various pro-growth oncogenes in a number of different cancer types. Nearly 10 years ago, miR-150 was identified as a potential biomarker for the prognosis and therapeutic outcome of colorectal cancer[324]. miRNAs have been shown previously to act as prognostic markers for certain cancer

types and other disease states; accordingly, this study sought to identify miRNAs which correlated with better survival and response to adjuvant chemotherapy in colorectal cancer patients and found that high miR-150 expression was in fact associated with both.

Several more recent studies have further elucidated the role of miR-150 in cancer progression demonstrating direct interactions with previously identified pro-cancer pathways. For example, miR-150 has been shown to target the oncogene, *Notch3*, in ovarian cancer cells leading to sensitization to paclitaxel therapy[325] as well as vascular epithelial growth factor A (VEGFA) in colorectal cancer resulting in reduced proliferation and angiogenesis[326]. This miRNA has also been shown to prevent the formation of metastases in lung and ovarian cancers[327,328]. One study found that miR-150 was significantly downregulated in CSCs of non-small-cell lung cancer (NSCLS), further investigation revealed that it could inhibit wingless (Wnt)-β-catenin signaling as well as high mobility group AT-hook 2 (HMAG2), both associated with cancer cell stemness; ectopic expression resulted in less lung CSC induced tumorigenesis and metastases[327]. Another very recent study has shown that ectopic expression of miR-150 via lentiviral transduction could inhibit ovarian cancer growth and metastases both *in vitro* and *in vivo*[328]. This group found that both insulin-like growth factor 1 receptor and insulin receptor substrate 1 (IGF1R and IRS1) were direct targets of miR-150. By downregulating IGF1R/IRS1, the downstream PI3K/AKT/mTOR growth pathway was less active in ovarian cancer cells[328]. High miR-150 expression has also been shown to inhibit the growth of melanoma and lung cancer via inhibition of the transcription factor c-Myb[329,330].

Of note, like other miRNAs which have a strong connection to cancer development, miR-150's impact is multifaceted, and has the potential to exhibit a pro-tumour role in some cases.

Cancer types which have been associated with high miR-150 expression include breast cancer, cervical cancer and lung cancer[331–333]. Thus, as the field of cancer therapeutics has already proven, the choice of therapy depends not only on the type of malignancy, it may also depend on the subtype and mutational or miRNA expression landscape of the tumour in question.

miR-150 and the immune system

The role of miR-150 in the immune system is also quite complex. The development and function of several immune cell types are under the control of miR-150, most often due to their association with transcription factor c-Myb which plays a critical role in controlling transcription at multiple stages of lymphocyte development[334]. For example, NK and invariant NK T (iNKT) cells are both impacted by miR-150 expression, but in a contrasting fashion. Deletion of miR-150 in mice impairs the development of NK cells while over-expression leads to reduced levels of iNKT cells in the thymus and peripheral lymphoid organs[335]. B cell differentiation has also been associated with miR-150 expression where high levels of miR-150 expression can result in a partial block of B cell development [336]. One group has also shown that increased miR-150 expression leads to enhanced levels of terminal effector $CD8^+$ T cells via downregulation of the transcription factor c-Myb[337] while another group demonstrated that T cell differentiation and effector function are dependant on miR-150 but this was not associated with c-Myb expression levels[338]. Interestingly, additional work has shown that miR-150 can increase the level of memory phenotype $CD8^+$ T cells via translational repression of Foxo1[339]. Of note, a recent study connected miR-150 directly to the anti-tumour immune response showing increasing activation of tumour specific $CD8^+$ T cells with high miR-150 expression[340].

Taken together, it is clear that the impact of miR-150 on the immune system is complex and likely dependant on a number of confounding factors ranging from the model being studied to the state of the immune system whether it be infected or uninfected, what type of infection, and finally the presence of malignancy or not.

5.2 Rationale and Hypothesis

Overcoming current clinical hurdles to deliver miRNA to the site of the tumour

While several studies have in fact demonstrated the potential benefit of overexpressing specific miRNAs to promote responsiveness to certain therapies, the delivery of miRNAs to the site of the tumour remains challenging. A distinct advantage of microRNAs over conventional chemotherapies is the ability to target cancer cells with enhanced specificity based on their unique miRNA profile. While conventional chemotherapeutics and small molecule therapies do aim to impact tumour cells largely while leaving normal tissues unharmed, they are almost always associated with off-target effects including damage to rapidly dividing normal tissues and/or non-specific entry due to shared receptors between cancer cells and some normal cells[341]. Even monoclonal antibodies, one of the most well targeted therapies available, have the potential to become less effective due to immune escape and/or ineffective entry into the tumour itself[342].

A plethora of strategies have been developed to increase the efficiency of miRNA delivery to tumour cells including packaging within liposomes, nanoparticles, or with compounds such as polyethylene glycol (PEG), and expression from lentiviral vectors or adeno-associated viruses (summarized in [341]), however, there remain challenges. The primary hurdle for miRNA based

therapy initially, was the very quick clearance after administration; 'naked' miRNAs are typically cleared via degradation or intracellular trapping within minutes or even seconds in the circulation, methods of protecting miRNAs as listed above have slowed this clearance significantly[341,343]. Though, many nanoparticles still unfortunately do not reach their intended target cells as they are taken up non-specifically by immune cells[344]. Physical barriers continue to exist for miRNA delivery even when the miRNA is protected from degradation by modifications or coating. Local and topical deliver of miRNAs has reduced off-target effects and enhanced target gene knockdown at the site of delivery for miRNAs with or without the addition of a carrier[345,346]. Direct delivery of lentiviral vectors expressing miRNAs have also shown promise. Of note, while local administration has improved miRNA uptake it would be unlikely to significantly impact metastatic disease. Thus, infection by OVs which replicate specifically in cancer cells could be the necessary bridge to deliver miRNAs to the site of the tumour at high enough levels to achieve successful gene knockdown.

An additional roadblock still stands in our way; it is well understood that only a select portion of cells within a tumour will actually be infected so we must rely on various additional mechanisms of OV killing such as the anti-tumour immune response and disruption of tumour vasculature to make any clinically significant impact[347,348]. As mentioned earlier, even with this arsenal of anti-tumour mechanisms, OVs still have yet to become standard of care due to their limited efficacy in most patients[167,349]. Our group (Wedge *et al.*, Nature Cancer, in revisions) and others have shown that virally derived miRNAs can be packaged within small EVs[350]. We aim to explore the findings of the previous chapter and the above-mentioned manuscript further by strategically expressing miRNAs which are more prone to EV packaging, virtually hijacking the EV

trafficking system of infected cells to impact gene expression in neighbouring uninfected cells. To this end, I have engineered the top five miRNAs that are exported into EVs as described in the previous chapter to determine if they are in fact exported to a higher level when over-expressed from VSV.

Hypothesis

The expression of naturally occurring miRNAs from VSV which become enriched in EVs following infection will further boost their packaging into EVs.

5.3 Results

Naturally occurring EV-miRNA sequences can be expressed from VSV

To confirm the presence of each EV-miRNA in EVs following infection I first completed qPCR analysis demonstrating that each miRNA is could be detected both in its pre-miRNA and mature forms at varying levels before and after infection using this method (**Figure 5.1**). Next, I cloned each of the five EV-miRNAs into VSV (both with and without VSV G protein) and rescued these viruses. To validate their expression and processing when expressed from a replicating VSV, qPCRs using specific probes for the mature form of each miRNA have been completed, verifying that each miRNA is in fact expressed and processed in MiaPaCa2 cells (a pancreatic cancer cell line in which the original RNA-seq experiment was performed) (**Figure 5.2**). I have also confirmed expression and processing from two additional cancer cell lines, ID8 (mouse ovarian cancer) and T47D (human breast cancer) (**Figure S5.1**).

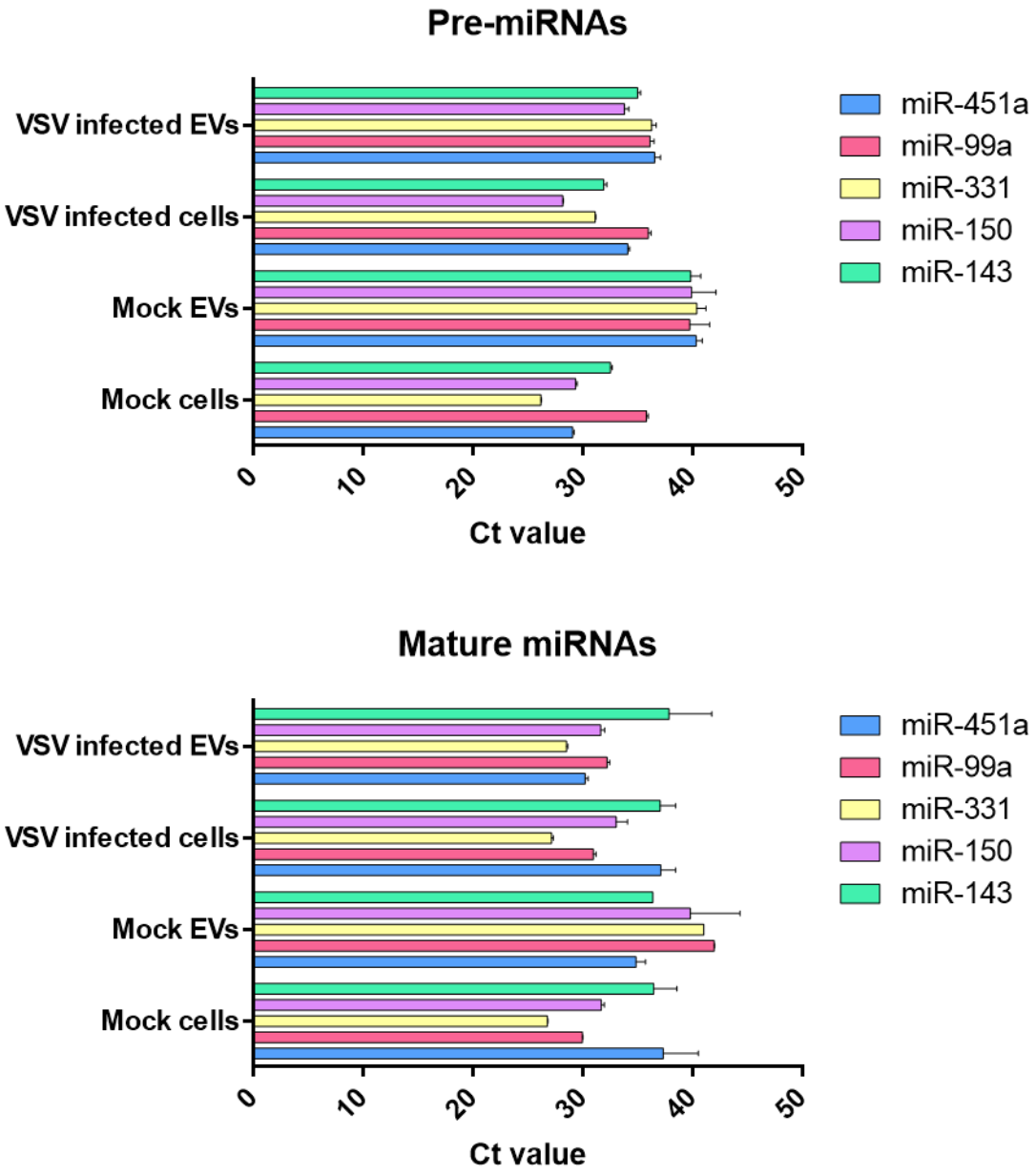

Figure 5.1 qPCR analysis demonstrating that each EV-miRNA can be detected in EVs before and after infection with VSVΔ51-GFP. Ct values have been used to represent the raw expression levels here as opposed to relative expression, as 'house-keeping' miRNAs tended to have altered expression following infection. Error bars represent standard error of mean (n=3 technical replicates).

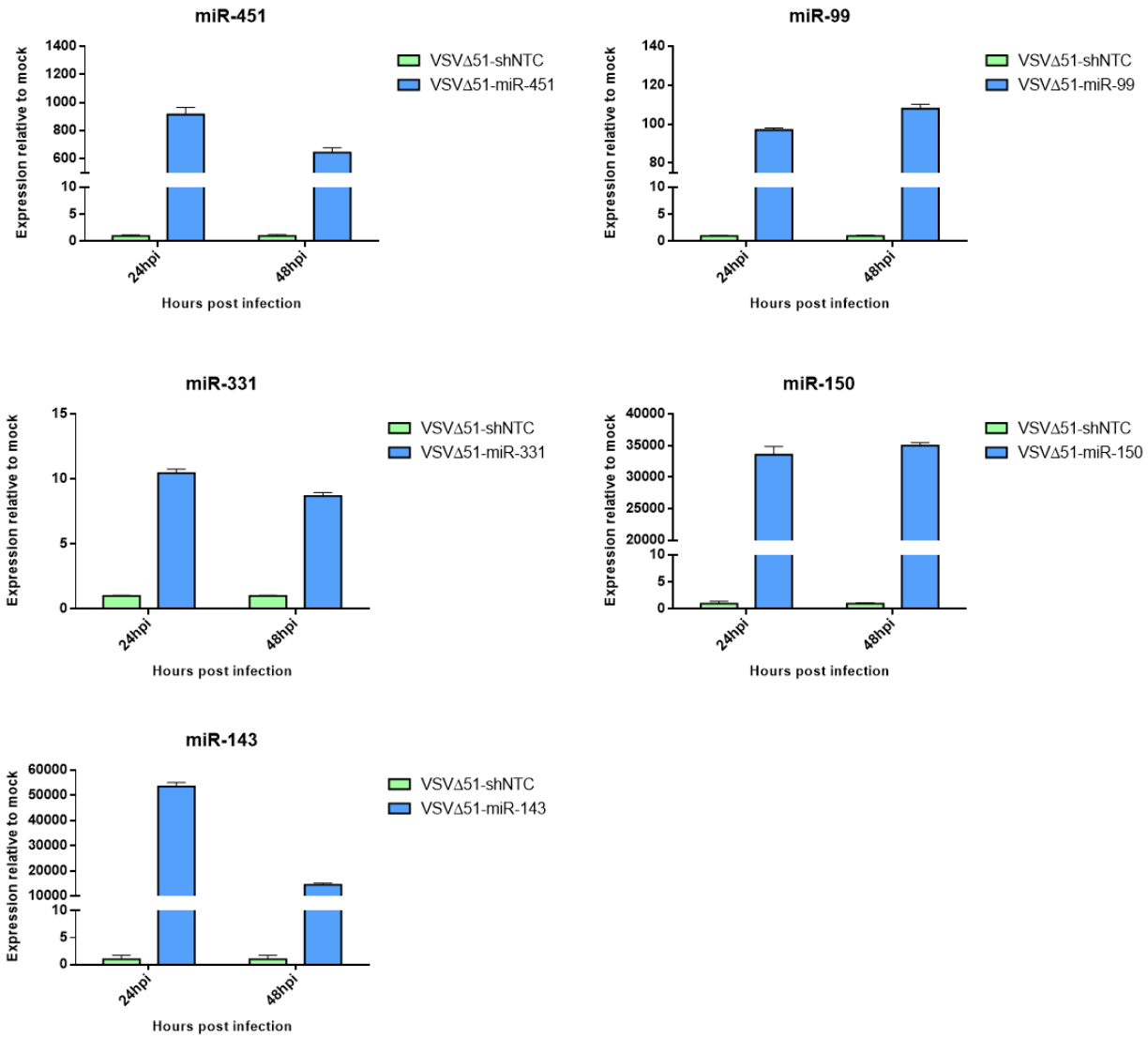

Figure 5.2 Relative expression of EV-miRNAs compared to cells infected with a non-targeting control (VSVΔ51-shNTC) in MiaPaCa2 (human pancreatic cancer) cells. Expression levels shown here represent the mature form of each microRNA. Cells were infected at MOI of 0.1 for 24 hours or 0.01 for 48hrs. The relative expression of each EV-miRNA following infection with the NTC has been set to 1. Error bars represent standard error of mean (n=1, 3 technical replicates).

Pre-miRNAs are more readily exported into EVs compared to mature miRNAs

To determine if miRNAs expressed from VSV are loaded into and/or delivered by EVs, I first engineered "G-less" or ΔG (non-infectious, unless G is provided transiently) versions of each recombinant virus. A non-spreading version of the virus is essential as VSV is quite small (~80nm)[152], in fact, it is similar in size to a small EV; therefore, it is impossible to separate the two populations by filtration steps. G-less VSV lacks the gene encoding the viral glycoprotein; therefore, these recombinant viruses are capable of infecting cells, replicating and packaging new virions, however these particles will be significantly less infectious due to their severely reduced capacity to bud from the host cell and infect other cells[171,351,352]. I have utilized the G-less versions of each virus to determine if the relative expression of each miRNA does in fact increase in EVs when expressed from VSV. Interestingly, the pre-mature form of each miRNA is present at very high levels compared to VSV-NTC infection, while the mature form is quite variable from miRNA to miRNA (**Figure 5.3**).

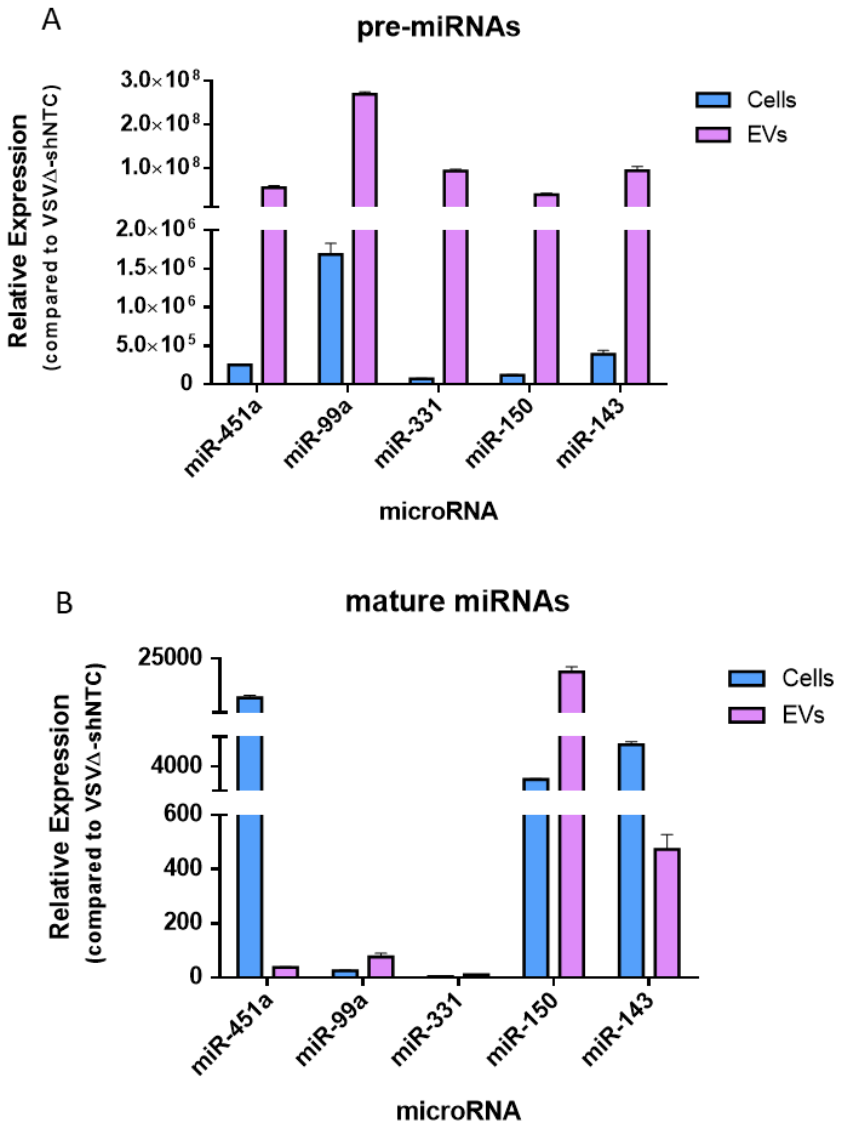

Figure 5.3 qPCR analysis demonstrates each EV-miRNA expressed from VSVΔ51 can be detected in cells and EVs. MiaPaCa2 cells were infected at MOI 3 with VSVΔ51 (G-less) expressing each miRNA for 48 hours. TaqMan qPCR probes for the (A) pre-miRNA versus the (B) mature miRNA for each virus were used to measure expression relative to the shNTC expressing virus. Error bars represent standard error of mean (n=1, 3 technical replicates).

Endogenous miRNAs are functional when expressed from VSV

Chapter 3 revealed some incongruencies between knockdown at the mRNA and protein levels following infection with amiRNAs expressed from VSV; however, qPCR is a very quick and simple way to determine if there may be any functionality to then follow-up with other methods to interrogate protein expression. Hence, qPCR analysis of two or more genes predicted to be targeted by each EV-miRNA (TargetScan.org prediction) was used to demonstrate that there is a significant decrease at the mRNA level of each gene (**Figure 5.4**).

More importantly, it was essential to develop a method to evaluate the functionality of each miRNA at the protein level. I began working with a commonly used commercially available dual reporter assay which utilizes *Firefly* luciferase as an internal control and *Renilla* luciferase as a reporter by cloning miRNA target sequences into the 3' UTR of the *Renilla* sequence. Unfortunately, after many trials I determined that the variability of luciferase expression following infection with VSV would not permit reliable comparisons to be made between viruses. Thus, I began testing a different vector (referred to as LSB-miR-X in accompanying figures) which encodes two fluorescent proteins, EBFP2 (internal control) and mKate2 (reporter with miRNA recognition sequence at 3' UTR).

As described above, miR-150 was of particular interest given its multifaceted participation in immune cell differentiation and activation as well as the potential for direct action on cancer cell growth and spread. Additionally, the entire pri-miR-150 was available in a mammalian expression vector from Addgene thus I was able to quickly PCR amplify the entire sequence, adding restriction enzyme sites to both ends for cloning into VSV to compare the efficacy of knockdown by pre-miRNA versus pri-miRNA expressing viruses.

The LSB-miR-150 reporter was available with two different target sequences located at the 3' UTR of mKate2, a miR-150-3p or a miR-150-5p recognition site. Thus, these vectors could easily distinguish which strand of the processed miR-150 was more active; in this case the 5p strand is reported to be the active guide strand and the 3p acts as the passenger strand. As expected, a significantly higher knockdown of mKate2 was observed when the miR-150-5p target sequence was transfected whereas only small decreases in mKate2 signal were observed for the miR-150-3p target sequence. Quite interestingly, this was only true for the pre-miR-150 expressing virus, not the pri-miR-150. In fact, VSV-pri-miR-150 did not knock down either target sequence (**Figure 5.5**).

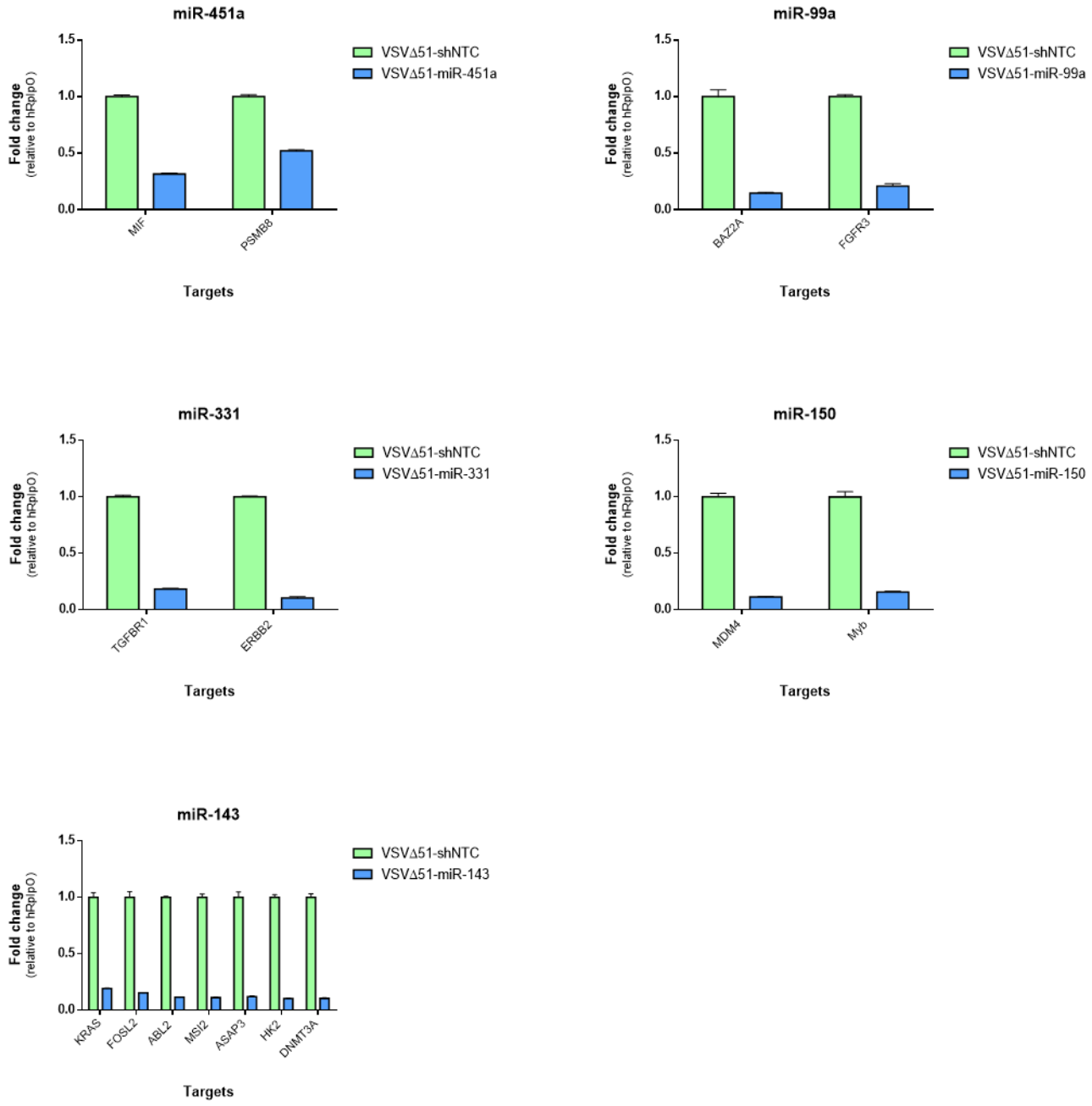

Figure 5.4 qPCR analysis demonstrates a significant decrease in the expression of genes targeted by each EV-miRNA expressing virus. 786-O cells were infected for 48 hours at an MOI of 3 with VSVΔ51ΔG. Error bars represent standard error of mean (n=1, 3 technical replicates).

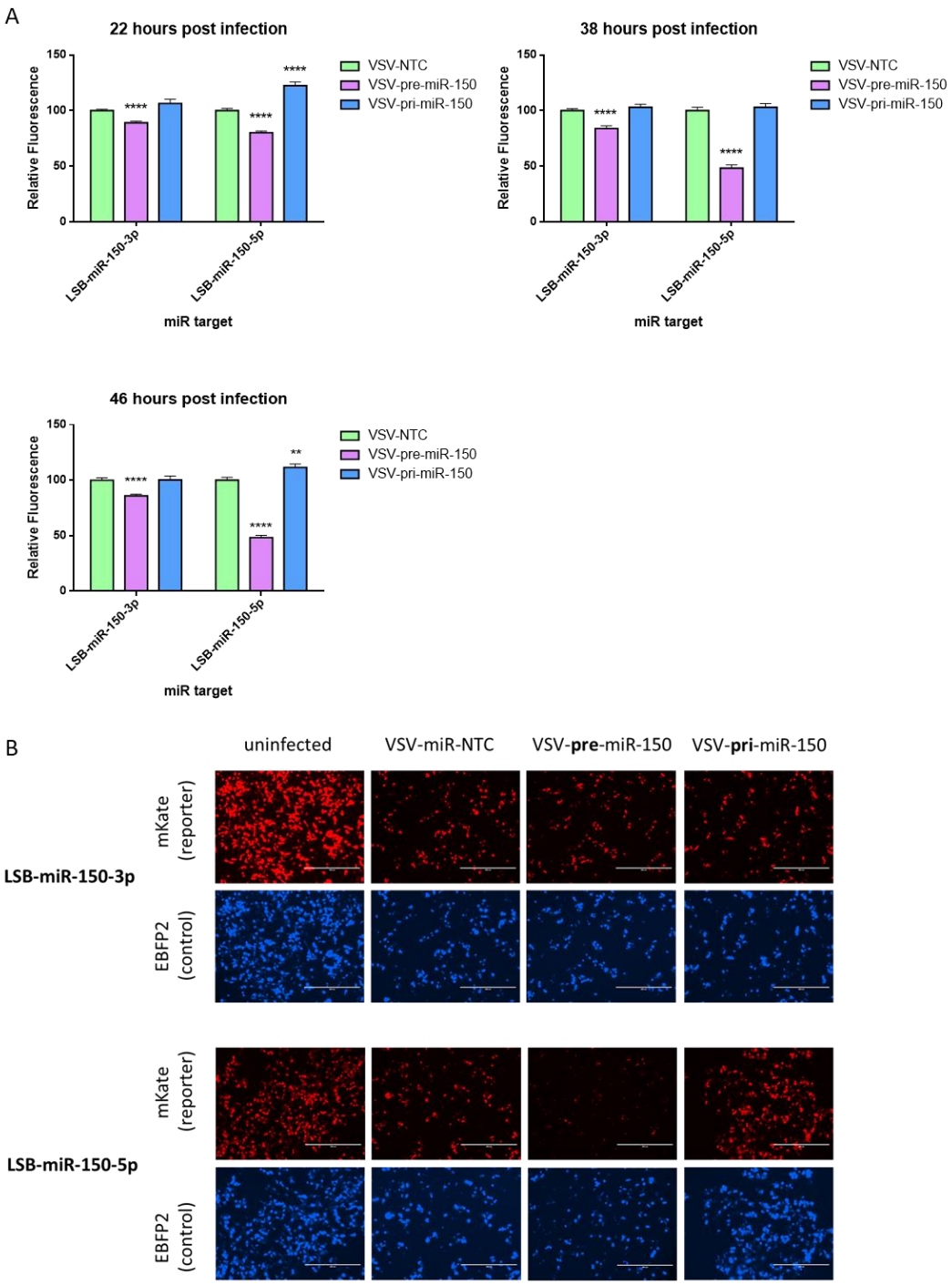

Figure 5.5 LSB-mKate dual-fluorescent reporter demonstrating knockdown of miR-150-5p target sequence by VSVΔ51-pre-miR-150. Cells were transfected with the reporter plasmid approximately 6 hours prior to infection at MOI 0.1. (A) The relative expression of mKate/EBFP2 is shown for each condition with VSV-shNTC set to 100%. Plates were scanned at 22, 38 and 46 hours post infection. (B) Fluorescent images were captured at 38 hours post infection. Error bars represent standard error of mean (n=10, 5 technical x 2 biological replicates). Unpaired two-tailed t-test was used to evaluate statistical significance (**P<0.01, ****P<0.0001).

Unfortunately, due to the inherently repetitive sequences within this backbone many of the reporters I have attempted to test do not produce a dual fluorescent signal before any infection has even taken place. After screening a number of colonies for each reporter, one intact miR-143-3p and 5p pair was identified and I completed a pilot test of the VSV-miR-143 (**Figure 5.6**). To expand our use of these vectors, I have re-purposed one of the 'functional' plasmids into an empty vector with a multiple cloning site to insert any miRNA target sequence of our choice within the 3' UTR of mKate. This will be a useful tool to not only test the function of the various miRNAs discussed here but may now be used as a quick method to screen the ability of any artificial miRNA to knock down a specific target.

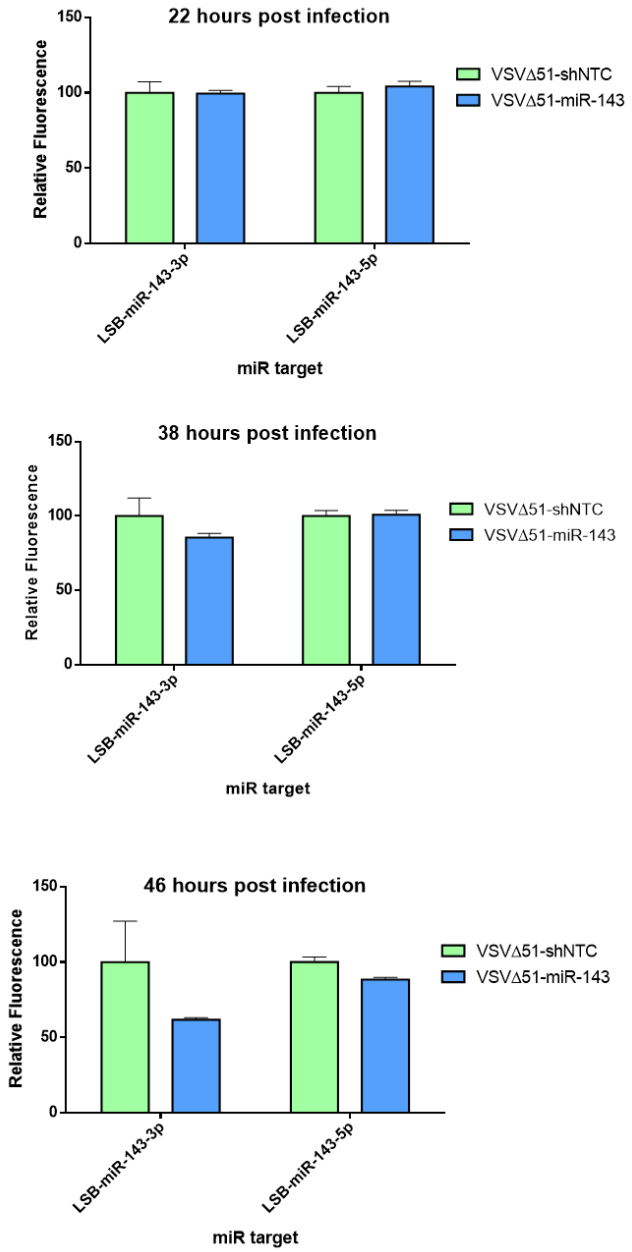

Figure 5.6 LSB-mKate dual-fluorescent reporter demonstrating knockdown of miR-143-3p target sequence by VSVΔ51-miR-143. Cells were transfected with the reporter plasmid approximately 6 hours prior to infection at MOI 0.1. (A) The relative expression of mKate/EBFP2 is shown for each condition with VSV-shNTC set to 100%. Plates were scanned at 22, 38 and 46 hours post infection. Due to the variability of infection there is a trend towards miR-143-3p knockdown at 46 hours post infection, however this is not technically significant (via t test comparing VSV-shNTC to VSV-miR-143). Error bars represent standard error of mean (n=5 technical replicates).

Expression of miR-150 from VSV can modulate the tumour immune profile

To begin to assess the functionality of miRNA-expressing VSVΔ51 in the *in vivo* setting, we sought to determine if changes to the tumour immune profile would be evident following VSV-miR-150 infection. The MC38 immunocompetent colorectal tumour model was selected for a pilot *in vivo* experiment. The decision to start with a colorectal cancer model was based on previous reports of improved survival and response to chemotherapy in colorectal cancer patients with high miR-150 expression in addition to further work showing decreased cell proliferation in multiple colorectal cancer tumour cell lines and human xenograft models following miR-150-5p transfection [324,326]. For this pilot experiment, I infected MC38 tumours intratumourally (IT) with either control VSV-shNTC or VSV-miR-150 (or PBS control) once daily for three days and collected both tumours and spleens six days after the last injection. Prior to beginning this experiment, I have also confirmed robust expression and processing of miR-150 expressed from VSV in the MC38 cell line via qPCR probing for the fully processed, mature, miR-150 (**Figure 5.7**). Importantly, while the stem-loop sequence of mmu-miR-150 (mouse) is slightly shorter than hsa-miR-150 (human; used here), the mature sequence of the two are identical (mirbase.org). Based on the previous results VSV-pre-miR-150 was used in this experiment not VSV-pri-miR-150.

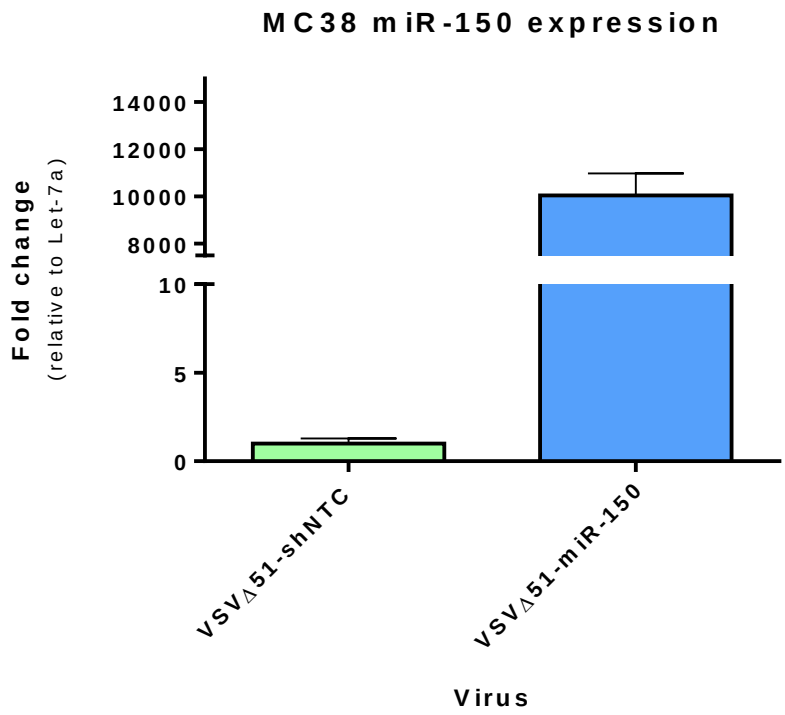

Figure 5.7 qPCR analysis of mature miR-150 expression from MC38 cells infected at MOI 0.1 for 24 hours. Error bars represent standard error of mean (n=1, 3 technical replicates).

I have assessed T cell activation, as well as a few markers for memory versus effector phenotype by flow cytometry. While the results of this initial experiment may not have been statistically significant there are a number of biologically notable trends which have encouraged us to move forward with further development of this aspect of the project. Intriguingly, the most noticeable changes among the T cell populations are occurring within the spleen samples rather than the tumours themselves (**Figure 5.8**). An interesting outcome given that the virus was delivered via the IT route. Following infection with VSV-miR-150 compared to VSV-shNTC there is a decrease in the proportion of $CD4^+$ T cells and an increase in $CD8^+$ T cell staining among splenocytes. We also observe an increase in CD44/CD122 single and double positive $CD8^+$ T staining representing a trend towards memory phenotype effector (gating strategy for flow analysis is shown in **Figure S2.1**).

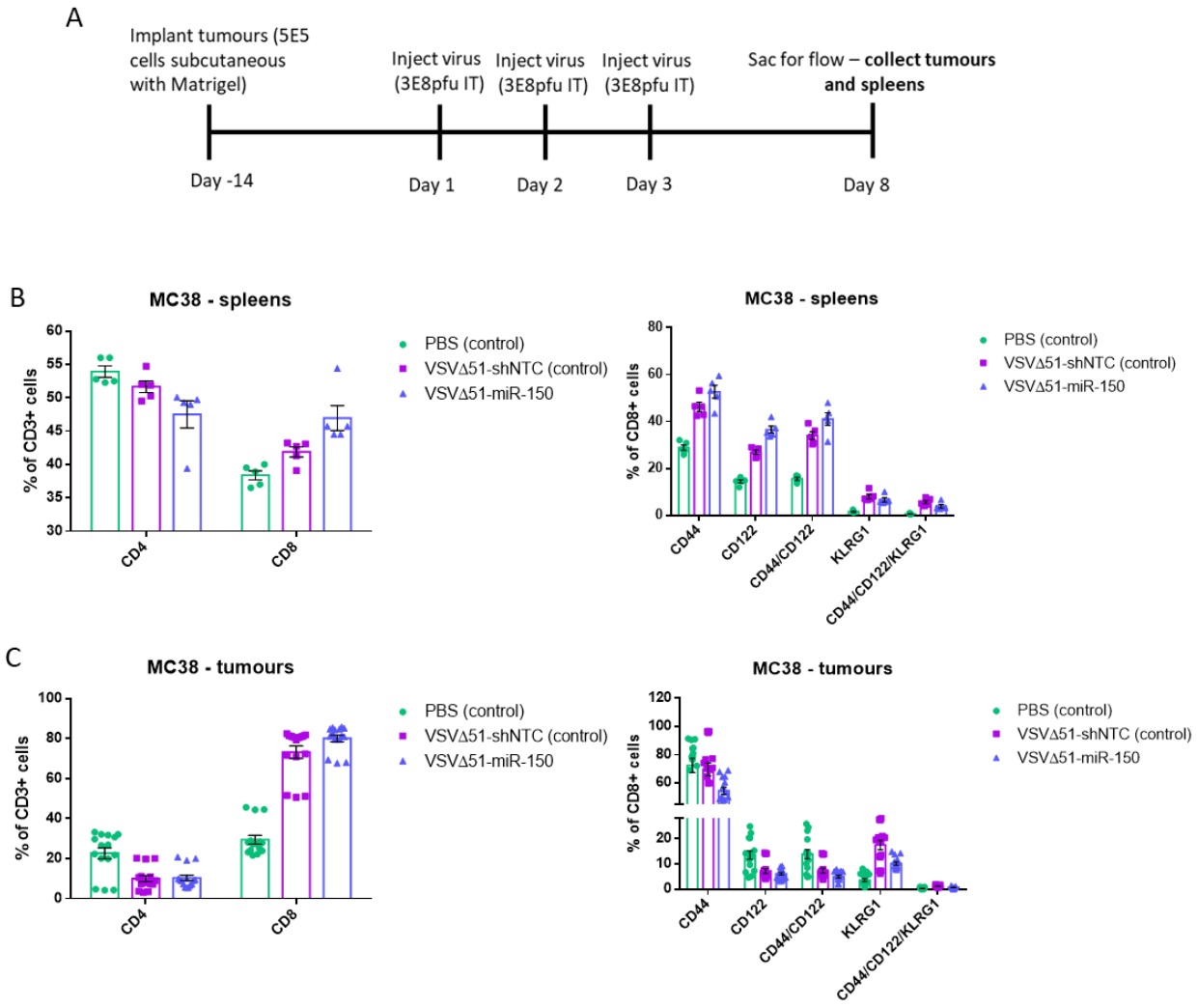

Figure 5.8 Flow cytometry analysis of MC38 (mouse colorectal cancer) cells infected with VSVΔ51-miR-150. (A) Tumours were injected with PBS (control), VSV-shNTC (control) or VSV-miR-150 for three consecutive days and tissues were harvested on day 8. Analysis of (B) splenocytes and (C) tumour cells demonstrate increased CD8+ T cell staining and a shift towards memory phenotype. Each point represents one animal on the splenocyte plots, the tumour samples were run in triplicate thus each point represents one of three technical replicates for five animals total (error bars represent standard error of mean). Unpaired two-tailed t-test comparing VSV-shNTC samples with VSV-miR-150 did not reveal any significant differences between samples.

5.4 Discussion and future directions

The expression of endogenous miRNAs has the potential to target multiple genes

A major advantage of encoding endogenous therapeutic miRNAs as opposed to specifically selected amiRNAs is the ability to knockdown multiple targets using only one miRNA. While qPCR analysis was performed on only two different genes for a majority of the miRNAs under investigation here, each was in fact able to knock down at least two predicted targets and could likely knockdown several more. To fully elucidate the range of genes which may be targeted by each virus, it would be ideal to perform RNA sequencing to compare the RNA profile of cells infected with the non-targeting virus compared to each miRNA. A simpler, more cost effect tool to elucidate the RNA landscape of infected cells could also include microarray analysis.

More importantly, I have established the ability of VSV-pre-miR-150 to knockdown its target sequence at the protein level. The marked difference between pre-miR-150 and pri-miR-150 functionality when expressed from VSV was rather surprising. Prior to infecting cells with each virus, I completed an initial experiment to determine if the pri-miR-150 expressed from a plasmid vector could knockdown the miR-150-5p recognition sequence while incurring minimal impact on the miR-150-3p recognition sequence and this was in fact the case (**Figure 5.9**). Thus, full processing of the pri-miRNA structure was possible prior to inserting it into the virus.

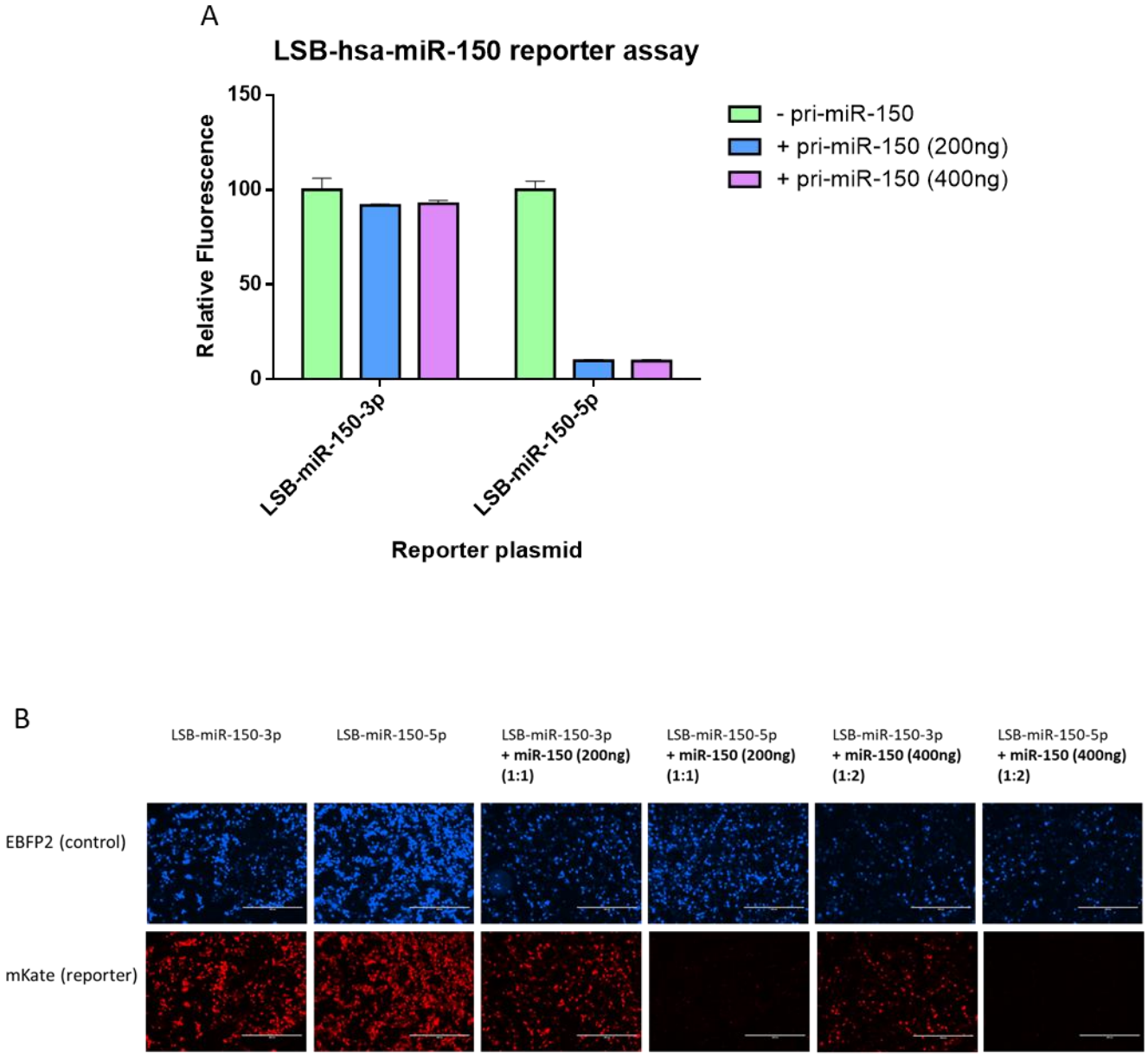

Figure 5.9 LSB-mKate dual-fluorescent reporter demonstrating knockdown of miR-150-5p target sequence by pri-miR-150 plasmid (pcDNA3.2) transfection. Cells were transfected with the reporter plasmid simultaneously with the pri-miR-150 plasmid. (A) The relative expression of mKate/EBFP2 is shown for each condition at 48 hours with LSB-mKate alone set to 100%. (B) Fluorescent images were also captured at 48 hours post transfection. Error bars represent standard error of mean (n=1, 5 technical replicates).

I originally predicted that the pri-miRNA expressing virus may be more effective than its pre-miRNA counterpart based on two related studies. The first is a study in which miR-1 was expressed from oncolytic adenovirus as a short hairpin RNA (shRNA), pre-miRNA, and pri-miRNA. Interestingly, this group found that mature miR-1 expression could be detected at the highest levels when expressed from the pri-miRNA, they also validated that processing was almost completely dependant on Drosha via knockout studies[353]. The next set of studies by tenOever *et al.,* also discussed in the previous chapters, involved the successful expression of pri-miR-124 from influenza A virus and Sindbis virus[354,355]. This group has also successfully inserted a library of artificial sequences into the miRNA-124 backbone for expression from the Influenza backbone[356]. The key difference between adenovirus and influenza when compared with VSV is that replication takes place in the nucleus, unlike VSV which replicates in the cytoplasm, meaning miRNAs expressed from these vectors should have full access to nuclear miRNA processing machinery required for pri-miRNA to pre-miRNA cleavage.

As mentioned previously, an additional study by tenOever *et al.* has shown that translocation of Drosha, required for canonical pri-miRNA processing, out of the nucleus and into the cytoplasm can occur as a result of infection with multiple viruses including VSV[254]. Accordingly, when this group expressed pri-miR-124-2 from Sindbis virus, also a cytoplasmic RNA virus, it was determined that miRNA processing could occur in a Dicer-dependant, Exportin-5 independent manner, establishing that processing could in fact occur in the cytoplasm completely (shown via knockdown of the respective proteins)[253]. Knock out of DGCR8, the RNA-binding protein of the microprocessor which partners with Drosha, revealed that processing could occur independent of DGCR8[253]. Drosha depletion experiments were not explored in this

study; however, the authors did report the presence of a heterogeneous mixture of miR-124 and 'miR-124 like' products of varying lengths thus concluding that an 'uncharacterized' processing pathway may be at play. Further work by the same group aimed to decipher whether a negative sense RNA virus could also produce functional miR-124, to this end they encoded miR-124 into the genome of VSV[357]. While they did demonstrate the ability of cells to process miR-124 expressed from VSV, the functionality was inferred by showing less induction of polypyrimidine tract-binding protein 1 (*Ptbp1*), a known miR-124 target, at the mRNA level compared to infection with VSV alone which has been shown to induce very high levels of *Ptbp1*[357]. Regulation at the protein level was not reported in this study.

The pri-miR-150 sequence carried by the engineered VSV discussed here is identical to the sequence expressed from the plasmid used to validate the dual-fluorescence reporter system (in fact the pri-miRNA expressing plasmid was used for PCR amplification of pri-miR-150 and the segment cloned into VSV was verified by sequencing); therefore, I predict that the main barrier to VSV-pri-miR-150's ability to knockdown its target compared to expression from the plasmid could still be access to efficient processing. The fluorescent reporter assay used here required a relatively high concentration of pri-miR-150 plasmid to successfully knock down its target; therefore, the assay itself may not be sensitive enough to detect a more subtle level of knockdown especially when cells are infected and dying.

While time constraints did not permit this experiment to be completed, miRNA processing could be rather easily determined using TaqMan qPCR probes which bind specifically to the mature miRNA versus the pre-miRNA and pri-miRNA to determine the stage at which the processing may have been stalled. Depletion or knockout of the main miRNA processing proteins

could also be combined with the LSB-mKate dual-fluorescent reporter system to determine at which steps of processing, delays could be occurring. Overall, it is difficult to directly compare the results of only a very small set of miRNAs as there can be significant differences in processing between different miRNAs due to a variety of factors.

Most importantly from a therapeutic standpoint, being able to quickly determine the sequence yielding the most functional knockdown is crucial and the LSB-mKate dual-fluorescent reporter is an ideal system to do so. While VSV-pre-miR-150 produced a much more efficient knockdown of its target in this case compared to VSV-pri-miR-150 this may not be the same across all miRNAs.

Using the new and improved dual-fluorescent reporter system (LSB-mKate) the remaining miRNA expressing viruses can be screened for functionality. More importantly, the ability to quickly modify this vector means we can easily explore the function of amiRNAs to further elucidate the challenges encountered in the previous chapter. Given the convenient 96-well format of this assay many amiRNAs may be engineered and tested after systematically changing key aspects of the stem-loop such as predicted Dicer and Drosha cleavage sites. The dual-fluorescent reporter plasmid may also be transfected into recipient cells which lack various components of the miRNA processing machinery to gain insight into the processing pathway being utilized by miRNAs expressed from VSV.

Pre-miRNAs expressed from VSV are more readily exported into EVs

As anticipated, all five miRNAs were loaded into EVs following infection. Interestingly, the level of each miRNA in the pre-miRNA state was much higher than mature miRNA (**Figure 5.3**).

Previous work by Gibbings *et al*., demonstrated similar results for amiRNAs expressed from the miR-451 cassette as well as miR-451 itself[249]. When comparing the amount of mature EV-miRNA retained within the cells versus EVs here, it was determined that in most cases there was more mature miRNA in the cell rather than the EV fraction. Alternatively, there was relatively low expression within cells overall for select miRNAs (miR-99 and miR-331). Of note, miR-150 is processed preferentially by Ago2 similar to miR-451, although, miR-150 is not completely dependant on Ago2[358]. The propensity for miR-150 to interact with Ago2 is intriguing, as one mechanism by which miRNAs are loaded into miRNAs is in fact binding to Ago2 protein which is then shuttled into EVs; thus, the high level of miR-150 in EVs in both mature and pre-mature state could be due to shuttling of Ago2 as miR-150 undergoes processing[359]. However, this does not necessarily explain why there was a higher proportion of mature miR-451 in the cell fraction compared to EVs. Of note, Gibbings *et al.* also reported a higher presence of mature miR-451 within cells compared with EVs but it is not completely understood why we see this pattern[249]. This experiment was completed at only one timepoint, so it is difficult to say if at an earlier or later point in time there may have been more copies of mature miRNAs in the EVs or not (i.e. are the EVs carrying miR-451 quickly taken back up by the cells or are they truly retain within the cell with pre-miR-451 being the primary exported species?). To fully elucidate the kinetics of EV release following infection it would be ideal to perform a time course experiment. A notable limitation of the described qPCR quantification of mature and pre-miRNAs here is the inability of the assay to distinguish pre-miRNA molecules that are within the viral genome in the cellular fraction versus those that are partially processed and have been released from the genome. Importantly, this is not the case for the mature miRNA molecules as the TaqMan mature miRNA

detection system can specially distinguish mature miRNAs from their unprocessed counterparts (described further in the methods section). Given that G-less versions of each virus were utilized for these infections, we do not expect any virions to be present in the EV fraction; thus, it should be noted that the proportion of pre-miRNAs being shuttled into EVs could be underestimated as some copies detected in the cells may be within the viral genome itself.

Overall, the robust loading of miR-150 into EVs in both its mature and pre-mature form along with high expression of the mature miRNA within the cells themselves, combined with its reported ability to act as an anticancer agent led us to move forward with this miRNA as a promising transgene for VSV.

VSV-miR-150 has the potential to synergize with other immunotherapies

While miR-150 plays a part in regulating a variety of areas of immune system function and development, we aimed to start with a small subset of T cell markers for this pilot experiment given the central role these cells play in the anti-tumour immune response. $CD8^+$ T cells are one of the most important components of the anti-tumour arsenal our immune system houses to keep transformed cells at bay each day. They have also become a primary target in the development of almost all immunotherapies currently in use and under development. Cytotoxic $CD8^+$ T cells survey the body regularly, killing unwanted pathogens and neoplastic cells while $CD4^+$ T play a critical role in maintaining the $CD8^+$ T response, importantly, preventing exhaustion[360].

We were interested in determining how the T cell population was impacted by miR-150 expression from VSV compared to viral infection alone (expressing a non-targeting shRNA). The initial framework and timing of the experiment was based on previous literature demonstrating

that $CD8^+$ T cell population numbers peak by seven days post infection with *Listeria monocytogenes* and six days with Vaccinia virus. Overall, this group found that there were more $CD8^+$ T cells present in blood collected from miR-150 wild type cells compared with their miR-$150^{-/-}$ counterparts. Within this population there were more memory phenotype cells ($CD44^{hi}/CD122^{hi}$) and of these there were a higher proportion of effector phenotype cells ($KLRG1^{hi}$)[338]. Though the results of the MC38 experiment did not reveal any significant change in the expression of KLRG1, we did see a trend towards increased CD44/CD122 expression in the splenocyte $CD8^+$ T cell population (**Figure 5.8**). The subtle changes we observed may have been more prominent with optimized timing. This experiment incorporated multiple components that diverged from the previously reported work including infection with an RNA virus rather than a DNA virus as well as overexpression of miR-150 as opposed to comparing wildtype expression with a knockout model. It will be ideal for future studies to incorporate a time course to determine the point at which the $CD8^+$ T cell population reaches its peak. Though unrefined, this pilot experiment did reveal an increase in the proportion of $CD8^+$ T cells in splenocytes with VSV-miR-150 infection, a promising result with opportunity for further optimization. We also report a slight decrease in the proportion of CD4 expression with VSV-miR-150 infection which is to be expected as miR-150 has been shown to be a negative regulator of $CD4^+$ T cells[361]. It will be informative in future experiments to incorporate counting beads to decipher a more quantitative picture of T cell infiltration and activation within the tumour and/or spleen.

Future experiments will also aim to look further into T cell function given that miR-150 expression has also been shown to impact the production of granzyme B, leading to more potent killing of target cells *in vivo* and *in vitro*[338]. It will also be crucial to decipher whether the increased

presence of T cells will act synergistically with the virus or contribute to the antiviral immune response, reducing the impact of the virus altogether. This initial experiment was not designed in such a way that an impact on tumour burden could be discernable as the tumours were allowed to grow far beyond a size that OV infection would have any impact. The strategy for this experiment was to ensure enough cells could be harvested to obtain robust flow cytometry readouts. Thus, additional follow-up experiments will include survival and tumour burden measurements for the MC38 model as well as other immunocompetent *in vivo* models in addition to titering experiments to determine if VSV-miR-150 is able to infect and replicate at a similar rate as the parental virus.

Looking forward to how VSV-miR-150 could contribute to the field of immunotherapeutic treatments currently under development, we can consider that responses to ICI therapy have been tied closely to high infiltration of effector memory tumour antigen-specific cytotoxic T cells[362]. Thus, it will be interesting to explore if infection with VSV-miR-150 can enhance the potency of ICI therapy by promoting an effector memory phenotype among T cells at the site of the tumour. The use of a model tumour antigen for future experiments could also contribute to determining the proportion of the T cell response that is specific to the tumour itself versus the antiviral response. Another group of new players in the immunotherapy arena are Bispecific T Cell Engagers (BiTES). BiTEs consist of two single chain variable fragments (scFv) connected by a flexible linker, one scFv binds to a T cell specific molecule (generally CD3) and the other binds a tumour-associated antigen, physically bringing T cells in physical contact with tumour cells[363]. There are currently a number of BiTEs undergoing clinical trials and there is in fact a small collection of BiTEs that have been incorporated into OVs[364]. The combination of VSV-miR-150

which aims to increase $CD8^+$ T cell expansion and differentiation could be a perfect partner for BiTE therapy which will enhance the targeting of T cells as the population grows.

Chapter 6: General discussion, future directions, and concluding statement

Re-claiming control of the EV delivery pipeline to deliver therapeutic cargo

Viruses have learned to hijack the cellular EV delivery system for their own selfish purposes, to create a pro-viral niche which encourages infection and discourages anti-viral immune activation[365,366]. Hidden within the cloak of these membrane bound vesicles, viral proteins and genetic material can fly under the immune surveillance radar toward uninfected cells to promote functions which will assist the virus in a variety of ways. For example, human immunodeficiency viruses (HIV) is capable of shuttling its own viral receptors to uninfected cells that normally do not express them to promote infection in a wider range of cell types[367,368]. Small viruses, such as hepatitis C virus (HCV), can hide entirely within EVs to avoid detection by neutralizing antibodies[369,370]. Some viruses have even been shown to alter the miRNA profile of EVs during infection. For example, Newcastle disease virus (NDV) has been shown to strategically alter the expression profile of miRNAs in EVs[371]. In fact, a miRNA array analysis of EVs derived from NDV infected HeLa cells has revealed an increase in the loading of at least three miRNAs (i.e. miR-198, miR-1184, and miR-1273f) known to decrease IFN-β mRNA and protein levels[371,372]. IFN-β plays a key role in activating antiviral signaling pathways; consequently, uninfected cells exposed to artificial vesicles (liposomes in this case) bearing these miRNAs were more sensitive to infection than naïve cells, revealing that EVs from infected cells are likely acting to promote a more pro-virus niche[371,372]. By encouraging the loading of specific miRNAs via overexpression from an OV, the engineered viruses described in this thesis can take control of the EV delivery system to destroy the tumour from within.

The expression of miRNAs from VSV could become a personalized treatment strategy

The scope of miRNA regulation over the human genome goes far beyond the knowledge we currently possess. These seemingly tiny players have an enormous role in the regulation of nearly all cellular processes ranging from cell growth and death pathways, metabolism, embryonic development, and many others[373–375]. Indeed, it has been estimated that miRNAs regulate at least 30% of protein-coding genes[375,376], this number is likely to increase as we learn more about miRNA processing and function. Consequently, harnessing the power of miRNAs to target an entire network of genes simultaneously has become an attractive development for the treatment of multiple diseases including cancer[377]. By using genetic manipulation via miRNA expression, the door has been opened to 'drug the undruggable'[378]. While many researches have began shifting this term to "difficult to drug" based on current advances, namely in the field of small molecule development, there are a number of highly dysregulated proteins associated with cancer development and prognosis that still have yet to be targeted by an effective standard of care treatment[379]. Notably, one group has elected to take down one of the most commonly mutated oncogenes, RAS, using RNA interference technology. Kalluri *et al.* have developed a novel system to specifically target mutated KRAS in pancreatic cancer cells via siRNA delivered within EVs[380]. This very promising example of EV delivery of a therapeutic RNA interference molecule has already reached clinical trials and is currently undergoing a phase I trial (ClinicalTrials.gov Identifier: NCT03608631). This exciting novel treatment strategy has re-enforced one of the main objectives of this project, to determine if we could manipulate EV packaging to preferentially load miRNAs overexpressed from VSV. By creating an EV sorting and packaging facility at the site of the tumour via infection we can bypass many of the time

consuming and likely expensive steps required to load and deliver EVs. Unlike the previous example, the proposed therapy described in this thesis does not require *ex vivo* production and loading of EVs.

While the contents of this thesis focus mainly on the objective of overcoming PARPi resistance as a therapeutic, there are endless other opportunities for miRNA therapy to play a part in the development of 'personalized medicine'. The advent of immunotherapeutic treatment has begun to steer cancer therapies toward more 'precise medicine' via monoclonal antibodies, CAR T therapy, etc. However, in an ideal world we would be able to specifically target genes, pathways, or proteins which have become dysregulated according to each unique tumour. This is of course a huge undertaking and the healthcare system is far from sequencing every single tumour. Alternatively, if we can follow mutational trends such as those used to predict PARPi treatment response and deploy miRNAs to mirror each condition we will be one step closer to personalized medicine.

By encoding endogenous miRNAs into VSV, the work described in this thesis has demonstrated the ability to target multiple genes by one OV while imparting drug sensitizing and immunomodulatory effects. There exist a number of tools to assist in the prediction of miRNA target genes (eg. TargetScan, MicroRNA Target Prediction Database, etc); however due to the complex nature of miRNA interactions it is essential to validate any predicted targets to determine their biological significance at the mRNA and protein level. As previously mentioned, an important next step will be to determine additional targets that could be impacted by our newly engineered viruses via RNA sequencing or RNA microarray analysis and further validation via western blot or reporter such as the dual-fluorescent reporter used here. By fully elucidating

the targets of each virus we might further expand the scope of their application to the treatment of diverse models or to overcome different types of drug resistance.

Are the miRNAs that are packaged in EVs functional and where do they go?

One of the most critical future directions for this work is to determine whether the miRNAs which are loaded in EVs from infected cells can in fact knockdown their respective targets in neighbouring uninfected cells. Several previous studies have proven the functionality of EV derived miRNA and mRNA in recipient cells and have implicated these extracellular RNAs in a variety of disease states including cancer[206,381]. In fact, as previously discussed, our group currently has one manuscript in revisions wherein we demonstrate the ability of an artificial miRNA to enter EVs and exert its effect on neighbouring uninfected cells (Wedge *et al*., in revisions). One of the goals for this project was to improve upon the current work by specifically selecting miRNAs which are preferentially loaded into EVs. Time constraints did not permit optimization of these experiments, but ideally the previously discussed dual-fluorescent reporter system will be used to measure knockdown of target sequences within uninfected cells following the transfer of EVs from VSV-miRNA infected cells. The results presented in Chapter 4 are however quite promising, wherein we can detect ~40% knockdown of BRCA1 and CHEK2 using G-less virus at an MOI of 1; previous work by our group has shown that only ~30% of cells or less can be expected to be infected at this MOI, thus there are likely extracellular miRNAs acting to knockdown targets in uninfected cells.

EV delivery of miRNAs represents a huge advantage over other miRNA delivery systems. Not only are the miRNAs well protected from degradation in these vesicles, EVs are far less

immunogenic and exhibit less toxicity than other carriers such as liposomes and nanoparticles[207,382]. And of course, one of the largest advantages for this proposed therapy is the natural production of miRNA loaded EVs from infected cells. Thus far, our group has not observed off-target effects of miRNA containing EVs during *in vivo* studies of previously developed miRNA expressing viruses. EVs have already been shown to selectively enter specific cells, in fact, *in vitro* tracking of EVs in co-cultured cell populations has revealed that these vesicles are more likely to enter the cell type from which they originated[383], thus, we expect EVs derived from virally infected cancer cells to primarily enter the surrounding cancer cells or those at distant sites by entering the circulatory system. While we do not anticipate systemic toxicity to occur as a result of EV spread based on previous experiments completed by our group, there are methods we can use to track the spread of EVs in addition to incorporating specific targeting systems on the EVs themselves if necessary. For example, *in vivo* imaging systems have been developed to allow for non-invasive tracking of marked EVs via bioluminescent imaging as well as fluorescence detection[384]. There are also exist methods for isolating EVs from tissues and plasma which may be used to investigate if the miRNAs are travelling to distant sites or remaining within the tumour[385,386]. If off-target EV trafficking becomes an issue, there are several tools which have been developed to send EVs on a targeted trajectory. For example, our group and others have taken advantage of the EV surface protein lysosome-associated membrane protein 2b (Lamp2b) to display various ligands on the outside of EVs to promote their uptake into specific cell types[387]. Specific targeting moieties can also be fused to transmembrane protein tetraspanins including CD9 and CD63, which are considered general markers of EVs due to their nearly ubiquitous expression across EV populations [388].

Combination therapy is standard practice for the treatment of cancer

The use of two or more therapeutics is now a mainstay for the treatment of nearly all types of cancer. This typically includes any or all therapeutic modalities including chemotherapy, radiation, surgery and most recently immunotherapy. The expression of a miRNA from VSV represents an interesting combination on its own, especially in the case of the immunomodulatory miR-150. Looking forward there could be opportunities to explore VSV-miRNA infection in collaboration with a number of other therapeutics. One of the simplest options will be determining if there is any limit to the quantity of miRNAs we can express from VSV. I have demonstrated the ability of VSV to successfully express two miR-182 hairpins, with the double hairpin virus achieving a more potent knockdown of multiple targets. Therefore, it is likely that multiple tandem miRNAs could be expressed from the same virus to target several genes simultaneously. More interestingly, both VSV-miR-182 and -miR-150 have the potential to synergize with additional immunotherapeutics such as ICI or BiTEs. PARPi mediated DNA damage has previously been shown to increase PD-L1 expression on cancer cells[389]. OVs themselves have also been shown to enhance the efficacy of ICI treatment by essentially turning a immunologically "cold" tumour "hot" by increasing immune infiltration and activation[390]. Taken together, a triple therapy including VSV-miR-182, ICI, and PARPi could act synergistically to decrease tumour burden and increase survival. The ability of BiTEs to synergize with OVs has been demonstrated as well, in fact, the expression of BiTEs from OVs themselves is a current area of investigation[364]. The ability of VSV-miR-150 to activate the adaptive immune system via $CD8^+$ T cell differentiation and activation could be just appetizing enough for the immune system to take a BiTE out of a tumour (increasing efficacy of BiTE treatment).

Concluding statement

The work described in this thesis has demonstrated the ability of oncolytic VSV to express several unique miRNAs which are functional within the infected cell and are also readily packaged within EVs. While the expression and processing of amiRNAs from VSV remains elusive, the use of naturally occurring endogenous miRNA sequences has opened the door to targeting multiple genes of interest simultaneously using only a single miRNA. The expression of miR-182 from VSV not only has the potential to overcome resistance as a late line therapy in tumours which have developed resistance to PARPi and/or platinum-based chemotherapy, it could also be investigated for use in tumours which are initially BRCA1/2 wild-type as a targeted first line therapeutic, as demonstrated here. Finally, the expression of miR-150 from VSV has the potential to work synergistically with additional immune-modulating therapies. In fact, the combination of miR-150 with miR-182 and PARPi could be the triple-threat therapy needed to induce cell death specifically in cancer cells while engaging the immune system to prevent recurrence in HR deficient cancers. The expression of miRNAs which may be delivered by EVs has the potential to impact protein expression across a variety of cells together with the tumour itself and the TME as a whole. There are several miRNAs which have been proposed as modulators of the TME, some are currently under investigation as potential therapeutics. Indeed, a collection of miRNAs which are known to be preferentially carried by EVs have been implicated as cancer suppressors as well. Thus, our current working model proposes the use of diverse miRNAs expressed from VSV which may be used alone or in combination with other complementary therapies, such as PARPi described here, to target the tumour and its supportive surrounding niche (Summarized in **Figure 6.1**).

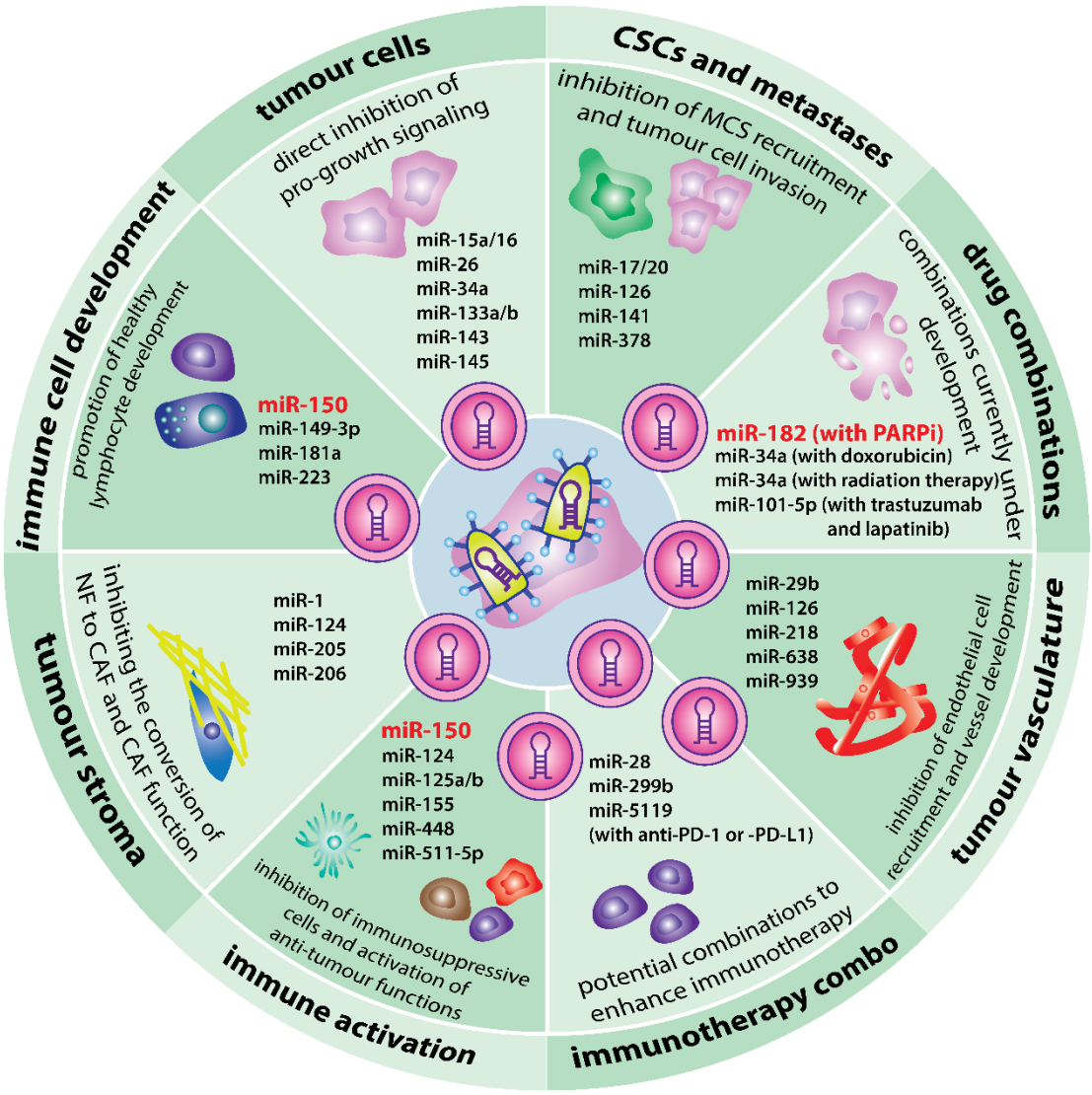

Figure 6.1 Summary of potential therapeutic anti-cancer miRNAs for expression from VSVΔ51 and delivery to TME by EVs. Tumour cells: miR-15a/16[391], miR-26[392], miR-34a[393], miR-133a/b[394], miR-143[395], miR-145[394]. CSCs and metastases: miR-17/20 cluster[396], miR-126[397], miR-141[398], miR-378[398]. Drug combinations: miR-34a (with doxorubicin)[399], miR-34a (with radiation therapy)[400], miR-101-5p (with trastuzumab and lapatinib)[401]. Tumour vasculature: miR-29b[402], miR-126[403], miR-218[404], miR-638[405], miR-939[406]. Immune activation: miR-124[407], miR-125a[408], miR-125b[409], miR-155[410], miR-448[411], miR-511-3p[412]. Immunotherapy combinations: miR-28 (with anti-PD-1 or PD-L1)[413], miR-200b (with anti-PD-1 or PD-L1)[414], miR-5119 (with anti-PD-1 or PD-L1)[415]. Tumour stroma: miR-1[416], miR-206[416], miR-205[417], miR-124[418]. (Abbreviations: NF - normal fibroblast; CAF – cancer associated fibroblast; PD-1 – programmed cell death protein 1, PD-L1 - programmed death – ligand 1; MSC – mesenchymal stem cell; CSC – cancer stem cell) [artwork created using Adobe Illustrator CS6]

References

1. Hanahan, D. & Weinberg, R. A. Hallmarks of cancer: The next generation. *Cell* **144**, 646–674 (2011).
2. Maacha, S. *et al.* Extracellular vesicles-mediated intercellular communication: Roles in the tumor microenvironment and anti-cancer drug resistance. *Mol. Cancer* **18**, 1–16 (2019).
3. Jamieson, T. R., Poutou, J. & Ilkow, C. S. Redirecting oncolytic viruses: Engineering opportunists to take control of the tumour microenvironment. *Cytokine and Growth Factor Reviews* **56**, 102–114 (2020).
4. Eble, J. A. & Niland, S. The extracellular matrix in tumor progression and metastasis. *Clin. Exp. Metastasis* **36**, 171–198 (2019).
5. Kalluri, R. The biology and function of fibroblasts in cancer. *Nat. Rev. Cancer* **16**, 582–598 (2016).
6. Hanahan, D. & Coussens, L. M. Accessories to the Crime: Functions of Cells Recruited to the Tumor Microenvironment. *Cancer Cell* **21**, 309–322 (2012).
7. Crupi, M. J. F., Bell, J. C. & Singaravelu, R. Concise Review: Targeting Cancer Stem Cells and Their Supporting Niche Using Oncolytic Viruses. *Stem Cells* **37**, 716–723 (2019).
8. Malhotra, V. & Perry, M. C. Classical chemotherapy: mechanisms, toxicities and the therapeutic window. *Cancer biology & therapy* **2**, (2003).
9. Goutsouliak, K. *et al.* Towards personalized treatment for early stage HER2-positive breast cancer. *Nature Reviews Clinical Oncology* **17**, 233–250 (2020).
10. Jabbour, E., Paul, S. & Kantarjian, H. The clinical development of antibody–drug conjugates — lessons from leukaemia. *Nature Reviews Clinical Oncology* 1–16 (2021). doi:10.1038/s41571-021-00484-2
11. Huang, L., Jiang, S. & Shi, Y. Tyrosine kinase inhibitors for solid tumors in the past 20 years (2001–2020). *Journal of Hematology and Oncology* **13**, 143 (2020).
12. Krauss, K. & Stickeler, E. Endocrine Therapy in Early Breast Cancer. *Breast Care* **15**, 337–346 (2020).
13. Bejarano, L., Jordão, M. J. C. & Joyce, J. A. Therapeutic targeting of the tumor microenvironment. *Cancer Discovery* **11**, (2021).
14. Roma-Rodrigues, C., Mendes, R., Baptista, P. V. & Fernandes, A. R. Targeting tumor microenvironment for cancer therapy. *International Journal of Molecular Sciences* **20**, (2019).
15. Miki, Y. *et al.* A strong candidate for the breast and ovarian cancer susceptibility gene BRCA1. *Science (80-.).* **266**, 66–71 (1994).
16. Wooster, R. *et al.* Localization of a breast cancer susceptibility gene, BRCA2, to chromosome 13q12-13. *Science (80-.).* **265**, 2088–2090 (1994).
17. Hall, J. M. *et al.* Linkage of early-onset familial breast cancer to chromosome 17q21. *Science (80-.).* **250**, 1684–1689 (1990).
18. Stratton, M. R. *et al.* Familial male breast cancer is not linked to the BRCA1 locus on chromosome 17q. *Nat. Genet.* **7**, 103–107 (1994).
19. Wooster, R. *et al.* Identification of the breast cancer susceptibility gene BRCA2. *Nature*

378, 789–792 (1995).
20. CDC - Hereditary Breast and Ovarian Cancer Syndrome - Gynecologic Cancer Curriculum - Inside Knowledge Campaign. Available at: https://www.cdc.gov/cancer/knowledge/provider-education/genetics/hboc-syndrome.htm. (Accessed: 18th August 2018)
21. Godet, I. & Gilkes, D. M. BRCA1 and BRCA2 mutations and treatment strategies for breast cancer. *Integr. cancer Sci. Ther.* **4**, (2017).
22. Gudmundsdottir, K. & Ashworth, A. The roles of BRCA1 and BRCA2 and associated proteins in the maintenance of genomic stability. *Oncogene* **25**, 5864–5874 (2006).
23. Smith, S. A., Easton, D. F., Evans, D. G. R. & Ponder, B. A. J. Allele losses in the region 17q12–21 in familial breast and ovarian cancer involve the wild–type chromosome. *Nat. Genet.* **2**, 128–131 (1992).
24. Gudmundsson, J. *et al.* Different Tumor Types from BRCA2 Carriers Show Wild-Type Chromosome Deletions on 13q12–q13. *Cancer Res.* **55**, (1995).
25. Canadian cancer statistics | Canadian Cancer Society. Available at: https://action.cancer.ca/en/research/cancer-statistics/canadian-cancer-statistics. (Accessed: 3rd May 2021)
26. Cancer Statistics Review, 1975-2017 - SEER Statistics. Available at: https://seer.cancer.gov/archive/csr/1975_2017/. (Accessed: 3rd May 2021)
27. Kuchenbaecker, K. B. *et al.* Risks of breast, ovarian, and contralateral breast cancer for BRCA1 and BRCA2 mutation carriers. *JAMA - J. Am. Med. Assoc.* **317**, 2402–2416 (2017).
28. Antoniou, A. *et al.* Average risks of breast and ovarian cancer associated with BRCA1 or BRCA2 mutations detected in case series unselected for family history: A combined analysis of 22 studies. *Am. J. Hum. Genet.* **72**, 1117–1130 (2003).
29. Chen, S. & Parmigiani, G. Meta-analysis of BRCA1 and BRCA2 penetrance. *J. Clin. Oncol.* **25**, 1329–1333 (2007).
30. Narod, S. A. Modifiers of risk of hereditary breast and ovarian cancer. *Nature Reviews Cancer* **2**, 113–123 (2002).
31. Hodgson, A. & Turashvili, G. Pathology of Hereditary Breast and Ovarian Cancer. *Front. Oncol.* **10**, 2026 (2020).
32. Lakhani, S. R. *et al.* The Pathology of Familial Breast Cancer: Histological Features of Cancers in Families Not Attributable to Mutations in BRCA1 or BRCA2. *Clin. Cancer Res.* **6**, (2000).
33. Lakhani, S. R. *et al.* The pathology of familial breast cancer: predictive value of immunohistochemical markers estrogen receptor, progesterone receptor, HER-2, and p53 in patients. *J Clin Oncol* **20**, 2310–2318 (2002).
34. Perou, C. M. *et al.* Molecular portraits of human breast tumours. *Nature* **406**, 747–752 (2000).
35. Semmler, L., Reiter-Brennan, C. & Klein, A. BRCA1 and breast cancer: A review of the underlying mechanisms resulting in the tissue-specific tumorigenesis in mutation carriers. *J. Breast Cancer* **22**, 1–14 (2019).
36. Singh, A. K. & Yu, X. Tissue-Specific Carcinogens as Soil to Seed BRCA1/2-Mutant Hereditary Cancers. *Trends in Cancer* **6**, 559–568 (2020).
37. Yoshida, R. Hereditary breast and ovarian cancer (HBOC): review of its molecular

characteristics, screening, treatment, and prognosis. *Breast Cancer* **1**, 3 (2020).
38. Widschwendter, M. *et al.* The sex hormone system in carriers of BRCA1/2 mutations: A case-control study. *Lancet Oncol.* **14**, 1226–1232 (2013).
39. Mullan, P. B., Quinn, J. E. & Harkin, D. P. The role of BRCA1 in transcriptional regulation and cell cycle control. *Oncogene* **25**, 5854–5863 (2006).
40. Savage, K. I. *et al.* Brca1 deficiency exacerbates estrogen-induced dna damage and genomic instability. *Cancer Res.* **74**, 2773–2784 (2014).
41. Fridlich, R., Annamalai, D., Roy, R., Bernheim, G. & Powell, S. N. BRCA1 and BRCA2 protect against oxidative DNA damage converted into double-strand breaks during DNA replication. *DNA Repair (Amst).* **30**, 11–20 (2015).
42. Nolan, E., Lindeman, G. J. & Visvader, J. E. Out-RANKing BRCA1 in Mutation Carriers. *Cancer Research* **77**, 595–600 (2017).
43. Li, W., Xiao, C., Vonderhaar, B. K. & Deng, C. X. A role of estrogen/ERα signaling in BRCA1-associated tissue-specific tumor formation. *Oncogene* **26**, 7204–7212 (2007).
44. Moslemi, M. *et al.* The association between ATM variants and risk of breast cancer: a systematic review and meta-analysis. *BMC Cancer* **21**, 1–12 (2021).
45. Swift, M., Sholman, L., Perry, M. & Chase, C. Malignant Neoplasms in the Families of Patients with Ataxia-Telangiectasia. *Cancer Res.* **36**, (1976).
46. Thorstenson, Y. R. *et al.* Contributions of ATM Mutations to Familial Breast and Ovarian Cancer. *Cancer Res.* **63**, (2003).
47. Suszynska, M. & Kozlowski, P. Summary of bard1 mutations and precise estimation of breast and ovarian cancer risks associated with the mutations. *Genes (Basel).* **11**, 1–18 (2020).
48. Khan, F. & Naab, T. BRCA1 and BRIP1 Mutations Associated with Triple Positive Invasive Poorly Differentiated Breast Ductal Carcinoma. *Am. J. Clin. Pathol.* **146**, 104–142 (2016).
49. Suszynska, M., Ratajska, M. & Kozlowski, P. BRIP1, RAD51C, and RAD51D mutations are associated with high susceptibility to ovarian cancer: Mutation prevalence and precise risk estimates based on a pooled analysis of ~30,000 cases. *J. Ovarian Res.* **13**, 1–11 (2020).
50. Erkko, H. *et al.* A recurrent mutation in PALB2 in Finnish cancer families. *Nature* **446**, 316–319 (2007).
51. Rahman, N. *et al.* PALB2, which encodes a BRCA2-interacting protein, is a breast cancer susceptibility gene. *Nat. Genet.* **39**, 165–167 (2007).
52. Tischkowitz, M. *et al.* Analysis of PALB2/FANCN-associated breast cancer families. *Proc. Natl. Acad. Sci. U. S. A.* **104**, 6788–6793 (2007).
53. Meijers-Heijboer, H. *et al.* Low-penetrance susceptibility to breast cancer due to CHEK2*1100delC in noncarriers of BRCA1 or BRCA2 mutations: The CHEK2-breast cancer consortium. *Nat. Genet.* **31**, 55–59 (2002).
54. Wu, X., Webster, S. R. & Chen, J. Characterization of Tumor-associated Chk2 Mutations. *J. Biol. Chem.* **276**, 2971–2974 (2001).
55. Vahteristo, P. *et al.* A CHEK2 genetic variant contributing to a substantial fraction of familial breast cancer. *Am. J. Hum. Genet.* **71**, 432–438 (2002).
56. Lord, C. J. & Ashworth, A. BRCAness revisited. *Nat. Rev. Cancer* **16**, 110–120 (2016).
57. Narod, S. A. & Foulkes, W. D. BRCA1 and BRCA2: 1994 and beyond. *Nature Reviews*

Cancer **4**, 665–676 (2004).
58. Greer, J. B. & Whitcomb, D. C. Role of BRCA1 and BRCA2 mutations in pancreatic cancer. *Gut* **56**, 601–605 (2007).
59. Gallagher, D. J. *et al.* Germline BRCA mutations denote a clinicopathologic subset of prostate cancer. *Clin. Cancer Res.* **16**, 2115–2121 (2010).
60. Alexandrov, L. B., Nik-Zainal, S., Siu, H. C., Leung, S. Y. & Stratton, M. R. A mutational signature in gastric cancer suggests therapeutic strategies. *Nat. Commun.* **6**, 1–7 (2015).
61. Couch, F. J. *et al.* The prevalence of BRCA2 mutations in familial pancreatic cancer. *Cancer Epidemiol. Biomarkers Prev.* **16**, 342–346 (2007).
62. Mersch, J. *et al.* Cancers associated with BRCA1 and BRCA2 mutations other than breast and ovarian. *Cancer* **121**, 269–275 (2015).
63. Gumaste, P. V. *et al.* Skin cancer risk in BRCA1/2 mutation carriers. *British Journal of Dermatology* **172**, 1498–1506 (2015).
64. Sugasawa, K. *et al.* A multistep damage recognition mechanism for global genomic nucleotide excision repair. *Genes Dev.* **15**, 507–521 (2001).
65. Mellon, I., Spivak, G. & Hanawalt, P. C. Selective removal of transcription-blocking DNA damage from the transcribed strand of the mammalian DHFR gene. *Cell* **51**, 241–249 (1987).
66. Lindahl, T. & Wood, R. D. Quality control by DNA repair. *Science* **286**, 1897–1905 (1999).
67. Hoeijmakers, J. H. J. Genome maintenance mechanisms for preventing cancer. *Nature* **411**, 366–374 (2001).
68. Sonoda, E., Hochegger, H., Saberi, A., Taniguchi, Y. & Takeda, S. Differential usage of non-homologous end-joining and homologous recombination in double strand break repair. *DNA Repair (Amst).* **5**, 1021–1029 (2006).
69. O'Driscoll, M. & Jeggo, P. A. The role of double-strand break repair - Insights from human genetics. *Nature Reviews Genetics* **7**, 45–54 (2006).
70. Jeggo, P. A. & Löbrich, M. DNA double-strand breaks: Their cellular and clinical impact? *Oncogene* **26**, 7717–7719 (2007).
71. Takata, M. *et al.* Homologous recombination and non-homologous end-joining pathways of DNA double-strand break repair have overlapping roles in the maintenance of chromosomal integrity in vertebrate cells. *EMBO J.* **17**, 5497–5508 (1998).
72. Kadyk, L. C. & Hartwell, L. H. Sister chromatids are preferred over homologs as substrates for recombinational repair in Saccharomyces cerevisiae. *Genetics* **132**, (1992).
73. Ma, Y., Lu, H., Schwarz, K. & Lieber, M. R. Repair of double-strand DNA breaks by the human non-homologous DNA end joining pathway: The iterative processing model. *Cell Cycle* **4**, 1193–1200 (2005).
74. Grawunder, U. *et al.* Activity of DNA ligase IV stimulated by complex formation with XRCC4 protein in mammalian cells. *Nature* **388**, 492–495 (1997).
75. Mimoris, T. & Hardin, J. A. *Mechanism of Interaction between Ku Protein and DNA**. *Journal of Biological Chemistry* **261**, (1986).
76. Scully, R., Panday, A., Elango, R. & Willis, N. A. DNA double-strand break repair-pathway choice in somatic mammalian cells. *Nature Reviews Molecular Cell Biology* **20**, 698–714 (2019).
77. Lee, J. H. & Paull, T. T. ATM activation by DNA double-strand breaks through the Mre11-

Rad50-Nbs1 complex. *Science (80-.).* **308**, 551–554 (2005).
78. Prakash, R., Zhang, Y., Feng, W. & Jasin, M. Homologous recombination and human health: The roles of BRCA1, BRCA2, and associated proteins. *Cold Spring Harb. Perspect. Biol.* **7**, a016600 (2015).
79. Roy, R., Chun, J. & Powell, S. N. BRCA1 and BRCA2: Different roles in a common pathway of genome protection. *Nature Reviews Cancer* **12**, 68–78 (2012).
80. Wright, W. D., Shah, S. S. & Heyer, W. D. Homologous recombination and the repair of DNA double-strand breaks. *Journal of Biological Chemistry* **293**, 10524–10535 (2018).
81. Powell, S. N. & Kachnic, L. A. Roles of BRCA1 and BRCA2 in homologous recombination, DNA replication fidelity and the cellular response to ionizing radiation. *Oncogene* **22**, 5784–5791 (2003).
82. Scully, R. *et al.* Association of BRCA1 with Rad51 in mitotic and meiotic cells. *Cell* **88**, 265–275 (1997).
83. Sharan, S. K. *et al.* Embryonic lethality and radiation hypersensitivity mediated by Rad51 in mice lacking Brca2. *Nature* **386**, 804–810 (1997).
84. Chen, J. *et al.* Stable interaction between the products of the BRCA1 and BRCA2 tumor suppressor genes in mitotic and meiotic cells. *Mol. Cell* **2**, 317–328 (1998).
85. Chen, J. J., Silver, D., Cantor, S., Livingston, D. M. & Scully, R. BRCA1, BRCA2, and Rad51 operate in a common DNA damage response pathway. in *Cancer Research* **59**, 1752s-1756s (American Association for Cancer Research Inc., 1999).
86. Yoshida, K. & Miki, Y. Role of BRCA1 and BRCA2 as regulators of DNA repair, transcription, and cell cycle in response to DNA damage. *Cancer Sci.* **95**, 866–871 (2004).
87. Li, M. L. & Greenberg, R. A. Links between genome integrity and BRCA1 tumor suppression. *Trends in Biochemical Sciences* **37**, 418–424 (2012).
88. Christensen, D. E., Brzovic, P. S. & Klevit, R. E. E2-BRCA1 RING interactions dictate synthesis of mono- or specific polyubiquitin chain linkages. *Nat. Struct. Mol. Biol.* **14**, 941–948 (2007).
89. Morris, J. R. & Solomon, E. BRCA1: BARD1 induces the formation of conjugated ubiquitin structures, dependent on K6 of ubiquitin, in cells during DNA replication and repair. *Hum. Mol. Genet.* **13**, 807–817 (2004).
90. Yu, X., Chini, C. C. S., He, M., Mer, G. & Chen, J. The BRCT Domain Is a Phospho-Protein Binding Domain. *Science (80-.).* **302**, 639–642 (2003).
91. Cantor, S. B. & Guillemette, S. Hereditary breast cancer and the BRCA1-associated FANCJ/BACH1/BRIP1. *Future Oncology* **7**, 253–261 (2011).
92. Wong, A. K. C. *et al.* Characterization of a carboxy-terminal BRCA1 interacting protein. *Oncogene* **17**, 2279–2285 (1998).
93. Lee, J. S., Collins, K. M., Brown, A. L., Lee, C. H. & Chung, J. H. hCds1-mediated phosphorylation of BRCA1 regulates the DNA damage response. *Nature* **404**, 201–204 (2000).
94. Tibbetts, R. S. *et al.* Functional interactions between BRCA1 and the checkpoint kinase ATR during genotoxic stress. *Genes Dev.* **14**, 2989–3002 (2000).
95. Gatei, M. *et al.* Ataxia telangiectasia mutated (ATM) kinase and ATM and Rad3 related kinase mediate phosphorylation of Brca1 at distinct and overlapping sites. In vivo assessment using phospho-specific antibodies. *J. Biol. Chem.* **276**, 17276–17280 (2001).

96. Hanenberg, H. & Andreassen, P. R. PALB2 (partner and localizer of BRCA2). *Atlas of Genetics and Cytogenetics in Oncology and Haematology* **22**, 484–490 (2018).
97. Wong, A. K. C., Pero, R., Ormonde, P. A., Tavtigian, S. V. & Bartel, P. L. RAD51 interacts with the evolutionarily conserved BRC motifs in the human breast cancer susceptibility gene brca2. *J. Biol. Chem.* **272**, 31941–31944 (1997).
98. Yang, H. *et al.* BRCA2 function in DNA binding and recombination from a BRCA2-DSS1-ssDNA structure. *Science (80-.).* **297**, 1837–1848 (2002).
99. Li, J. *et al.* DSS1 is required for the stability of BRCA2. *Oncogene* **25**, 1186–1194 (2006).
100. Venkitaraman, A. R. How do mutations affecting the breast cancer genes BRCA1 and BRCA2 cause cancer susceptibility? *DNA Repair* **81**, 102668 (2019).
101. Anczuków, O. *et al.* Does the nonsense-mediated mRNA decay mechanism prevent the synthesis of truncated BRCA1, CHK2, and p53 proteins? *Hum. Mutat.* **29**, 65–73 (2008).
102. Findlay, G. M. *et al.* Accurate classification of BRCA1 variants with saturation genome editing. *Nature* **562**, 217–222 (2018).
103. Rebbeck, T. R. *et al.* Association of type and location of BRCA1 and BRCA2 mutations with risk of breast and ovarian cancer. *JAMA - J. Am. Med. Assoc.* **313**, 1347–1361 (2015).
104. Cline, M. S. *et al.* BRCA Challenge: BRCA Exchange as a global resource for variants in BRCA1 and BRCA2. *PLoS Genet.* **14**, e1007752 (2018).
105. Lord, C. J. & Ashworth, A. Mechanisms of resistance to therapies targeting BRCA-mutant cancers. *Nat. Med.* **19**, 1381–1388 (2013).
106. Whicker, M. E., Lin, Z. P., Hanna, R., Sartorelli, A. C. & Ratner, E. S. MK-2206 sensitizes BRCA-deficient epithelial ovarian adenocarcinoma to cisplatin and olaparib. *BMC Cancer* **16**, 550 (2016).
107. Amé, J.-C., Spenlehauer, C. & de Murcia, G. The PARP superfamily. *BioEssays* **26**, 882–893 (2004).
108. Bitler, B. G., Watson, Z. L., Wheeler, L. J. & Behbakht, K. PARP inhibitors: Clinical utility and possibilities of overcoming resistance. *Gynecol. Oncol.* **147**, 695–704 (2017).
109. Chambon, P., Weill, J. D. & Mandel, P. Nicotinamide mononucleotide activation of a new DNA-dependent polyadenylic acid synthesizing nuclear enzyme. *Biochem. Biophys. Res. Commun.* **11**, 39–43 (1963).
110. Satoh, M. S. & Lindahl, T. Role of poly(ADP-ribose) formation in DNA repair. *Nature* **356**, 356–358 (1992).
111. Ström, C. E. *et al.* Poly (ADP-ribose) polymerase (PARP) is not involved in base excision repair but PARP inhibition traps a single-strand intermediate. *Nucleic Acids Res.* **39**, 3166–3175 (2011).
112. Luis Polo, A. M. *et al.* Efficient Single-Strand Break Repair Requires Binding to Both Poly(ADP-Ribose) and DNA by the Central BRCT Domain of XRCC1. *CellReports* **26**, 573-581.e5 (2019).
113. Cook, S. A. & Tinker, A. V. PARP Inhibitors and the Evolving Landscape of Ovarian Cancer Management: A Review. *BioDrugs* (2019). doi:10.1007/s40259-019-00347-4
114. Lord, C. J. & Ashworth, A. PARP inhibitors: Synthetic lethality in the clinic. *Science* **355**, 1152–1158 (2017).
115. Farmer, H. *et al.* Targeting the DNA repair defect in BRCA mutant cells as a therapeutic strategy. *Nature* **434**, 917–921 (2005).

116. Bryant, H. E. *et al.* Specific killing of BRCA2-deficient tumours with inhibitors of poly(ADP-ribose) polymerase. *Nature* **434**, 913–917 (2005).
117. ARUN, B., AKAR, U., GUTIERREZ-BARRERA, A. M., HORTOBAGYI, G. N. & OZPOLAT, B. The PARP inhibitor AZD2281 (Olaparib) induces autophagy/mitophagy in BRCA1 and BRCA2 mutant breast cancer cells. *Int. J. Oncol.* **47**, 262–268 (2015).
118. Clements, K. E. *et al.* Loss of E2F7 confers resistance to poly-ADP-ribose polymerase (PARP) inhibitors in BRCA2-deficient cells. *Nucleic Acids Res.* **46**, 8898–8907 (2018).
119. Giovannini, S., Weller, M.-C., Repmann, S., Moch, H. & Jiricny, J. Synthetic lethality between BRCA1 deficiency and poly(ADP-ribose) polymerase inhibition is modulated by processing of endogenous oxidative DNA damage. *Nucleic Acids Res.* (2019). doi:10.1093/nar/gkz624
120. Dziadkowiec, K. N., Gąsiorowska, E., Nowak-Markwitz, E. & Jankowska, A. PARP inhibitors: review of mechanisms of action and BRCA1/2 mutation targeting. *Prz. menopauzalny = Menopause Rev.* **15**, 215–219 (2016).
121. Jiang, X., Li, W., Li, X., Bai, H. & Zhang, Z. Current status and future prospects of PARP inhibitor clinical trials in ovarian cancer. *Cancer Manag. Res.* **11**, 4371–4390 (2019).
122. Jones, P., Wilcoxen, K., Rowley, M. & Toniatti, C. Niraparib: A Poly(ADP-ribose) Polymerase (PARP) Inhibitor for the Treatment of Tumors with Defective Homologous Recombination. *J. Med. Chem.* **58**, 3302–3314 (2015).
123. Murai, J. *et al.* Trapping of PARP1 and PARP2 by clinical PARP inhibitors. *Cancer Res.* **72**, 5588–5599 (2012).
124. Hopkins, T. A. *et al.* PARP1 trapping by PARP inhibitors drives cytotoxicity in both cancer cells and healthy bone marrow. *Mol. Cancer Res.* **17**, 409–419 (2019).
125. Shen, Y., Aoyagi-Scharber, M. & Wang, B. Trapping poly(ADP-Ribose) polymerase. *Journal of Pharmacology and Experimental Therapeutics* **353**, 446–457 (2015).
126. Pommier, Y., O'Connor, M. J. & De Bono, J. Laying a trap to kill cancer cells: PARP inhibitors and their mechanisms of action. *Science Translational Medicine* **8**, 362ps17-362ps17 (2016).
127. Kim, G. *et al.* FDA approval summary: Olaparib monotherapy in patients with deleterious germline BRCA-mutated advanced ovarian cancer treated with three or more lines of chemotherapy. *Clin. Cancer Res.* **21**, 4257–4261 (2015).
128. Tutt, A. *et al.* Oral poly(ADP-ribose) polymerase inhibitor olaparib in patients with BRCA1 or BRCA2 mutations and advanced breast cancer: A proof-of-concept trial. *Lancet* **376**, 235–244 (2010).
129. Gorodetska, I., Kozeretska, I. & Dubrovska, A. BRCA genes: The role in genome stability, cancer stemness and therapy resistance. *Journal of Cancer* **10**, 2109–2127 (2019).
130. Antolin, A. A. *et al.* The kinase polypharmacology landscape of clinical PARP inhibitors. *Sci. Rep.* **10**, (2020).
131. FDA Approves Olaparib, Rucaparib to Treat Prostate Cancer - National Cancer Institute. Available at: https://www.cancer.gov/news-events/cancer-currents-blog/2020/fda-olaparib-rucaparib-prostate-cancer. (Accessed: 11th May 2021)
132. Lim, J. & Tan, D. S. P. Understanding Resistance Mechanisms and Expanding the Therapeutic Utility of PARP Inhibitors. *Cancers (Basel).* **9**, 109 (2017).
133. Gogola, E., Rottenberg, S. & Jonkers, J. Resistance to PARP Inhibitors: Lessons from

Preclinical Models of BRCA-Associated Cancer. **3**, 235–254 (2019).
134. Noordermeer, S. M. & van Attikum, H. PARP Inhibitor Resistance: A Tug-of-War in BRCA-Mutated Cells. *Trends Cell Biol.* **0**, (2019).
135. Kim, D. S., Camacho, C. V. & Kraus, W. L. Alternate therapeutic pathways for PARP inhibitors and potential mechanisms of resistance. *Experimental and Molecular Medicine* **53**, 42–51 (2021).
136. Rottenberg, S. *et al.* High sensitivity of BRCA1-deficient mammary tumors to the PARP inhibitor AZD2281 alone and in combination with platinum drugs. *Proc. Natl. Acad. Sci. U. S. A.* **105**, 17079–84 (2008).
137. Jaspers, J. E. *et al.* BRCA2-deficient sarcomatoid mammary tumors exhibit multidrug resistance. *Cancer Res.* **75**, 732–741 (2015).
138. Callaghan, R., Luk, F. & Bebawy, M. Inhibition of the multidrug resistance P-glycoprotein: Time for a change of strategy? *Drug Metabolism and Disposition* **42**, 623–631 (2014).
139. Pettitt, S. J. *et al.* Genome-wide and high-density CRISPR-Cas9 screens identify point mutations in PARP1 causing PARP inhibitor resistance. *Nat. Commun.* **9**, 1–14 (2018).
140. Gogola, E. *et al.* Selective Loss of PARG Restores PARylation and Counteracts PARP Inhibitor-Mediated Synthetic Lethality. *Cancer Cell* **33**, 1078-1093.e12 (2018).
141. Cortez, D. Preventing replication fork collapse to maintain genome integrity. *DNA Repair (Amst).* **32**, 149–157 (2015).
142. Chaudhuri, A. R. *et al.* Replication fork stability confers chemoresistance in BRCA-deficient cells. *Nature* **535**, 382–387 (2016).
143. Edwards, S. L. *et al.* Resistance to therapy caused by intragenic deletion in BRCA2. *Nature* **451**, 1111–1115 (2008).
144. Kondrashova, O. *et al.* Secondary somatic mutations restoring RAD51C and RAD51D associated with acquired resistance to the PARP inhibitor rucaparib in high-grade ovarian carcinoma. *Cancer Discov.* **7**, 984–998 (2017).
145. Ter Brugge, P. *et al.* Mechanisms of therapy resistance in patient-derived xenograft models of brca1-deficient breast cancer. *J. Natl. Cancer Inst.* **108**, (2016).
146. Bunting, S. F. *et al.* 53BP1 inhibits homologous recombination in brca1-deficient cells by blocking resection of DNA breaks. *Cell* **141**, 243–254 (2010).
147. Bajrami, I. *et al.* Genome-wide profiling of genetic synthetic lethality identifies CDK12 as a novel determinant of PARP1/2 inhibitor sensitivity. *Cancer Res.* **74**, 287–297 (2014).
148. Choi, Y. E. *et al.* Platinum and PARP Inhibitor Resistance Due to Overexpression of MicroRNA-622 in BRCA1-Mutant Ovarian Cancer. *Cell Rep.* **14**, 429–439 (2016).
149. Du, Y. *et al.* Blocking c-Met–mediated PARP1 phosphorylation enhances anti-tumor effects of PARP inhibitors. *nature.com*
150. Tapodi, A., Debreceni, B., Hanto, K., … Z. B.-J. of B. & 2005, undefined. Pivotal role of Akt activation in mitochondrial protection and cell survival by poly (ADP-ribose) polymerase-1 inhibition in oxidative stress. *Elsevier*
151. Teng, P., Bateman, N., Darcy, K., … C. H.-G. & 2015, undefined. Pharmacologic inhibition of ATR and ATM offers clinically important distinctions to enhancing platinum or radiation response in ovarian, endometrial, and cervical. *Elsevier*
152. Kaufman, H. L., Kohlhapp, F. J. & Zloza, A. Oncolytic viruses: a new class of immunotherapy drugs. *Nat Rev Drug Discov* **14**, 642–662 (2015).

153. Mesev, E. V., LeDesma, R. A. & Ploss, A. Decoding type I and III interferon signalling during viral infection. *Nat. Microbiol.* **4**, 914–924 (2019).
154. Choi, A. H., O'Leary, M. P., Fong, Y. & Chen, N. G. From benchtop to bedside: A review of oncolytic virotherapy. *Biomedicines* **4**, 1–20 (2016).
155. Pikor, L. A., Bell, J. C. & Diallo, J.-S. Oncolytic Viruses: Exploiting Cancer's Deal with the Devil. *Trends in Cancer* **1**, 266–277 (2015).
156. Matsuda, T., Karube, H. & Aruga, A. A Comparative Safety Profile Assessment of Oncolytic Virus Therapy Based on Clinical Trials. *Ther. Innov. Regul. Sci.* **52**, 430–437 (2018).
157. Rehman, H., Silk, A. W., Kane, M. P. & Kaufman, H. L. Into the clinic: Talimogene laherparepvec (T-VEC), a first-in-class intratumoral oncolytic viral therapy. *J. Immunother. Cancer* **4**, 53 (2016).
158. Zeng, W. *et al.* The oncolytic herpes simplex virus vector G47Δ effectively targets breast cancer stem cells. *Oncol. Rep.* **29**, 1108–1114 (2013).
159. Breitbach, C. J. *et al.* Oncolytic vaccinia virus disrupts tumor-associated vasculature in humans. *Cancer Res.* **73**, 1265–1275 (2013).
160. Leoni, V. *et al.* A fully-virulent retargeted oncolytic HSV armed with IL-12 elicits local immunity and vaccine therapy towards distant tumors. *PLoS Pathog.* **14**, e1007209 (2018).
161. Liu, Z. *et al.* Modifying the cancer-immune set point using vaccinia virus expressing re-designed interleukin-2. *Nat. Commun.* **9**, 4682 (2018).
162. Freedman, J. D. *et al.* An Oncolytic Virus Expressing a T-cell Engager Simultaneously Targets Cancer and Immunosuppressive Stromal Cells. *Cancer Res.* **78**, 6852–6865 (2018).
163. Eckert, E. C. *et al.* Generation of a Tumor-Specific Chemokine Gradient Using Oncolytic Vesicular Stomatitis Virus Encoding CXCL9. *Mol. Ther. - Oncolytics* **16**, 63–74 (2020).
164. Chesney, J. *et al.* Randomized, open-label phase II study evaluating the efficacy and safety of talimogene laherparepvec in combination with ipilimumab versus ipilimumab alone in patients with advanced, unresectable melanoma. *J. Clin. Oncol.* **36**, 1658–1667 (2018).
165. Bourgeois-Daigneault, M.-C. *et al.* Neoadjuvant oncolytic virotherapy before surgery sensitizes triple-negative breast cancer to immune checkpoint therapy. *Sci. Transl. Med.* **10**, eaao1641 (2018).
166. Gulley, J. L. *et al.* Role of antigen spread and distinctive characteristics of immunotherapy in cancer treatment. *J. Natl. Cancer Inst.* **109**, 1–9 (2017).
167. Harrington, K., Freeman, D. J., Kelly, B., Harper, J. & Soria, J. C. Optimizing oncolytic virotherapy in cancer treatment. *Nature Reviews Drug Discovery* (2019). doi:10.1038/s41573-019-0029-0
168. Lemos de Matos, A., Franco, L. S. & McFadden, G. Oncolytic Viruses and the Immune System: The Dynamic Duo. *Molecular Therapy - Methods and Clinical Development* **17**, 349–358 (2020).
169. Everts, A., Bergeman, M., McFadden, G. & Kemp, V. Simultaneous tumor and stroma targeting by oncolytic viruses. *Biomedicines* **8**, 1–20 (2020).
170. Balachandran, S. & Barber, G. Vesicular Stomatitis Virus (VSV) Therapy of Tumors. *IUBMB Life* **50**, 135–138 (2000).

171. Lichty, B. D., Power, A. T., Stojdl, D. F. & Bell, J. C. Vesicular stomatitis virus: re-inventing the bullet. *Trends Mol. Med.* **10**, 210–216 (2004).
172. Stojdl, D. F. *et al.* Exploiting tumor-specific defects in the interferon pathway with a previously unknown oncolytic virus. *Nat. Med.* **6**, 821–825 (2000).
173. Hastie, E., Cataldi, M., Marriott, I. & Grdzelishvili, V. Z. Understanding and altering cell tropism of vesicular stomatitis virus. *Virus Research* **176**, 16–32 (2013).
174. Bukreyev, A., Skiadopoulos, M. H., Murphy, B. R. & Collins, P. L. Nonsegmented Negative-Strand Viruses as Vaccine Vectors. *J. Virol.* **80**, 10293–10306 (2006).
175. Finkelshtein, D., Werman, A., Novick, D., Barak, S. & Rubinstein, M. LDL receptor and its family members serve as the cellular receptors for vesicular stomatitis virus. *Proc. Natl. Acad. Sci. U. S. A.* **110**, 7306–7311 (2013).
176. Critchley-Thorne, R. J. *et al.* Impaired interferon signaling is a common immune defect in human cancer. *Proc. Natl. Acad. Sci. U. S. A.* **106**, 9010–5 (2009).
177. Bell, J. C., Garson, K. A., Lichty, B. D. & Stojdl, D. F. Oncolytic viruses: programmable tumour hunters. *Curr. Gene Ther.* **2**, 243–54 (2002).
178. Balachandran, S. & Barber, G. Vesicular Stomatitis Virus (VSV) Therapy of Tumors. *IUBMB Life* **50**, 135–138 (2000).
179. Stojdl, D. F. *et al.* VSV strains with defects in their ability to shutdown innate immunity are potent systemic anti-cancer agents. *Cancer Cell* **4**, 263–275 (2003).
180. Her, L.-S., Lund, E. & Dahlberg, J. E. Inhibition of Ran Guanosine Triphosphatase-Dependent Nuclear Transport by the Matrix Protein of Vesicular Stomatitis Virus. *Science (80-.).* **276**, (1997).
181. Von Kobbe, C. *et al.* Vesicular stomatitis virus matrix protein inhibits host cell gene expression by targeting the nucleoporin Nup98. *Mol. Cell* **6**, 1243–1252 (2000).
182. Barr, J. N., Whelan, S. P. J. & Wertz, G. W. Transcriptional control of the RNA-dependent RNA polymerase of vesicular stomatitis virus. *Biochimica et Biophysica Acta - Gene Structure and Expression* **1577**, 337–353 (2002).
183. Whelan, S. P. J. & Wertz, G. W. Transcription and replication initiate at separate sites on the vesicular stomatitis virus genome. *Proc. Natl. Acad. Sci. U. S. A.* **99**, 9178–9183 (2002).
184. Virus Replication. in *Fenner's Veterinary Virology* 17–45 (Elsevier, 2017). doi:10.1016/b978-0-12-800946-8.00002-7
185. Raux, H. *et al.* The Matrix Protein of Vesicular Stomatitis Virus Binds Dynamin for Efficient Viral Assembly. *J. Virol.* **84**, 12609–12618 (2010).
186. Obuchi, M., Fernandez, M. & Barber, G. N. Development of Recombinant Vesicular Stomatitis Viruses That Exploit Defects in Host Defense To Augment Specific Oncolytic Activity. *J. Virol.* **77**, 8843–8856 (2003).
187. Naik, S., Nace, R., Barber, G. N. & Russell, S. J. Potent systemic therapy of multiple myeloma utilizing oncolytic vesicular stomatitis virus coding for interferon-B. *Cancer Gene Ther.* **19**, 443–450 (2012).
188. Goel, A. *et al.* Radioiodide imaging and radiovirotherapy of multiple myeloma using VSV(Δ51)-NIS, an attenuated vesicular stomatitis virus encoding the sodium iodide symporter gene. *Blood* **110**, 2342–2350 (2007).
189. Naik, S. *et al.* Curative one-shot systemic virotherapy in murine myeloma. *Leukemia*

(2012). doi:10.1038/leu.2012.70
190. Merchan, J. R. *et al.* Relationship of infusion duration to safety, efficacy, and pharmacodynamics (PD): Second part of a phase I-II study using VSV-IFNβ-NIS (VV1) oncolytic virus in patients with refractory solid tumors. *J. Clin. Oncol.* **38**, 3090–3090 (2020).
191. https://www.cancer.gov/about-cancer/treatment/clinical-trials/intervention/vsv-hifnbeta-nis.
192. Lee, R. C., Feinbaum, R. L. & Ambrost, V. *The C. elegans Heterochronic Gene lin-4 Encodes Small RNAs with Antisense Complementarity to &II-14*. *Cell* **75**, (1993).
193. Alles, J. *et al.* An estimate of the total number of true human miRNAs. *Nucleic Acids Res.* **47**, 3353–3364 (2019).
194. Plotnikova, O., Baranova, A. & Skoblov, M. Comprehensive Analysis of Human microRNA–mRNA Interactome. *Front. Genet.* **10**, 933 (2019).
195. Maffioletti, E., Tardito, D., Gennarelli, M. & Bocchio-Chiavetto, L. Micro spies from the brain to the periphery: new clues from studies on microRNAs in neuropsychiatric disorders. *Front. Cell. Neurosci.* **8**, 75 (2014).
196. Bartel, D. P. MicroRNAs: target recognition and regulatory functions. *Cell* **136**, 215–33 (2009).
197. Rodriguez, A., Griffiths-Jones, S., Ashurst, J. L. & Bradley, A. Identification of mammalian microRNA host genes and transcription units. *Genome Res.* **14**, 1902–1910 (2004).
198. Cai, X., Hagedorn, C. H. & Cullen, B. R. Human microRNAs are processed from capped, polyadenylated transcripts that can also function as mRNAs. *RNA* **10**, 1957–1966 (2004).
199. Hammond, S. M. An overview of microRNAs. *Advanced Drug Delivery Reviews* **87**, 3–14 (2015).
200. Yang, J.-S., Maurin, T. & Lai, E. C. Functional parameters of Dicer-independent microRNA biogenesis. *RNA* **18**, 945–57 (2012).
201. Yang, J.-S. *et al.* Conserved vertebrate mir-451 provides a platform for Dicer-independent, Ago2-mediated microRNA biogenesis. *Proc. Natl. Acad. Sci.* **107**, 15163–15168 (2010).
202. Yang, S. *et al.* Widespread regulatory activity of vertebrate microRNA* species. *RNA* **17**, 312–326 (2011).
203. Ruby, J. G., Jan, C. H. & Bartel, D. P. Intronic microRNA precursors that bypass Drosha processing. *Nature* **448**, 83–86 (2007).
204. Berezikov, E., Chung, W. J., Willis, J., Cuppen, E. & Lai, E. C. Mammalian Mirtron Genes. *Mol. Cell* **28**, 328–336 (2007).
205. Zhang, J. *et al.* Exosome and Exosomal MicroRNA: Trafficking, Sorting, and Function. *Genomics. Proteomics Bioinformatics* **13**, 17–24 (2015).
206. Valadi, H. *et al.* Exosome-mediated transfer of mRNAs and microRNAs is a novel mechanism of genetic exchange between cells. *Nat. Cell Biol.* **9**, 654–659 (2007).
207. Samanta, S. *et al.* Exosomes: new molecular targets of diseases. *Acta Pharmacol. Sin.* **39**, 501–513 (2018).
208. Whiteside, T. L. Tumor-Derived Exosomes and Their Role in Cancer Progression. in *Advances in Clinical Chemistry* **74**, 103–141 (Academic Press Inc., 2016).
209. Atay, S. & Godwin, A. K. Tumor-derived exosomes. *Commun. Integr. Biol.* **7**, e28231

(2014).
210. Li, I. & Nabet, B. Y. Exosomes in the tumor microenvironment as mediators of cancer therapy resistance. *Molecular Cancer* **18**, (2019).
211. Gurunathan, S., Kang, M.-H., Jeyaraj, M., Qasim, M. & Kim, J.-H. Review of the Isolation, Characterization, Biological Function, and Multifarious Therapeutic Approaches of Exosomes. *Cells* **8**, 307 (2019).
212. Melo, S. A. *et al.* Cancer Exosomes Perform Cell-Independent MicroRNA Biogenesis and Promote Tumorigenesis. *Cancer Cell* **26**, 707–721 (2014).
213. Chen, C. *et al.* Real-time quantification of microRNAs by stem-loop RT-PCR. *Nucleic Acids Res.* **33**, (2005).
214. Breast Cancer - Canada.ca. Available at: https://www.canada.ca/en/public-health/services/chronic-diseases/cancer/breast-cancer.html. (Accessed: 16th November 2019)
215. Lisio, M. A., Fu, L., Goyeneche, A., Gao, Z. H. & Telleria, C. High-grade serous ovarian cancer: Basic sciences, clinical and therapeutic standpoints. *International Journal of Molecular Sciences* **20**, (2019).
216. Ovarian Cancer – Cancer Care Ontario. Available at: https://www.cancercareontario.ca/en/types-of-cancer/ovarian-cancer. (Accessed: 16th November 2019)
217. Collignon, J., Lousberg, L., Schroeder, H. & Jerusalem, G. Triple-negative breast cancer: treatment challenges and solutions. *Breast cancer (Dove Med. Press.* **8**, 93–107 (2016).
218. Neff, R. T., Senter, L. & Salani, R. BRCA mutation in ovarian cancer: testing, implications and treatment considerations. *Ther. Adv. Med. Oncol.* **9**, 519–531 (2017).
219. Yamauchi, H. & Takei, J. Management of hereditary breast and ovarian cancer. *International Journal of Clinical Oncology* **23**, 45–51 (2018).
220. Padamsee, T. J., Wills, C. E., Yee, L. D. & Paskett, E. D. Decision making for breast cancer prevention among women at elevated risk. *Breast Cancer Research* **19**, 1–12 (2017).
221. Paluch-Shimon, S. *et al.* Prevention and screening in BRCA mutation carriers and other breast/ovarian hereditary cancer syndromes: ESMO clinical practice guidelines for cancer prevention and screening. *Ann. Oncol.* **27**, v103–v110 (2016).
222. Swanson, C. L. & Bakkum-Gamez, J. N. Options in Prophylactic Surgery to Prevent Ovarian Cancer in High-Risk Women: How New Hypotheses of Fallopian Tube Origin Influence Recommendations. *Current Treatment Options in Oncology* **17**, 20 (2016).
223. Matulonis, U. A. *et al.* Ovarian cancer. *Nat. Rev. Dis. Prim.* **2**, (2016).
224. Survival statistics for ovarian cancer - Canadian Cancer Society. Available at: https://www.cancer.ca/en/cancer-information/cancer-type/ovarian/prognosis-and-survival/survival-statistics/?region=on. (Accessed: 4th May 2021)
225. Vaughan, S. *et al.* Rethinking ovarian cancer: Recommendations for improving outcomes. *Nature Reviews Cancer* **11**, 719–725 (2011).
226. Pouptsis, A., Swafe, L., Patwardhan, M. & Stavraka, C. Surgical and Systemic Treatment of Hereditary Breast Cancer: A Mini-Review With a Focus on BRCA1 and BRCA2 Mutations. *Frontiers in Oncology* **10**, 2325 (2020).
227. Valachis, A., Nearchou, A. D. & Lind, P. Surgical management of breast cancer in BRCA-mutation carriers: A systematic review and meta-analysis. *Breast Cancer Research and*

Treatment **144**, 443–455 (2014).
228. Tung, N. M. *et al.* Management of hereditary breast cancer: American society of clinical oncology, American society for radiation oncology, and society of surgical oncology guideline. *J. Clin. Oncol.* **38**, 2080–2106 (2020).
229. Pfeffer, S. *et al.* Identification of Virus-Encoded MicroRNAs. *Science (80-.).* **304**, 734–736 (2004).
230. Skalsky, R. L. & Cullen, B. R. Viruses, microRNAs, and host interactions. *Annual Review of Microbiology* **64**, 123–141 (2010).
231. Mishra, R., Kumar, A., Ingle, H. & Kumar, H. The Interplay Between Viral-Derived miRNAs and Host Immunity During Infection. *Frontiers in Immunology* **10**, 3079 (2020).
232. Kincaid, R. P., Burke, J. M. & Sullivan, C. S. RNA virus microRNA that mimics a B-cell oncomiR. *Proc. Natl. Acad. Sci. U. S. A.* **109**, 3077–3082 (2012).
233. Gillet, N. *et al.* Mechanisms of leukemogenesis induced by bovine leukemia virus: Prospects for novel anti-retroviral therapies in human. *Retrovirology* **4**, 18 (2007).
234. Lei, X. *et al.* A Kaposi's Sarcoma-Associated Herpesvirus MicroRNA and Its Variants Target the Transforming Growth Factor Pathway To Promote Cell Survival. *J. Virol.* **86**, 11698–11711 (2012).
235. Brown, B. D., Venneri, M. A., Zingale, A., Sergi, L. S. & Naldini, L. Endogenous microRNA regulation suppresses transgene expression in hematopoietic lineages and enables stable gene transfer. *Nat. Med.* **12**, 585–591 (2006).
236. Ruiz, A. J. & Russell, S. J. MicroRNAs and oncolytic viruses. *Current Opinion in Virology* **13**, 40–48 (2015).
237. Iorio, M. V. & Croce, C. M. microRNA involvement in human cancer. *Carcinogenesis* **33**, 1126–1133 (2012).
238. Guduric-Fuchs, J. *et al.* Selective extracellular vesicle-mediated export of an overlapping set of microRNAs from multiple cell types. *BMC Genomics* **13**, 1–14 (2012).
239. Gupta, S. K., Bang, C. & Thum, T. Circulating MicroRNAs as biomarkers and potential paracrine mediators of cardiovascular disease. *Circulation: Cardiovascular Genetics* **3**, 484–488 (2010).
240. Contu, R., Latronico, M. V. G. & Condorelli, G. Circulating MicroRNAs as potential biomarkers of coronary artery disease: A promise to be fulfilled? *Circulation Research* **107**, 573–574 (2010).
241. Kosaka, N., Iguchi, H. & Ochiya, T. Circulating microRNA in body fluid: A new potential biomarker for cancer diagnosis and prognosis. *Cancer Science* **101**, 2087–2092 (2010).
242. Mittelbrunn, M. *et al.* Unidirectional transfer of microRNA-loaded exosomes from T cells to antigen-presenting cells. *Nat. Commun.* **2**, 1–10 (2011).
243. Collino, F. *et al.* Microvesicles derived from adult human bone marrow and tissue specific mesenchymal stem cells shuttle selected pattern of miRNAs. *PLoS One* **5**, e11803 (2010).
244. Yang, S. *et al.* Conserved vertebrate mir-451 provides a platform for Dicer-independent, Ago2-mediated microRNA biogenesis. *Proc. Natl. Acad. Sci. U. S. A.* **107**, 15163–15168 (2010).
245. Lin, S. & Gregory, R. I. MicroRNA biogenesis pathways in cancer. *Nature Reviews Cancer* **15**, 321–333 (2015).
246. Lin, R. J. *et al.* microRNA signature and expression of Dicer and Drosha can predict

prognosis and delineate risk groups in neuroblastoma. *Cancer Res.* **70**, 7841–7850 (2010).
247. Merritt, W. M. *et al.* Dicer, Drosha, and Outcomes in Patients with Ovarian Cancer. *N. Engl. J. Med.* **359**, 2641–2650 (2008).
248. Maurin, T., Cazalla, D., Yang, S., Bortolamiol-Becet, D. & Lai, E. C. RNase III-independent microRNA biogenesis in mammalian cells. *RNA* **18**, 2166–73 (2012).
249. Reshke, R. *et al.* Reduction of the therapeutic dose of silencing RNA by packaging it in extracellular vesicles via a pre-microRNA backbone. *Nat. Biomed. Eng.* **4**, 52–68 (2020).
250. Li, X. & Zou, X. An overview of RNA virus-encoded microRNAs. *ExRNA* **1**, 1–5 (2019).
251. Zhan, S., Wang, Y. & Chen, X. RNA virus-encoded microRNAs: biogenesis, functions and perspectives on application. *ExRNA* **2**, 1–7 (2020).
252. Rouha, H., Thurner, C. & Mandl, C. W. Functional microRNA generated from a cytoplasmic RNA virus. *Nucleic Acids Res.* **38**, 8328–8337 (2010).
253. Shapiro, J. S., Varble, A., Pham, A. M. & Tenoever, B. R. Noncanonical cytoplasmic processing of viral microRNAs. *RNA* **16**, 2068–2074 (2010).
254. Shapiro, J. S. *et al.* Drosha as an interferon-independent antiviral factor. *Proc. Natl. Acad. Sci. U. S. A.* **111**, 7108–7113 (2014).
255. Benitez, A. A. *et al.* In Vivo RNAi Screening Identifies MDA5 as a Significant Contributor to the Cellular Defense against Influenza A Virus. *Cell Rep.* **11**, 1714–1726 (2015).
256. Lewis, B. P., Shih, I. H., Jones-Rhoades, M. W., Bartel, D. P. & Burge, C. B. Prediction of Mammalian MicroRNA Targets. *Cell* **115**, 787–798 (2003).
257. Brennecke, J., Stark, A., Russell, R. B. & Cohen, S. M. Principles of microRNA-target recognition. in *PLoS Biology* **3**, 0404–0418 (Public Library of Science, 2005).
258. Castle, J. C. *et al.* Mutated tumor alleles are expressed according to their DNA frequency. *Sci. Rep.* **4**, 4743
259. Chang, K., Marran, K., Valentine, A. & Hannon, G. J. Creating an miR30-based shRNA vector. *Cold Spring Harb. Protoc.* **8**, 631–635 (2013).
260. Turner, N. C. *et al.* A synthetic lethal siRNA screen identifying genes mediating sensitivity to a PARP inhibitor. *EMBO J.* **27**, 1368–1377 (2008).
261. Gebert, L. F. R. & MacRae, I. J. Regulation of microRNA function in animals. *Nature Reviews Molecular Cell Biology* **20**, 21–37 (2019).
262. Dou, D., Revol, R., Östbye, H., Wang, H. & Daniels, R. Influenza A virus cell entry, replication, virion assembly and movement. *Frontiers in Immunology* **9**, 1 (2018).
263. Fang, Z. & Rajewsky, N. The impact of miRNA target sites in coding sequences and in 3'UTRs. *PLoS One* **6**, (2011).
264. Forman, J. J. & Coller, H. A. The code within the code: MicroRNAs target coding regions. *Cell Cycle* **9**, 1533–1541 (2010).
265. Pei, Y. *et al.* Quantitative evaluation of siRNA delivery in vivo. *RNA* **16**, 2553–2563 (2010).
266. Veldhoen, S., Laufer, S. D., Trampe, A. & Restle, T. Cellular delivery of small interfering RNA by a non-covalently attached cell-penetrating peptide: Quantitative analysis of uptake and biological effect. *Nucleic Acids Res.* **34**, 6561–6573 (2006).
267. Sakai, W. *et al.* Functional Restoration of BRCA2 Protein by Secondary BRCA2 Mutations in BRCA2-Mutated Ovarian Carcinoma. *Cancer Res.* **69**, 6381–6386 (2009).
268. Pulliam, N. *et al.* Cancer Therapy: Preclinical An Effective Epigenetic-PARP Inhibitor Combination Therapy for Breast and Ovarian Cancers Independent of BRCA Mutations.

(2018). doi:10.1158/1078-0432.CCR-18-0204
269. Passaro, C. *et al.* PARP inhibitor olaparib increases the oncolytic activity of dl922-947 in invitro and invivo model of anaplastic thyroid carcinoma. *Mol. Oncol.* **9**, 78–92 (2015).
270. Vikas, P., Borcherding, N., Chennamadhavuni, A. & Garje, R. Therapeutic Potential of Combining PARP Inhibitor and Immunotherapy in Solid Tumors. *Frontiers in Oncology* **10**, 570 (2020).
271. Ning, J., Wakimoto, H., Peters, C., Martuza, R. L. & Rabkin, S. D. Rad51 degradation: Role in oncolytic virus-poly (ADP Ribose) polymerase inhibitor combination therapy in glioblastoma. *J. Natl. Cancer Inst.* **109**, (2017).
272. Peyraud, F. & Italiano, A. Combined parp inhibition and immune checkpoint therapy in solid tumors. *Cancers* **12**, 1–28 (2020).
273. Ding, L. *et al.* PARP Inhibition Elicits STING-Dependent Antitumor Immunity in Brca1-Deficient Ovarian Cancer. *Cell Rep.* **25**, 2972-2980.e5 (2018).
274. Shen, J. *et al.* PARPI triggers the STING-dependent immune response and enhances the therapeutic efficacy of immune checkpoint blockade independent of BRCANEss. *Cancer Res.* **79**, 311–319 (2019).
275. Dhanwani, R., Takahashi, M. & Sharma, S. Cytosolic sensing of immuno-stimulatory DNA, the enemy within. *Current Opinion in Immunology* **50**, 82–87 (2018).
276. Pantelidou, C. *et al.* Parp inhibitor efficacy depends on CD8+ T-cell recruitment via intratumoral sting pathway activation in brca-deficient models of triple-negative breast cancer. *Cancer Discov.* **9**, 722–737 (2019).
277. Lee, E. K. & Konstantinopoulos, P. A. PARP inhibition and immune modulation: scientific rationale and perspectives for the treatment of gynecologic cancers. *Ther. Adv. Med. Oncol.* **12**, 1758835920944116 (2020).
278. Dunphy, G. *et al.* Non-canonical Activation of the DNA Sensing Adaptor STING by ATM and IFI16 Mediates NF-κB Signaling after Nuclear DNA Damage. *Mol. Cell* **71**, 745-760.e5 (2018).
279. Robert, C. A decade of immune-checkpoint inhibitors in cancer therapy. *Nature Communications* **11**, 1–3 (2020).
280. Wei, S. C., Duffy, C. R. & Allison, J. P. Fundamental mechanisms of immune checkpoint blockade therapy. *Cancer Discovery* **8**, 1069–1086 (2018).
281. Pardoll, D. M. The blockade of immune checkpoints in cancer immunotherapy. *Nature Reviews Cancer* **12**, 252–264 (2012).
282. Zou, W. & Chen, L. Inhibitory B7-family molecules in the tumour microenvironment. *Nature Reviews Immunology* **8**, 467–477 (2008).
283. Jiao, S. *et al.* PARP inhibitor upregulates PD-L1 expression and enhances cancer-associated immunosuppression. *Clin. Cancer Res.* **23**, 3711–3720 (2017).
284. Cai, H., Yan, L., Liu, N., Xu, M. & Cai, H. IFI16 promotes cervical cancer progression by upregulating PD-L1 in immunomicroenvironment through STING-TBK1-NF-kB pathway. *Biomed. Pharmacother.* **123**, (2020).
285. Bellucci, R. *et al.* Interferon-γ-induced activation of JAK1 and JAK2 suppresses tumor cell susceptibility to NK cells through upregulation of PD-L1 expression. *Oncoimmunology* **4**, (2015).
286. Lassen, U. Combining PARP inhibition with PD-1 inhibitors. *The Lancet Oncology* **20**,

1196–1198 (2019).
287. Strickland, K. C. *et al.* Association and prognostic significance of BRCA1/2-mutation status with neoantigen load, number of tumor-infiltrating lymphocytes and expression of PD-1/PD-L1 in high grade serous ovarian cancer. *Oncotarget* **7**, 13587–13598 (2016).
288. Darb-Esfahani, S. *et al.* Prognostic impact of programmed cell death-1 (PD-1) and PD-ligand 1 (PD-L1) expression in cancer cells and tumorinfiltrating lymphocytes in ovarian high grade serous carcinoma. *Oncotarget* **7**, 1486–1499 (2016).
289. Wen, W. X. & Leong, C. O. Association of BRCA1- And BRCA2-deficiency with mutation burden, expression of PD-L1/ PD-1, immune infiltrates, and T cell-inflamed signature in breast cancer. *PLoS One* **14**, (2019).
290. Smith, S. & Weller, S. K. HSV-I and the cellular DNA damage response. *Future Virology* **10**, 383–397 (2015).
291. Kanai, R. *et al.* Oncolytic virus-mediated manipulation of DNA damage responses: Synergy with chemotherapy in killing glioblastoma stem cells. *J. Natl. Cancer Inst.* **104**, 42–55 (2012).
292. Lilley, C. E., Schwartz, R. A. & Weitzman, M. D. Using or abusing: viruses and the cellular DNA damage response. *Trends in Microbiology* **15**, 119–126 (2007).
293. Passaro, C. *et al.* Ionizing radiation enhances dl922-947-mediated cell death of anaplastic thyroid carcinoma cells. *Endocr. Relat. Cancer* **20**, 633–647 (2013).
294. Calin, G. A. *et al.* Frequent deletions and down-regulation of micro-RNA genes miR15 and miR16 at 13q14 in chronic lymphocytic leukemia. *Proc. Natl. Acad. Sci. U. S. A.* **99**, 15524–15529 (2002).
295. Calin, G. A. *et al.* Human microRNA genes are frequently located at fragile sites and genomic regions involved in cancers. *Proc. Natl. Acad. Sci. U. S. A.* **101**, 2999–3004 (2004).
296. Blenkiron, C. *et al.* MicroRNA expression profiling of human breast cancer identifies new markers of tumor subtype. *Genome Biol.* **8**, (2007).
297. Meng, F. *et al.* Involvement of Human Micro-RNA in Growth and Response to Chemotherapy in Human Cholangiocarcinoma Cell Lines. *Gastroenterology* **130**, 2113–2129 (2006).
298. Iorio, M. V. *et al.* MicroRNA-205 regulates HER3 in human breast cancer. *Cancer Res.* **69**, 2195–2200 (2009).
299. Hu, W. Z. *et al.* Functional miRNAs in breast cancer drug resistance. *OncoTargets and Therapy* **11**, 1529–1541 (2018).
300. Mihanfar, A., Fattahi, A. & Nejabati, H. R. MicroRNA-mediated drug resistance in ovarian cancer. *Journal of Cellular Physiology* **234**, 3180–3191 (2019).
301. Moskwa, P. *et al.* miR-182-Mediated Downregulation of BRCA1 Impacts DNA Repair and Sensitivity to PARP Inhibitors. *Mol. Cell* **41**, 210–220 (2011).
302. Krishnan, K. *et al.* MicroRNA-182-5p targets a network of genes involved in DNA repair. *RNA* **19**, 230–242 (2013).
303. Choi, J. G. *et al.* Multiplexing seven miRNA-Based shRNAs to suppress HIV replication. *Mol. Ther.* **23**, 310–320 (2015).
304. Villarreal, L. P., Holland, J. J. & Breindl, M. Determination of Molar Ratios of Vesicular Stomatitis Virus Induced RNA Species in BHK21Cells. *Biochemistry* **15**, 1663–1667 (1976).

305. Iverson, L. E. & Rose, J. K. Localized attenuation and discontinuous synthesis during vesicular stomatitis virus transcription. *Cell* **23**, 477–484 (1981).
306. Keung, M. Y., Wu, Y., Badar, F. & Vadgama, J. V. Response of Breast Cancer Cells to PARP Inhibitors Is Independent of BRCA Status. *J. Clin. Med.* **9**, 940 (2020).
307. Li, J., Yuan, H., Xu, H., Zhao, H. & Xiong, N. Hypoxic cancer-secreted exosomal miR-182-5p promotes glioblastoma angiogenesis by targeting kruppel-like factor 2 and 4. *Mol. Cancer Res.* **18**, 1218–1231 (2020).
308. Ohno, S. *et al.* Systemically injected exosomes targeted to EGFR deliver antitumor microRNA to breast cancer cells. *Mol. Ther.* **21**, 185–91 (2013).
309. Jayson, G. C., Kohn, E. C., Kitchener, H. C. & Ledermann, J. A. Ovarian cancer. *Lancet* **384**, 1376–1388 (2014).
310. Heeke, A. L. *et al.* Prevalence of Homologous Recombination-Related Gene Mutations Across Multiple Cancer Types. *JCO Precis. Oncol.* **2018**, (2018).
311. Pilié, P. G., Tang, C., Mills, G. B. & Yap, T. A. State-of-the-art strategies for targeting the DNA damage response in cancer. *Nature Reviews Clinical Oncology* **16**, 81–104 (2019).
312. Johnson, N. *et al.* Compromised CDK1 activity sensitizes BRCA-proficient cancers to PARP inhibition. *Nat. Med.* **17**, 875–82 (2011).
313. Johnson, S. F. *et al.* CDK12 Inhibition Reverses De Novo and Acquired PARP Inhibitor Resistance in BRCA Wild-Type and Mutated Models of Triple-Negative Breast Cancer. *Cell Rep.* **17**, 2367–2381 (2016).
314. Bryant, H. E. & Helleday, T. Inhibition of poly (ADP-ribose) polymerase activates ATM which is required for subsequent homologous recombination repair. *Nucleic Acids Res.* **34**, 1685–91 (2006).
315. Yazinski, S. A. *et al.* ATR inhibition disrupts rewired homologous recombination and fork protection pathways in PARP inhibitor-resistant BRCA-deficient cancer cells. *Genes Dev.* **31**, 318–332 (2017).
316. Fang, Y. *et al.* Sequential Therapy with PARP and WEE1 Inhibitors Minimizes Toxicity while Maintaining Efficacy. *Cancer Cell* **35**, 851-867.e7 (2019).
317. Garcia, T. B. *et al.* A small-molecule inhibitor of WEE1, AZD1775, synergizes with olaparib by impairing homologous recombination and enhancing DNA damage and apoptosis in acute leukemia. *Mol. Cancer Ther.* **16**, 2058–2068 (2017).
318. Du, Y. *et al.* Blocking c-Met-mediated PARP1 phosphorylation enhances anti-tumor effects of PARP inhibitors. *Nat. Med.* **22**, 194–201 (2016).
319. Turner, N. C. *et al.* A synthetic lethal siRNA screen identifying genes mediating sensitivity to a PARP inhibitor. *EMBO J.* **27**, 1368–1377 (2008).
320. McCabe, N. *et al.* Deficiency in the repair of DNA damage by homologous recombination and sensitivity to poly(ADP-ribose) polymerase inhibition. *Cancer Res.* **66**, 8109–8115 (2006).
321. Neijenhuis, S., Bajrami, I., Miller, R., Lord, C. J. & Ashworth, A. Identification of miRNA modulators to PARP inhibitor response. *DNA Repair (Amst).* **12**, 394–402 (2013).
322. Pamuła-Piłat, J., Tęcza, K., Kalinowska-Herok, M. & Grzybowska, E. Genetic 3'UTR variations and clinical factors significantly contribute to survival prediction and clinical response in breast cancer patients. *Sci. Rep.* **10**, 1–15 (2020).
323. Roe, C. J., Siddiqui, M. T., Lawson, D. & Cohen, C. RNA in Situ Hybridization for Epstein-

Barr Virus and Cytomegalovirus: Comparison with in Situ Hybridization and Immunohistochemistry. *Appl. Immunohistochem. Mol. Morphol.* **27**, 155–159 (2019).
324. Yanlei, M. *et al.* miR-150 as a potential biomarker associated with prognosis and therapeutic outcome in colorectal cancer. *Gut* **61**, 1447–1453 (2012).
325. Kim, T. H. *et al.* miR-150 enhances apoptotic and anti-tumor effects of paclitaxel in paclitaxel-resistant ovarian cancer cells by targeting Notch3. *Oncotarget* **8**, (2017).
326. Chen, X. *et al.* miR-150-5p suppresses tumor progression by targeting VEGFA in colorectal cancer. *Aging (Albany. NY).* **10**, 3421–3437 (2018).
327. Dai, F. Q. *et al.* miR-150-5p Inhibits Non-Small-Cell Lung Cancer Metastasis and Recurrence by Targeting HMGA2 and β-Catenin Signaling. *Mol. Ther. - Nucleic Acids* **16**, 675–685 (2019).
328. Zhang, Q. *et al.* FoxP3-miR-150-5p/3p suppresses ovarian tumorigenesis via an IGF1R/IRS1 pathway feedback loop. *Cell Death Dis.* **12**, 1–16 (2021).
329. Sun, X., Zhang, C., Cao, Y. & Liu, E. MiR-150 suppresses tumor growth in melanoma through downregulation of myb. *Oncol. Res.* **27**, 317–323 (2019).
330. Zhang, J., Luo, N., Luo, Y., oncology, Z. P.-… journal of & 2012, undefined. microRNA-150 inhibits human CD133-positive liver cancer stem cells through negative regulation of the transcription factor c-Myb. *spandidos-publications.com* doi:10.3892/ijo.2011.1242
331. Li, H. *et al.* MiR-150 promotes cellular metastasis in non-small cell lung cancer by targeting FOXO4. *Sci. Rep.* **6**, 1–11 (2016).
332. Liu, Y., Li, X., Zhang, H. & Huang, Y. MIAT inhibits proliferation of cervical cancer cells through regulating miR-150-5p. *Cancer Cell Int.* **20**, 1–10 (2020).
333. Huang, S. *et al.* MiR-150 promotes human breast cancer growth and malignant behavior by targeting the pro-apoptotic purinergic P2X7 receptor. *PLoS One* **8**, (2013).
334. Bender, T. P. Potential Roles For C-Myb Thoughout Early Lymphocyte Development. in *Myb Transcription Factors: Their Role in Growth, Differentiation and Disease* 81–105 (Springer Netherlands, 2007). doi:10.1007/978-1-4020-2869-4_4
335. Bezman, N. A., Chakraborty, T., Bender, T. & Lanier, L. L. MiR-150 regulates the development of NK and iNKT cells. *J. Exp. Med.* **208**, 2717–2731 (2011).
336. Xiao, C. *et al.* MiR-150 Controls B Cell Differentiation by Targeting the Transcription Factor c-Myb. *Cell* **131**, 146–159 (2007).
337. Chen, Z. *et al.* miR-150 Regulates Memory CD8 T Cell Differentiation via c-Myb. *Cell Rep.* **20**, 2584–2597 (2017).
338. Smith, N. L., Wissink, E. M., Grimson, A. & Rudd, B. D. MiR-150 Regulates Differentiation and Cytolytic Effector Function in CD8+ T cells. *Sci. Rep.* **5**, 16399 (2015).
339. Ban, Y. H. *et al.* miR-150-Mediated Foxo1 Regulation Programs CD8+ T Cell Differentiation. *Cell Rep.* **20**, 2598–2611 (2017).
340. Kim, T. D. *et al.* MicroRNA-150 modulates intracellular Ca 2+ levels in naïve CD8+ T cells by targeting TMEM20. *Sci. Rep.* **7**, (2017).
341. Chen, Y., Gao, D.-Y. & Huang, L. In vivo delivery of miRNAs for cancer therapy: Challenges and strategies ☆. (2014). doi:10.1016/j.addr.2014.05.009
342. Weiner, L. M., Surana, R. & Wang, S. Monoclonal antibodies: Versatile platforms for cancer immunotherapy. *Nature Reviews Immunology* **10**, 317–327 (2010).
343. Yu, B., Zhao, X., Lee, J. L. & Lee, R. J. Targeted delivery systems for oligonucleotide

therapeutics. *AAPS Journal* **11**, 195–203 (2009).
344. Garzon, R., Marcucci, G. & Croce, C. M. Targeting microRNAs in cancer: Rationale, strategies and challenges. *Nature Reviews Drug Discovery* **9**, 775–789 (2010).
345. Møller, H. G. *et al.* A systematic review of MicroRNA in glioblastoma multiforme: Micro-modulators in the mesenchymal mode of migration and invasion. *Molecular Neurobiology* **47**, 131–144 (2013).
346. Schneider, M. R. MicroRNAs as novel players in skin development, homeostasis and disease. *British Journal of Dermatology* **166**, 22–28 (2012).
347. Achard, C. *et al.* Lighting a Fire in the Tumor Microenvironment Using Oncolytic Immunotherapy. *EBioMedicine* **31**, 17–24 (2018).
348. Russell, S. J., Peng, K.-W. & Bell, J. C. Oncolytic virotherapy. *Nat Biotech* **30**, 658–670 (2012).
349. Martin, N. T. & Bell, J. C. Oncolytic Virus Combination Therapy: Killing One Bird with Two Stones. *Molecular Therapy* **26**, 1414–1422 (2018).
350. Koppers-Lalic, D., Hogenboom, M. M., Middeldorp, J. M. & Pegtel, D. M. Virus-modified exosomes for targeted RNA delivery; A new approach in nanomedicine. *Advanced Drug Delivery Reviews* **65**, 348–356 (2013).
351. Lemay, C. G. *et al.* Harnessing oncolytic virus-mediated antitumor immunity in an infected cell vaccine. *Mol. Ther.* **20**, 1791–9 (2012).
352. Galivo, F. *et al.* Single-cycle viral gene expression, rather than progressive replication and oncolysis, is required for VSV therapy of B16 melanoma. *Gene Ther.* **17**, 158–170 (2010).
353. Brachtlova, T. *et al.* Expression of Oncolytic Adenovirus-Encoded RNAi Molecules Is Most Effective in a pri-miRNA Precursor Format. *Mol. Ther. - Oncolytics* **19**, 332–343 (2020).
354. Varble, A. & Tenoever, B. R. Implications of RNA virus-produced miRNAs. *RNA Biol.* **8**, 190–194 (2011).
355. Shapiro, J. S., Varble, A., Pham, A. M. & Tenoever, B. R. Noncanonical cytoplasmic processing of viral microRNAs. *RNA* **16**, 2068–2074 (2010).
356. Varble, A. *et al.* An in vivo RNAi screening approach to identify host determinants of virus replication. *Cell Host Microbe* **14**, 346–56 (2013).
357. Langlois, R. A., Shapiro, J. S., Pham, A. M. & Tenoever, B. R. In vivo delivery of cytoplasmic RNA virus-derived miRNAs. *Mol. Ther.* **20**, 367–375 (2012).
358. Ma, H., Zhang, J. & Wu, H. Designing Ago2-specific siRNA/shRNA to avoid competition with endogenous miRNAs. *Mol. Ther. - Nucleic Acids* **3**, e176 (2014).
359. Groot, M. & Lee, H. Sorting Mechanisms for MicroRNAs into Extracellular Vesicles and Their Associated Diseases. *Cells* **9**, (2020).
360. Raskov, H., Orhan, A., Christensen, J. P. & Gögenur, I. Cytotoxic CD8+ T cells in cancer and cancer immunotherapy. *British Journal of Cancer* **124**, 359–367 (2021).
361. Sang, W. *et al.* MicroRNA-150 negatively regulates the function of CD4+ T cells through AKT3/Bim signaling pathway. *Cell. Immunol.* **306**–**307**, 35–40 (2016).
362. Principe, N. *et al.* Tumor Infiltrating Effector Memory Antigen-Specific CD8+ T Cells Predict Response to Immune Checkpoint Therapy. *Front. Immunol.* **11**, 1 (2020).
363. Huehls, A. M., Coupet, T. A. & Sentman, C. L. Bispecific T-cell engagers for cancer immunotherapy. *Immunology and Cell Biology* **93**, 290–296 (2015).
364. Heidbuechel, J. P. W. & Engeland, C. E. Oncolytic viruses encoding bispecific T cell

engagers: a blueprint for emerging immunovirotherapies. *J. Hematol. Oncol.* **14**, 63 (2021).
365. Bello-Morales, R., Ripa, I. & López-Guerrero, J. A. Extracellular vesicles in viral spread and antiviral response. *Viruses* **12**, (2020).
366. Raab-Traub, N. & Dittmer, D. P. Viral effects on the content and function of extracellular vesicles. *Nature Reviews Microbiology* **15**, 559–572 (2017).
367. Rozmyslowicz, T. *et al.* Platelet- and megakaryocyte-derived microparticles transfer CXCR4 receptor to CXCR4-null cells and make them susceptible to infection by X4-HIV. *AIDS* **17**, 33–42 (2003).
368. Mack, M. *et al.* Transfer of the chemokine receptor CCR5 between cells by membrane-derived microparticles: A mechanism for cellular human immunodeficiency virus 1 infection. *Nat. Med.* **6**, 769–775 (2000).
369. Xiao, F. *et al.* Hepatitis C Virus Cell-Cell Transmission and Resistance to Direct-Acting Antiviral Agents. *PLoS Pathog.* **10**, (2014).
370. Brimacombe, C. L. *et al.* Neutralizing Antibody-Resistant Hepatitis C Virus Cell-to-Cell Transmission. *J. Virol.* **85**, 596–605 (2011).
371. Zhou, C. *et al.* Exosomes carry microRNAs into neighboring cells to promote diffusive infection of newcastle disease virus. *Viruses* **11**, (2019).
372. Witwer, K. W., Sisk, J. M., Gama, L. & Clements, J. E. MicroRNA Regulation of IFN-β Protein Expression: Rapid and Sensitive Modulation of the Innate Immune Response. *J. Immunol.* **184**, 2369–2376 (2010).
373. Rottiers, V. & Näär, A. M. MicroRNAs in metabolism and metabolic disorders. *Nature Reviews Molecular Cell Biology* **13**, 239–251 (2012).
374. Gross, N., Kropp, J. & Khatib, H. MicroRNA signaling in embryo development. *Biology* **6**, (2017).
375. Shu, J., Resende E Silva, B. V., Gao, T., Xu, Z. & Cui, J. Dynamic and modularized MicroRNA regulation and its implication in human cancers. *Sci. Rep.* **7**, 1–17 (2017).
376. MacFarlane, L.-A. & R. Murphy, P. MicroRNA: Biogenesis, Function and Role in Cancer. *Curr. Genomics* **11**, 537–561 (2010).
377. Hanna, J., Hossain, G. S. & Kocerha, J. The potential for microRNA therapeutics and clinical research. *Frontiers in Genetics* **10**, 478 (2019).
378. Dang, C. V., Reddy, E. P., Shokat, K. M. & Soucek, L. Drugging the 'undruggable' cancer targets. *Nature Reviews Cancer* **17**, 502–508 (2017).
379. Duffy, M. J. & Crown, J. Drugging "undruggable" genes for cancer treatment: Are we making progress? *International Journal of Cancer* **148**, 8–17 (2021).
380. Kamerkar, S. *et al.* Exosomes facilitate therapeutic targeting of oncogenic KRAS in pancreatic cancer. *Nature* **546**, 498–503 (2017).
381. Wang, M. *et al.* Emerging Function and Clinical Values of Exosomal MicroRNAs in Cancer. *Molecular Therapy - Nucleic Acids* **16**, 791–804 (2019).
382. Ha, D., Yang, N. & Nadithe, V. Exosomes as therapeutic drug carriers and delivery vehicles across biological membranes: current perspectives and future challenges. *Acta Pharmaceutica Sinica B* **6**, 287–296 (2016).
383. Sancho-Albero, M. *et al.* Exosome origin determines cell targeting and the transfer of therapeutic nanoparticles towards target cells. *J. Nanobiotechnology* **17**, 16 (2019).

384. Betzer, O. *et al.* Advances in imaging strategies for in vivo tracking of exosomes. *Wiley Interdisciplinary Reviews: Nanomedicine and Nanobiotechnology* **12**, e1594 (2020).
385. Hurwitz, S. N., Olcese, J. M. & Meckes, D. G. Extraction of Extracellular Vesicles from Whole Tissue. *J. Vis. Exp.* (2019). doi:10.3791/59143
386. Brennan, K. *et al.* A comparison of methods for the isolation and separation of extracellular vesicles from protein and lipid particles in human serum. *Sci. Rep.* **10**, 1–13 (2020).
387. Jafari, D. *et al.* Designer Exosomes: A New Platform for Biotechnology Therapeutics. *BioDrugs* **34**, 567–586 (2020).
388. Stickney, Z., Losacco, J., McDevitt, S., Zhang, Z. & Lu, B. Development of exosome surface display technology in living human cells. *Biochem. Biophys. Res. Commun.* **472**, 53–59 (2016).
389. Peyraud, F. & Italiano, A. Combined parp inhibition and immune checkpoint therapy in solid tumors. *Cancers* **12**, 1–28 (2020).
390. Hwang, J. K., Hong, J. & Yun, C. O. Oncolytic viruses and immune checkpoint inhibitors: Preclinical developments to clinical trials. *International Journal of Molecular Sciences* **21**, 1–26 (2020).
391. Kasar, S. *et al.* Systemic in vivo lentiviral delivery of miR-15a/16 reduces malignancy in the NZB de novo mouse model of chronic lymphocytic leukemia. *Genes Immun.* **13**, 109–119 (2012).
392. Ji, J. *et al.* MicroRNA Expression, Survival, and Response to Interferon in Liver Cancer. *N. Engl. J. Med.* **361**, 1437–1447 (2009).
393. Suzuki, H. I. & Miyazono, K. Dynamics of microRNA biogenesis: crosstalk between p53 network and microRNA processing pathway. doi:10.1007/s00109-010-0650-1
394. Qiu, T. *et al.* MiR-145, miR-133a and miR-133b inhibit proliferation, migration, invasion and cell cycle progression via targeting transcription factor Sp1 in gastric cancer. *FEBS Lett.* **588**, 1168–1177 (2014).
395. Osaki, M. *et al.* MicroRNA-143 regulates human osteosarcoma metastasis by regulating matrix metalloprotease-13 expression. *Mol. Ther.* **19**, 1123–1130 (2011).
396. Yu, Z. *et al.* microRNA 17/20 inhibits cellular invasion and tumor metastasis in breast cancer by heterotypic signaling. *Proc. Natl. Acad. Sci. U. S. A.* **107**, 8231–8236 (2010).
397. Zhang, Y. *et al.* MiR-126 and miR-126 * repress recruitment of mesenchymal stem cells and inflammatory monocytes to inhibit breast cancer metastasis. *Nat. Cell Biol.* **15**, 284–294 (2013).
398. Ell, B. *et al.* Tumor-Induced Osteoclast miRNA Changes as Regulators and Biomarkers of Osteolytic Bone Metastasis. *Cancer Cell* **24**, 542–556 (2013).
399. Zhao, Y. *et al.* Combination therapy with bioengineered miR-34a prodrug and doxorubicin synergistically suppresses osteosarcoma growth. *Biochem. Pharmacol.* **98**, 602–613 (2015).
400. Cortez, M. A. *et al.* In vivo delivery of miR-34a sensitizes lung tumors to radiation through RAD51 regulation. *Mol. Ther. - Nucleic Acids* **4**, e270 (2015).
401. Normann, L. S. *et al.* MicroRNA in combination with HER2-targeting drugs reduces breast cancer cell viability in vitro. *Sci. Rep.* **11**, 10893 (2021).
402. Chou, J. *et al.* GATA3 suppresses metastasis and modulates the tumour

microenvironment by regulating microRNA-29b expression. *Nat. Cell Biol.* **15**, 201–213 (2013).
403. Png, K. J., Halberg, N., Yoshida, M. & Tavazoie, S. F. A microRNA regulon that mediates endothelial recruitment and metastasis by cancer cells. *Nature* **481**, 190–196 (2012).
404. Guan, B. *et al.* Tumor-suppressive microRNA-218 inhibits tumor angiogenesis via targeting the mTOR component RICTOR in prostate cancer. *Oncotarget* **8**, 8162–8172 (2017).
405. Cheng, J. *et al.* Downregulation of miRNA-638 promotes angiogenesis and growth of hepatocellular carcinoma by targeting VEGF. *Oncotarget* **7**, 30702–30711 (2016).
406. Di Modica, M. *et al.* Breast cancer-secreted miR-939 downregulates VE-cadherin and destroys the barrier function of endothelial monolayers. *Cancer Lett.* **384**, 94–100 (2017).
407. Wei, J. *et al.* MiR-124 inhibits STAT3 signaling to enhance T cell-mediated immune clearance of glioma. *Cancer Res.* **73**, 3913–3926 (2013).
408. Zhao, J. L. *et al.* Forced activation of notch in macrophages represses tumor growth by upregulating MIR-125a and disabling tumor-associated macrophages. *Cancer Res.* **76**, 1403–1415 (2016).
409. Chaudhuri, A. A. *et al.* MicroRNA-125b Potentiates Macrophage Activation. *J. Immunol.* **187**, 5062–5068 (2011).
410. He, M., Xu, Z., Ding, T., Kuang, D. M. & Zheng, L. MicroRNA-155 regulates inflammatory cytokine production in tumor-associated macrophages via targeting C/EBPβ. *Cell. Mol. Immunol.* **6**, 343–352 (2009).
411. Lou, Q. *et al.* MiR-448 targets IDO1 and regulates CD8+ T cell response in human colon cancer. *J. Immunother. Cancer* **7**, (2019).
412. Squadrito, M. L. *et al.* MiR-511-3p Modulates Genetic Programs of Tumor-Associated Macrophages. *Cell Rep.* **1**, 141–154 (2012).
413. Li, Q. *et al.* miR-28 modulates exhaustive differentiation of T cells through silencing programmed cell death-1 and regulating cytokine secretion. *Oncotarget* **7**, 53735–53750 (2016).
414. Grenda, A. *et al.* Tissue MicroRNA Expression as a Predictor of Response to Immunotherapy in NSCLC Patients. *Front. Oncol.* **10**, 3267 (2021).
415. Zhang, M. *et al.* miRNA-5119 regulates immune checkpoints in dendritic cells to enhance breast cancer immunotherapy. *Cancer Immunol. Immunother.* **69**, 951–967 (2020).
416. Shen, H. *et al.* Reprogramming of Normal Fibroblasts into Cancer-Associated Fibroblasts by miRNAs-Mediated CCL2/VEGFA Signaling. *PLoS Genet.* **12**, (2016).
417. Du, Y. E. *et al.* MiR-205/YAP1 in activated fibroblasts of breast tumor promotes VEGF-independent angiogenesis through STAT3 signaling. *Theranostics* **7**, 3972–3988 (2017).
418. Mitra, A. K. *et al.* MicroRNAs reprogram normal fibroblasts into cancer-associated fibroblasts in ovarian cancer. *Cancer Discov.* **2**, 1100–1108 (2012).

Contributions of collaborators

This project would not have been possible without the guidance and support of many members of the Bell and Ilkow labs as well as others at the OHRI. Specific contributions are listed below:

1. Development of the colony counting macro was completed in collaboration with Julien Yockell-Lelievre (Stanford lab, OHRI).
2. The RNA-sequencing experiment described in Chapter 3 (Figure 3.1) was completed previously by Marie-Ève Wedge and analyzed by Dr. Adrian Pelin.
3. Western blots in Chapter 4 (Figure 4.2) were completed in collaboration with Dr. Mathieu Crupi.
4. All *in vivo* studies were completed with the assistance of Christiano Tanese De Souza and Julia Petryk.
5. The flow cytometry experiment in Chapter 5 (Figure 5.8) was completed in collaboration with Dr. Mathieu Crupi, Dr. Vera Tang and Zaid Taha.

Appendices

A1: Chapter 2 supplemental information

Supplemental Table 1. miRNA oligonucleotide sequences

microRNA	Sense sequence (5'→3')	Antisense sequence (5'→3')
shNTC (miR-30 cassette)	TCGAGAAGGTATATTGCTGTTGACAGTG AGCGAACTGGTTTACATGTCGACTAATA GTGAAGCCACAGATGTATTAGTCGACAT GTAAACCAGTGTGCCTACTGCCTCGG	CTAGCCGAGGCAGTAGGCACACTGGT TTACATGTCGACTAATACATCTGTGGCT TCACTATTAGTCGACATGTAAACCAGTT CGCTCACTGTCAACAGCAATATACCTTC
451miR-BRCA1	TCGACTTGGGAATGGCAAGGCACAAAG TGTGACCACATATTTATGTGGTCACACT TTGTATCTTGCTATACCCAGAAAGCTAGC	CTAGGCTAGCTTTCTGGGTATAGCAAGA TACAAAGTGTGACCACATAAATATGTGG TCACACTTTGTGCCTTGCCATTCCCAAG
451miR-BRCA2	TCGACTTGGGAATGGCAAGGTACAGGAT ATGCGAATTAAGAATAATTCGCATATCCT GTCTCTTGCTATACCCAGAAA	CTAGTTTCTGGGTATAGCAAGAGACAG GATATGCGAATTATTCTTAATTCGCATA TCCTGTACCTTGCCATTCCCAAG
451miR-BRCA1 (new-human)	TCGACTTGGGAATGGCAAGGTTGAATGT TCCTCAAAGTTTTCCCTTTGAGGAACGTT CACTCTTGCTATACCCAGAAA	CTAGTTTCTGGGTATAGCAAGAGTGAA CGTTCCTCAAAGGGAAAACTTTGAGGA ACATTCAACCTTGCCATTCCCAAG
451miR-BRCA1 (new-mouse)	TCGACTTGGGAATGGCAAGGTCACCTTCA CCAAAGCTAGTATGAGCTTTGGTGAGGGT GCTCTTGCTATACCCAGAAA	CTAGTTTCTGGGTATAGCAAGAGCACCC TCACCAAAGCTCATACTAGCTTTGGTGAA GGTGACCTTGCCATTCCCAAG
30miR-BRCA1	TCGAGAAGGTATATTGCTGTTGACAGTG AGCGAACAAAGTGTGACCACATATTTTA GTGAAGCCACAGATGTAAAATATGTGGT CACACTTTGTGTGCCTACTGCCTCGG	CTAGCCGAGGCAGTAGGCACACAAAG TGTGACCACATATTTTACATCTGTGGCT TCACTAAAATATGTGGTCACACTTTGTT CGCTCACTGTCAACAGCAATATACCTTC
150miR-BRCA1	TCGACTCCCCATGGCCCTGAAATATGTGG TCACACTTTGTGCTGGGCTCAGACCCAAA GTGGACGCCATATTTCAGGGACCTGGGGAC	CTAGGTCCCCAGGTCCCTGAAATATGGCG TCCACTTTGGGTCTGAGCCCAGCACAAAG TGTGACCACATATTTCAGGGCCATGGGGAG
99miR-BRCA1	TCGACCCATTGGCATAAAATATGTGGTCAC ACTTTGTGGTGAAGTGGACCGCACAAATTG TCTCCACGTATTCTGTGTCAGTGTG	CTAGCACACTGACACAGAATACGTGGAGA CAATTTGTGCGGTCCACTTCACCACAAAGT GTGACCACATATTTTATGCCAATGGG

143miR-BRCA1	TCGAGCGCAGCGCCCTGTCTCCCAGCCTAC ATAGTGTGACCGCATATTAGGTCAGTTGGG AGTCAAATATGTGGTCACACTTTGTAGGAA GAGAGAAGTTGTTCTGCAGC	CTAGGCTGCAGAACAACTTCTCTCTTCCTA CAAAGTGTGACCACATATTTGACTCCCAAC TGACCTAATATGCGGTCACACTATGTAGGC TGGGAGACAGGGCGCTGCGC
331miR-BRCA1	TCGAGAGTTTGGTTTTGTTTGGGTTTGACAA AGTTGTGATCACATATCGCCCAGATCAAACC AGAAATATGTGGTCACACTTTGTCCAACCTA AGCTC	CTAGGAGCTTAGGTTGGACAAAGTGTGACC ACATATTTCTGGTTTGATCTGGGCGATATGT GATCACAACTTTGTCAAACCCAAACAAAACC AAACTC
hsa-miR-451a	TCGACTTGGGAATGGCAAGGAAACCGTTAC CATTACTGAGTTTAGTAATGGTAATGGTTCT CTTGCTATACCCAGA	CTAGTCTGGGTATAGCAAGAGAACCATTAC CATTACTAAACTCAGTAATGGTAACGGTTTC CTTGCCATTCCCAAG
hsa-miR-150	TCGACTCCCCATGGCCCTGTCTCCCAACCC TTGTACCAGTGCTGGGCTCAGACCCTGGT ACAGGCCTGGGGGACAGGGACCTGGGGAC	CTAGGTCCCCAGGTCCCTGTCCCCCAGGCCT GTACCAGGGTCTGAGCCCAGCACTGGTACA AGGGTTGGGAGACAGGGCCATGGGGAG
hsa-miR-331	TCGAGAGTTTGGTTTTGTTTGGGTTTGTT CTAGGTATGGTCCCAGGGATCCCAGATC AAACCAGGCCCCTGGGCCTATCCTAGAA CCAACCTAAGCTC	CTAGGAGCTTAGGTTGGTTCTAGGATAGGC CCAGGGGCCTGGTTTGATCTGGGATCCCTG GGACCATACCTAGAACAAACCCAAACAAAA CCAAACTC
hsa-miR-99a	TCGACCCATTGGCATAAACCCGTAGATCC GATCTTGTGGTGAAGTGGACCGCACAAG CTCGCTTCTATGGGTCTGTGTCAGTGTG	CTAGCACACTGACACAGACCCATAGAAGCG AGCTTGTGCGGTCCACTTCACCACAAGATCG GATCTACGGGTTTATGCCAATGGG
hsa-miR-143	TCGAGCGCAGCGCCCTGTCTCCCAGCCTG AGGTGCAGTGCTGCATCTCTGGTCAGTTG GGAGTCTGAGATGAAGCACTGTAGCTCAG GAAGAGAGAAGTTGTTCTGCAGC	CTAGGCTGCAGAACAACTTCTCTCTTCCTGA GCTACAGTGCTTCATCTCAGACTCCCAACTG ACCAGAGATGCAGCACTGCACCTCAGGCTG GGAGACAGGGCGCTGCGC
hsa-miR-182 (x1)	CTCGAGACAGACCGAGGCCTCCCCAGCTCCTGGGGGGAGCTGCTTGCCTCCCCCCGTTTTTGGCAATGG TAGAACTCACACTGGTGAGGTAACAGGATCCGGTGGTTCTAGACTTGCCAACTATGGGGCGAGGACTCA GCCGGCACCCTGTGCACAGCCAGCGAGGGAAGGGCCGGGCGATCGCGCTAGC	
hsa-miR-182 (x2)	CTCGAGGGCGCGCCACAGACCGAGGCCTCCCCAGCTCCTGGGGGGAGCTGCTTGCCTCCCCCCGTTTTT GGCAATGGTAGAACTCACACTGGTGAGGTAACAGGATCCGGTGGTTCTAGACTTGCCAACTATGGGGC GAGGACTCAGCCGGCACCCTGTGCACAGCCAGCGAGGGAAGGGCCGGACAGACCGAGGCCTCCCCAG CTCCTGGGGGGAGCTGCTTGCCTCCCCCCGTTTTTGGCAATGGTAGAACTCACACTGGTGAGGTAACAG GATCCGGTGGTTCTAGACTTGCCAACTATGGGGCGAGGACTCAGCCGGCACCCTGTGCACAGCCAGCG AGGGAAGGGCCGGGCGATCGCGCTAGC	

Supplemental Table 2. **PCR and qPCR primers**

Gene	Forward sequence (5’-3’)	Reverse sequence (5’-3’)
18S (human/mouse)	CTCAACACGGGAAACCTCAC	CGCTCCACCAACTAAGAACG
RPlP0 (human)	TTAAACCCTGCGTGGCAATCC	TTAAACCCTGCGTGGCAATCC
VSV insert sequencing (G)	CAGTAGTTGGAAAAGCTCTATTGCC	
pri-miR-150 insert	TATACTCGAGGGAGTGGGTGTGCAGTTTC	TATAGCTAGCACTTTGCGCATCACACAGAG
hRGS17 (human)	GGAGAGTATCCAGGTCCTAGAG	CACTGTATTCTGTTCGGAGGAAC
hFOXO3 (human)	TCTACGAGTGGATGGTGCGTTG	CTCTTGCCAGTTCCCTCATTCTG
hCHEK2 (human)	GACCAAGAACCTGAGGAGCCTA	GGATCAGATGACAGCAGGAGTTC
hSMARCD3 (human)	CAGGAGATCAGTGCTCTGGACA	GAGCAGGTCTTGGACATAGCCT
CDKN1B (human)	ATAAGGAAGCGACCTGCAACCG	TTCTTGGGCGTCTGCTCCACAG
BRCA1 (human)	CTTAGAGTGTCCCATCTGTCTGG	CAGCATGCAAAATTTGCAAAATATG
BRCA1 (mouse)	CTTAGAGTGTCCGATCTGTTTGG	CAGCATACAAAATTTGCAAAATATG
BRCA2 (human)	GAAGAACCTTTAGATTTAATTACAAGTC	GTATACAGCTGTTTATGAGAACACG
BRCA2 (mouse)	CGTCAGTTTAACAAAGATTTAATGTC	GTATATATAGAGCTGCTTAGGAGAAC
KRAS (human)	CAGTAGACACAAAACAGGCTCAG	TGTCGGATCTCCCTCACCAATG
FOSL2 (human)	CAGCCAGCTTGTTCCTCT	GATCAAGACCATTGGCACCA
ABL2 (human)	CGGACACTGAAGAAACAGGTGG	GTCTCTTTGCTTTCGAGGCAGTG
MSI2 (human)	GCAGACCTCACCAGATAGCCTT	AAGCCTCTGGAGCGTTTCGTAG
ASAP3 (human)	TTCATAGTCCTTCCATGCCTTC	CTGCGCTCTTCAAGAACCT
HK2 (human)	GAGTTTGACCTGGATGTGGTTGC	CCTCCATGTAGCAGGCATTGCT
DNMT3A (human)	CCTGCTTTATGGAGTTTGACCT	GTAACCTTCCCGGTATGAACAG
MIF (human)	AGAACCGCTCCTACAGCAAGCT	GGAGTTGTTCCAGCCCACATTG
MDM4 (human)	GTATCAGAGCAGTTAGGTGTTGG	GACTTAGAGTCCTCCAGGTCATC
TGFBR1 (human)	GCCAGTCCTAAGTCTGCAAT	GGTCTTGCCCATCTTCACA
PSMB8 (human)	GGGACTGGAAGAATTCTGTGG	GCTCCTGGCTGACTTCTAGT
Myb (human)	GGGAACAGATGGGCAGAAATCG	GCTGGCTTTTGAAGACTCCTGC
ERBB2 (human)	GGAAGTACACGATGCGGAGACT	ACCTTCCTCAGCTCCGTCTCTT
BAZ2A (human)	GTGTGAGATACAGTAGATAAGCCA	ACTGAAACCCTCTCCTTCCT
FGFR3 (human)	TCCATCTCCTGGCTGAAGAACG	TGTTCTCCACGACGCAGGTGTA

Supplemental Table 3. Antibodies used for flow cytometry analysis.

Antibody	Fluorophore	Channel	Concentration	Catalogue number
eBioscience™ Fixable Viability Dye	eFluor780	APC-Cy7	1:1000	65-0865-14
CD4	V500	AmCyan	1:300	560783
CD8	Pe-Cy7	Pe-Cy7	1:300	100722
CD3	PerCp Cy5.5	PerCp Cy5.5	1:100	100218
CD45	AF700	AF700	1:300	103218
CD25	BV650	Qdot655	1:100	564021
KLRG1	PE-Dazzle 594	PE-Texas Red	1:100	138424
CD44	FITC	FITC	1:100	103022
CD122	PE	PE	1:100	105906

All flow antibodies were purchased from BD Bioscience except viability dye (Thermo Fisher Scientific).

Colony forming macro for ImageJ analysis

(The following protocol begins by stitching together images acquired using ArrayScan VTI HCS, if images are acquired by other methods these initial steps may be skipped)

```
//Get starting time
getDateAndTime(year,month,dayOfWeek,dayOfMonth,hour,minute,second,millisecond);
H0=hour;
M0=minute;
S0=second;
run("Set Measurements...", "shape redirect=None decimal=0");

//Sets up directories
dir1=getDirectory("Choose images directory");
dir2=getDirectory("Choose results directory");

setBatchMode(false);

//Create field array
Fields=newArray(143,142,141,140,139,138,137,136,135,134,133,132,100,99,98,97,96,95,94,93,92,91,90
,131,101,64,63,62,61,60,59,58,57,56,89,130,102,65,36,35,34,33,32,31,30,55,88,129,103,66,37,16,15,14,
13,12,29,54,87,128,104,67,38,17,"04","03","02",11,28,53,86,127,105,68,39,18,"05","00","01",10,27,52,
85,126,106,69,40,19,"06","07","08","09",26,51,84,125,109,70,41,20,21,22,23,24,25,50,83,124,108,71,4
2,43,44,45,46,47,48,49,82,123,109,72,73,74,75,76,77,78,79,80,81,122,110,111,112,113,114,115,116,11
7,118,119,120,121);

//Creates items list
list=getFileList(dir1);

//Create an Array for all the wells
Wells=newArray(list.length/144);

//Create an Array for all the Plates
Plates=newArray(list.length/144);

//Create an Array for the colonies
Colonies=newArray(list.length/144);

//Process each well one at a time
for(i=0; i < list.length/144; i++)
{
        showProgress(i+1, list.length);

//create well name
        name=list[i*144];
        name=substring(name, 0,36);
```

```
//processing the well
	for(j=0; j < 144; j++)
	{
		open(dir1+name+Fields[j]+"d0.tiff");
		run("Subtract Background...", "rolling=50 light");
		run("Flip Vertically");
	}
	run("Images to Stack", "name=Stack title=[] use");
	run("Make Montage...", "columns=12 rows=12 scale=1");
	run("Properties...", "channels=1 slices=1 frames=1 unit=pixel pixel_width=1 pixel_height=1
voxel_depth=1.0000000");
	run("Duplicate...", "title=temp");
	setAutoThreshold("Triangle");
	run("Threshold...");
	run("Convert to Mask");
	run("Options...", "iterations=2 count=1 do=Erode");
	run("Options...", "iterations=10 count=1 do=Dilate");
	run("Fill Holes");
	run("Options...", "iterations=5 count=1 do=Erode");
	run("Options...", "iterations=10 count=1 do=Dilate");
	run("Analyze Particles...", "size=30000-Infinity clear add");
	Count=roiManager("count");
	for(j=0; j < Count; j++)
	{
		roiManager("Select", Count-(j+1));
		roiManager("Measure");
		Ratio=getResult("AR", 0);
		if (Ratio>3)
		{
			roiManager("Delete");
		}
		run("Clear Results");
	}
	roiManager("Select All");
	roiManager("Combine");
	setBackgroundColor(0, 0, 0);
	run("Clear Outside");
	run("Invert");
	roiManager("Show None");
	roiManager("Show All");
	roiManager("Show None");
	run("Invert");
	run("Fill Holes");
	run("Scale...", "x=.5 y=.5 interpolation=None create");
	selectWindow("temp");
	close();
	rename("temp");
```

```
        run("Options...", "iterations=10 count=4 do=Dilate");
        run("Watershed");
        run("Scale...", "x=2 y=2 interpolation=None create");
        selectWindow("temp");
        close();
        roiManager("Select All");
        roiManager("Delete");
        run("Analyze Particles...", "size=30000-Infinity clear add");
        close();
        roiManager("Show All");

        //Save the image after Flattening it
        run("Flatten");
        name=substring(name, 20,36);
        plate=substring(name, 0,11);
        well=substring(name, 12, 15);
        saveAs("Jpeg", dir2+name+".jpg");

        //Save the colony counts
        Count=roiManager("count");
        if (Count>=1)
{
        roiManager("Select All");
        roiManager("Delete");
}
        Colonies[i]=Count;
        Plates[i]=plate;
        Wells[i]=well;

        while (nImages>0)
        {
         selectImage(nImages);
         close();
   }
}

//Create table using the Colonies array and save it as an excel file
run("Clear Results");
for(i=0; i < list.length/144; i++)
{
        setResult("Plate", i, Plates[i]);
        setResult("Well", i, Wells[i]);
        setResult("Colonies", i, Colonies[i]);
}

saveAs("Results", dir2+"April24_T47D_1.csv");

//Get finishing time
```

```
getDateAndTime(year,month,dayOfWeek,dayOfMonth,hour,minute,second,millisecond);
H1=hour;
M1=minute;
S1=second;
H=H1-H0;
M=M1-M0;
S=S1-S0;
showMessage("All done!", "Time elapsed: "+H+" hours, "+M+" minutes and "+S+" seconds");
```

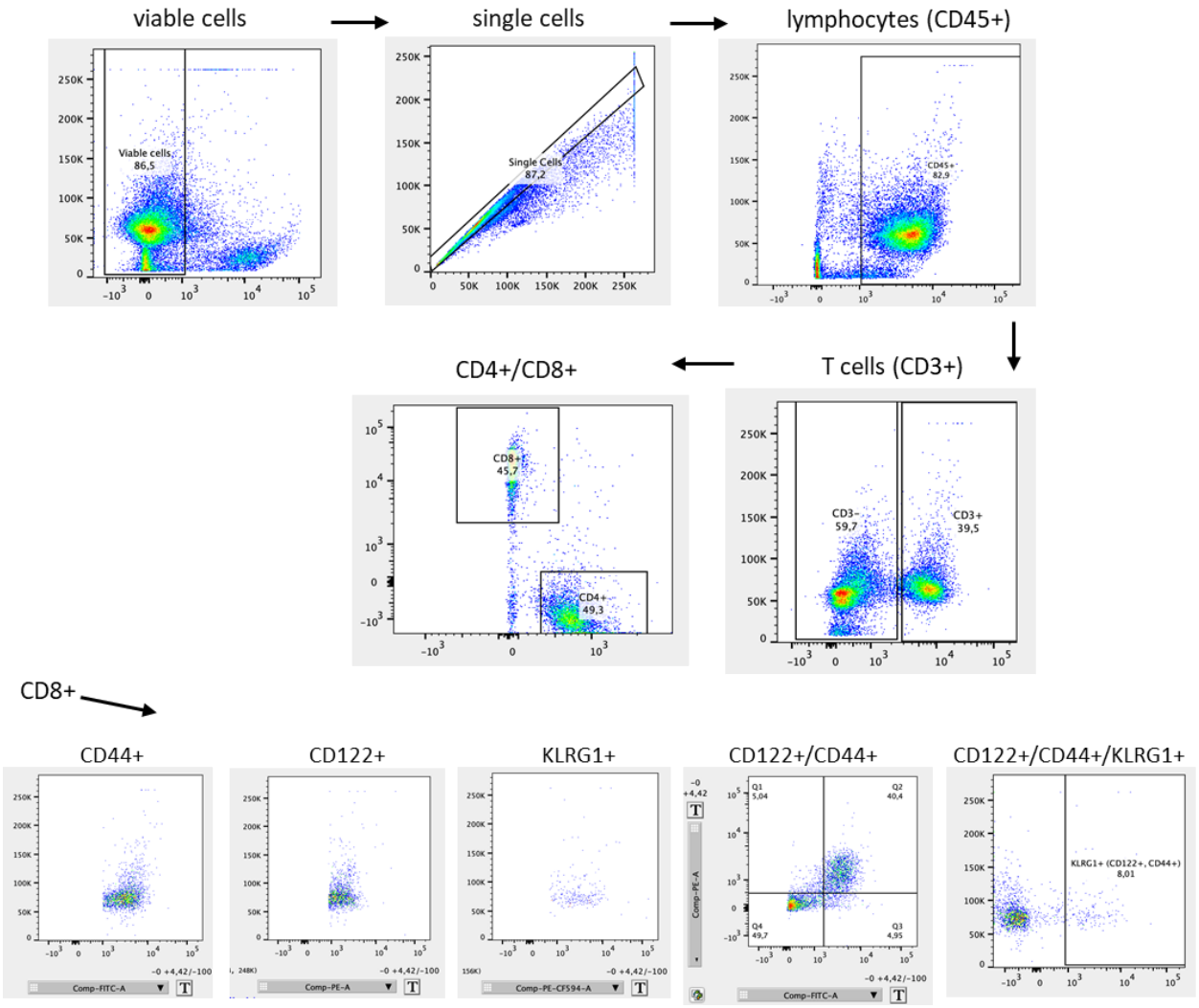

Figure S2.1 Gating strategy for MC38 flow experiment

A2: Chapter 3 supplemental information

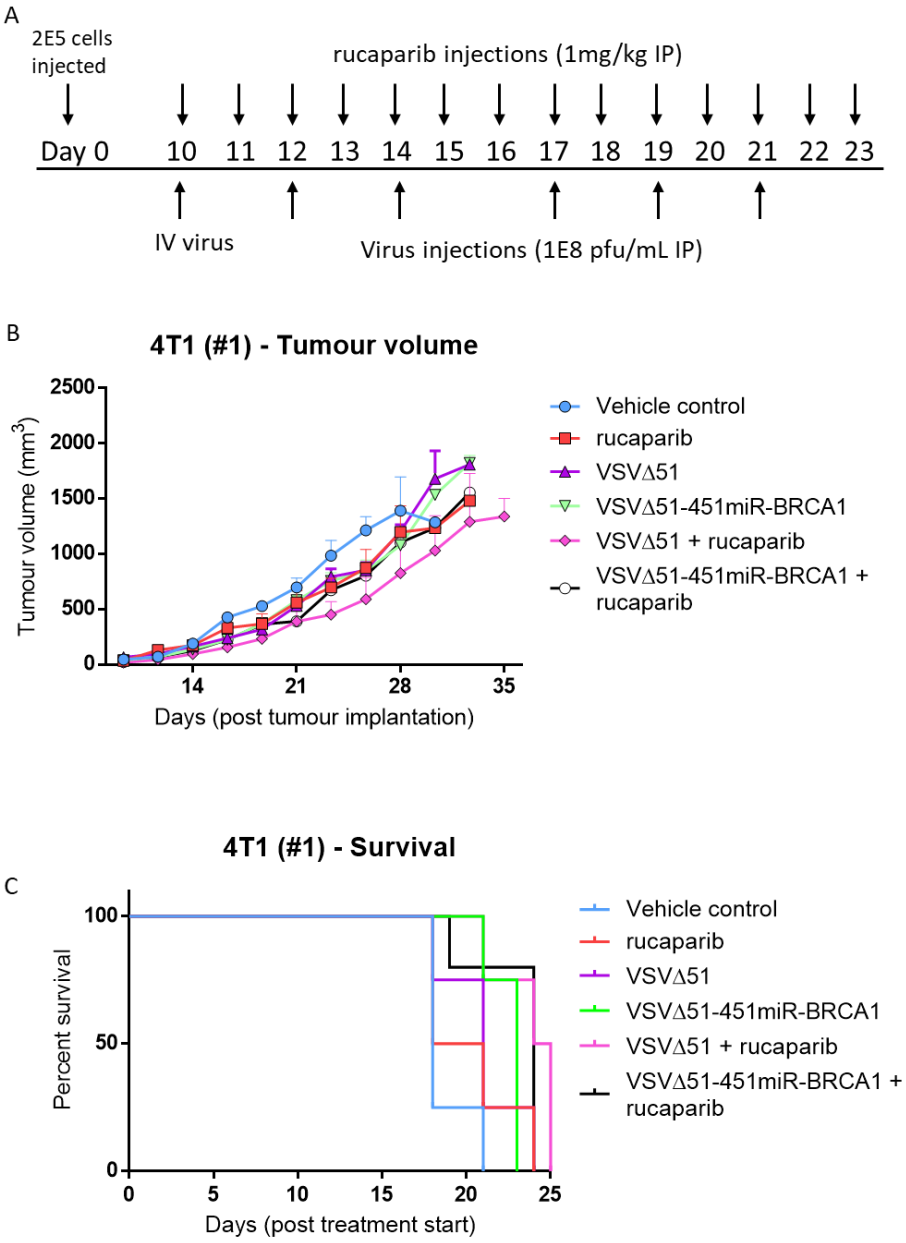

Figure S3.1 VSVΔ51-451miR-BRCA1 infection combined with rucaparib (1mg/kg) does not control tumour growth or increase survival in the 4T1 in vivo model. (A) Treatment was performed as shown above beginning 10 days post-tumour implantation. (B) Tumour measurements were completed three-times per week and (C) survival was determined when mice reached end-point either due to large tumour burden (>15x15mm) or respiratory distress.

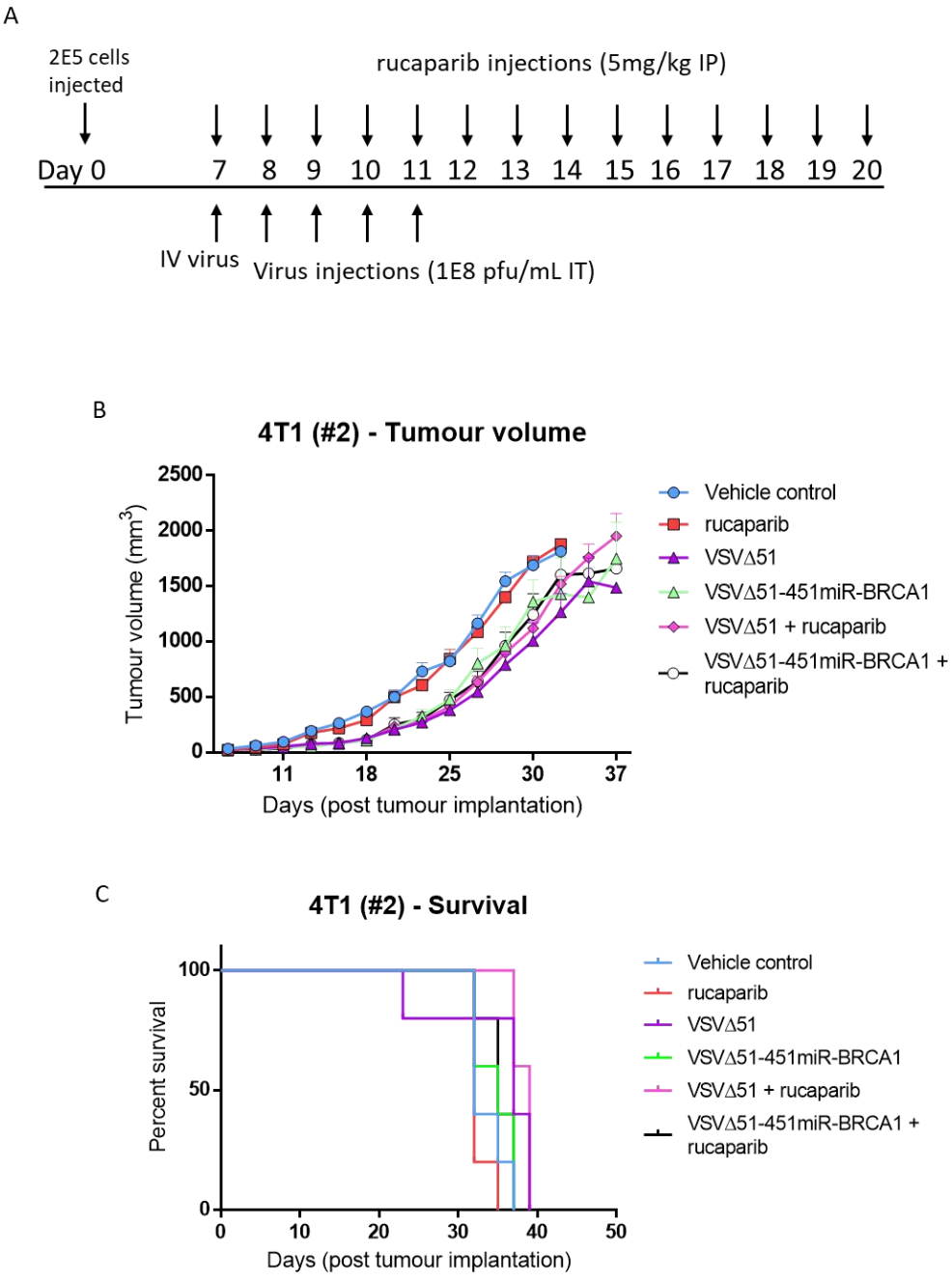

Figure S3.2 VSVΔ51-451miR-BRCA1 infection combined with rucaparib (5mg/kg) has a small impact on tumour burden but does not impact overall survival the 4T1 in vivo model. (A) Treatment was performed as shown above beginning 7 days post-tumour implantation. (B) Tumour measurements were completed three-times per week and (C) survival was determined when mice reached end-point either due to large tumour burden (>15x15mm) or respiratory distress.

miR-451 cassette design strategy

1. Sequence selection – search for a 17nt sequence (reverse compliment to the mRNA target site) with the following characteristics using http://www.geneinfinity.org/sms/sms_DNApatterns.html:
    a) Position 1 = T (may be replaced with A if needed, try to avoid G and C)
    b) Position 10 and 11 = CC (may be replaced with G if needed)
    c) Position 11 – 17 must contain up to 3 G-C pairs (may increase to a maximum of 4)

    Note: The terminal loop sequence does not impact miRNA maturation
2. Extend sequence 5nt to produce the 22nt 5' guide strand
3. Trim 4nt and reverse compliment to produce the 18nt 3' passenger strand
4. Replace position 23 (on the passenger strand) by extending the guide strand by 1nt (try to use a sequence that will create a mismatch at this point)
5. Create a mismatch at position +35 (to create a bulge)

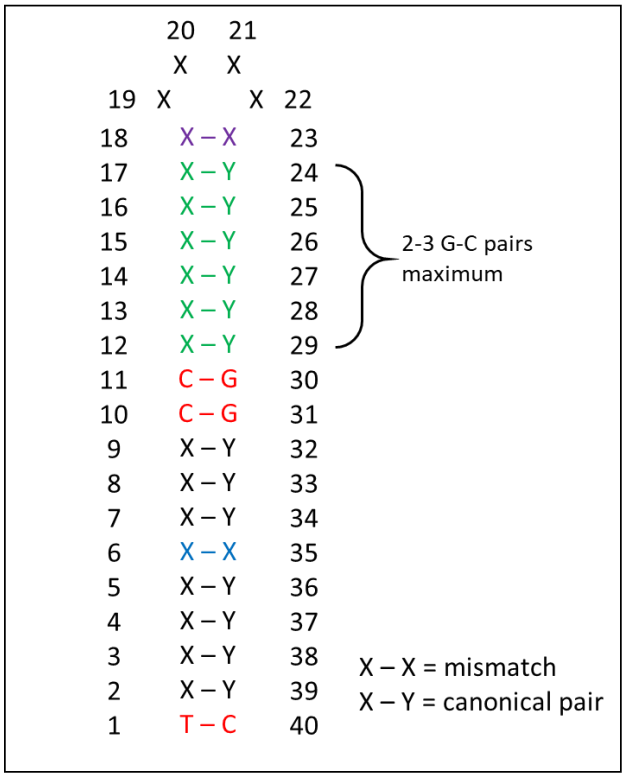

Figure S3.3 miR-451 design strategy. The approach described here was formulated based on two previous publications which aimed to reveal characteristics critical for optimal miRNA processing of miR-451[200,201].

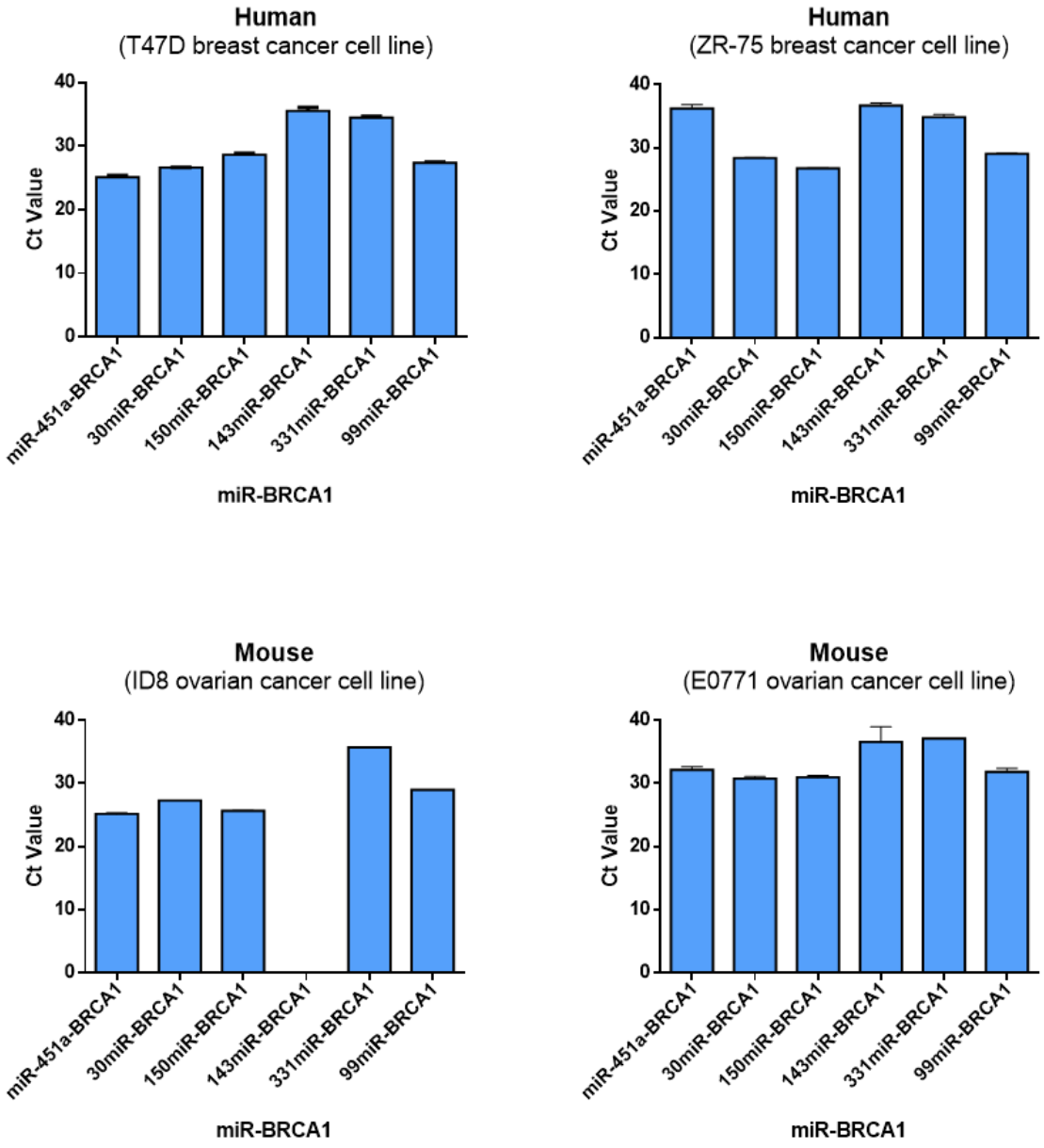

Figure S3.4 qPCR analysis demonstrating expression of the mature BRCA1 amiRNAs expressed from VSVΔ51 in human (T47D and ZR-75) and mouse (ID8 and E0771) cell lines. Cells were infected at MOI 0.1 for 24 hours prior to RNA isolation. Error bars represent standard error of mean (n=3 technical replicates).

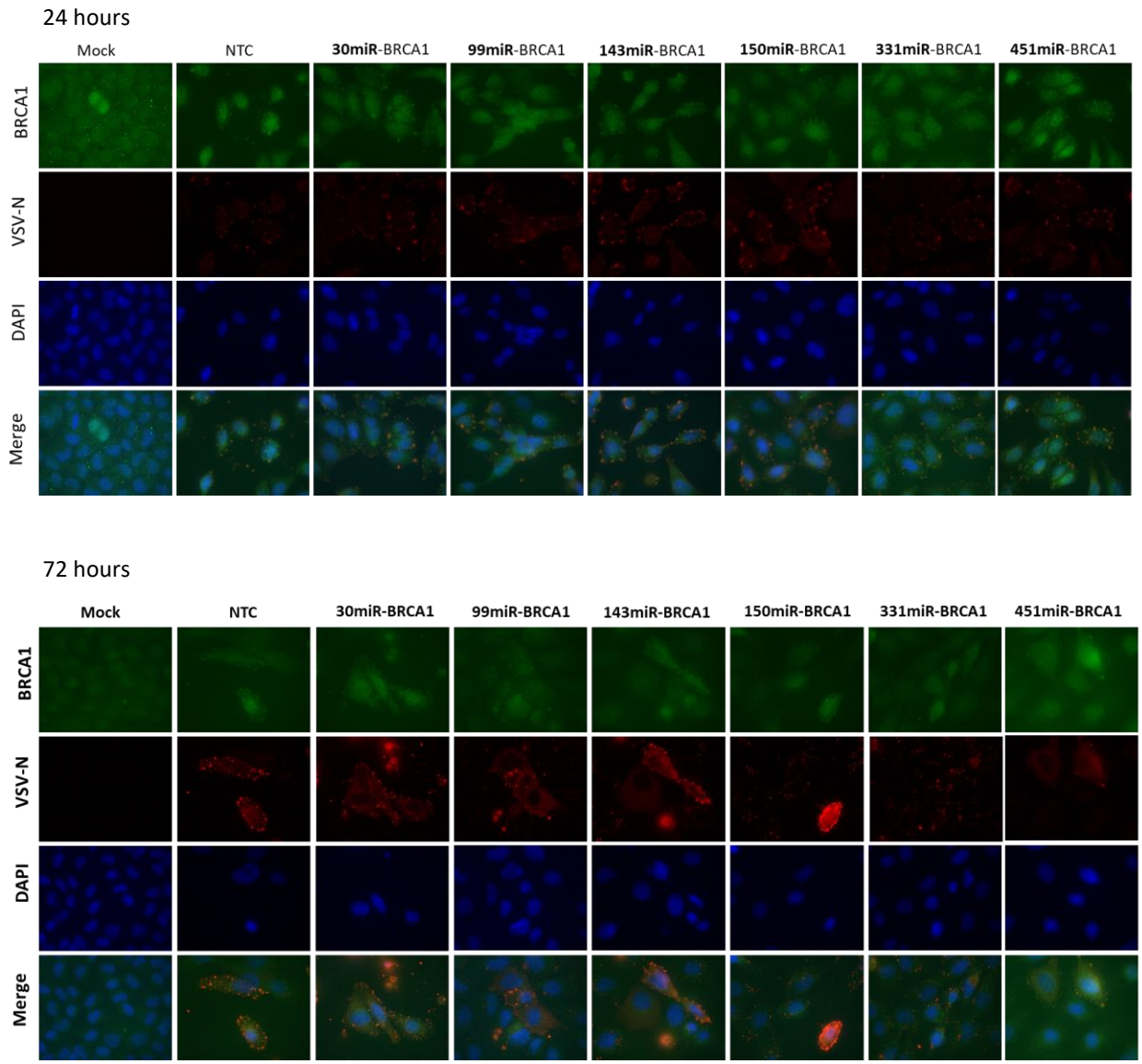

Figure S3.5 Immunofluorescence demonstrating no change in BRCA1 protein expression following infection with G-less VSVΔ51-miR-BRCA1 viruses. ID8 cells were infected at MOI 1 for 24 and 72 hours. VSV-N staining has been included here to ensure there was sufficient infection using the non-replicating versions of each virus.

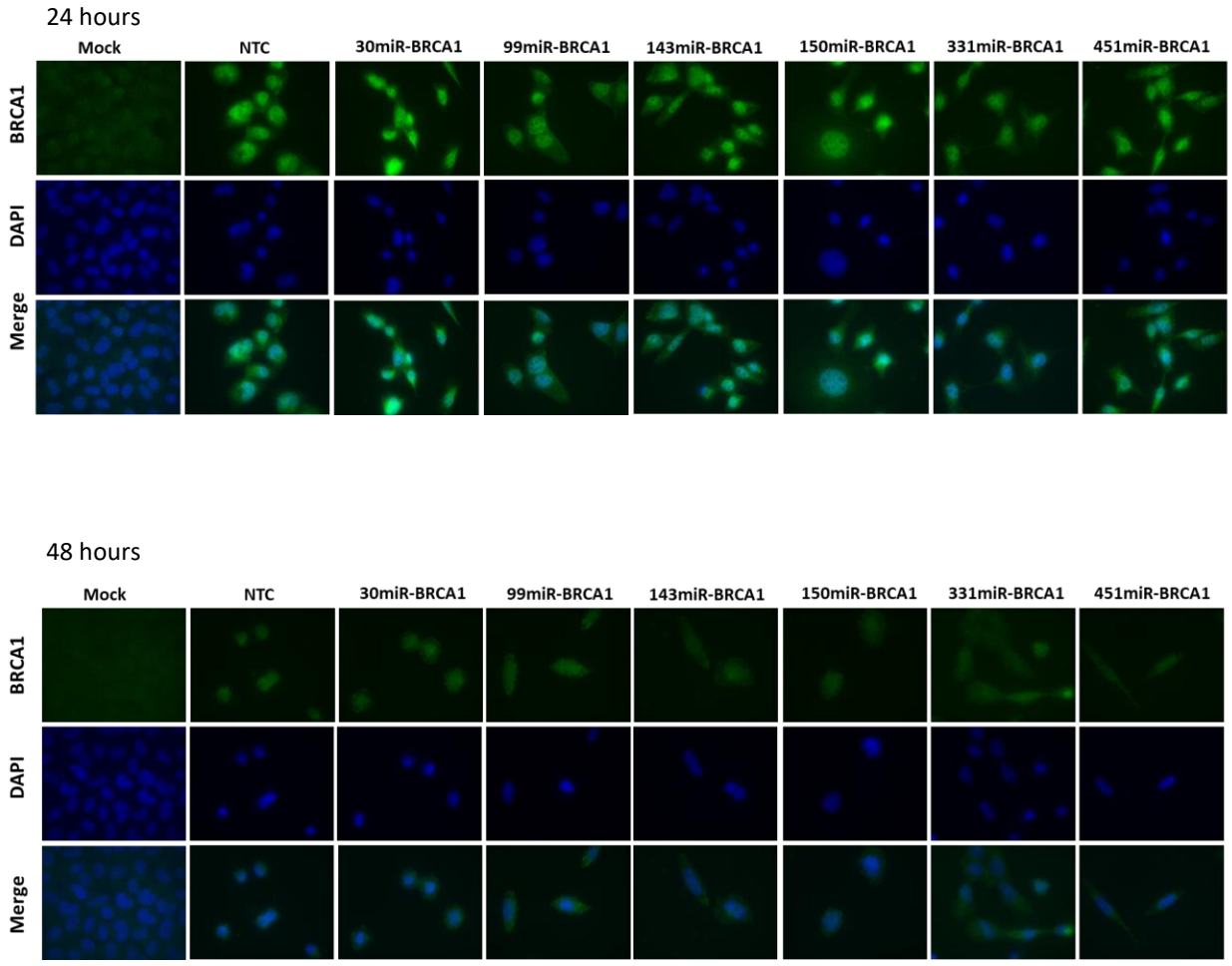

Figure S3.6 Immunofluorescence demonstrating no change in BRCA1 protein expression following infection with replicating VSVΔ51-miR-BRCA1 viruses. ID8 cells were infected at MOI 0.1 for 24 and 48 hours.

A3: Chapter 5 supplemental information

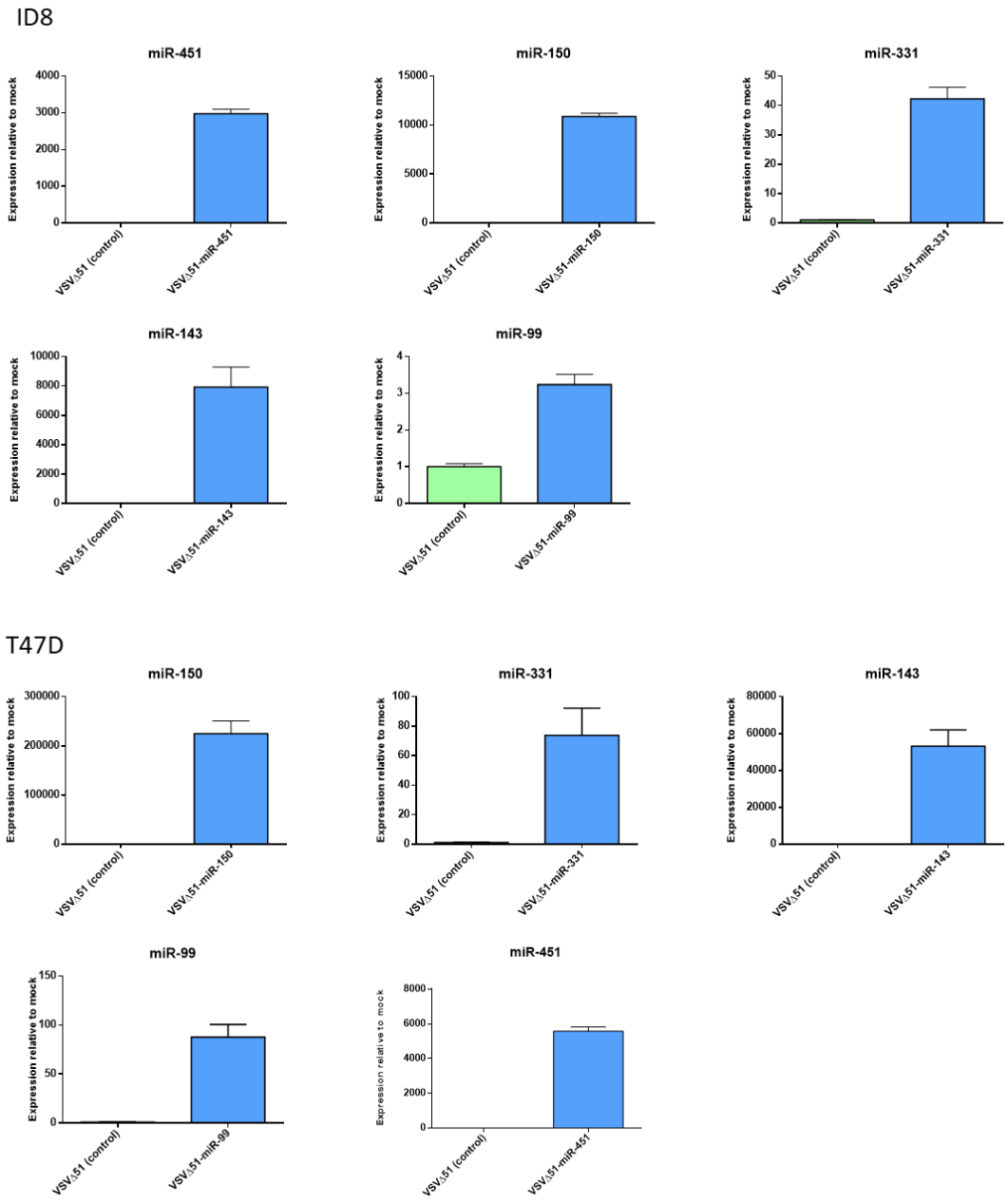

Figure S5.1 Relative expression of EV-miRNAs (mature form) from additional cell lines to demonstrate the versatility of these viruses to produce miRNAs across varying cell types. Expression is relative to the non-targeting control (shNTC) in ID8 and T47D cells. Cells were infected at MOI of 0.1 for 24 hours. The relative expression of each EV-miRNA following infection with the NTC has been set to 1. Error bars represent standard error of mean (n=1, 3 technical replicates).

A4: Engineering and characterization of a novel complementary nanoluciferase based biosensor for the rapid screening of SARS-CoV-2 therapeutics

Preface

The contents of this appendix contain a concise collection of results which have been previously published (listed below). Each manuscript was very collaborative; thus, I have specifically highlighted experiments which I was closely involved with.

1. Emily E. F. Brown*, Reza Rezaei*, **Taylor R. Jamieson***, Jaahnavi Dave*, Nikolas T. Martin, Mathieu J.F. Crupi, Stephen Boulton, Sarah Tucker, Jessie Duong, Joanna Poutou, Adrian Pelin, Hamed Yasavoli-Sharahi, Zaid Taha, Rozanne Arulanandam, Abera Surendran, Mina Ghahremani, Chantal Matar, Jean-Simon Diallo, Ragunath Singaravelu, John C. Bell , Carolina S. Ilkow, and Taha Azad. **Characterization of Critical Determinants of ACE2-RBD Interaction.** *International Journal of Molecular Sciences* 22(5), 2268 (2021). (*equal authorship contribution)

2. Taha Azad, Ragunath Singaravelu, Zaid Taha, **Taylor R. Jamieson**, Stephen Boulton, Mathieu J.F. Crupi, Nikolas T. Martin, Joanna Poutou, Mina Ghahremani, Adrian Pelin, Kazem Nouri, Christopher Boyd Marshall, Rozanne Arulanandam, Emily E.F. Brown, Nouf Alluqmani, Reuben Samson, Anne-Claude Gingra, Bill Cameron, Peter A. Greer, Carolina S. Ilkow, Jean-Simon Diallo, John C. Bell. **Nanoluciferase complementation-based biosensor reveals the importance of N-linked glycosylation of SARS-CoV-2 Spike for viral entry.** *Molecular therapy*, 21 (2021).

Introduction

In December 2019, a novel coronavirus was identified which we now know as SARS-CoV-2, the causative agent of coronavirus disease 2019 (covid-19)[1]. SARS-CoV-2 belongs to the large family of viruses *Coronaviridae*. These enveloped viruses comprise a large positive-sense RNA genome and are responsible for respiratory and intestinal infections in both humans and animals[2]. As of May 26, 2021, there have been more than 168 million reported cases of covid-19 globally and more than 3.4 million deaths[3]. Currently, there are more than 500 different covid-19 therapeutic drugs under development and more than 400 undergoing clinical trials[4]. A rapid method for screening the efficacy of therapeutics which aim to disrupt the host-viral interaction is clearly needed.

We have used the recently developed Nanoluciferase (or NanoLuc) Binary Technology (NanoBiT) to create a biosensor assay to investigate the host-viral interactions of SARS-CoV-2. Entry of the SARS-CoV-2 virus into mammalian cells occurs through binding of the viral Spike (S) protein to the Angiotensin Converting Enzyme 2 (ACE2) host receptor, via the receptor binding domain (RBD) of the S protein[5]. The NanoBiT system features a split NanoLuc protein separated into a large fragment (LgBiT) and a smaller fragment (SmBiT), each bound to proteins of interest[6]. In our case, RBD has been bound to LgBiT and ACE2 has been bound to SmBiT, both with a glycine-serine linker between the NanoBit and its respective protein to allow for enhanced flexibility (**Figure A4.1**). Importantly, SmBiT and LgBiT possess inherently low affinity for binding one another and rely on the interaction of their fused partner proteins to come together. Thus, the SARS-CoV-2-NanoBiT biosensor described here may be used to evaluate changes in the ability of the RBD to bind ACE2 through changes in luminescence with addition of the NanoLuc substrate.

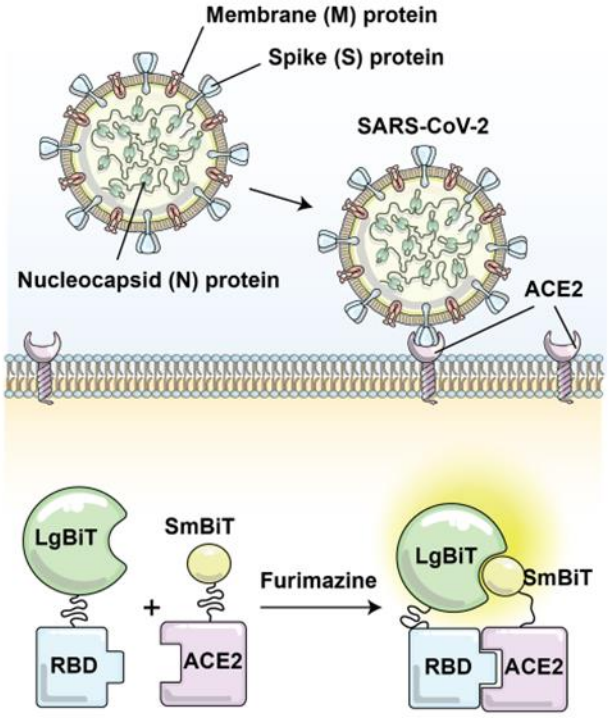

Figure A4.1 NanoLuc Binary Technology (NanoBiT) biosensor design. LgBiT has been linked to the SARS-CoV-2 spike protein RBD and SmBiT has been linked to the ACE2 receptor. When successful interaction of the two sub-units occurs, luminescence will be detectable with the addition of furimazine (NanoLuc substrate).

Methodology

Cell lines

HEK293T (ATCC® CRL-3216) human embryonic kidney cells were obtained from ATCC. Cells were maintained in Dulbecco's Modified Eagle's Medium (Gibco, Gaithersburg, MD, USA), supplemented with 10% FBS (VWR, Mississauga, ON, Canada) and 1% penicillin/streptomycin (Invitrogen, Grand Island, NY, USA). Cells were incubated in a humidified 37°C incubator at 5% CO_2. Cells are routinely tested for mycoplasma by PCR testing and used for up to 20 passages after thawing.

Plasmid construction

Inserts outlined in Table S1 (Supplemental information available online for article 2 listed above https://www.cell.com/molecular-therapy-family/molecular-therapy/fulltext/S1525-0016(21)00074-5#supplementaryMaterial) were ordered from GenScript. Bioreporter subunits were cloned into the BamHI/NotI sites of pcDNA3.1 to generate mammalian expression constructs. SARS-CoV-2 RBD-TMD WT and mutant constructs were cloned into the BamHI/NotI sites of pcDNA3.1 or the XhoI/NheI sites of VSV backbone plasmid.

In vitro NanoLuc assay

293T cells (3E5 cells) were plated in 12-well plates in triplicate 24 hours before transfection. Five hundred nanograms of the bioreporter constructs was transfected using PolyJet transfection reagent (SignaGen Laboratories). After 48 hours, supernatant or cell lysates were collected. Cells were lysed using passive lysis buffer (Promega). NanoLuc luciferase assays were performed using

one of two substrates: FMZ (Nano-Glo cell reagent, Promega) or native CTZ (3.33 mM final concentration; Nanolight Technologies-Prolume, Pinetop, AZ, USA). A synergy microplate reader (BioTek, Winooski, VT, USA) was used to measure luminescence. Results are presented as RLU normalized to control. The data presented are the mean of three independent experiments.

Bioreporter-based neutralization assay

For the neutralization assay with monoclonal antibodies and patient sera, 5 µg of RBD-LgBiT containing cell lysates was incubated at 37^{o}C for 25 min with candidate antibodies or serum. Then, 50 µg of SmBiT-ACE2-transfected cell lysate was added and then incubated for an additional 5 min at room temperature. The amount of mentioned protein was determined using a bicinchoninic acid (BCA) assay, and it refers to total protein. Subsequently, a luciferase assay was performed. The following monoclonal RBD antibodies were tested in the bioreporter-based neutralization assay: 1A9 (GeneTex, GTX632604); 2414 (Active Motif, 91349), 1414 (Active Motif, 91361), 273074 (Abcam, ab273074), 40592 (Sino Biological, 40592-MM57), 9ACA (GenScript, 5B7D7), 11D11F2 (GenScript), 10G6H5 (Genscript), HC2001 (GenScript), and L00847 (Genscript Biotech).

Virus rescue

To rescue the recombinant VSV viruses expressing SARS-CoV-2 RBD or RBD-TMD, HEK293T cells were infected with vaccinia virus expressing T7 RNA polymerase (MOI = 0.5) for 2 h. Inoculum was removed and cells were transfected with the viral backbone plasmid along with T7 RNA polymerase-driven expression plasmids for VSV N, L, and P genes. Forty-eight hours post

transfection, the recombinant virus was collected, filtered (0.2 μm) and plaque purified in Vero cells.

In vivo vaccination studies

Female 6-week-old BALB/C mice (Charles River Laboratories, Malvern, PA, USA) were vaccinated intravenously with 1E7 plaque-forming units (PFU) of VSVΔ51-expressing RBD-TMD WT or mutants (N331A or N343A). Sera were collected from mice using saphenous vein bleeds at days 7 and 14 post-inoculation using sera collection tubes. Blood was incubated on ice for 30 min and then centrifuged to separate sera.

VSV-S neutralization assay

VSV pseudotyped with SARS-CoV-2 spike (VSV-S) was a kind gift from Dr. Sean Whelan (Washington University, St. Louis, MO, USA). Vero E6 cells were seeded in 96-well plates such that 4E5 cells were in each well at the time of infection. Serial dilutions of mouse sera were performed and then co-incubated with an equal volume of VSV-S (2,000 PFU per well) and incubated for 1 h at 37°C. After 1 h, media on the cell were replaced with 60 μL of the virus/serum and incubated for 1 h at 37°C. Wells were then topped up with carboxymethylcellulose (CMC) in DMEM supplemented with 10% FBS for a final concentration of 3% CMC and incubated 24 h at 34°C. GFP foci were imaged and counted using a Cellomics ArrayScan VTI HCS reader.

SDS-PAGE electrophoresis and immunoblotting

Whole-cell lysates were obtained by lysing cells in radioimmunoprecipitation assay (RIPA) buffer (pH 7.4; 25 mM Tris-HCl, 150 mM NaCl, 1% Nonidet P-40 [NP-40], 0.5% sodium deoxycholate,

SDS) and 1× protease inhibitor cocktail (Roche) on ice. Protein concentration was measured by a Pierce BCA assay (Thermo Scientific), and 10 µg of cell extract was mixed into DTT-Laemmli buffer and boiled for 5 min. Samples were resolved using the NuPAGE SDS-PAGE system (Invitrogen) and transferred to a nitrocellulose membrane. Blots were probed with primary antibodies, including anti-FLAG (1:1,000, MilliporeSigma, F3165), anti-β-actin (1:10,000, Sigma, A5441), anti-hemagglutinin (HA) (1:1,000, Sigma, H6908), anti-RBD (1:1,000, RayBiotech, 130-10759), and anti-S (1:1,000, GeneTex, 1A9), and then washed and probed with the appropriate secondary antibodies, including anti-mouse, anti-rabbit (MilliporeSigma, A9169) or anti-goat (Abcam, Cambridge, UK, ab97110). Blots were imaged using the ChemiDoc MP imaging system (Bio-Rad Laboratories, Mississauga, ON, Canada). Clarity western enhanced chemiluminescence (ECL) substrate (Bio-Rad) was used to visualize the blot.

Statistical analysis

All graphs and statistical analyses were generated using Excel or GraphPad Prism v.8. Means of two groups were compared using a two-tailed unpaired Student's t test. Means of more than two groups were compared by one-way ANOVA with a Dunnett's or Tukey's multiple comparison correction. Alpha levels for all tests were 0.05, with a 95% confidence interval. Error was calculated as the standard deviation (SD). Measurements were taken from distinct samples. For all analyses, $*p < 0.05$, $**p < 0.01$, $***p < 0.001$, $****p < 0.0001$; n.s., not significant. Data were reproduced by two different operators.

Results and discussion

Design and validation of a nanoluciferase complementation-based biosensor for the rapid screening of covid-19 therapeutic strategies

Using published sequences and structural homology analysis, we designed a SARS-CoV-2 RBD sequence spanning residues 331 to 524 of the S protein for one component of the biosensor, fused to LgBiT. The other component, SmBiT, was fused to the soluble ectodomain of ACE2 (residues 1 to 740) as this has been shown to be adequate to interact with RBD[7]. Various secretion signals were tested in addition to a series of codon optimizations to ensure enough of each interacting component could be produced and secreted to produce robust luminescent signal. We have shown that both cell lysates and supernatants from cells co-transfected with RBD and ACE2 NanoBiT constructs produce strong luminescence (**Figure A4.2A**). The orientation of the fusion to LgBiT and SmBiT for each component was also finalized after comparing each version head to head with the best signal coming from the combination of SmBiT-ACE2 and RBD-LgBiT. Additionally, pre-incubation of each NanoBiT component with recombinant protein (recombinant ACE2 prior to adding RBD-LgBiT or recombinant RBD prior to adding SmBiT-ACE2) resulted in a reduction in signal demonstrating that our biosensor could be used to identify molecules with interrupt the host-viral interaction of ACE2-RBD (**Figure A4.2B** – demonstrates addition of recombinant RBD).

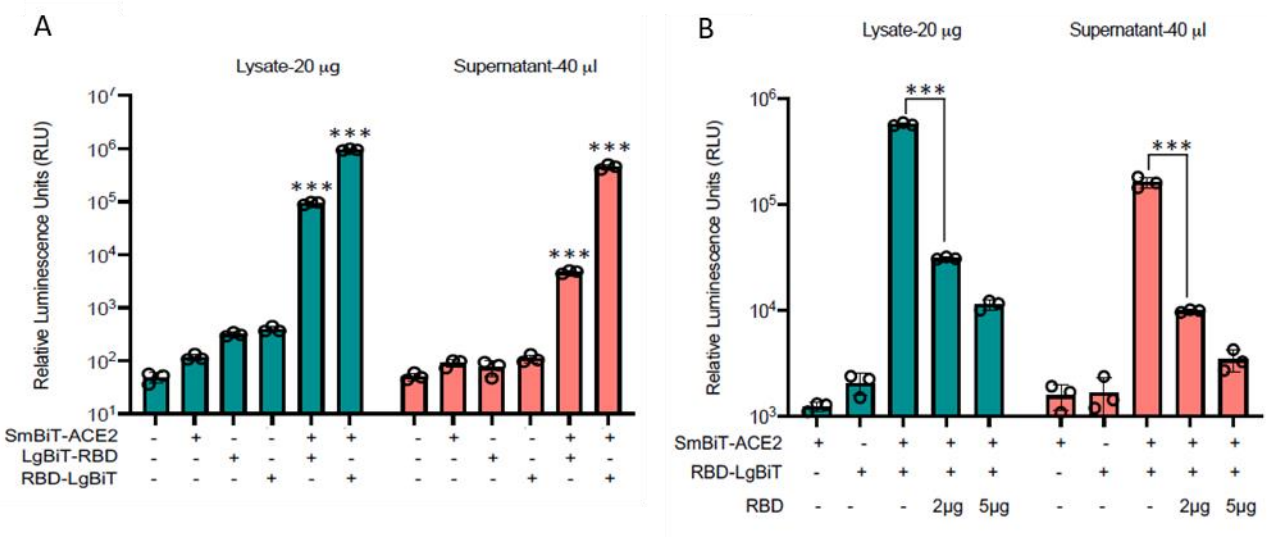

Figure A4.2 Biosensor validation assay measuring luminescence from both cell lysates and supernatants. (A) 293T cells were either transfected individually with ACE2/RBD or co-transfected with both and luciferase activity was measured 48 hours later. Only the combination of ACE2/RBD resulted in significant luminescence signal, with the RBD-LgBiT orientation outperforming LgBiT-RBD. (B) Luciferase assay following pre-incubation of SmBiT-ACE2 with recombinant RBD demonstrating competitive inhibition in a dose-dependant manner of the NanoBiT ACE2/RBD interaction.

SARS-CoV-2 biosensor can identify critical residues for ACE2-RBD interaction

We used previously reported mutational analysis of the ACE2 catalytic domain to guide our interrogation of SARS-CoV-2 host-viral interaction by incorporating mutations shown to disrupt the ACE2-RBD interaction for SARS-CoV-1. Additionally, using previously identified critical residues of SARS-CoV-1 RBD, we tested homologous residues of SARS-CoV-2 RBD using our biosensor[8,9]. All the ACE2 mutations resulted in substantial loss of signal when tested in the biosensor assay (**Figure A4.3**). All the mutations of RBD also resulted in a loss of signal with four of the mutations resulting in more than 80% loss of luminescence, highlighting their importance for binding ACE2 (**Figure A4.4**). Overall, these mutational analyses demonstrate that this biosensor can serve as a useful method for analyzing the SARS-CoV-2 host-viral interaction.

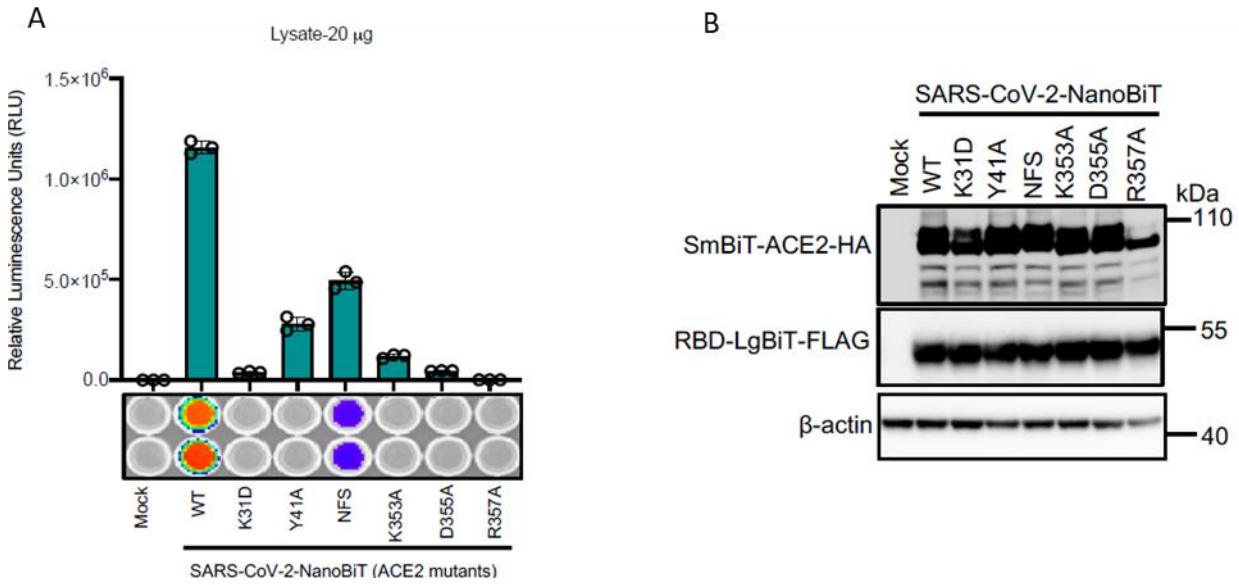

Figure A4.3 Luciferase assay investigating critical residues of ACE2. 293T cells were transfected with each individual ACE2 mutant with the wildtype RBD and harvested after 48 hours. (A) A loss of luminescence signal was observed for all mutations (B) despite robust expression of each construct shown by western blot analysis.

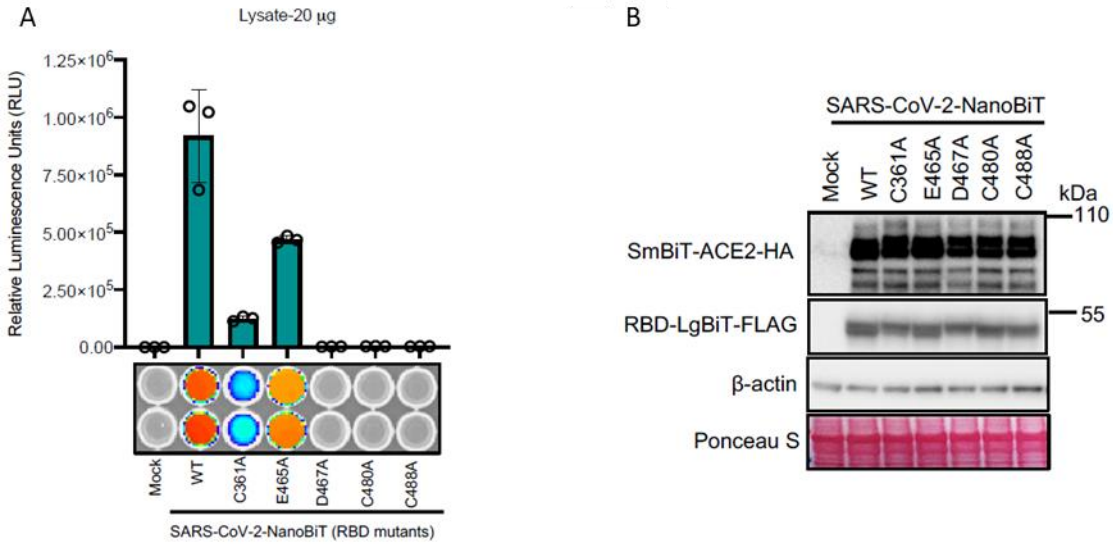

Figure A4.4 Luciferase assay investigating critical residues of RBD. 293T cells were transfected with each individual RBD mutant with the wildtype ACE2 and harvested after 48 hours. (A) A loss of luminescence signal was observed for all mutations (B) despite robust expression of each construct shown by western blot analysis.

SARS-CoV-2 biosensor is inhibited by neutralization antibodies

Monoclonal antibodies are currently under investigation as a potential SARS-CoV-2 therapeutic[10]. We have screened thirteen different commercially available monoclonal antibodies against RBD for their ability to inhibit the SARS-CoV-2 biosensor and found that many of them (9/13) could significantly reduce the ACE2-RBD interaction with a number able to also inhibit interaction of SARS-CoV-1 RBD with ACE2 (**Figure A4.5**).

Emerging RBD mutations around the globe impact ACE2-RBD interaction

Sequencing of the SARS-CoV-2 genome has revealed multiple emerging mutations of RBD: V367F (France and Hong Kong/China), N354D (China), A435S (Finland), F342L (England), K458R and V483R (United States). The SARS-CoV-2 biosensor has shown that these mutations result in variable binding to ACE2 with V367F resulting in 3-fold enhancement in ACE2 binding and F342L resulting in less interaction. Recognizing that these mutations may be present in patients treated with monoclonal antibodies we tested the ability of two of the previously tested neutralizing antibodies to block the interaction of the mutated versions of RBD with ACE2, revealing that the mutated RBD proteins could still be recognized (**Figure A4.6**).

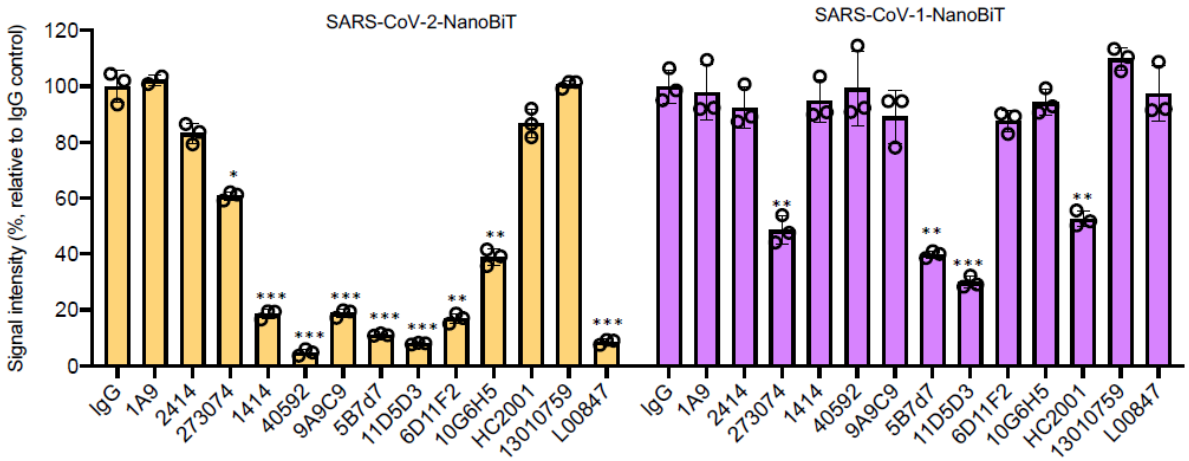

Figure A4.5 Luciferase assay representing the ability of commercial antibodies against SARS-CoV-2 to inhibit RBD/ACE2 interaction. RBD-LgBiT containing cell lysates from 293T cells were incubated with antibodies for 25 minutes at 37ºC prior to combination with SmBiT-ACE2 cell lysates, then incubated an additional 5 minutes at room temperature prior to measuring luminescence.

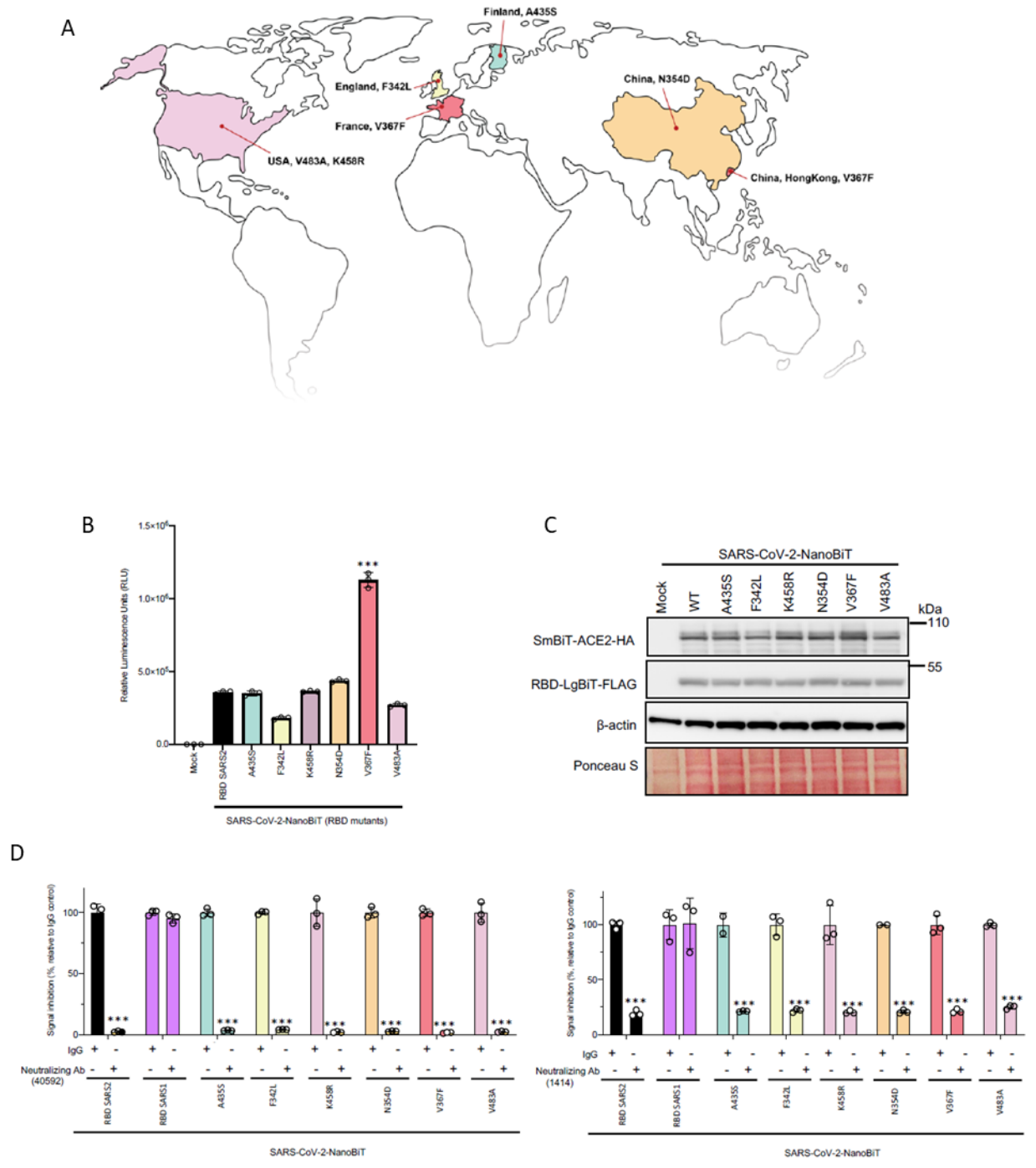

Figure A4.6 Emerging global mutant strains of RBD (A) result in (B) varying levels of interaction with ACE2, (C) despite similar expression of each construct shown by western blot analysis. (D) Neutralizing antibodies capable of disrupting the SARS-CoV-2 RBD interaction with ACE2 are still effective after introducing emerging mutations.

Additional mutations of both RBD and ACE2 impact the host-viral interaction

Many therapeutics currently under development target the RBD of the SARS-CoV-2 S protein, meaning that mutations in this domain could render potential therapeutics ineffective. Importantly, studies correlating mutations in RBD with infectivity have revealed that certain mutations lead to more infectious strains of the virus[11]. Building on the sensitivity of our biosensor to identify changes in ACE2-RBD interaction for previously reported mutations we probed deeper into the ACE2-RBD structure and identified 22 sites in the ACE2 sequence that are predicted to interact directly with RBD and 25 sites in RBD that are predicted to interact with ACE2. To test the impact of each ACE2 mutation we investigated their interactions with both SARS-CoV-2 RBD and SARS-CoV-2 S1. We included the full S1 sequence as a binding partner here considering that the RBD is located within this subunit of the S protein and binding may be impacted when expressed within the full subunit. Additionally, we included the SARS-CoV-1 RBD as many residues are conserved between the two viruses. There was a significant alteration of interaction for 12 of the 22 ACE2 mutants when combined with SARS-CoV-2 RBD and 13 when combined with SARS-CoV-2 S1 (12 of which overlapped with RBD expressed alone). There were 14 mutations which resulted in a significant change in interaction with ACE2 for the SARS-CoV-1 mutations (10 overlapping with SARS-CoV-2 RBD) (**Figure A4.7**). We have also determined that 21 of the 25 SARS-CoV-2 RBD mutants significantly reduced binding with ACE2 with one mutation increasing binding to a significant level (**Figure A4.8**). Experiments completed by our group have also shown that the RBD mutants which retained ACE2 binding capacity to some extent were still vulnerable to neutralizing antibody treatment as well. This important finding demonstrates that RBD mutations are unlikely to hinder the ability to develop an effective vaccine.

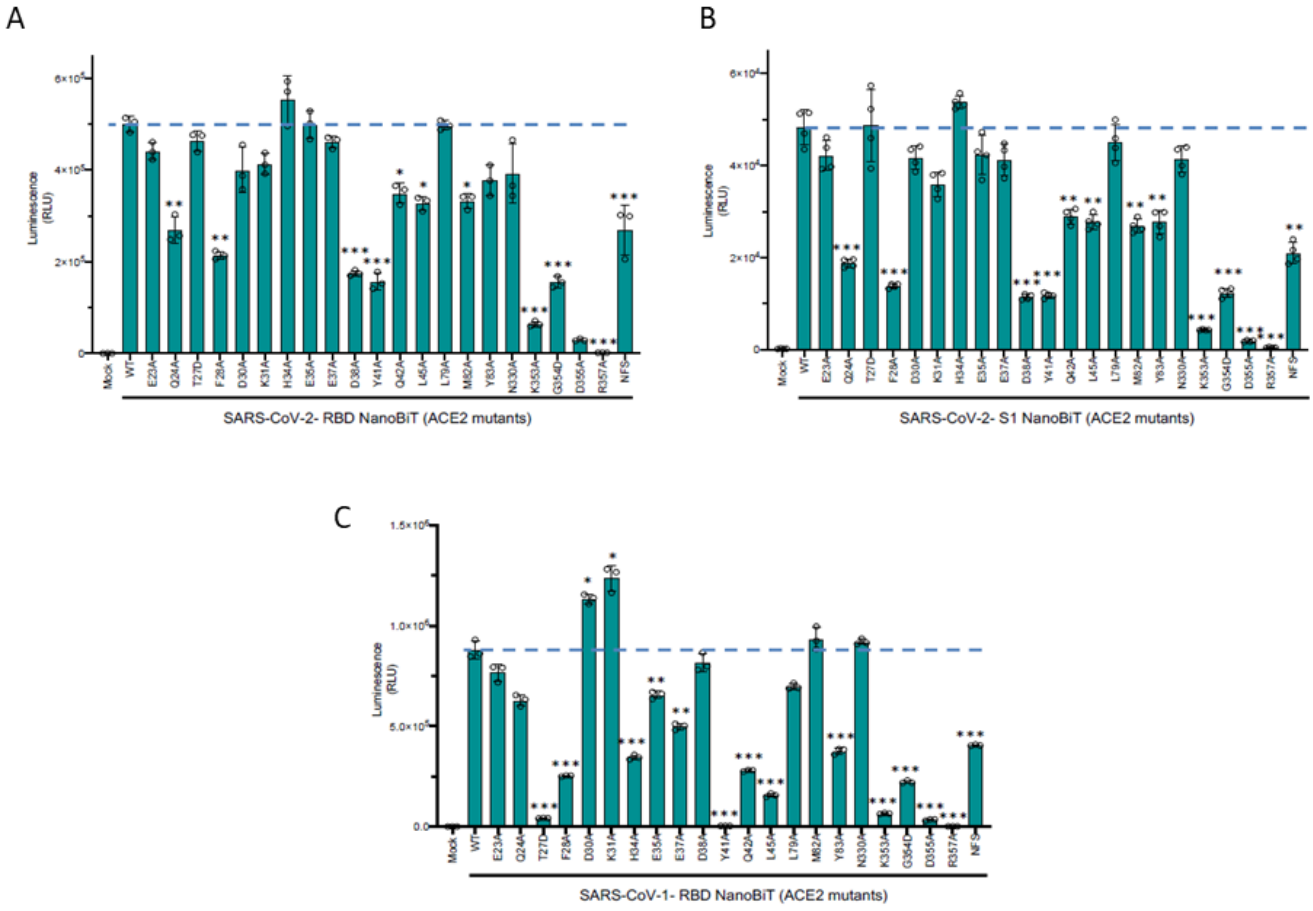

Figure A4.7 Luciferase assay demonstrating the interaction of critical ACE2 residue mutations with (A) SARS-CoV-2 RBD, (B) SARS-CoV-2 S1, and (C) SARS-CoV-1 RBD. Each construct was expressed at a similar level via western blot (not shown here). Lysates from 293T cells transfected with each mutant SmBiT-ACE2 were combined with those from above listed wildtype RBD-LgBiT components.

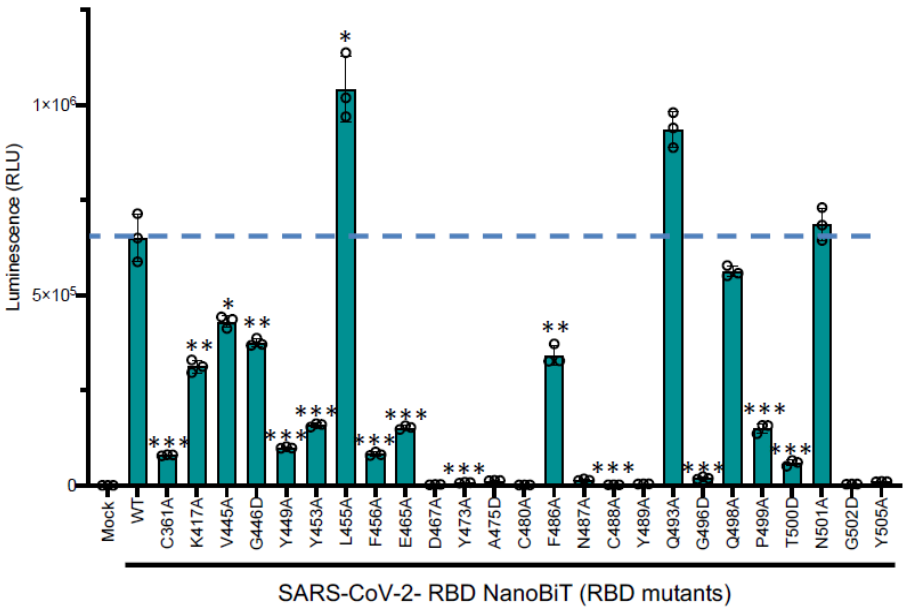

Figure A4.8 Luciferase assay demonstrating the interaction of critical RBD residue mutations with ACE2. Each construct was expressed at a similar level via western blot (not shown here). Lysates from 293T cells transfected with mutant RBD-LgBiT components were combined with wildtype SmBiT ACE2.

Glycosylation plays an important role in the host-viral interaction

Antigen glycosylation has been shown to play a key role in adaptive immune responses[12]. We have evaluated the necessity for N-linked glycosylation at previously reported sites within the RBD[13] for successful ACE2-RBD interaction using our biosensor as well as antigenicity by vaccinating mice with mutated versions of these sites followed by ELISA and neutralization assays. In comparison to the wildtype RBD, mutants which lack glycosylation (N331A and N343A) demonstrated a significant decrease in ACE2 binding via the biosensor assay (**Figure A4.9**). We then immunized mice with VSVΔ51 constructs expressing either the wildtype RBD or the mutated versions, collected sera and measured RBD-specific IgG levels, demonstrating a significant decrease in response for the N343 mutation. Similarly, we observed a decreased production of neutralizing antibodies for animals vaccinated with VSVΔ51-N343A, via neutralization assay using VSV expressing spike as a pseudovirus for SARS-CoV-2 (**Figure A4.10**).

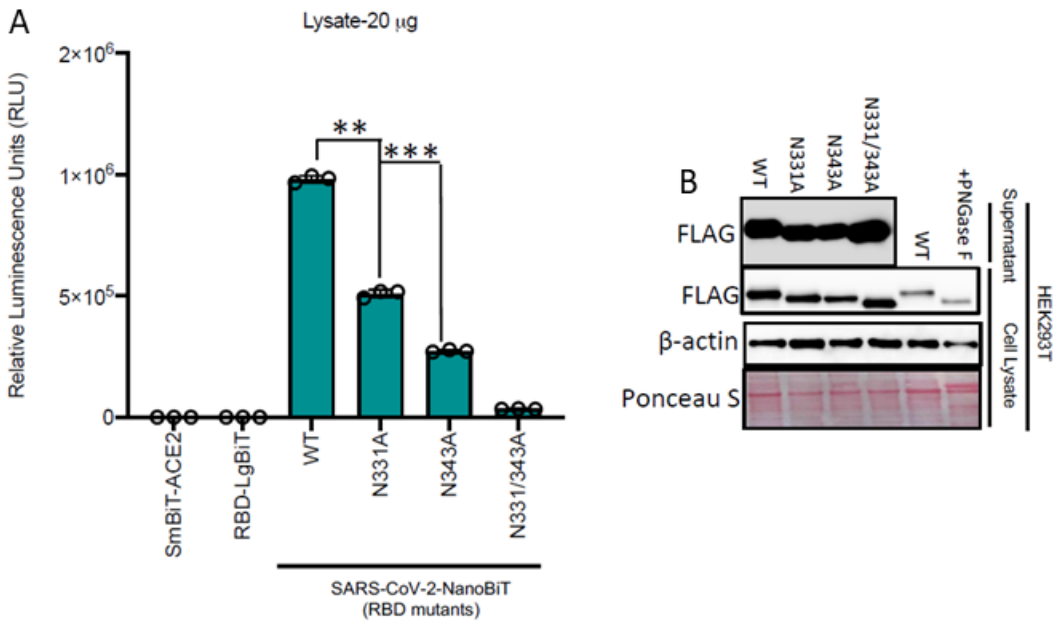

Figure A4.9 Luciferase assay demonstrating a decrease in RBD-ACE2 interaction following mutation of critical glycosylation sites on RBD (A). (B) Western blot analysis shows a small reduction in molecular weight following mutation of glycosylation sites, this is confirmed by treatment of the wildtype component with PNGase F (glycosidase to remove N-linked oligosaccharides from wildtype RBD).

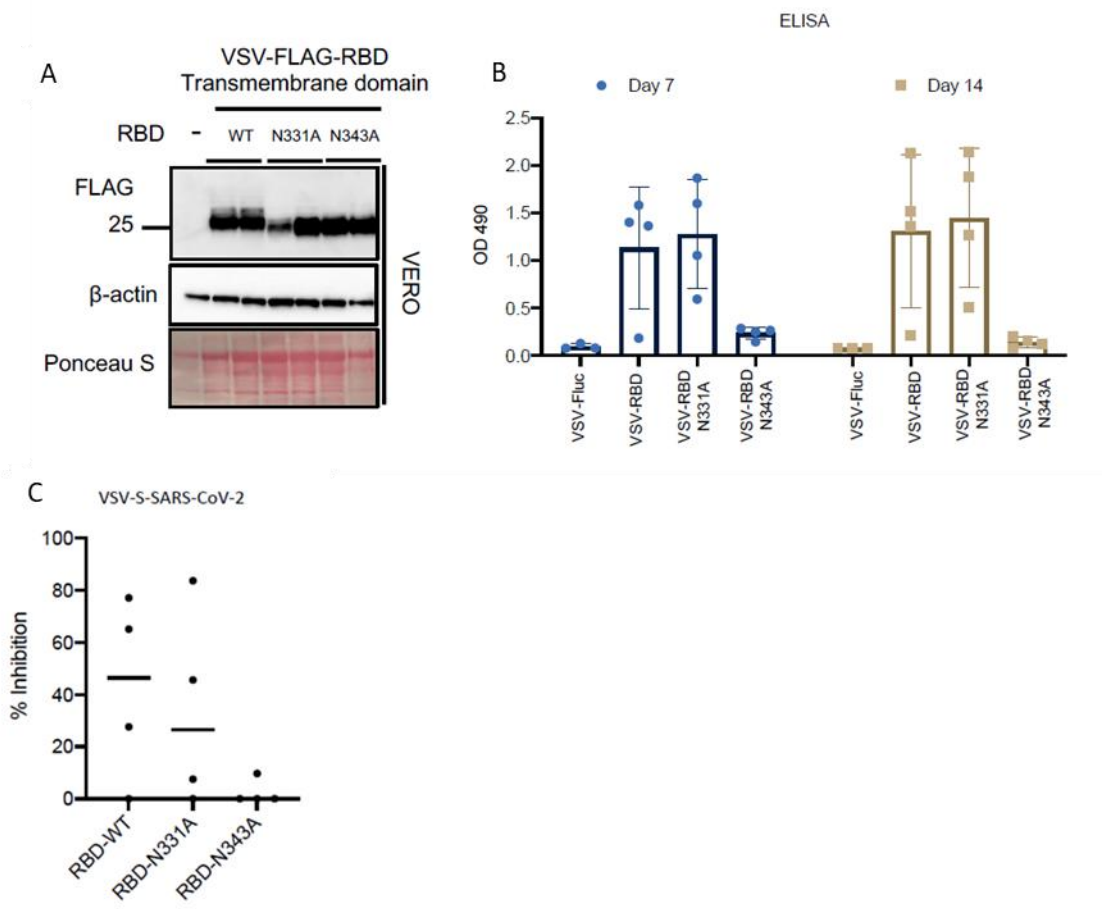

Figure A4.10 Glycosylation of RBD is required for the development of RBD specific antibodies. (A) Western blot analysis confirms the expression and loss of glycosylation for VSVΔ-RBD mutants (N331A and N343A). (B) ELISA measuring RBD-specific IgG levels at days 7 and 14 post vaccination show decreased production of RBD antibodies for RBD-N343A mutation. (C) Similarly, neutralization of a VSV-spike pseudovirus using serum from vaccinated mice after 14 days is reduced for RBD-N343A.

Conclusion

The results of these two studies demonstrate that the SARS-CoV-2-NanoBiT biosensor is a versatile tool for the rapid screening of novel SARS-CoV-2 therapies, it can also be used to identify critical mutations of ACE2-RBD interaction. We also highlight two key glycosylation sites which not only play a role in host-viral interaction but contribute to the development of a neutralizing antibody response against the SARS-CoV-2 spike protein.

References

1. Hu, B., Guo, H., Zhou, P. & Shi, Z. L. Characteristics of SARS-CoV-2 and COVID-19. *Nature Reviews Microbiology* (2020). doi:10.1038/s41579-020-00459-7
2. *Chapter 31. Coronaviruses | Elsevier Enhanced Reader*. doi:http://dx.doi.org/10.1016/B978-0-12-375156-0.00031-X
3. COVID-19 Map - Johns Hopkins Coronavirus Resource Center. Available at: https://coronavirus.jhu.edu/map.html. (Accessed: 26th May 2021)
4. COVID-19 Vaccine and Therapeutic Drugs Tracker. Available at: https://biorender.com/covid-vaccine-tracker. (Accessed: 26th May 2021)
5. Hoffmann, M. *et al.* SARS-CoV-2 Cell Entry Depends on ACE2 and TMPRSS2 and Is Blocked by a Clinically Proven Protease Inhibitor. *Cell* **181**, 271-280.e8 (2020).
6. Dixon, A. S. *et al.* NanoLuc Complementation Reporter Optimized for Accurate Measurement of Protein Interactions in Cells. *ACS Chem. Biol.* **11**, 400–408 (2016).
7. Wong, S. K., Li, W., Moore, M. J., Choe, H. & Farzan, M. A 193-Amino Acid Fragment of the SARS Coronavirus S Protein Efficiently Binds Angiotensin-converting Enzyme 2. *J. Biol. Chem.* **279**, 3197–3201 (2004).
8. Han, D. P., Penn-Nicholson, A. & Cho, M. W. Identification of critical determinants on ACE2 for SARS-CoV entry and development of a potent entry inhibitor. *Virology* **350**, 15–25 (2006).
9. Wong, S. K., Li, W., Moore, M. J., Choe, H. & Farzan, M. A 193-Amino Acid Fragment of the SARS Coronavirus S Protein Efficiently Binds Angiotensin-converting Enzyme 2* Downloaded from. *J. Biol. Chem.* **279**, 3197–3201 (2004).
10. Wang, C. *et al.* A human monoclonal antibody blocking SARS-CoV-2 infection. *Nat. Commun.* **11**, (2020).
11. Chen, J., Wang, R., Wang, M. & Wei, G.-W. Mutations strengthened SARS-CoV-2 infectivity. *J. Mol. Biol.* **432**, 5212–5226 (2020).
12. Wolfert, M. A. & Boons, G. J. Adaptive immune activation: Glycosylation does matter. *Nature Chemical Biology* **9**, (2013).
13. Watanabe, Y., Allen, J. D., Wrapp, D., McLellan, J. S. & Crispin, M. Site-specific glycan analysis of the SARS-CoV-2 spike. *Science (80-.).* **369**, (2020).

A5: Development of multipronged vaccine strategies against the novel SARS-CoV-2 virus

Preface

The contents of this appendix contain a concise collection of results which have either been previously published or are currently being prepared for publication. Each aspect of this project was exceedingly collaborative; thus, I have selected experiments to summarize here which I was closely involved with. My direct contribution has been primarily in the development and validation of our VSV candidates in addition to the design and optimization of the neutralization assay. I will describe the overall scope of the project here and go into greater detail for the aspects I am directly involved with.

The figures below have been selected from the following publications:

1. Taha Azad*, Ragunath Singaravelu*, Mathieu J.F. Crupi*, **Taylor R. Jamieson***, Jaahnavi Dave, Emily E.F. Brown, Reza Rezaei, Zaid Taha, Stephen Boulton, Nikolas T. Martin, Abera Surendran, Joanna Poutou, Mina Ghahremani, Kazem Nouri, Jack T. Whelan, Jessie Duong, Sarah Tucker, Jean-Simon Diallo, John C. Bell, and Carolina S. Ilkow. **Implications for SARS-CoV-2 Vaccine Design: Fusion of Spike Glycoprotein Transmembrane Domain to Receptor-Binding Domain Induces Trimerization**. *Membranes,* 2020, *10*(9), 215. (*equal authorship contribution)

2. Single dose replicating poxvirus vector-based RBD vaccine drives robust humoral and T cell immune response against SARS-CoV-2 infection (in preparation)

Introduction

As of May 2021, there are 92 SARS-CoV-2 vaccines undergoing clinal trials and at least 77 pre-clinical vaccines under development[1]. As the pandemic began to progress in Canada and across the globe, our group realized that an opportunity to help those most at risk for serious infection using the oncolytic viral vectors we already have experience engineering was upon us. Cancer patients are known to be at higher risk of developing complications as a result of SARS-CoV-2 infection and are more likely to require hospitalization compared to those without cancer[2]. We are currently working with three different viral vectors, each with a solid track record of safety as vaccine candidates, to combat the SARS-CoV-2 virus. VSV, MVA (Modified Vaccinia Ankara), and Vaccinia virus (VacV) – Tiantan strain have all been previously approved for use as vaccine platforms, respectively against Ebola, MERS-CoV, and smallpox viruses[3–5]. To date, we have achieved our most promising results using the VacV Tiantan backbone; thus, the current work we are moving forward and will submit for publication shortly focuses primarily on our VacV candidates.

While we aim to develop a single-dose vaccine capable of achieving protection against SARS-CoV-2, there have been many examples of vaccines for which multiple dosing (also known as a "boost") is needed to enhance both humoral and cellular immune responses[6]. There are two different strategies of boosting, homologous or heterologous. Homologous prime-boost entails repeated inoculation with the same vaccine, whereas heterologous boosting involves a different formulation/vector for the subsequent vaccination. Some studies have shown benefits to the heterologous approach, reporting improved T cell responses compared to homologous prime-

boost strategies[7]. We are currently testing both options for our different vaccine platforms. Finally, to enhance the safety of the VSV platform we have engineered one candidate in which the VSV glycoprotein has been replaced with the glycoprotein of Junín virus (JUNV). JUNV is an enveloped, negative stranded RNA virus belonging to the *Arenaviridae* family of viruses, it is the causative agent of Argentine hemorrhagic fever[8]. The aim of pseudotyping the VSV vector is two-fold: (1) limit the inherent neurotropism of VSV[9] and (2) reduce the strong anti-VSV G immune response, directing neutralizing antibody production to our antigen of interest[10]. Each vaccine backbone expresses the region of the SARS-CoV-2 Spike protein known as the receptor binding domain (RBD). This critical portion of the Spike protein is not only responsible for binding the host receptor, Angiotensin-Converting Enzyme 2 (ACE2)[11], it has also been identified as an immunodominant target of the SARS-CoV-2 antibody response in infected patients[12,13].

Methodology

Construct design

The TOH-VAC1 antigen construct consists of the receptor binding domain (RBD) of the SARS-CoV-2 spike protein (amino acid residues 331-524) fused to its transmembrane (TM) domain (residues 1208-1270) via a 3x GGGGS linker (the accession number used for spike sequences is MW070087.1). Upstream of the RBD coding sequence is a murine IL-12 signal peptide followed by a GGSGGG linker. At the C-terminal end of the TM region is an HA-Tag for convenient detection. The CovAg construct is expressed by the Vaccinia early/late H5R promoter (GenBank accession number: LR877630.1). For recombinant virus selection and tracking of viral growth, genes encoding firefly luciferase and eGFP were incorporated under a separate early/late

promoter (composed of O2L and A12L promoters) separated by a P2A sequence. The entire construct noted above was flanked by homology arms for B13R and B14R loci in Vaccinia.

VSV rescue

To rescue the recombinant VSV viruses expressing SARS-CoV-2 RBD or RBD-TMD, HEK293T cells were infected with vaccinia virus expressing T7 RNA polymerase (MOI = 0.5) for 2 h. Inoculum was removed and cells were transfected with the viral backbone plasmid along with T7 RNA polymerase-driven expression plasmids for VSV N, L, and P genes. Forty-eight hours post transfection, the recombinant virus was collected, filtered (0.22 μM) and plaque purified in Vero cells. VSV-G protein expression was provided transiently to rescue VSV-pseudotyped with Junín glycoprotein.

Dot blot assay

U-2 OS cells, infected with VSV viruses at an MOI of 0.1, were harvested 24 h post-infection in RIPA buffer supplemented with 1x protease/phosphatase inhibitor cocktail (Cell Signaling Technology, Danvers, MA, USA, Cat. #5872S) on ice. Protein concentration was determined by BCA assay, and 10 μg of whole cell lysates was directly loaded onto nitrocellulose membrane (Bio-Rad Laboratories) with 1 h incubation at room temperature. After blocking in 5% milk in TBS-T, membranes were probed with either mouse anti-RBD clone 5B7D7 (GenScript, Cat.#A02056), clone 6D11F2 (GenScript, Cat.#A02055), or clone 40592 (Sino Biological, Wayne, PA, USA); mouse anti-VSV-G clone 8G5F11 (Kerafast, Boston, MA, Cat.#EB0010), or rabbit anti-β-actin clone 13E5 (Cell Signaling Technology, Cat.#4970S) as a loading control; ectodomain ACE2 and goat anti-ACE2 (R&D Systems, Minneapolis, MN, USA, Cat.#AF933), or sera from BALB/cJ mice (The Jackson

Laboratory, Bar Harbor, ME, USA) immunized with SARS-CoV-2 spike. Blots were then washed and probed with appropriate secondary antibodies: anti-mouse, anti-rabbit (MilliporeSigma, Cat. #A9169) or anti-goat (Abcam, Cambridge, UK, Cat.#ab97110). Blots were imaged using the ChemiDoc MP imaging system (Bio-Rad Laboratories, Mississauga, ON, USA). Clarity Western ECL Substrate (Bio-Rad) was used to visualize the blot.

Immunofluorescence

U-2 OS cells (ATCC) were seeded on glass coverslips and were either infected with Tiantan (TT) CovAg or MVA CovAg at an MOI of 0.1 the next day or left untreated as control (mock). 24 hr post infection, cells were washed once with ice cold PBS containing 0.5 mM CaCl2 and 1 mM MgCl2 (PBSCM) and subsequently fixed with 4% (w/v) paraformaldehyde (PF) in PBSCM for 20 minutes at 4°C. After this, PF was quenched with 50 mM NH4Cl (in PBS) for 5 min. The cells were then either permeabilized with 0.2% (v/v) Triton X-100 at room temperature for 4 min or left untreated as control. Permeabilization was stopped by washing the cells twice for 5 min with PBSCM and non-specific binding was then blocked by incubating the cells with 1% BSA (w/v) in PBSCM for 20 minutes. Cells were then incubated with serum (1:100 in PBSCM)) for 1 h at room temperature, then washed 3 times for 5 min with 0.1% BSA (w/v) in PBSCM and incubated for 1 h at room temperature with the secondary antibody (Goat-anti-Mouse-IgG-Alexa-555-, Invitrogen Cat # A32727, 1:500 in 1% (w/v) BSA in PBSCM). Serum was obtained from a mouse 117 days after it was primed with VSV-Cov3 (1E7 pfu SQ) and boosted with MVA-Cov3 (1E7 pfu SQ). Unbound secondary antibody was then removed by washing three times with PBSCM as described above. Coverslips were then washed once with PBS, mounted on glass microscope

slides using ProLong™ Gold Antifade Mountant with DAPI (Invitrogen™) and dried at room temperature overnight in the dark.

Pseudovirus neutralization assay

Vero E6 cells were seeded in 96-well plates such that there were 40, 000 cells per well at the time of infection. Serum was first diluted in a separate 96-well at a 1:10 dilution in serum free DMEM and a serial 1 in 2 dilution series was performed. VSV pseudotyped with the SARS-CoV-2 spike glycoprotein was then added to the serum in an equal volume of serum free DMEM for a final dilution of 2000 pfu per well and incubated for 1hr at 37^{o}C. After 1hr, media on the cell was replaced with 60uL of the virus/serum and incubated for 1hr at 37^{o}C. Wells were then topped up with carboxymethylcellulose (CMC) in DMEM (supplemented with 10% FBS) for a final concentration of 3% CMC and incubated 24hrs at 34^{o} C. GFP foci were imaged and counted using a Cellomics ArrayScan VTI HCS Reader.

A comprehensive outline of the neutralization assay protocol has recently been accepted for publication in the Journal of Visualized Experiments. The complete text has been inserted in the following appendix (**Appendix A6**).

ELISA

Nunc Maxisorp flat-bottom plates were coated overnight at 4°C with 125 ng of RBD (prepared in-house). The following day, the RBD solution was removed, the plates were washed with PBS-Tween (0.1% Tween 20) and blocked with 3% skim milk solution for 1 hour. Mouse sera from vaccinated mice were then serially diluted and added to the plates to incubate for 2 hours at

room temperature. In addition, a positive and negative control was added to each plate comprised of a monoclonal RBD antibody (1 µg/ml; Cat No: MBS434247, Anti-RBD Domain (SARS-CoV2-Spike), monoclonal antibody, MyBioSource, CA, USA) and a pool of sera taken from mice vaccinated with empty viral vector. Following the 2 hour incubation, plates were washed with PBS-Tween and incubated with anti-mouse IgG conjugated to HRP (1:3000; Cat No: Cat No:314930, Goat anti-Mouse IgG (H+L) Secondary Antibody, HRP, Invitrogen) for 1 hour at room temperature. Plates were then developed using SigmaFast OPD solution and measured at 490 nm using a Biotek microplate reader.

All experimental absorbance readings were normalized relative to the blank and the positive control (monoclonal RBD antibody at 1 µg/ml) and fit using a quadratic binding polynomial assuming 1:1 binding. The fitting was performed using a Monte Carlo simulation with the non-linear curve fitting tool in QtGrace. The reciprocal antibody titer (LDF) was determined by interpolating the dilution factor that intersected with a minimum detection threshold defined by 10x the standard deviation of the responses from mice vaccinated with wildtype virus, or to a fixed value of 0.025 (whichever was larger).

Results and discussion

The RBD-transmembrane region of spike protein is necessary for trimerization

We have recently published our findings demonstrating that fusion of the SARS-CoV-2 spike protein transmembrane domain (TMD) to the RBD induces trimerization[14]. As stated previously, the RBD has been shown to be a crucial antigen for mounting a successful immune response, consequently several vaccine candidates have utilized RBD as a target antigen. Previous work has shown that expression of the spike protein ectodomain results in trimerization and this has served as a blueprint for vaccine development [15,16]. We have now demonstrated that the spike protein TMD induces trimerization of the RBD, a key piece of information for vaccine platforms using RBD as a target antigen (**Figure A5.1 D**)[14]. We first demonstrated that RBD fused to the TMB (RBD-TMD) results in a multiple banding pattern when run on and SDS-PAGE gel with a 25kDa band representing the monomeric RBD construct, in addition to a 75kDa and a faint 150kDa band likely due to trimerization and oligomerization. Thermal denaturation indeed led to elimination of the higher molecular weight bands (**Figure A5.1 A**). Under native gel conditions the intensity of the 75kDa band was enhanced and again could be eliminated by boiling (**Figure A5.1 B**). To investigate whether the TMD was responsible for trimerization, we repeated the native PAGE analysis on RBD alone and did not detect the 75kDa band (**Figure A5.1 C**).

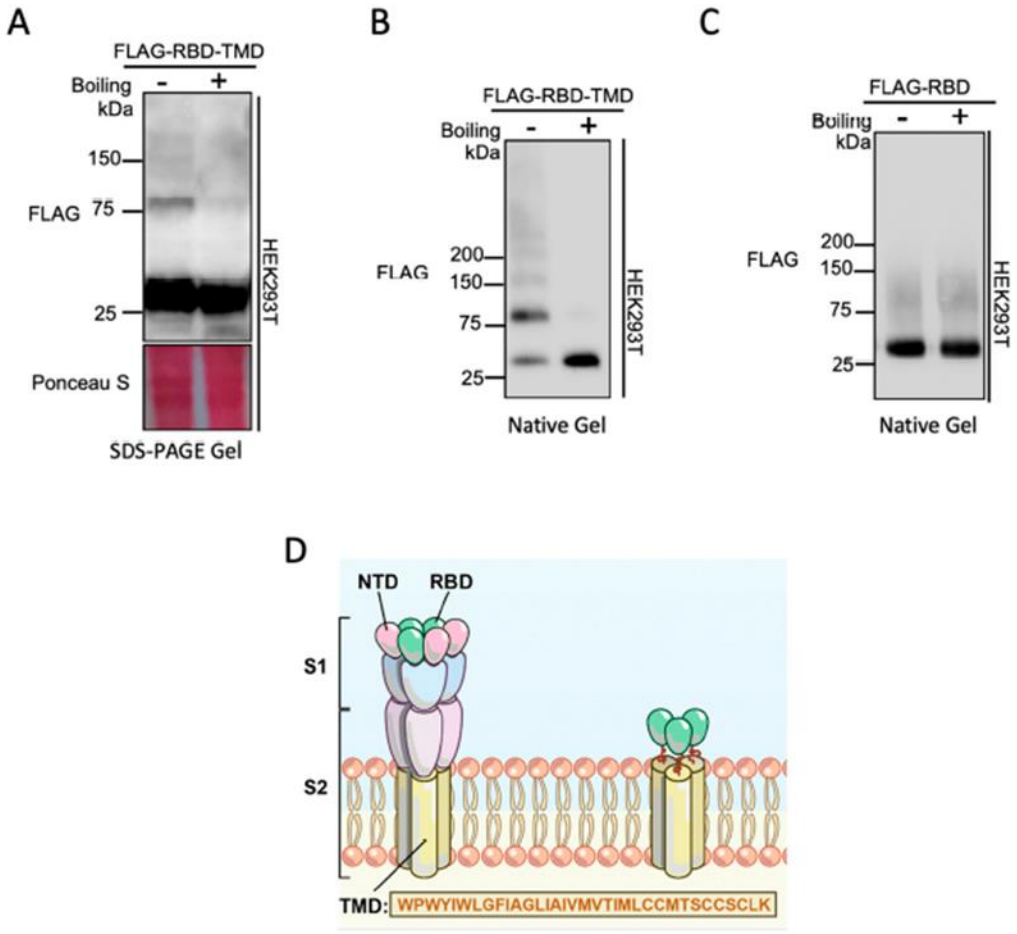

Figure A5.1 Fusion of the transmembrane domain of SARS-CoV-2 spike protein induces trimerization of RBD. (A) SDS-PAGE analysis demonstrates multiple band pattern when RBD is fused to TMD and expressed from 293T cells, with higher molecular weight bands eliminated after boiling. (B) Native-PAGE immunoblot of RBD-TMD with and without boiling. (C) Native-PAGE immunoblot of RBD alone with and without boiling. (D) Schematic of SARS-CoV-2 spike protein with RBD fused to TMD. N-terminal domain (NTD); receptor-binding domain (RBD); transmembrane domain (TMD).

To determine whether the RBD-TMD protein possessed functional and antigenic conformation we then engineered a VSVΔ51 expressing RBD-TMD. Dot blot analysis confirmed that commercially available neutralizing antibodies as well as mouse sera immunized with SARS-CoV-2 spike protein could recognize the RBD-TMD construct (**Figure A5.2 A and B**). Additionally, this construct retained the capacity to interact with the ACE2 receptor protein (**Figure A5.2 C**).

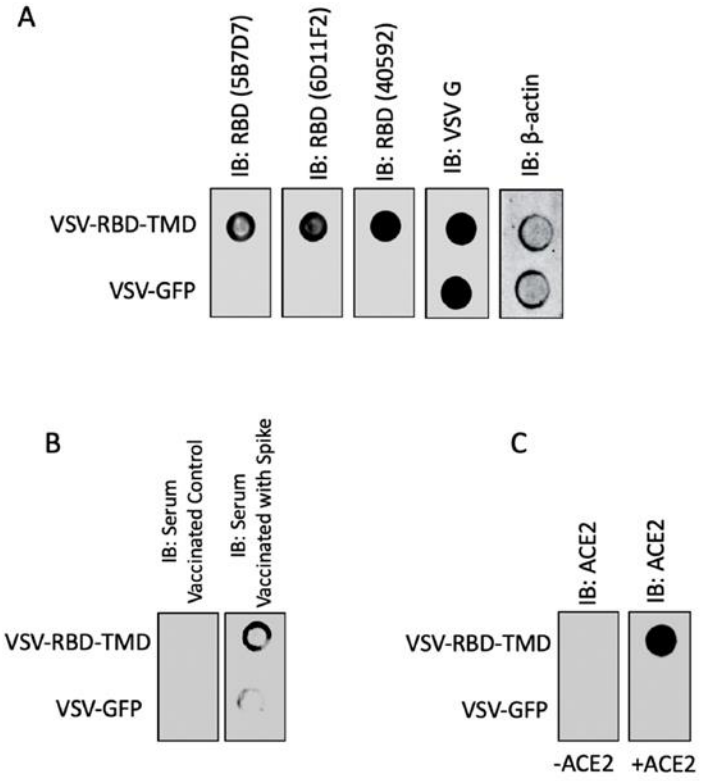

Figure A5.2 RBD-TMD retains antigenicity and functional conformation when expressed from VSVΔ51. U-2 OS cells were infected with VSV expressing either GFP or RBD-TM at MOI 0.1 for 24 hours and probed via dot blot analysis with (A) RBD antibodies, (B) sera from mice immunized with SARS-CoV-2 spike, or (C) recombinant ACE2 with ACE2 antibody.

Validating the expression and localization of encoded antigens

To demonstrate the expression as well as localization of the encoded RBD-TMD from each vector (**Figure A5.3 A**) we have completed western blot, flow analysis, and immunofluorescent imaging demonstrating that RBD is present at the extracellular surface of infected cells. My main role has been the rescue and production of our VSV vectors; thus, I have included samples of immunofluorescent detection of antigens expressed from the VSVΔ51 and VSV-wildtype-JUNV pseudotyped vectors, in addition to the MVA and Tiantan candidates which will be the focus of the remainder of the results discussed here (**Figure A5.3 B, C, D**). We have also confirmed trimerization of RBD-TMD expressed from VacV, similarly to VSV-RBD-TMD discussed above.

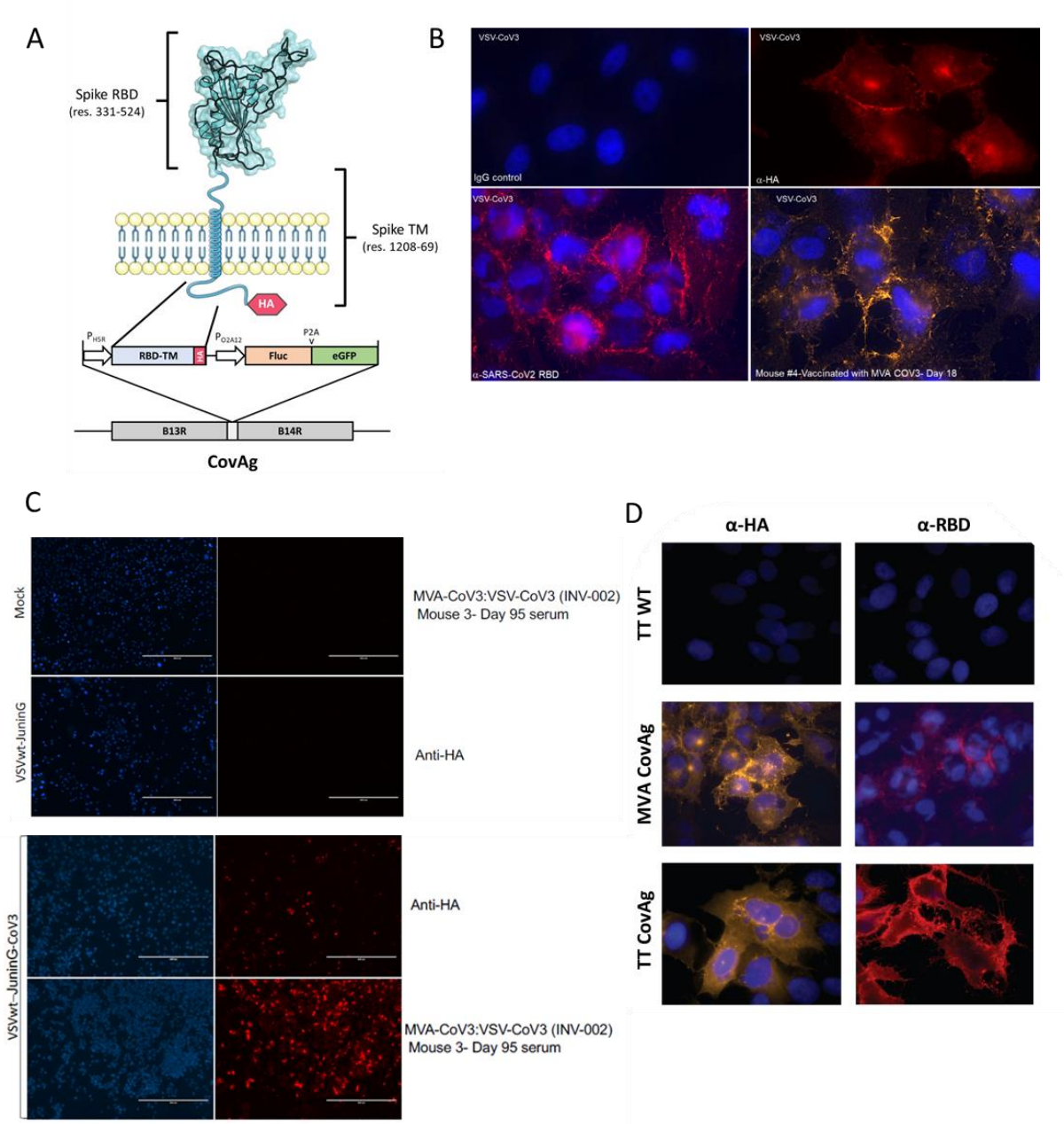

Figure A5.3 Schematic depiction of SARS-CoV-2 spike RBD construct and immunofluorescent imaging confirming expression of RBD. (A) Schematic depiction of SARS-CoV-2 RBD construct. Immunofluorescence validating expression of RBD (or CovAg/CoV3) from (B) VSVΔ51 and (C) VSV-wildtype-pseudotyped with Junín G; vero E6 cell were infected for 24 hours with each virus and stained for either α-HA or α-RBD. We have also utilized the serum from a mouse identified by the neutralization assay to have very robust expression of neutralizing antibodies to validate expression of our construct here (labelled MVA/VSV-CoV3 INV002). (D) Immunofluorescence of MVA/Tiantan (TT) CovAg constructs with α-HA or α-RBD antibodies; U-2 OS cells were infected approximately 24 hours before staining.

Vaccinia virus – Tiantan strain is our most promising SARS-CoV-2 vaccine vector

Natural infection with SARS-CoV-2 has been shown to produce both mucosal (IgA) and systemic antibody responses (IgG); therefore, we have opted to test multiple routes of infection for our vaccine vectors, including intranasal (IN) administration in addition to intraperitoneal (IP) and subcutaneous (SC)[17]. We currently have a number of *in vivo* studies underway to determine (1) best route of administration, (2) is prime-boost required, and (3) if prime-boost is needed whether homologous or heterologous will be more beneficial. My primary contribution to this project, after the initial virus rescues, has been following the humoral responses against the SARS-CoV-2 RBD antigen (T cell response is under investigation by other members of the group using interferon-γ ELISPOT assays). To measure the ability of our vaccine candidates to induce a neutralizing antibody response I have developed a high throughput protocol to measure neutralization of pseudotyped VSV expressing the Spike glycoprotein of SARS-CoV-2 (in collaboration with senior technicians Ricardo Marius and Xiaohong He). This assay has been complemented with ELISA data to capture the full spectrum of IgG antibodies which bind RBD present in the serum of vaccinated mice. Initial experiments comparing Tiantan with MVA revealed that Tiantan could elicit significantly higher antibody responses, measured by ELISA, when administered both IN and IP, whereas SC administration resulted in substantially lower antibody titers overall (**Figure A5.4 A** and **B**). When comparing each route of administration with or without a homologous boost using the Tiantan (or TOH-VAC1) vaccine, both ELISA and neutralization assays confirmed IN and IP as the most effective routes (**Figure A5.4 C** and **D**).

Moving forward, we followed the long-term antibody response after a single dose of Tiantan administered IN or IP, compared with a homologous prime/boost regimen. The results of our neutralization assays thus far have correlated very well with ELISAs measuring antibodies

against SARS-CoV-2 RBD-specific IgG. Interestingly, we have seen very strong responses with the prime alone and thus far no distinct improvement with the boost (**Figure A5.4 E-H**). Very importantly, our neutralization curves for TOH-VAC1 (Tiantan) are well in line with convalescent serum from patients. More recently, we have demonstrated the ability of TOH-VAC1 to induce a humoral immune response in our first non-human primate study wherein rhesus macaques were vaccinated with a single dose of TOH-VAC1 intramuscularly (**Figure A5.5**).

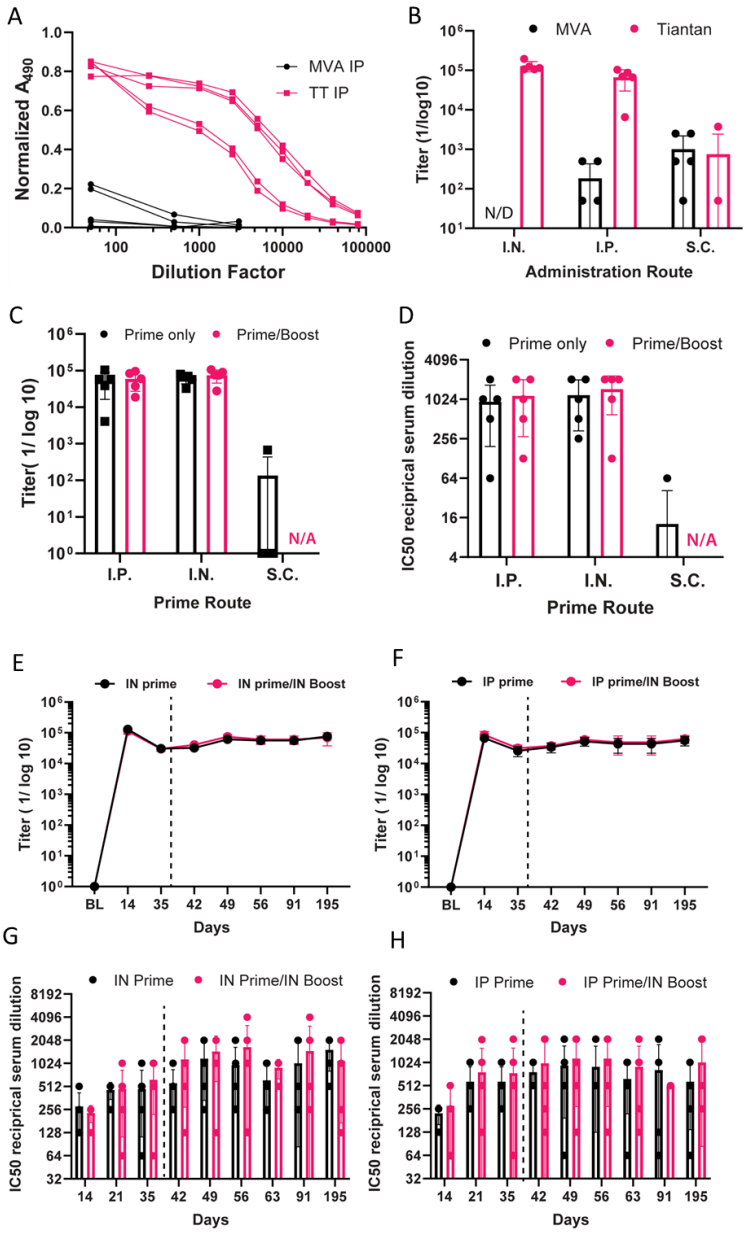

Figure A5.4 Comparison of MVA and Tiantan (TT) RBD vaccine antibody responses using different routes of administration and long-term humoral responses for TT vaccine. (A) Normalized ELISA absorbance vs. serum dilution factors for mice vaccinated I.P. with MVA (black) or TT (red) RBD-TM. (B) Reciprocal titers from RBD ELISAs for MVA and TT vaccines inoculated via different administration routes. N/D indicates values were not detectable. (C) Endpoint titers of TT CovAg vaccinated mice with and without boosts for various routes of administration. Data was acquired at day 49, 14 days after the boost injection date. (D) VSV-S neutralization IC50 values for samples described in panel C. (E+F) Antibody endpoint titers over 195-day duration for IN (E) or IP primed (F) mice. The vertical dashed line depicts the boost date. (G+H) VSV-S neutralization IC50 values over 195 days for prime only and prime/boost vaccinations given either IP (G) or IN (H).

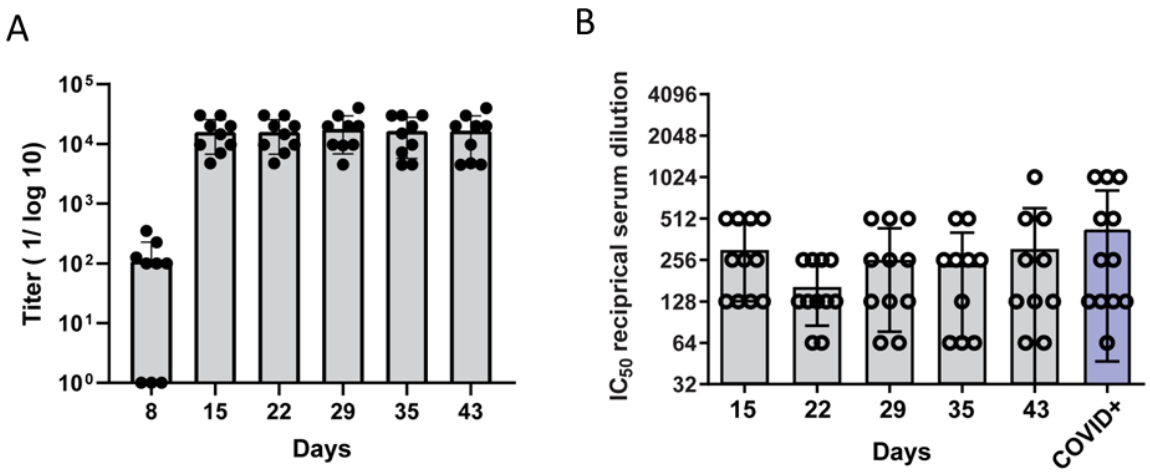

Figure A5.5 Investigation of Tiantan RBD (TOH-VAC1) vaccine efficacy in Rhesus macaques with comparison to patients previously infected with SARS-CoV-2. (A) Endpoint antibody titers for RBD specific antibodies from macaques vaccinated intramuscularly (IM) with TOH-VAC1 determined by ELISA. (B) VSV-S neutralization assay results from macaques vaccinated IM with TOH-VAC1 (COVID+ represents human donor neutralization data for serum collected approximately 3 months post-infection). Each point represents an individual animal (n=11) or human donor (n=12).

Conclusion

We have described here multiple advantages of using the Tiantan viral backbone compared to current vaccine standards including: (1) only one dose is required to induce antibody titers similar to previously infected patients, (2) VacV is quite stable at room temperature and will therefore be easier to ship and distribute to remote sites[18] (our group has successfully demonstrated similar stability of both MVA and Tiantan candidates), (3) by encoding the spike receptor-binding domain (RBD) only we may also decrease the risk of vaccine-induced immune thrombotic thrombocytopenia which has been associated with Spike protein expression and is currently under investigation[19]. Future work aims to determine the level of protection this 'one shot' vaccine can achieve against SARS-CoV-2 infection *in vivo*.

References

1. Covid-19 Vaccine Tracker: Latest Updates - The New York Times. Available at: https://www.nytimes.com/interactive/2020/science/coronavirus-vaccine-tracker.html. (Accessed: 28th May 2021)
2. Liang, W. *et al.* Cancer patients in SARS-CoV-2 infection: a nationwide analysis in China. *The Lancet Oncology* **21**, 335–337 (2020).
3. Koch, T. *et al.* Safety and immunogenicity of a modified vaccinia virus Ankara vector vaccine candidate for Middle East respiratory syndrome: an open-label, phase 1 trial. *Lancet Infect. Dis.* **20**, 827–838 (2020).
4. Suder, E., Furuyama, W., Feldmann, H., Marzi, A. & de Wit, E. The vesicular stomatitis virus-based Ebola virus vaccine: From concept to clinical trials. *Human Vaccines and Immunotherapeutics* **14**, 2107–2113 (2018).
5. Chen, Z. *et al.* Mucosal immunization induces a higher level of lasting neutralizing antibody response in mice by a replication-competent smallpox vaccine: Vaccinia Tiantan strain. *J. Biomed. Biotechnol.* **2011**, (2011).
6. Woodland, D. L. Jump-starting the immune system: Prime-boosting comes of age. *Trends in Immunology* **25**, 98–104 (2004).
7. Kardani, K., Bolhassani, A. & Shahbazi, S. Prime-boost vaccine strategy against viral infections: Mechanisms and benefits. *Vaccine* **34**, 413–423 (2016).
8. Grant, A. *et al.* Junín virus pathogenesis and virus replication. *Viruses* **4**, 2317–2339 (2012).
9. Hastie, E., Cataldi, M., Marriott, I. & Grdzelishvili, V. Z. Understanding and altering cell tropism of vesicular stomatitis virus. *Virus Research* **176**, 16–32 (2013).
10. Rose, N. F., Roberts, A., Buonocore, L. & Rose, J. K. Glycoprotein Exchange Vectors Based on Vesicular Stomatitis Virus Allow Effective Boosting and Generation of Neutralizing Antibodies to a Primary Isolate of Human Immunodeficiency Virus Type 1. *J. Virol.* **74**, 10903–10910 (2000).
11. Lan, J. *et al.* Structure of the SARS-CoV-2 spike receptor-binding domain bound to the ACE2 receptor. *Nature* **581**, 215–220 (2020).
12. Premkumar, L. *et al.* The receptor-binding domain of the viral spike protein is an immunodominant and highly specific target of antibodies in SARS-CoV-2 patients. *Sci. Immunol.* **5**, (2020).
13. Piccoli, L. *et al.* Mapping Neutralizing and Immunodominant Sites on the SARS-CoV-2 Spike Receptor-Binding Domain by Structure-Guided High-Resolution Serology. *Cell* **183**, 1024-1042.e21 (2020).
14. Azad, T. *et al.* Implications for SARS-CoV-2 Vaccine Design: Fusion of Spike Glycoprotein Transmembrane Domain to Receptor-Binding Domain Induces Trimerization. *Membranes (Basel).* **10**, 215 (2020).
15. Daniel Wrapp *et al. Cryo-EM structure of the 2019-nCoV spike in the prefusion conformation | Science*. *science* **367**, 1260–1263 (2020).
16. Walls, A. C. *et al.* Structure, Function, and Antigenicity of the SARS-CoV-2 Spike Glycoprotein. *Cell* **181**, 281-292.e6 (2020).
17. Krammer, F. SARS-CoV-2 vaccines in development. *Nature* **586**, (2020).
18. Newman, F. K., Frey, S. E., Blevins, T. P., Yan, L. & Belshe, R. B. Stability of undiluted and diluted vaccinia-virus vaccine, Dryvax. *J. Infect. Dis.* **187**, 1319–1322 (2003).
19. Cines, D. B. & Bussel, J. B. SARS-CoV-2 Vaccine–Induced Immune Thrombotic Thrombocytopenia. *N. Engl. J. Med.* (2021). doi:10.1056/nejme2106315

A6: Detection of SARS-CoV-2 neutralizing antibodies using high-throughput fluorescent imaging of pseudovirus infection

jove

Detection of SARS-CoV-2 Neutralizing Antibodies using High-Throughput Fluorescent Imaging of Pseudovirus Infection

Taylor R. Jamieson[1,2], Joanna Poutou[1,2], Ricardo Marius[1,2], Xiaohong He[1], Reza Rezaei[1,2], Taha Azad[1,2], Carolina S. Ilkow[1,2]

[1] Ottawa Hospital Research Institute [2] Department of Biochemistry, Microbiology and Immunology, University of Ottawa

Corresponding Author

Carolina S. Ilkow
cilkow@ohri.ca

Citation

Jamieson, T.R., Poutou, J., Marius, R., He, X., Rezaei, R., Azad, T., Ilkow, C.S. Detection of SARS-CoV-2 Neutralizing Antibodies using High-Throughput Fluorescent Imaging of Pseudovirus Infection. *J. Vis. Exp.* (), e62486, doi:10.3791/62486 (2021).

Date Published

May 18, 2021

DOI

10.3791/62486

URL

jove.com/t/62486

Abstract

As the COVID-19 pandemic caused by severe acute respiratory syndrome coronavirus 2 (SARS-CoV-2) continues to evolve, it has become evident that the presence of neutralizing antibodies against the virus may provide protection against future infection. Thus, as the creation and translation of effective COVID-19 vaccines continues at an unprecedented speed, the development of fast and effective methods to measure neutralizing antibodies against SARS-CoV-2 will become increasingly important to determine long-term protection against infection for both previously infected and immunized individuals. This paper describes a high-throughput protocol using vesicular stomatitis virus (VSV) pseudotyped with the SARS-CoV-2 spike protein to measure the presence of neutralizing antibodies in convalescent serum from patients who have recently recovered from COVID-19. The use of a replicating pseudotyped virus eliminates the necessity for a containment level 3 facility required for SARS-CoV-2 handling, making this protocol accessible to virtually any containment level 2 lab. The use of a 96-well format allows for many samples to be run at the same time with a short turnaround time of 24 h.

Introduction

In December 2019, a novel coronavirus was identified, which we now know as SARS-CoV-2, the causative agent of coronavirus disease 2019 (COVID-19)[1]. SARS-CoV-2 is a betacoronavirus belonging to the *Coronaviridae* family. These enveloped viruses comprise a large positive-sense RNA genome and are responsible for respiratory and intestinal infections in both humans and animals[2]. As of May 2021 there have been more than 157 million reported cases of COVID-19 globally and more than 3.2 million deaths[3]. The development of an effective vaccine has become the primary goal of researchers around the globe with at least 77 preclinical

vaccines under investigation and 90 currently undergoing clinical trials[4].

Coronaviruses encode four structural proteins including the spike protein (S), nucleocapsid (N), envelope protein (E), and the membrane protein (M). Entry of SARS-CoV-2 requires interaction of the receptor-binding domain (RBD) of S with the host receptor, human angiotensin-converting enzyme 2 (hACE2), and subsequent membrane fusion following proteolytic cleavage by host cellular serine protease, transmembrane protease serine 2 (TMPRSS2)[5,6,7,8,9,10]. Humoral immunodominance of the S protein of SARS-CoV has been previously reported and has now been shown also for SARS-CoV-2[11,12,13]. Indeed, neutralizing antibody responses against S have been detected in convalescent serum from SARS-CoV patients 24 months after infection[14], highlighting their critical role in the long-term immune response. The S protein has been identified as a promising vaccine target and has thus become a key component of most vaccines under development[15,16].

While the rapid detection of neutralizing antibodies is a critical aspect of vaccine development, it may also shed light on the rate of infection and sero-epidemiologic surveillance in impacted areas[17]. A replication-competent VSV pseudotyped with the SARS-CoV-2 S glycoprotein, in place of the wild-type VSV glycoprotein, to study SARS-CoV-2 infection in biosafety level 2 settings was kindly donated by Whelan and co-workers[18]. VSV expressing spike (VSV-S) will be utilized to determine the neutralizing antibody response against SARS-CoV-2 spike protein. As the VSV-S used here also expresses enhanced green fluorescent protein (eGFP), eGFP foci may be detected within 24 h to quantify infection, whereas plaque formation can take 48 to 72 h. Summarized here is a simple and effective protocol to determine the ability of convalescent patient serum to neutralize VSV-S-eGFP infection. This method may also be easily adapted to interrogate other potential therapeutics that aim to disrupt the host-viral interaction of SARS-CoV-2 S protein.

Protocol

1. Plating cells (Day 1) for the production and quantification of SARS-CoV-2 pseudovirus

1. Preparation for tissue culture
    1. Warm 1x Dulbecco's Phosphate-Buffered Saline (DPBS); Dulbecco's Modified Eagle Medium (DMEM) containing 10% Fetal Bovine Serum (FBS) and 1% penicillin/streptomycin (optional); and 0.25% trypsin-ethylenediamine tetraacetic acid (EDTA) to 37 °C in a water bath for approximately 15 min.
    2. Disinfect a tissue culture hood with 70% ethanol, and place tissue culture dishes, Pasteur pipettes, and serological pipettes in the tissue culture hood as needed. Remove PBS, DMEM, and trypsin from the water bath, and disinfect with 70% ethanol prior to placing in the tissue culture hood.
2. Plating and maintaining cells
    1. Grow Vero E6 cells in DMEM (containing 10% FBS) in T75 tissue culture flasks or 15 cm tissue culture dishes in a 37 °C incubator with 5% CO_2. Passage the cells as needed when cells are 80-90% confluent.
    2. Wash the cells by adding 10 mL of 1x PBS to each dish and gently rocking 4-5 times; aspirate the PBS. Add 3 mL of trypsin-EDTA to each dish, rock the plate to ensure the entire surface is covered. Incubate the cells at 37 °C with 5% CO_2

for approximately 5 min, or until the cells have detached.

3. Add 7 mL of DMEM (containing 10% FBS) to deactivate the trypsin, and resuspend the cells by pipetting up and down several times. Spin down the cells to remove the trypsin using a benchtop centrifuge at 500 × *g* for 5 min, aspirate the media without disturbing the cell pellet, and resuspend the cells in 10 mL of DMEM (containing 10% FBS). If cells are required for future experiments, place 1 mL in a new dish containing 15 mL of fresh DMEM (containing 10% FBS).
4. Count the cells using an automated cell counter or hemocytometer, and add approximately 1×10^7 cells to each 15 cm plate, and incubate at 37 °C with 5% CO_2 until they are 100% confluent (1-2 days).

2. VSV-S-EGFP pseudovirus preparation

1. Infection
    1. Infect cells at multiplicity of infection (MOI) 0.01 with VSV-S-eGFP stock virus in 12 mL of serum-free DMEM for 1 h at 37 °C with 5% CO_2, occasionally rocking the plates. Replace the inoculum with fresh DMEM (containing 2% FBS and 20 mM HEPES, pH 7.7), and move to an incubator set to 34 °C with 5% CO_2.

        NOTE: A temperature of 34 °C is required for the propagation of VSV-S-eGFP in cell culture.
    2. Collect cell supernatants upon observation of extensive cytopathic effect (CPE) and cell detachment, approximately 48 h post-infection. Use a fluorescent microscope to visualize the extensive expression of eGFP by infected cells starting at 24 h post-infection.
2. Collection
    1. Centrifuge the supernatants using a benchtop centrifuge for 5 min at 1,000 × *g* at 4 °C to remove the cell debris. Aliquot the supernatant to avoid multiple freeze-thaw cycles, and store at -80 °C.

3. Titering the VSV-S-eGFP pseudovirus

1. Serial dilution to determine viral titer
    1. Plate Vero E6 cells on 6-well plates at a seeding density of 6×10^5 cells per well in DMEM (with 10% FBS), and incubate overnight at 37 °C with 5% CO_2.

        NOTE: Vero cells that overexpress TMPRSS2 and hACE2 can also be used.
    2. Set up a 10-fold serial dilution series of the VSV-S-eGFP virus in cold serum-free DMEM by placing 900 µL of media in seven microcentrifuge tubes. Label tubes from 1 to 7. Add 100 µL of the viral stock to the first tube and vortex briefly. Transfer 100 µL of diluted virus from tube 1 to tube 2 and vortex briefly; continue until tube 7.
    3. Aspirate the medium from all wells of the 6-well plate containing Vero E6 cells, and replace with 500 µL of dilutions 10^{-2} to 10^{-7}. Incubate the plates for 45 min at 37 °C with 5% CO_2, gently rocking every 15 min.
    4. Aspirate the inoculum and replace with overlay containing a 1:1 mixture of 2x DMEM and 6% carboxymethyl cellulose (CMC), final concentration of 3% CMC, supplemented with 10% FBS; incubate at 34 °C with 5% CO_2 for 48 h.

NOTE: Pre-warm the overlay mixture in a 37 °C water bath for 15 min during the infection step. A 1:1 mixture of 1% agarose with 2x DMEM supplemented with 10% FBS may be used in place of CMC. To overlay with agarose, boil 1% agarose (in dH_2O) and mix with cold 2x DMEM. Ensure the mixture is a suitable temperature before adding to the cell monolayer (approximately 37-40 °C). If agarose is used for the overlay, cells must be fixed by incubating in 2 mL of 3:1 methanol:acetic acid for at least one hour prior to staining.

2. Staining and calculating viral titer

    1. Visualize plaques by staining with crystal violet or direct visualization of eGFP under a fluorescent microscope.

    2. To stain plates, aspirate the overlay, wash once with PBS, then add 2 mL of 0.1% crystal violet (in 80% methanol and dH_2O) to each well. Place on a plate rocker for approximately 20 min at room temperature prior to de-staining. Remove the crystal violet, and gently wash each well twice using dH_2O or PBS.

    NOTE: Washing and staining steps should be performed gently by pipetting slowly towards the side of each well to ensure the cell monolayer remains intact throughout the procedure.

    3. Allow plates to dry for at least 1 h prior to counting plaques. Ensure that plaque counts are obtained from wells containing 20 to 200 plaques. To calculate the titer of the virus in plaque-forming units (PFU) per mL, multiply the dilution factor of the well counted with the volume of infection, and divide this number from the plaques present in the respective well.

$$titer\ (pfu/mL) = \frac{number\ of\ plaques}{dilution\ factor\ \times\ volume\ of\ infection}$$

4. Plating cells (Day 1) for the measurement of neutralization of SARS-CoV-2 pseudovirus by commercially available antibodies and convalescent patient serum

1. Preparation for tissue culture

    1. Prepare medium and tissue culture hood as described in section 1. In addition, prepare the necessary number of 96 well plates to accommodate a minimum of 2 replicates per sample (i.e., 1 plate per 6 samples); add additional replicates if sample volume permits.

2. Plating and maintaining cells

    1. Grow and maintain Vero E6 cells as described in section 1. Prepare at least 10 mL of cell suspension per 96-well plate at a concentration of 2×10^5 cells per mL (plate 1.5×10^5 cells per mL for assays performed after 48 h, if needed). Add 100 µL of cell suspension to each well of a 96-well plate using a multichannel pipette, and incubate for 24 h at 37 °C with 5% CO_2.

    NOTE: Mix the cell suspension well, and rock each plate gently in all directions to ensure even distribution of cells.

5. Antibody or serum dilutions and infections (Day 2)

NOTE: This protocol can be applied to measure the neutralization of VSV-S-eGFP by both commercially available antibodies and patient serum, as well as serum collected from animals for pre-clinical vaccine development studies. *Take note of the additional steps listed when handling patient/ animal serum samples.

1. Serial dilution series

1. Prior to diluting serum samples, heat-inactivate each sample in a 56 °C water bath for 30 min to inactivate complement. Ensure necessary safety precautions are taken when handling patient samples; only open sample containers when in the tissue culture hood, and ensure appropriate containment level 2 personal protective equipment is worn.
2. Set up the dilution series in an empty 96-well plate (Plate 1).
3. Begin all dilutions in Row A of the 96-well plate in 80 µL. *For patient samples, begin the dilution series at 1 in 10 by placing 8 µL of serum in 72 µL of serum-free DMEM (with 1% penicillin/streptomycin).
   NOTE: The concentration of neutralizing antibody used will depend on the activity predicted by the manufacturer. For the SARS-CoV-2 Spike neutralizing antibody used here (see the **Table of Materials**), start with 5 µg/mL to observe at least 50% neutralization.
4. Add 40 µL of of serum-free DMEM (with 1% penicillin/streptomycin) to rows B to G, and 80 µL to row H. Do not add virus to row H, as it serves as a cell-only control.
5. Using a 12-well multichannel pipette, mix and transfer 40 µL of diluted serum or antibody from row A to row B. Mix and repeat until row F, discard 40 µL from row F. Do not add serum to row G as it represents the virus-only control row.

2. Infection and overlay

1. Prepare an appropriate volume of diluted VSV-S-eGFP to treat each well at MOI 0.05 (or 2000 pfu). (When completing this calculation, keep in mind that only 60 µL of the total 80 µL volume will be moved onto the cells; therefore, be sure to multiply the volume of the virus by 1.33 to maintain 2000 pfu).
   NOTE: As VSV-S-eGFP is temperature-sensitive, ensure viral stocks remain on ice whenever not in use, and avoid multiple freeze-thaw cycles as titers will differ after repeated freezing.
2. Add 40 µL of diluted virus to each well in rows A to G of Plate 1 and mix by pipetting up and down 4-5 times. Incubate the plate for 1 h at 37 °C with 5% CO_2.
3. Remove the plate containing cells from the incubator (Plate 2), and carefully aspirate the media from all wells. Transfer 60 µL of antibody/virus mixture from Plate 1 to Plate 2, and incubate for 1 h at 37 °C with 5% CO_2, rocking the plate every 20 min.
4. Top up each well with 140 µL of overlay containing CMC in DMEM for a final concentration of 3% CMC (with 10% FBS and 1% penicillin/streptomycin). Place Plate 2 in an incubator set to 34 °C with 5% CO_2 for approximately 24 h before imaging.
   NOTE: Pre-warm the overlay mixture in a 37 °C water bath for 15 min during the infection step.

6. Imaging and quantification (Day 3)

1. Image plates using an automated fluorescent imager (using a fluorescein isothiocyanate (FITC) filter or an alternative filter with an excitation wavelength of 488 nm). Quantify viral infection by creating a protocol that automatically identifies and counts individual eGFP foci. If an automatic counting feature is not available, use ImageJ software to quantify the number of eGFP foci.

Representative Results

This protocol outlines a rapid and effective method for detecting neutralizing antibodies against SARS-CoV-2 S protein via inhibition of VSV-S-eGFP pseudovirus infection (quantifiable by loss of eGFP foci detected). A schematic representation of the protocol is depicted in **Figure 1**. It is recommended that a commercially available antibody be used as a positive control each time the assay is run to ensure the consistency of the assay. Here, we demonstrate a dilution curve using a commercially available neutralizing IgG antibody against SARS-CoV-2 Spike RBD compared to an IgG control (see the **Table of Materials** for details about both antibodies; **Figure 2**).

Convalescent patient samples were collected approximately three months post SARS-CoV-2 infection, and pseudovirus neutralization was determined using the method described above (**Figure 3**). Importantly, minimal background inhibition was observed using healthy donor serum. Furthermore, of note, this assay distinguishes between patients with high symptom severity versus those with milder disease based on the need for hospitalization. In line with other reports, we have observed within our small cohort that hospitalized patients tend to demonstrate increased neutralizing capacity than those who did not require hospitalization[19,20]. While this may not always be the case for hospitalized versus non-hospitalized patient samples, the ability of the assay to differentiate varying degrees of neutralization is an asset. There may also be cases in which the neutralizing ability of the patient serum is much higher than those demonstrated here. If necessary, the starting dilution of patient serum may be adjusted, or additional dilution steps may be carried out on an additional plate.

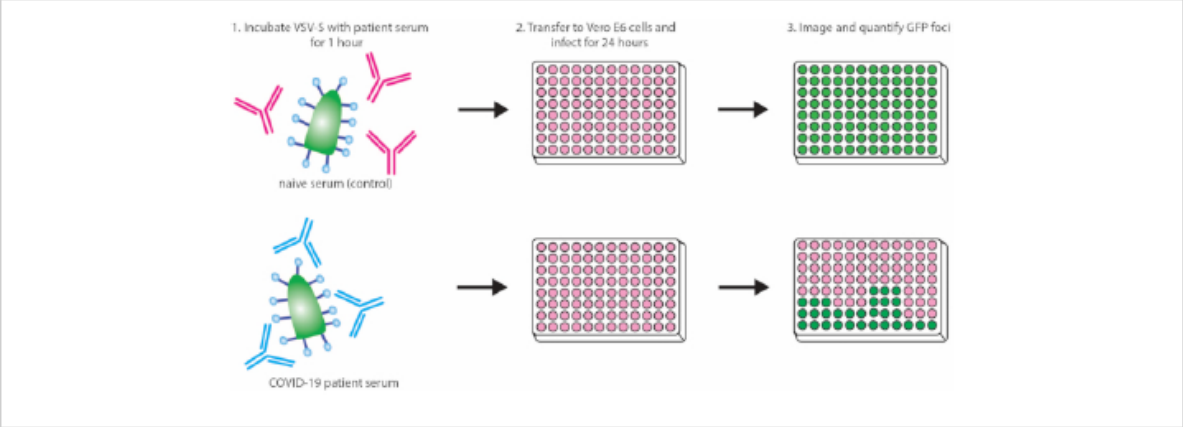

Figure 1: Protocol outline demonstrating neutralization of VSV-S-eGFP by convalescent serum. Abbreviations: VSV = vesicular stomatitis virus; eGFP = enhanced green fluorescent protein; COVID-19 = coronavirus disease. Please click here to view a larger version of this figure.

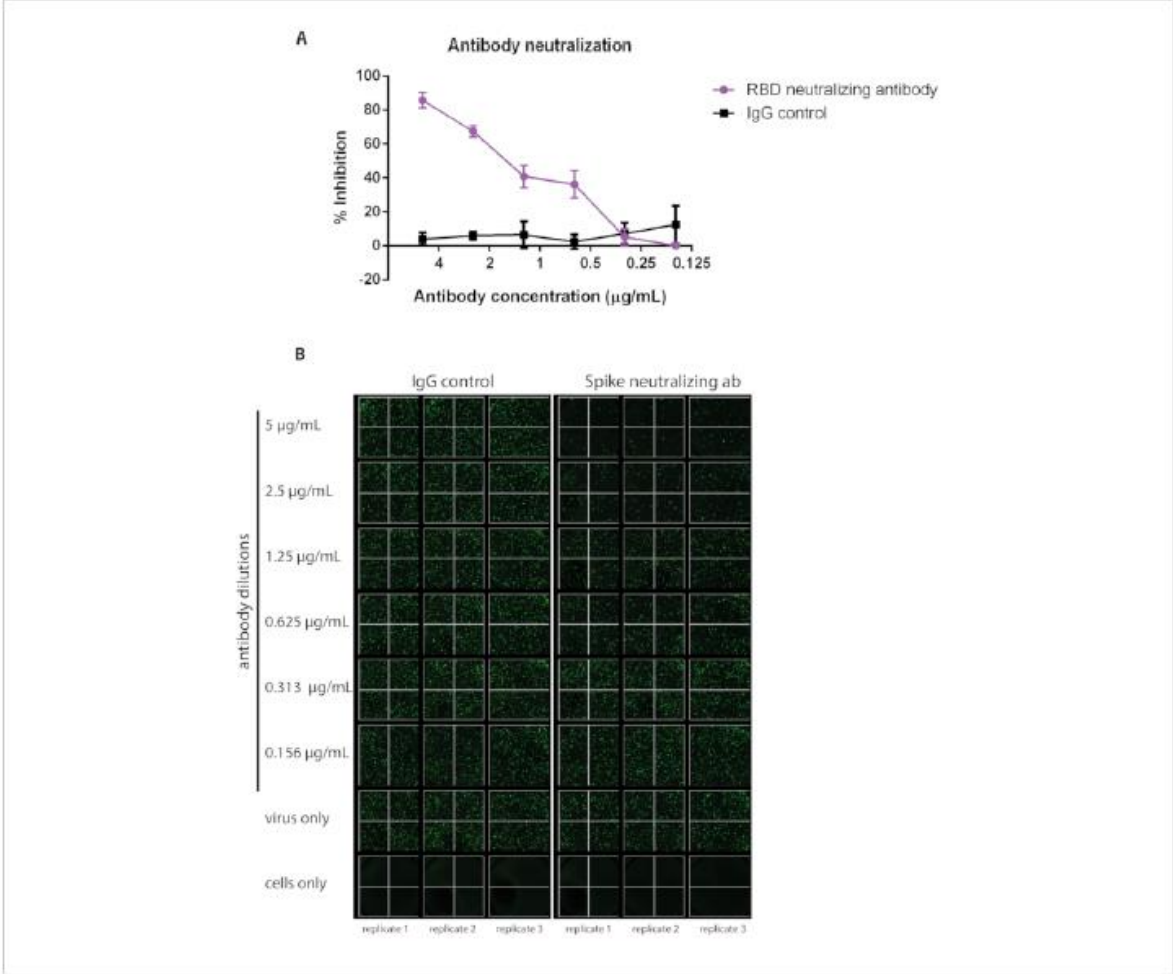

Figure 2: A commercially available neutralizing antibody against SARS-CoV-2 has been used as an example of a positive control alongside IgG as a negative control. The ability of neutralizing antibodies to inhibit viral infection will vary; refer to the information available for the specific antibody purchased to determine which concentration to begin the dilution curve (samples were run in triplicate, error bars represent ± SD). (**A**) Percent inhibition has been calculated based on the number of eGFP foci detected via (**B**) fluorescent imaging. Abbreviations: SARS-CoV-2 = severe acute respiratory syndrome coronavirus 2; IgG = immunoglobulin; SD = standard deviation; eGFP = enhanced green fluorescent protein; RBD = receptor-binding domain. Please click here to view a larger version of this figure.

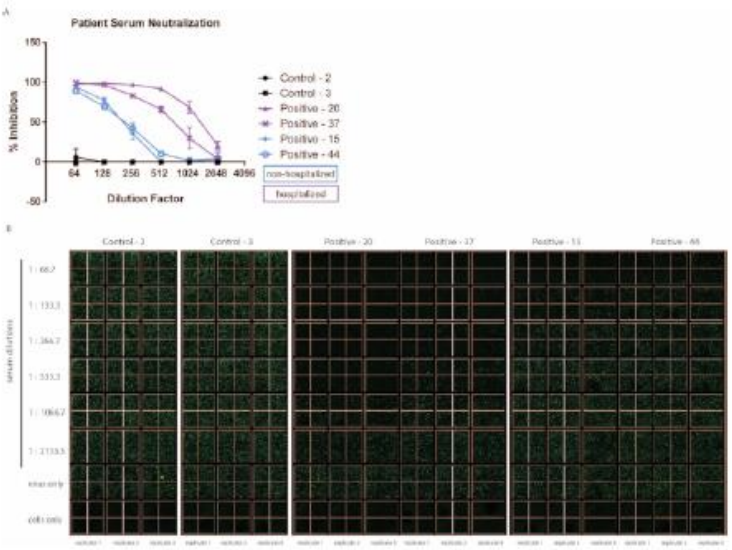

Figure 3: The ability of convalescent serum from patients to neutralize VSV-S-eGFP varies depending on the severity of symptoms. Patient serum samples were collected approximately 3 months post-SARS-CoV-2 infection, and control samples were collected from uninfected patients (samples were run in triplicate, error bars represent ± SD). (**A**) Percent inhibition has been calculated based on the number of eGFP foci detected via (**B**) fluorescent imaging. Abbreviations: SARS-CoV-2 = severe acute respiratory syndrome coronavirus 2; SD = standard deviation; eGFP = enhanced green fluorescent protein. Please click here to view a larger version of this figure.

Discussion

The method described here may be adapted to suit varying lab environments and resources as needed. Importantly, the main limitation of this protocol is the necessity for a containment level 2 space and tissue culture hood. The application of a replicating RNA virus pseudotyped with the SARS-CoV-2 spike, such as VSV-S-eGFP, is a formidable alternative to the SARS-CoV-2 virus, which requires a containment level 3 working area, but may remain a limitation for some groups. All other steps described here are quite flexible and may be performed in nearly any containment level 2 lab. For example, the use of a fluorescent imager with an automated counting feature is not necessary. The 96-well format used here means that only approximately 4 fields of view are required to image nearly the entire well using the lowest objective available (2x).

A manual fluorescent microscope may be used to image multiple fields of each well, and ImageJ (free software) can then be used to quantify eGFP foci. Additionally, we have chosen to use the 96-well format to use the lowest volume of serum possible as well as keeping consumable usage to a minimum. If a fluorescent microscope is unavailable, this protocol may be scaled up to a 6- or 12-well format to detect

plaque formation after crystal violet fixation and staining (similar to the viral titer protocol described above). The most critical consideration to keep in mind when performing this protocol is the temperature sensitivity of VSV-S-eGFP. When working with VSV-S-eGFP, always aliquot the virus into small volumes to avoid multiple freeze-thaw cycles, and keep the virus on ice whenever possible. Additionally, robust fluorescent signal may be detected after 24 h; however, we have acquired similar results after imaging at 20 to 28 h post infection.

There are several methods available to detect the presence of antibodies against SARS-CoV-2, including the gold-standard enzyme-linked immunosorbent assay (ELISA) assay, which quantifies the total amount of antibodies against S[21,22]. Here, we have outlined a fast and reliable method to specifically detect neutralizing antibodies against the immunodominant SARS-CoV-2 spike protein in convalescent serum from patients. We have improved the classical plaque-reduction neutralization test (PRNT) by successfully adapting to a 96-well format, which allows for the detection of neutralizing antibodies in a large number of samples within 24 h by automated quantification of pseudovirus infection, allowing for quick turnaround of final data reports. In addition to detecting neutralizing antibodies within serum, this method can be adapted to perform high-throughput screening of other therapeutic strategies, which aim to directly inhibit the SARS-CoV-2 spike protein interaction with hACE2, such as monoclonal antibodies, recombinant soluble hACE2, or protease inhibitors, to impede viral entry[23]. With the emergence of several SARS-CoV-2 spike protein variants, it is also important to note that this method may be applied to determine if similar neutralization levels occur following infection with different variants of the virus[24].

Other examples of available methods to detect antibodies against SARS-CoV-2 include ELISAs, lentivirus-based assays, and commercial kits to evaluate the neutralizing capacity of serum samples. While the commonly used IgM- or IgG-binding ELISAs are an effective method to determine the presence of antibody concentration to track previous infection or immunization, they are unable to distinguish the binding antibodies' neutralizing capacity[25]. Pseudotyped lentivirus-based neutralization assays have an improved safety profile, by using non-replicative viral particles as opposed to replicating VSV-S-eGFP; however, this creates a barrier in terms of testing capacity as lentiviral titers tend to be much lower[26,27]. There are several commercially available kits that measure the ability of antibodies to block infection via competitive inhibition of the SARS-CoV-2 spike protein (RBD specifically) binding with the hACE2 receptor following incubation with convalescent serum (e.g., CUSABIO, GenScript, Abnova). While many of these kits have reputable sensitivity and specificity, they also tend to be relatively expensive and therefore not ideal for a large volume of samples. The protocol provided here is fast, reliable, and inexpensive. This high-throughput method may be used to test many samples, achieving a robust readout within 24 h.

Disclosures

The authors have no competing financial interests related to this publication.

Acknowledgments

We would like to thank the Whelan lab for generously providing the VSV-S-eGFP virus used in this protocol (described in Case *et al.* 2020). We also thank Drs. Bill Cameron and Juthaporn Cowan (and team) for collecting the patient blood samples (REB protocol ID 20200371-01H). The

authors disclose receipt of the following financial support for the research, authorship, and/or publication of this article: This work was funded by the generous support from the Ottawa Hospital Foundation and a grant from the Canadian Institutes of Health Research (#448323) and a Fast Grant from the Thistledown foundation for COVID-19 Science to C.S.I. T.R.J. is funded by an Ontario Graduate Scholarship and cluster Mitacs fellowship. JP is funded by a cluster Mitacs fellowship. T.A. is funded by a CIHR Banting Fellowship. We would also like to thank all the individuals who participated and donated their blood samples for this study.

References

1. Hu, B., Guo, H., Zhou, P., Shi, Z.L. Characteristics of SARS-CoV-2 and COVID-19. *Nature Reviews Microbiology*. **19** (3), 141-154 (2021).
2. Burrell, C. J., Howard, C. R., Murphy, F. A. Coronaviruses. *Fenner and White's Medical Virlogy*. 437-446 (2017).
3. COVID-19 Map. Johns Hopkins Coronavirus Resource Center. https://coronavirus.jhu.edu/map.html.
4. Zimmer, C., Corum, J., Wee, S. L. Covid-19 vaccine tracker. The New York Times. https://www.nytimes.com/interactive/2020/science/coronavirus-vaccine-tracker.html.
5. Hoffmann, M. et al. SARS-CoV-2 cell entry depends on ACE2 and TMPRSS2 and is blocked by a clinically proven protease inhibitor. *Cell*. **181** (2), 271-280.e8 (2020).
6. Letko, M., Marzi, A., Munster, V. Functional assessment of cell entry and receptor usage for SARS-CoV-2 and other lineage B betacoronaviruses. *Nature Microbiology*. **5**, 562-569 (2020).
7. Azad, T. et al. Nanoluciferase complementation-based bioreporter reveals the importance of N-linked glycosylation of SARS-CoV-2 Spike for viral entry. *Molecular Therapy*. S1525-0016(21)00074-5 (2021).
8. Brown, E. E. F. et al. Characterization of critical determinants of ACE2-SARS CoV-2 RBD interaction. *International Journal of Molecular Sciences*. **22** (5), 2268 (2021).
9. Azad, T. et al. SARS-CoV-2 S1 NanoBiT: a Nanoluciferase complementation-based biosensor to rapidly probe SARS-CoV-2 receptor recognition. *Biosensors and Bioelectronics*. **180**, 113122 (2021).
10. Azad, T. et al. Implications for SARS-CoV-2 vaccine design: Fusion of Spike glycoprotein transmembrane domain to receptor-binding domain induces trimerization. *Membranes*. **10** (9), 215 (2020).
11. Cao, Z. et al. Potent and persistent antibody responses against the receptor-binding domain of SARS-CoV spike protein in recovered patients. *Virology Journal*. **7**, 299 (2010).
12. To, K. K. W. et al. Temporal profiles of viral load in posterior oropharyngeal saliva samples and serum antibody responses during infection by SARS-CoV-2: an observational cohort study. *The Lancet Infectious Diseases*. **20** (5), 565-574 (2020).
13. Gao, Q. et al. Development of an inactivated vaccine candidate for SARS-CoV-2. *Science*. **369** (6499), 77-81 (2020).
14. Liu, W. et al. Two-year prospective study of the humoral immune response of patients with severe acute respiratory syndrome. *Journal of Infectious Diseases*. **193** (6), 792-795 (2006).

15. Dong, Y. et al. A systematic review of SARS-CoV-2 vaccine candidates. *Signal Transduction and Targeted Therapy*. **5** (1), 237 (2020).

16. Amanat, F., Krammer, F. SARS-CoV-2 vaccines: Status report. *Immunity*. **52** (4), 583-589 (2020).

17. Amanat, F. et al. A serological assay to detect SARS-CoV-2 seroconversion in humans. *Nature Medicine*. **26** (7), 1033-1036 (2020).

18. Case, J. B. et al. Neutralizing antibody and soluble ACE2 inhibition of a replication-competent VSV-SARS-CoV-2 and a clinical isolate of SARS-CoV-2. *Cell Host and Microbe*. **28** (3), 475-485.e5 (2020).

19. Garcia-Beltran, W. F. et al. Journal Pre-proof COVID-19 neutralizing antibodies predict disease severity and survival. *Cell*. **184** (2), 476-488.e11 (2020).

20. Zeng, C. et al. Neutralizing antibody against SARS-CoV-2 spike in COVID-19 patients, health care workers, and convalescent plasma donors. *JCI insight*. **5** (22) (2020).

21. Whitman, J. D. et al. Evaluation of SARS-CoV-2 serology assays reveals a range of test performance. *Nature Biotechnology*. **38** (10), 1174-1183 (2020).

22. Ainsworth, M. et al. Performance characteristics of five immunoassays for SARS-CoV-2: a head-to-head benchmark comparison. *The Lancet Infectious Diseases*. **20** (12), 1390-1400 (2020).

23. Sharifkashani, S. et al. Angiotensin-converting enzyme 2 (ACE2) receptor and SARS-CoV-2: Potential therapeutic targeting. *European Journal of Pharmacology*. **884**, 173455 (2020).

24. Burki, T. Understanding variants of SARS-CoV-2. *The Lancet*. **397** (10273), 462 (2021).

25. Jayamohan, H. et al. SARS-CoV-2 pandemic: a review of molecular diagnostic tools including sample collection and commercial response with associated advantages and limitations. *Analytical and Bioanalytical Chemistry*. **413** (1), 49-71 (2020).

26. Nie, J. et al. Quantification of SARS-CoV-2 neutralizing antibody by a pseudotyped virus-based assay. *Nature Protocols*. **15** (11), 3699-3715 (2020).

27. Crawford, K. H. D. et al. Protocol and reagents for pseudotyping lentiviral particles with SARS-CoV-2 spike protein for neutralization assays. *Viruses*. **12** (5), 513 (2020).

A7: Curriculum Vitae

Taylor Rae Jamieson-Datzkiw

Education

UNIVERSITY OF OTTAWA, OTTAWA, ON — 2016-present
MD/PhD in Microbiology and Immunology (Faculty of Medicine)
Centre for Innovative Cancer Research, Ontario Hospital Research Institute

UNIVERSITY OF WINNIPEG, WINNIPEG, MB — 2011-15
B.Sc. Honours in Biochemistry and Biology
Honours thesis title: "Mechanistic evaluation of metformin's anticancer activity"

Scholarships & Awards

Canadian Graduate Scholarships – Doctoral Award (CIHR)	2021-present
University of Ottawa PhD Excellence Scholarship	2021-22
Mitacs Accelerate program internship	2020-21
Ontario Graduate Scholarship	2020-21
University of Ottawa PhD Excellence Scholarship	2020-21
Canadian Graduate Scholarship – Masters Award (CIHR)	2019-20
Ontario Graduate Scholarship (declined)	2019-20
University of Ottawa PhD Excellence Scholarship	2019-20
Ontario Graduate Scholarship	2018-19
University of Ottawa PhD Excellence Scholarship	2018-19
University of Ottawa Aboriginal Students Scholarship	2018
Mount Royal University - .cAISES Conference Travel Scholarship	2018
National Indian Brotherhood (NIB) Trust Fund Scholarship	2017-18
University of Ottawa PhD Entrance Scholarship	2017-21
Indspire Scholarship Award	2017
University of Ottawa MD/PhD Tuition Scholarship	2016-23
Dean's Honour List (University of Winnipeg)	2011-16
NSERC Aboriginal Ambassador in the Natural Sciences and Engineering	2015
Dr. Charles Code Scholarship in Biology (University of Winnipeg)	2014
NSERC Undergraduate Student Research Award	2014
Health Sciences Centre Leaders in Service Excellence Award	2014
Indspire Scholarship Award	2013
Alaa S. Abd-El-Aziz Aboriginal Student Award (University of Winnipeg)	2013
Health Sciences Centre Volunteer Enterprises Award Scholarship	2013
Manitoba Blue Cross Scholarship (University of Winnipeg)	2011
Chancellor's Special Entrance Award (University of Winnipeg)	2011
Platinum Jets Scholarship	2011
Horace Patterson Foundation Award	2011
Manitoba Youth Leadership Scholarship	2011

Conferences & Professional Development

OTTAWA HOSPITAL RESEARCH DAY - OTTAWA, ON 2020
Elevator Pitch finalist and poster presentation
Title: Nanoluciferase complementation-based biosensor for rapid screening of potential SARS-CoV-2 therapeutic agents and seroconversion

OTTAWA HOSPITAL RESEARCH DAY - OTTAWA, ON 2019
Poster presentation
Title: A double dose of DNA damage: Overcoming PARPi resistance using targeted oncolytic viruses

CANADIAN CANCER RESEARCH CONFERENCE - OTTAWA, ON 2019
Poster presentation
Title: A double dose of DNA damage: Overcoming PARPi resistance using targeted oncolytic viruses

BIOCANRX SUMMIT4CI – VICTORIA, BC 2019
Poster presentation
Title: A double dose of DNA damage: Overcoming PARPi resistance using targeted oncolytic viruses
*Recipient of HQP travel scholarship

AMERICAN ASSOCIATION FOR CANCER RESEARCH, ANNUAL GENERAL MEETING – ATLANTA, GA 2019
Poster presentation
Title: A double dose of DNA damage: Overcoming drug resistance using targeted oncolytic viruses
*Recipient of Minority Scholar in Cancer Research travel award

UNIVERSITY OF OTTAWA BIOCHEMISTRY, IMMUNOLOGY AND MICROBIOLOGY POSTER DAY - OTTAWA, ON 2019
Poster presentation
Title: A double dose of DNA damage: Overcoming PARPi resistance using targeted oncolytic viruses

CANADIAN COMMISSION FOR UNESCO AND LET'S TALK SCIENCE PRESENT EQUITY, INCLUSION AND THE FUTURE OF STEM LEARNING - OTTAWA, ON 2018
Panelist
Session: Women in post-secondary STEM

OTTAWA HOSPITAL RESEARCH INSTITUTE (OHRI) RESEARCH DAY – OTTAWA, ON 2018
Poster presentation
Title: A double dose of DNA damage: Overcoming PARPi resistance using targeted oncolytic viruses

NANOSCALE FLOW CYTOMETRY SYMPOSIUM – OTTAWA, ON 2018
Symposium attendee

INTERDISCIPLINARY STUDENT RESEARCH CONFERENCE ON HEALTHCARE (ISRCH) – OTTAWA, ON 2018
Conference organizer
Role: VP promotions and conference photographer

.CAISES (MAANOMATAPOYA: FIRST STEPS CONFERENCE) – CALGARY, AB 2018
Oral presentation/panelist
Sessions: 'Indigenous identity in post-secondary and the workplace' and 'volunteering for mentorship and professional organizations'

ASIST (APPLIED SUICIDE INTERVENTION SKILLS TRAINING) WORKSHOP – TORONTO, ON 2017
Workshop attendee

CLINICAL INVESTIGATOR TRAINING ASSOCIATION OF CANADA (CITAC) – TORONTO, ON 2016
Conference attendee

2ND ANNUAL BIOPHYSICAL SOCIETY MEETING – WINNIPEG, MB 2016
Conference attendee

PRAIRIE UNIVERSITY BIOLOGY SYMPOSIUM (PUBS) – WINNIPEG, MB 2015
Oral Presentation (and conference volunteer)
Title: Mechanistic Evaluation of Diabetes Drug Metformin's Anticancer Activity

Research Experience

UNIVERSITY OF OTTAWA: FACULTY OF MEDICINE 2017- present

PhD Student (Co-Supervisors: Dr. Carolina Ilkow and Dr. John Bell)

Following my first year of medical school, I worked in Dr. Ilkow's lab as a summer intern. One year later (June 2018) I began my PhD studies and have now mastered several new techniques (virus cloning and propagation, *in vivo* injections and dissection, qPCR and western blot, etc.), and presented at a number of conferences/meetings.

UNIVERSITY OF MANITOBA: FACULTY OF MEDICINE 2015-16

Student Research Assistant (Supervisor: Dr. Denice Bay)

Responsibilities included setting up Dr. Bay's new lab space, training new lab members, managing lab protocols and orders, and completing a research project on antimicrobial resistance testing.

UNIVERSITY OF WINNIPEG: FACULTY OF SCIENCE 2014-15

NSERC Undergraduate Studies Research Award (USRA) recipient (Supervisor: Dr. Anuraag Shrivastav)

I completed a research project centered on breast cancer cell signaling and assisted lab members when needed (this project was continued as an Honours thesis).

Teaching & Mentorship

LET'S TALK SCIENCE – UNIVERSITY OF OTTAWA 2016- present

Classroom volunteer and Aboriginal Mentorship Program (AMP) mentor

I plan and facilitate activities at various schools and afterschool programs to teach children of all ages concepts in science and encourage an interest in science as a career. As an AMP mentor, I work with a small group of Indigenous students from the rural outskirts of Ottawa to create science fair projects for a final presentation and full day event at the University of Ottawa each year.

Recent article featuring my involvement with AMP: 'Guiding the way for Indigenous youth: MD/PhD student proves the value of mentorship', published in the University of Ottawa's Faculty of Medicine MedPoint News.https://med.uottawa.ca/en/news/guiding-way-indigenous-youth-mdphd-student-proves-valuementorship

UNIVERSITY OF MANITOBA 2015-16

Mentor/trainer for new lab members

As the student research assistant in Dr. Bay's group at the University of Manitoba it was my responsibility, along with our graduate student, to train the incoming students, assist them in planning their daily activities in the lab and troubleshoot when needed.

LET'S TALK SCIENCE – UNIVERSITY OF WINNIPEG 2014-15

Daycare planning committee member

I planned and facilitated activities at the University of Winnipeg Daycare to teach the children concepts in science through fun games and projects to spark their interest in the field of science.

UNIVERSITY OF WINNIPEG 2012-15

First Year Biology Lab Demonstrator

Assisted in lab exercises, including animal dissections, microscope skills, spectrophotometric assays, etc.

Leadership & Volunteerism

LET'S TALK CANCER 2020-present

Co-Coordinator

Let's Talk Cancer is a sub-section of the larger Let's Talk Science program. As a co-coordinator I work with a small team of graduate students to deliver activities and lessons to middle and high school students primarily focused on cancer biology, extending as far as health sciences in general. Our goal is to engage students in learning more about cancer, its origin and treatments, as well as what it is like to be a graduate student to help guide education and career decisions they may encounter after graduating from high school

BIOCANRX 2020-present

HQP (highly qualified personnel) working group member and 'Insider Series' coordinator

The HQP working group is responsible for assisting in the planning and delivery of HQP training activities at the annual BioCanRx Summit for Cancer Immunotherapy. As HQP members, we provide input regarding topics for trainee workshops and seminars, we also evaluate and rank HQP award competitions. The Covid-19 pandemic has inspired a subset of our group to create the 'Insider Series' wherein we have delivered a number of online workshops and panel discussions to engage HQP across Canada who were required to spend a significant amount of time working from home due to laboratory shut-downs.

INDIGENOUS PHYSICIANS ASSOCIATION OF CANADA 2018-present

Student member

The Indigenous Physicians Association of Canada is a national organization that aims to improve the health of Indigenous communities. I was recently granted funding to attend the 2018 conference and annual general meeting where I was able to interact with students, residents and physicians from across the country. Issues discussed at this meeting revolved around Indigenous physician wellness, including workshops on building resilience, discussions on policy regarding physician wellness and cultural teachings.

CHEO BUDDY PROGRAM, CAMP QUALITY 2017-20

Medical student volunteer

This is a program that matches medical students from the University of Ottawa with children undergoing long-term cancer treatment. The benefits of these one-on-one relationships are three-fold: medical students get to see the hospital from a patient's perspective as opposed to a place of education, patients are given a new friend to spend time with while in hospital, and most importantly, parents are given the much-needed chance to leave their child's hospital room while the Buddy is visiting.

MEDICAL CURIOSITY ON STAGE, UNIVERSITY OF OTTAWA 2018-19

Actor/presenter

Medical Curiosity is a part of the 'Curiosity on Stage' program that runs regularly at the Canadian Science and Technology Museum. We are a group of medical students (supervised by a physician from the uOttawa medical school) that organize monthly programs to educate the public on common medical issues such as strokes, heart attacks, and fractures.

INDIGENOUS HEALTH INTEREST GROUP, UNIVERSITY OF OTTAWA 2017-18

Executive member

As a member of this group I have attended numerous workshops and seminars related to Indigenous culture and health. As a member of the leadership team, I applied for funding to run events, recruited speakers and planned many workshops, all with the common interest of teaching our fellow classmates about Indigenous health.

ONCOLOGY INTEREST GROUP, UNIVERSITY OF OTTAWA 2017-18

Executive member

I worked with a small team of students responsible for applying for the necessary funding to run our events and plan activities aimed at exploring the various sub-specialties of oncology, research opportunities, and patient experiences. We successfully offered more than 15 hours of activities for our group members.

APPLIED SUICIDE INTERVENTION SKILLS TRAINING (ASIST) 2018

Co-organizer

ASIST is a workshop that provides people from any field with the skills to recognize an individual at risk of committing self-harm or suicide, followed by a step-by-step approach to assisting the individual initiate a plan for short-term safety. Working alongside a fellow medical student, I worked to obtain funding from the Faculty of Medicine to bring ASIST training to uOttawa.

CHILDREN'S HOSPITAL, WINNIPEG HEALTH SCIENCES CENTRE 2010-16

Book corner volunteer

I completed weekly shifts at the Children's Hospital as a library volunteer. I was responsible for taking books and movies from the "Book Corner" library inside the Children's Hospital onto the wards for children and families that were unable to come down to the library. I would also read to children that needed a visitor.

Employment

NEW DIRECTIONS FOR CHILDREN, YOUTH, ADULTS, AND FAMILIES 2012-16

Support worker

I was a support worker for the Empowering People in the Community (EPC) program. I was responsible for providing support to individuals that had developmental delays, physical disabilities and/or mental health concerns. My duty as a support worker was to work one-on-one with individuals to assist them in being a part of the community and reaching individual goals.

Peer Reviewed Publications

1. **Taylor R. Jamieson**, Joanna Poutou, Ricardo Marius, Xiaohong He, Reza Rezaei, Taha Azad, and Carolina S. Ilkow. Detection of SARS-CoV-2 Neutralizing Antibodies Using High-Throughput Fluorescent Imaging of Pseudovirus Infection. *Journal of Visualized Experiments*, accepted for publication May 2021.

2. Reza Rezaei, Abera Surendran, Ragunath Singaravelu, **Taylor R. Jamieson**, Parisa Taklifi, Joanna Poutou, Taha Azad, Carolina S. Ilkow. Detection of SARS-CoV-2 Receptor-binding Domain Antibody Using a HiBiT-based Bioreporter. *Journal of Visualized Experiments*, accepted for publication May 2021.

3. Emily E. F. Brown*, Reza Rezaei*, **Taylor R. Jamieson***, Jaahnavi Dave*, Nikolas T. Martin, Mathieu J.F. Crupi, Stephen Boulton, Sarah Tucker, Jessie Duong, Joanna Poutou, Adrian Pelin, Hamed Yasavoli-Sharahi, Zaid Taha, Rozanne Arulanandam, Abera Surendran, Mina Ghahremani, Chantal Matar, Jean-Simon Diallo, Ragunath Singaravelu, John C. Bell , Carolina S. Ilkow, and Taha Azad. Characterization of Critical Determinants of ACE2-RBD Interaction. *International Journal of Molecular Sciences* 22(5), 2268 (2021). (*equal authorship contribution)

4. Marie-Eve Wedge, Victoria A. Jennings, Giuseppe Pugliese, Joanna Poutou, Mathieu Crupi, **Taylor R. Jamieson**, Brian J. Laight, Meaghan Boileau, Sarwat Tahsin Khan, Hayley E. McKay, Larissa Pikor, Adrian Pelin, Elaine Rose, Emily E.F. Brown, Natalie Crawford, Christiano Tanese de Souza, Almohanad Alkayyal, Abera Surendran, Ragunath Singaravelu, Dominic G. Roy, Julia Petryk, Gemma Migneco, Benjamin McSweeney, Mary Lynn Cottee, Egon J. Jacobus, Brian Keller, Avijit Chatterjee, Rebecca C. Auer, Jean-Simon Diallo, Derrick Gibbings, Benjamin R. tenOever, Alan Melcher, John C. Bell and Carolina S. Ilkow. Virally programmed extracellular vesicles sensitize cancer cells to oncolytic virus and small molecule therapy. *Nature Cancer*, currently under revisions.

5. Taha Azad, Reza Rezaei, Ragunath Singaravelu, **Taylor R. Jamieson**, Mathieu J F Crupi, Abera Surendran, Joanna Poutou, Parisa Taklifi, Juthaporn Cowan, Donald William Cameron, and Carolina S Ilkow. A high-throughput nanobit-based serological assay detects SARS-CoV-2 seroconversion. *Nanomaterials* 11(3), 1-9 (2021).

6. **Taylor R. Jamieson**, Joanna Poutou, and Carolina Ilkow. Redirecting oncolytic viruses: Engineering opportunists to take control of the tumour microenvironment. *Cytokine and Growth Factor Reviews* 56, 102-114 (2020).

7. Taha Azad*, Ragunath Singaravelu*, Mathieu J.F. Crupi*, **Taylor R. Jamieson***, Jaahnavi Dave, Emily E.F. Brown, Reza Rezaei, Zaid Taha, Stephen Boulton, Nikolas T. Martin, Abera Surendran, Joanna Poutou, Mina Ghahremani, Kazem Nouri, Jack T. Whelan, Jessie Duong, Sarah Tucker, Jean-Simon Diallo, John C. Bell, and Carolina S. Ilkow. Implications for SARS-CoV-2 Vaccine Design: Fusion of Spike Glycoprotein Transmembrane Domain to Receptor-Binding Domain Induces Trimerization. *Membranes,* 2020, *10*(9), 215. (*equal authorship contribution)

8. Taha Azad, Ragunath Singaravelu, Zaid Taha, **Taylor R. Jamieson**, Stephen Boulton, Mathieu J.F. Crupi, Nikolas T. Martin, Joanna Poutou, Mina Ghahremani, Adrian Pelin, Kazem Nouri, Christopher Boyd Marshall, Rozanne Arulanandam, Emily E.F. Brown, Nouf Alluqmani, Reuben Samson, Anne-Claude Gingra , Bill Cameron, Peter A. Greer, Carolina S. Ilkow, Jean-Simon Diallo, John C. Bell. Nanoluciferase complementation-based biosensor reveals the importance of N-linked glycosylation of SARS-CoV-2 Spike for viral entry. *Molecular therapy*, 21 (2021).

9. Carmine J. Slipski*, **Taylor R. Jamieson***, George G. Zhanel, and Denice C. Bay. Riboswitch associated guanidinium selective efflux pumps frequently transmitted on proteobacterial plasmids increase Escherichia coli biofilm tolerance to disinfectants. *Journal of Bacteriology*, 202 (2020). (* equal authorship contribution)

10. **Taylor R. Jamieson** and Anuraag Shrivastav. Mechanistic evaluation of diabetes drug metformin's anticancer activity. Honours Thesis. University of Winnipeg, Winnipeg, Manitoba. April 2015.

Media Interviews

1. uOttawa student helping to create new cancer-killing viruses for breast, ovarian cancer treatment receives award (text interview). uOttawa Media, November 24, 2020. https://media.uottawa.ca/news/uottawa-student-helping-create-new-cancer-killing-viruses-breast-ovarian-cancer-treatment

2. Ottawa researcher awarded for work on new cancer-killing viruses. CityNews (Ottawa), November 24, 2020 (text interview). https://ottawa.citynews.ca/local-news/ottawa-researcher-awarded-for-work-on-new-cancer-killing-viruses-2903115

3. A cancer killer? Canadian researcher wins award for virus that could potentially destroy ovarian and breast cancer (text interview). Yahoo! News, November 24, 2020. https://ca.finance.yahoo.com/news/cancer-breast-ovarian-treatment-221024211.html

4. This Ottawa PhD student creates viruses for the forces of good (radio interview). CBC As It Happens, November 30, 2020. https://www.cbc.ca/radio/asithappens/as-it-happens-monday-edition-1.5822123/this-ottawa-phd-student-creates-viruses-for-the-forces-of-good-1.5822125

5. Canadian scientist receives Mitacs Prize for using viruses to treat cancer (news broadcast). CTV Your Morning, November 30, 2020. https://www.ctvnews.ca/health/canadian-scientist-receives-mitacs-prize-for-using-viruses-to-treat-cancer-1.5210128

6. Using viruses in the fight against cancer – Young researcher creates viruses capable of neutralizing breast & ovarian cancer (news broadcast). CTV News, December 5, 2020. https://www.ctvnews.ca/video?clipId=2094216

7. Taylor Jamieson-Datzkiw is hoping to change the narrative about viruses with her now award-winning research (news broadcast). CBC News – Our Ottawa, December 12, 2020. https://www.cbc.ca/player/play/1831028291505

8. Front Line Diaries: Taylor Jamieson-Datzkiw (news broadcast). CTV News Ottawa – Front Line Diaries, May 6, 2021. https://ottawa.ctvnews.ca/video?clipId=2197090